UNIVERSITÀ DEGLI STUDI DI PADOVA

DIPARTIMENTO DI ELETTRONICA E INFORMATICA

Tesi di Dottorato di Ricerca in

Ingegneria Elettronica e delle Telecomunicazioni

XIV Ciclo

Multicarrier Multiuser Asynchronous Communications

Andrea Tonello

Il Coordinatore	**Il Tutore**	**Il Dottorando**
Prof. Enrico Zanoni	Prof. Silvano Pupolin	Dott. Andrea Tonello

14 Dicembre 2001

A. A. 1998 - 2001

To Milena

CONTENTS

PREFACE

This thesis summarizes some of the research activity I have done during my stay at the University of Padova for my "dottorato di ricerca", 1999-2001. It conceptually consists of a continuation of the work on multicarrier communication systems for my "laurea" thesis. I am particularly indebted to Prof. Silvano Pupolin who supervised both dissertations and was inspiring in suggesting an interesting research topic. I wish to acknowledge Dr. Nicola Laurenti for the interesting discussions and the fruitful collaboration that originated the analysis results included in Chapters 10 and 11. I wish to say that this thesis has greatly benefited by the broad exposure to theoretical and practical research problems that I had at Bell Laboratories – Lucent Technologies – NJ – USA. I express my appreciation to many of the Bell Labs colleagues that I have had the opportunity to work with for several years, in particular to Dr. James P. Seymour who has understood and supported my decision of going back to the academia. The topics included in Chapter 5 and 9, i.e., optimum multicarrier-user detection and turbo multicarrier-user decoding, have found inspiration from the research I have done on space-time bit-interleaved codes during the summer 2000 at Bell Labs.

Andrea Tonello, Padova 12.14.2001

ABSTRACT

Communication systems based on multicarrier modulation have raised great attention in recent years for both wireline and wireless broadband applications. The main motivation being the robustness of this modulation approach to highly time dispersive channels that potentially simplifies the equalization task at the receiver. Most of the work in literature has focused on the single user channel, the broadcast channel, and the synchronous multiuser channel. It lacks to consider the asynchronous multiple access channel and its impact on the design and performance of a multicarrier modulation based system.

This has motivated our work that is synthesized by the objective of developing a formal and unified analysis of multicarrier modulation over an asynchronous multiple access channel. That is, multiple users wish to transmit their multicarrier signal to a receiver by sharing a common communication channel. Users are asynchronous, i.e., they have a certain amount of temporal and carrier frequency misalignment with respect to a reference at the receiver. This model is appropriate to describe the uplink of a mobile wireless communication system (mobile to base link) such as the uplink of a satellite system, of a wireless local are network (WLAN), or of a mobile cellular system. We assume, in general, propagation through frequency selective time-variant fading channels. With the appropriate variations the model may be used also to describe a wireline system where a set of terminals communicates with a central receiver, e.g., a computer.

Several different ways are possible to access the common channel. We propose and deeply investigate a simple method, referred to as multicarrier multiple access (MC-MA) that is obtained by combining multicarrier modulation with frequency division multiplexing. First, a number of sub-carriers (tones) are allocated inside the available spectrum. Then, subsets of carriers are assigned to distinct users and are used for multicarrier modulation. The key design features of these architectures are the choice of the sub-carrier spacing, the sub-carrier multiplexing strategy, and the shape of the transmit filters. Efficient digital implementations of the transmitters are possible and in such a case the system is referred to as multitone multiple access (MT-MA).

In a MC-MA system multiple users transmit their information signals through multiple narrow band pipes (sub-channels). The sub-channels have a certain degree of temporal

and frequency overlapping as a function of the shape of the sub-channel shaping filters, the sub-carrier spacing, the tone multiplexing scheme, the frequency selective communication channel, and the temporal/carrier frequency misalignments.

This thesis is articulated over three main themes:

A. The description of efficient digital system implementations.

B. The definition of optimal and sub-optimal receivers.

C. The impact on complexity and performance of the system design parameters and channel characteristics.

We start investigating particular implementations that deploy the discrete Fourier transform (DFT) and are an extension of the discrete multitone modulation (DMT) or the filtered multitone modulation (FMT) to the multiple access scenario.

Then, we study the problem of defining the optimum multicarrier multiuser demodulator. The resulting receiver comprises a front-end structure followed by a maximum a posteriori processor. The demodulator is optimum in the probabilistic sense and is capable of delivering optimum soft information on the transmitted bits/symbols of all users. We analyze the structure of the front-end receiver considering both static and time-variant frequency selective fading channels in the presence of temporal and carrier frequency asynchronism. Efficient digital implementations are possible and are based on using a bank of adaptive polyphase digital filters.

Since the complexity of the optimum demodulator grows exponentially with the number of users, the number of sub-channels, and the channel memory, we propose several simplified detection approaches. These are based on iterative detection schemes where soft/hard information is exchanged between sub-trellises that are obtained by partitioning the full hyper trellis that describes the hidden multiple-input multiple-output Markov model. For instance, iterative per-symbol detection is a simple approach that performs detection by iteratively exchanging soft/hard information between the symbol detectors at the matched filter bank outputs.

Channel coding is also considered, and iterative (turbo) multicarrier-user detection and decoding is proposed as a practical decoding solution when interleaved codes are deployed.

We point out that some analogy exists with space-time coded multiple antenna systems. The approach we followed for the treatment of the channel coding problem and the iterative multicarrier-user detection/decoding approach is inspired by the extensive work we have done on the design and decoding of space-time bit-interleaved codes.

Single carrier detection turns out to be a sub-optimal approach where detection is independently made on each sub-channel front-end output. For instance this is the conventional technique used in a DMT system where the receiver consists of a DFT

module followed by a one-tap equalizer per channel. It is a simple approach that may yield good performance in DMT-MA systems when we carefully choose the sub-carrier allocation, the distribution of power, and we add time and frequency guards. For this reason we extensively study the DMT-MA system through the analysis of its performance and capacity limits.

With regard to an asynchronous DMT-MA Gaussian channel, we attack the non-trivial problem of determining an inner bound to both the capacity of a given user link and the region of achievable information rates for joint reliable communications, i.e., capacity region. Such capacity inner bounds are treated as random variables since they depend upon the time and frequency offsets as well as upon several system parameters. The associated complementary cumulative distribution functions are defined and are evaluated for several system scenarios characterized by different tone assignment schemes and strategies of power allotment to sub-carriers.

The analytical and numerical results of this thesis suggest that optimal multicarrier detection should be deployed in multicarrier multiuser systems. Practical implementation through simplified detection schemes yields good performance. The effectiveness of simplified detection can be improved with the control of the interference components through the appropriate design of the transmit filters, the sub-carrier spacing, and the sub-carrier multiplexing. Further improvements are expected with dynamic tone assignments and ad hoc power allocation across sub-carriers. Therefore, the appropriate design of the system can tradeoff between demodulation complexity and spectral efficiency such that the performance of the system is maximized.

SOMMARIO[1]

Recentemente i sistemi di comunicazione basati sulla modulazione multiportante hanno suscitato particolare interesse per applicazioni a larga banda sia fisse che radio. La principale motivazione risiede nella robustezza di questo approccio di modulazione in canali altamente tempo dispersivi che potenzialmente semplifica l'equalizzazione. La maggior parte del lavoro in letteratura ha preso in esame il canale singolo utente, il canale broadcast, ed il canale multiutente sincrono, senza analizzare in dettaglio il canale multiutente asincrono ed il suo impatto sul progetto e la prestazione di un sistema multiportante.

Ciò ha motivato il nostro lavoro che può essere sintetizzato nell'obiettivo di sviluppare un'analisi formale ed unificata della modulazione multiportante in un canale ad accesso multiplo asincrono. Utenti multipli desiderano trasmettere il loro segnale multiportante ad un ricevitore condividendo un canale di comunicazione. Gli utenti sono asincroni, cioè possiedono un certo grado di asincronismo temporale e di frequenza di portante rispetto ad un riferimento al ricevitore. Questo modello è appropriato per descrivere l'uplink di un sistema radiomobile (collegamento mobile-base), ad esempio l'uplink di un sistema satellitare, di un sistema radiomobile cellulare, o di una rete radio locale (WLAN). In generale noi consideriamo canali con fading tempo variante e selettivo in frequenza. Con le appropriate variazioni il modello può essere impiegato per descrivere un sistema cablato ove un insieme di terminali comunica con un ricevitore centrale ad es. un computer.

Il canale comune può essere condiviso in vari modi. Noi proponiamo ed ampliamente analizziamo un metodo semplice, denominato accesso multiplo multiportante (MC-MA) che si ottiene combinando la modulazione multiportante con la multiplazione a divisione di frequenza. Dapprima un certo numero di sottoportanti (toni) è allocato nello spettro disponibile. Quindi sottoinsiemi di portanti sono assegnati ad utenti distinti ed utilizzati per la modulazione multiportante. Le principali caratteristiche di queste architetture sono la scelta della spaziatura di portante, la strategia di multiplazione dei toni, e il progetto dei filtri di trasmissione. Implementazioni digitali efficienti sono possibili ed il

[1] This section is a translation to Italian of the previous abstract.

sistema in tal caso è denominato accesso multiplo multitono (MT-MA).

In un sistema MC-MA utenti multipli trasmettono i loro segnali informativi attraverso sottocanali a banda stretta. I sottocanali hanno un certo grado di sovrapposizione temporale e frequenziale come funzione della forma dei filtri di trasmissione, della spaziatura di portante, della presenza di un canale selettivo in frequenza, e di disallineamenti temporali e frequenziali.

Questa tesi si articola in tre tematiche principali:

A. *Descrizione di implementazioni digitali efficienti.*
B. *Definizione di ricevitori ottimi e sub-ottimi.*
C. *Impatto dei parametri di progetto e delle caratteristiche del canale sulla complessità e sulle prestazioni.*

Iniziamo analizzando particolari implementazioni basate sull'impiego della trasformata discreta di Fourier (DFT) e che sono una estensione della modulazione multitono discreta (DMT) o di quella multitono filtrata (FMT) al contesto ad accesso multiplo.

Quindi studiamo il problema di definire il demodulatore multiportante multiutente ottimo. Il ricevitore risultante comprende una struttura front-end seguita da un processore maximum a posteriori. Il demodulatore è ottimo nel senso probabilistico ed è capace di fornire informazione soft ottima sui bit/simboli di tutti gli utenti. Analizziamo la struttura del front-end considerando sia canali selettivi in frequenza quasi statici che tempo varianti, in presenza di asincronismo temporale e di portante. Implementazioni efficienti digitali sono possibili e basate su banchi di filtri digitali adattativi polifase.

Poiché la complessità del demodulatore ottimo cresce esponenzialmente con il numero degli utenti, il numero di sottocanali, e la memoria del canale, proponiamo schemi semplificati di demodulazione. Questi sono basati su tecniche iterative dove informazione soft/hard viene scambiata tra sottotralicci ottenuti partizionando l'iper-treliccio che descrive il sottostante modello multi-ingresso multi-uscita di Markov. Per esempio, la demodulazione iterativa per-simbolo è uno schema semplice basato sullo scambio iterativo di inforamziuone hard/soft tra i "simbol detectors" all'uscita del banco di filtri adattati.

Consideriamo anche la codifica di canale e proponiamo l'utilizzo di codici con interleavers e decodifica semplificata ottenuta concatenando iterativamente la demodulazione multiutente-portante con la decodifica (turbo decodifica).

Sottolineiamo che una qualche analogia esiste con i sistemi multiantenna con codifica spazio temporale. L'approccio seguito per il trattamento del problema della codifica di canale e la decodifica multiportante-utente iterativa trova ispirazione nell'estensivo lavoro che abbiamo svolto sul progetto e decodifica di sistemi spazio temporali con codici con bit interlevears. La demodulazione singola-portante è un approccio

semplificato ove la demodulazione è effettuata elaborando indipendentemente ciascuna delle uscite al front-end. Per esempio questa è la tecnica convenzionale utilizzata nel sistema DMT dove il ricevitore consiste di un modulo DFT seguito da equalizzazione di sottocanale ad un tappo. È un approccio semplice che dà buone prestazioni nel sistema DMT-MA ove si scelgano opportunamente l'allocazione dei toni tra gli utenti, la distribuzione della potenza, e si utilizzino intervalli di guardia nel tempo ed in frequenza. Per questa ragione approfondiamo lo studio del sistema DMT-MA in termini di prestazioni e limiti di capacità.

Con riferimento al canale DMT-MA Gaussiano asincrono, affrontiamo il non semplice problema di determinare un "inner bound" alla capacità del canale di un dato utente e alla regione delle velocità di trasmissione per comunicazioni congiuntamente affidabili, cioè regione di capacità. Tali limiti di capacità sono trattati come variabili aleatorie poiché dipendono dagli offset di tempo e frequenza così come da parametri di sistema. Valutiamo le corrispondenti distribuzioni di probabilità complementari per vari sistemi caratterizzati da diversi schemi di assegnazione delle sottoportanti e strategie di distribuzione della potenza sulle sottoportanti.

I risultati analitici e quelli numerici suggeriscono di impiegare nei sistemi multiportante multiutente la demodulazione ottima multiportante. L'implementazione pratica basata su schemi semplificati dà buone prestazioni. La valenza degli schemi semplificati può essere incrementata con il controllo delle componenti interferenziali attraverso il progetto dei filtri di trasmissione, della spaziatura delle sottoportanti e della multiplazione delle stesse. Ulteriori miglioramenti possono essere ottenuti con allocazioni dinamiche dei toni e del profilo di potenza associato. Ne consegue che le prestazioni del sistema vengono massimizzate attraverso il progetto accurato con un compromesso tra complessità di demodulazione ed efficienza spettrale.

1 INTRODUCTION

In this thesis we assess the analysis of multiuser communication systems that are based on multicarrier modulation techniques. Communications are through an asynchronous multiple access channel. That is, multiple users wish to transmit their information signals to a receiver by sharing a common communication channel. Users are asynchronous meaning that they have a certain amount of temporal and carrier frequency misalignment with respect to a reference point at the receiver. This model is appropriate to describe both the uplink of a satellite system and the uplink of a mobile wireless communication system such as a wireless LAN or a macro cellular system.

In general, several different ways are possible to access the common channel. We propose a simple method, referred to as multicarrier multiple access, that is obtained by combining multicarrier modulation with frequency division multiplexing. First, a number of sub-carriers are allocated inside the available spectrum. Then, subsets of carriers are assigned to distinct users and are used for multicarrier modulation.

The objective of this thesis is to build a formal and unified study of the key characteristics of an asynchronous multicarrier multiple access system. We focus on the design of efficient digital implementations, on the derivation of optimal and sub-optimal receivers, on the impact on performance of the system design parameters and channel characteristics.

1.1 Background and Problem Statement

Multicarrier modulation has been widely investigated for application to communication systems with high data rate requirements. Chang originally derived the conditions for the transmission of orthogonal band-limited signals [17]. Weinstein and Ebert proposed the practical implementation through the use of the discrete Fourier transform (DFT) [85]. Hirosaki studied the deployment of filtered multicarrier modulation and its efficient implementation via DFT [33]-[34]. Cimini investigated the deployment of orthogonal frequency division multiplexing (OFDM) over a wireless channel [22]. In the context of wireline applications it has been standardized for the high data rate transmission over the copper pair in the advanced digital subscriber line system (ADSL) [3]. In the context of broadcast wireless applications it as been standardized in the digital audio broadcast

system (DAB) [39] and in the digital video broadcast system (DVB) [26]. It has also been standardized for application to wireless LAN, e.g., IEEE 802.11a [35] and HIPERLAN2 [27].

The main advantage of multicarrier modulation is its high spectral efficiency and its proven robustness to frequency selective channels that simplifies the equalization task in highly time dispersive channels. However, the above proposals are limited to consider respectively the single user link, the broadcast link, and the multiple access link where the common media is accessed with a time division protocol. More recently, several proposals have considered the combination of multicarrier modulation with code division multiple access (CDMA) for application to cellular mobile communications [18], [19], [30], [38], [79]. An overview can be found in [57].

This thesis is motivated by the interest on investigating in a comprehensive fashion the impact of deploying multicarrier modulation in asynchronous multiple access channels. That is, multiple users wish to transmit their information to a receiver by sharing a common communication channel. Users are asynchronous meaning that they have a certain amount of temporal and carrier frequency misalignment with respect to a reference point at the receiver. This model is appropriate to describe the uplink of a mobile wireless communication system such as the uplink of a satellite system, of a wireless local are network (WLAN) or of a mobile cellular system. We assume, in general, propagation through frequency selective time-variant fading channels. With the appropriate variations the model may be used also to describe a wireline system where a set of terminals communicates with a central receiver, e.g., a computer.

The common channel can be shared among users in a time division, a frequency division, or a code division mode. We investigate a simple method that is obtained by combining multicarrier modulation with frequency division multiplexing. First, a number of carriers are allocated inside the available spectrum. Then, subsets of carriers are assigned to distinct users and are used for multicarrier modulation. We refer to the resulting system as multicarrier multiple access (MC-MA). Various methods of multiplexing the sub-carriers across users can be deployed, e.g., orthogonal or non-orthogonal schemes, static or dynamic allocations.

We consider special forms of multicarrier multiple access where M parallel information streams (with data rate $1/T_0$ each) are transmitted over sub-carriers uniformly spaced by $1/T_1$, with $T_1/T_0 = M/N \leq 1$. Each user is assigned a subset of sub-carriers, which corresponds to setting to zero some of the M data streams. Each data stream is filtered, and then it is carrier modulated. When the transmit filters are identical, an efficient implementation of the transmitter comprises a carrier mapping device, an M-point inverse Fast Fourier Transform (IFFT), followed by a bank of low rate filters and a serial to parallel conversion. When the transmit filters are rectangular

windows, strictly time limited, the discrete-time system implementation is referred to as discrete multitone multiple access (DMT-MA)[2]. More in general the users transmit their information through filtered/shaped sub-channels that may overlap in time and frequency. The corresponding discrete-time implementation is referred to as filtered multitone multiple access (FMT-MA) since it can be viewed as an extension of the FMT modulation concept [7], [9], [15], [20], [21].

In an asynchronous MC-MA wireless system, the receiver sees a multitude of signals that, in general, have propagated through independent frequency selective fading channels, and have relative time offsets, and carrier frequency offsets that differ from zero. The key objectives of this work are outlined below.

A. Describe multicarrier multiuser architectures and in particular multiuser DMT and FMT digital implementations.

B. Consider an asynchronous scenario where users transmit their signals through a time-variant frequency selective channel and are received with distinct time offsets, and frequency offsets.

C. Devise the optimal multicarrier multiuser demodulator.

D. Consider the channel coding problem and investigate decoding algorithms based on turbo (iterative) demodulation and decoding.

E. Derive simplified demodulation/decoding strategies.

F. Derive efficient digital implementations of both the MC-MA transmitter and receiver.

G. Study how the design of the transmit filters and the tone allocation strategy affects the demodulation/decoding complexity and the system performance.

The literature lacks a general analysis of such a scenario. Some investigation on the timing and carrier frequency synchronization requirements in multiuser pulse-shaped OFDM is presented in [84]. The effect of the time offsets in a DMT-MA system with sub-optimal single user detection can be found in [36]. A technique for compensating time and frequency misalignments based on feedback control in a DMT-MA system is presented in [77]. On the other hand a rich literature can be found on the study of receivers for DMT modulation in single user applications in the presence of timing errors, frequency offsets, and multipath fading, e.g., [52]-[53] and associated references. An overview of equalization methods for DMT transceivers is presented in [47]. An overview of FMT architectures for broadband digital subscriber lines is given in [21]. A comparison of DMT and FMT with Gaussian pulses in a radio channel can be found in [37]. Decision feedback equalizer structures for FMT systems in a single link wireless scenario are described in [8].

[2] Often discrete multitone modulation (DMT) is referred to as orthogonal frequency division multiplexing (OFDM). We prefer to denote with OFDM a broader category of multicarrier modulation schemes that deploy DFT based methods.

With regard to Objective C we wish to formulate the optimal receiver for a multicarrier multiuser system. We pursue the concept of joint detection of signals transmitted over multiple-input multiple- output (MIMO) channels [78]. This approach has found application also in the context of optimal detection of asynchronous CDMA signals [82]. The resulting receiver structure comprises a front-end structure followed by a maximum a posteriori processor that runs the BCJR algorithm [5] with an appropriate metric. It has elements of novelty since it exploits the parallelism that characterizes a MC-MA system. In particular, efficient digital implementations of the FMT-MA front-end receiver are studied for both static and time-variant frequency selective channels.

The channel coding problem (Objective D) is basically a problem of coding for MIMO channels. We see a similarity to the space-time coding problem in multiple antennas systems [55], [61]-[66]. The main difference is that coding is done across frequencies instead of across antenna elements. In particular we propose the deployment of bit-interleaved codes and describe decoding based on the iterative (turbo) concatenation of the multicarrier-user detector and the channel decoders [44]. It should be noted that the proposed detector is an optimum soft-in soft-out module. That is, it provides the a posteriori probabilities of the data bits/symbols transmitted by all users and accepts the corresponding a priori probabilities.

The complexity of this optimal detector grows exponentially with the number of sub-carriers, users, and the channel time-frequency memory. In turn, the channel time-frequency memory is a function not only of the propagation media characteristics, and the amount of time-frequency offset that is experienced by the users, but it also depends on the shape of the transmit filters and the tone allocation strategy. We analytically study the effect of such design issues.

Further, we seek for complexity reduction approaches. The proposals are based on iterative detection schemes where soft/hard information is exchanged between sub-trellises that are obtained by partitioning the full hyper trellis that describes the hidden MIMO Markov model.

Single carrier detection turns out to be a sub-optimal approach where detection is made independently over each sub-channel front-end output. For instance this is the conventional technique used in a DMT system where the receiver consists of a DFT module followed by one-tap equalizer per channel. Single carrier detection is a simple approach that may yield good performance in DMT-MA systems when we carefully choose the sub-carrier allocation, the distribution of power, and we add time and frequency guards. For this reason we extensively study the DMT-MA system through the analysis of its performance and capacity limits.

With regard to an asynchronous DMT-MA Gaussian channel, we attack the non-trivial problem of determining an inner bound to both the capacity of a given user link and the region of achievable information rates for joint reliable communications, i.e., capacity region [23]. Such capacity inner

bounds are treated as random variables since they depend upon the time and frequency offsets as well as upon several system parameters. The associated complementary cumulative distribution functions are defined and are evaluated for several system scenarios characterized by different tone assignment schemes and strategies of power allotment to sub-carriers.

In the next section we overview the organization of this thesis.

1.2 Overview of the Thesis

Chapter 2 presents a brief review of multicarrier modulation in a single user link. The objective is to establish the relation between analog and digital implementations, and to clarify the terminology used in this work.

In Chapter 3 we consider a multiuser communication link. We describe multiple access methods that are based on combining multicarrier modulation with time division, frequency division, and code division multiple access. We focus on transmit architectures that combine multicarrier modulation with sub-carrier multiplexing (MC-MA).

In Chapter 4 we describe the asynchronous multiple access channel model that is used throughout this work. Since we mostly consider wireless applications, the propagation media is assumed to be characterized by frequency selective time-variant fading.

In Chapter 5 we first devise the optimal multicarrier multiuser demodulator. Then, we consider simplified sub-optimal demodulators.

In Chapter 6 the implementation of the front-end receiver that is deployed in a multiuser multicarrier demodulator is investigated in detail. Efficient digital implementations are derived.

Chapter 7 deals with simplified single carrier detection in multicarrier multiple access with rectangular transmit filters, as well as with the discrete-time counterpart, i.e., DMT-MA.

In Chapter 8 we assess the impact of the system design (in terms of transmit filter shape and tone multiplexing strategy) on the interference components that arise at the receiver front-end output in the presence of a frequency selective channel with time and frequency offsets. Further, we report simulation results to exemplify the performance of multicarrier-user detection and single carrier detection in an asynchronous multiuser scenario.

Chapter 9 considers the deployment of channel coding. In particular we consider bit-interleaved codes and propose practical decoding based on turbo multicarrier-user detection and decoding. More specific topics are considered in the last two chapters.

In Chapter 10 we assess the performance analysis of single user detection in discrete multitone multiple access. To simplify the understanding of the impact of many system parameters we first

consider performance in an AWGN asynchronous channel. Then, we consider the performance in a frequency selective fading channel. Finally, we address the impact of fast fading, i.e., of a channel that varies over the DMT block duration.

In Chapter 11 we attack the non-trivial problem of deriving the capacity region of a discrete multitone multiple access Gaussian channel.

Finally in Chapter 12 we draw the main conclusions.

1.3 Related Publications

Some contents and novel ideas of this thesis have been published in [68]-[73]. The interested reader is also referred to [58], [60], [50] where the turbo demodulation and decoding approach is applied to the context of coded M-DPSK signals, and to [61]-[66] where we deal with the design of space-time bit interleaved codes and iterative space-time demodulation-decoding. The problem of generating optimal soft statistics in demapping devices is addressed in [59]. The characterization and modeling of multiple-input multiple-output broadband wireless channels is considered in [13]. An overview of multicarrier modulation and code division multiple access is given in [57]. In [57] we have also investigated the DMT-MA synchronous system and in particular we have studied the capacity of it as a function of the tone multiplexing strategy.

2 FROM MULTICARRIER MODULATION TO MULTITONE MODULATION

The term multicarrier modulation comprises a broad variety of methods. The common concept is the transmission of the information through multiple narrow band pipes (sub-channels) obtained by partitioning the available spectrum. The sub-channels may overlap in time and/or in frequency. If certain conditions are fulfilled the sub-channels are orthogonal such that no intersymbol and intercarrier interference is introduced.

In this chapter we revise the multicarrier modulation concept starting from its analog implementation. We then consider a discrete-time implementation and we refer to is as multitone modulation. Filtered multitone modulation (FMT) is a special form of it that can be efficiently implemented with an inverse discrete Fourier transform followed by a polyphase filter bank. An FMT modulator simplifies to the popular discrete multitone (DMT) modulator when the filtering operation does not take place.

2.1 Multicarrier Modulation Concept and Notation

The main concept behind multicarrier modulation is the simultaneous transmission of parallel data streams through sub-channels that are obtained by partitioning the available spectrum. The data streams are shaped with sub-channel interpolation filters and modulate sub-carriers that are allocated in the spectrum. We start describing an analog implementation of the multicarrier modulator.

2.1.1 Analog Implementation

An analog implementation of a multicarrier transmitter is depicted in Fig. 2.1. The information bit stream to be transmitted is first mapped to a complex data stream whose symbols belong to a finite alphabet, for instance to the M-QAM signal set [48]. The data stream is serial to parallel (S/P) converted into M data streams $a^k(lT_0)$, $k = 0,..., M-1$, $l = -\infty,...,+\infty$, that are referred to as *sub-channel data streams*. The *sub-channel data rate* is $W_0 = 1/T_0$ with $T_0 = NT$. In general, we assume $N \geq M$.

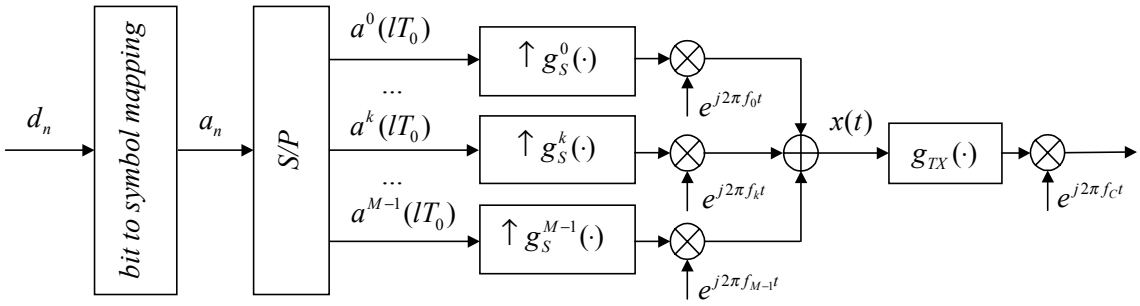

Fig. 2.1. Analog multicarrier modulator (complex representation).

Each sub-channel data stream is passed through an *interpolation filter* $g_S^k(t)$. The interpolation filter output modulates a sub-carrier f_k, yielding [3]

$$x^k(t) = \sum_{l=-\infty}^{\infty} a^k(lT_0) g_S^k(t - lT_0)\, e^{j2\pi f_k t}. \tag{2.1}$$

We assume the sub-carriers to belong to the frequency band $[0,\ W]$ with $W = 1/T$ *transmission rate*. Note that the interpolation filter shapes the sub-channel temporal and frequency response.

If we rewrite (2.1) as follows

$$\begin{aligned} x^k(t) &= \sum_{l=-\infty}^{\infty} \underbrace{a^k(lT_0) e^{j2\pi f_k lT_0}}_{\tilde{a}^k(lT_0)} \underbrace{g_S^k(t - lT_0) e^{j2\pi f_k (t - lT_0)}}_{g_T^k(t - lT_0)} \\ &= \sum_{l=-\infty}^{\infty} \tilde{a}^k(lT_0) g_T^k(t - lT_0) \end{aligned} \tag{2.2}$$

the output signal from the *k-th* sub-carrier modulator (oscillator) is the convolution of the rotated data sequence $\tilde{a}^k(lT_0) = a^k(lT_0) e^{j2\pi f_k lT_0}$ with the *sub-channel transmit filter* $g_T^k(t) = g_S^k(t) e^{j2\pi f_k t}$. The sub-channel transmit filter is obtained by a frequency shift of the interpolation filter.

The baseband *multicarrier signal* is obtained by summing up all sub-channel signals, i.e.,

$$x(t) = \sum_{k=0}^{M-1} x^k(t). \tag{2.3}$$

The multicarrier signal (2.3) may be further filtered with a broadband filter $g_{TX}(t)$, and bandpass modulated with carrier f_C, e.g., to radio frequency.

Assuming uniformly spaced sub-carriers, the *sub-channel transmission rate* (or *nominal sub-channel bandwidth*) is $W_1 = 1/T_1$ with $T_1 = MT$. In such a case the sub-carriers are defined as $f_k = k/T_1$. Further, if $N = M$ the sub-carriers are $f_k = k/T_0$, thus we can simply write

[3] For easy of notation we include the factor T_0 in the filter impulse response.

$$x^k(t) = \sum_{l=-\infty}^{\infty} a^k(lT_0) g_T^k(t - lT_0) \tag{2.4}$$

with $g_T^k(t) = g_S^k(t) e^{j\frac{2\pi}{N}kt}$. Therefore, the rotation of the data sequence does not take place. Note that the case $N = M$ corresponds to the *minimal sub-carrier spacing*.

When the sub-channel interpolation filter is identical for all sub-channels, i.e., $g_S^k(t) = g(t)$ for $k = 0,...,M-1$, we refer to it as *prototype filter*. The sub-channel transmit filters are then obtained by the frequency shift of the given prototype filter.

2.1.2 Sub-channel Filter Design

Let us assume transmission over an ideal channel and let us assume a receiver front-end structure that is matched to the bank of sub-channel transmit filters (see Chapters 5-8). Then, the receiver outputs may exhibit intersymbol interference (ISI) on each sub-channel and intercarrier interference (ICI) across sub-channels. The ISI and ICI terms depend upon the shape of the filters and the sub-carrier spacing. To avoid the presence of such interference components the system has to be designed in accordance to a generalized Nyquist criterion [7], [9], [15], [21]. Some natural choices for the sub-channel filters are reported below[4].

1. Time limited rectangular filters [5] (Fig. 2.2),

$$g(t) = \frac{1}{\sqrt{T_0}} \text{rect}\left(\frac{t - T_0/2}{T_0}\right) \tag{2.5}$$

$$G(f) = \sqrt{T_0} e^{-j\pi T_0 f} \text{ sinc}\left(T_0 f\right). \tag{2.6}$$

2. Frequency limited rectangular filters [5] (Fig. 2.3),

$$g(t) = \frac{1}{\sqrt{T_0}} \text{sinc}\left(\frac{t}{T_0}\right) \tag{2.7}$$

$$G(f) = \sqrt{T_0}\, \text{rect}\left(T_0 f\right). \tag{2.8}$$

3. Gaussian filters (Fig. 2.4),

$$g(t) = \sqrt{\frac{\alpha}{\sqrt{\pi/2}T_0}}\, e^{-(\frac{\alpha}{T_0}t)^2} \tag{2.9}$$

$$G(f) = \sqrt{\frac{T_0\sqrt{2\pi}}{\alpha}}\, e^{-(\frac{\pi T_0}{\alpha}f)^2}. \tag{2.10}$$

with $\alpha = \pi f_{3dB} T_0 \sqrt{2/\ln 2}$, and f_{3dB} cut-off frequency.

---

[4] The definitions correspond to filters with energy one. In the figures we normalize both the impulse and the frequency response such that they have the peak equal to one. The sub-carriers are assumed uniformly spaced with minimal spacing, i.e., N=M.

[5] $\text{rect}(t) = \{1 \text{ if } t \in [-0.5,\ 0.5];\ \ 0 \text{ if } t \notin [-0.5,\ 0.5]\}$; $\text{sinc}(t) = \sin(\pi t)/(\pi t)$.

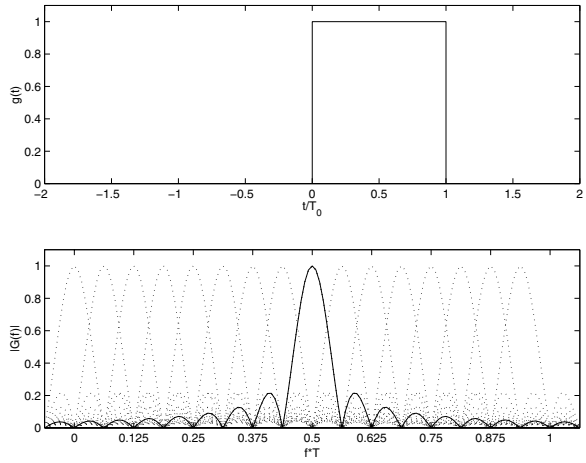

Fig. 2.2. Time limited prototype filter. *M=N=16*.

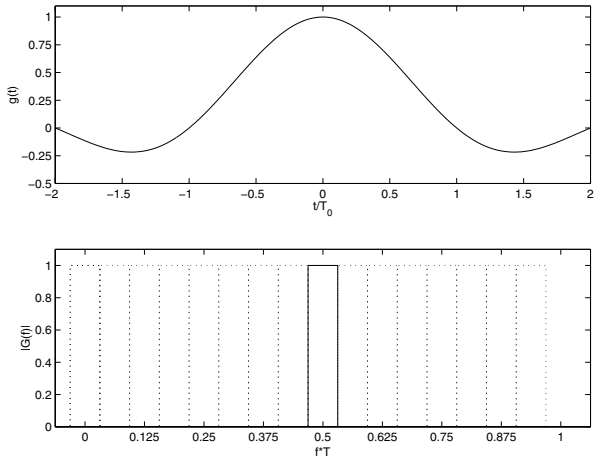

Fig. 2.3. Frequency limited prototype filter. *M=N*=16.

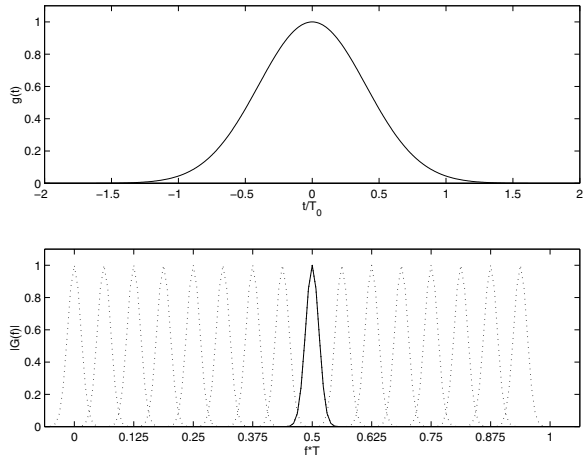

Fig. 2.4. Gaussian prototype filter. *M=N*=16, $f_{3dB}T_0$=0.33.

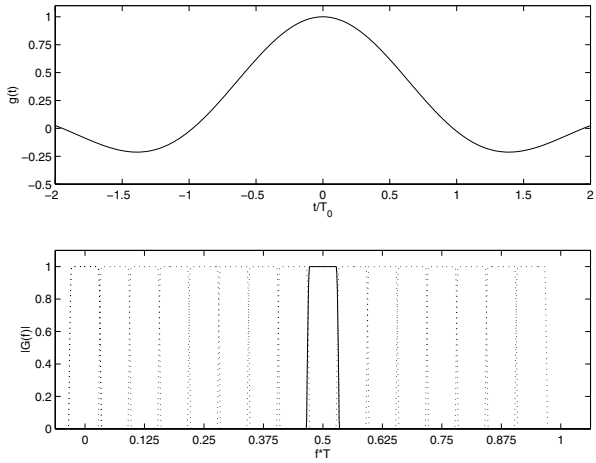

Fig. 2.5. Square-root-raised-cosine prototype filter. *M=N*=16, α=0.1.

4. Square-root raised cosine (sqrrc) filters (Fig. 2.5),

$$g(t)=\frac{1}{\sqrt{T_0}}\frac{\sin(\pi(1-\alpha)t/T_0)+4\alpha t/T_0\cos(\pi(1+\alpha)t/T_0)}{\pi t/T_0(1-(4\alpha t/T_0)^2} \tag{2.11}$$

$$G(f)=\begin{cases}\sqrt{T_0} & 0\le|f|\le f_1/T_0\\ \sqrt{T_0}\cos(\frac{\pi}{2}(\frac{T_0|f|-f_1}{\alpha})) & f_1/T_0<|f|\le f_2/T_0\\ 0 & |f|>f_2/T_0\end{cases} \tag{2.12}$$

with $0\le\alpha\le1$, $f_1=\frac{1}{2}(1-\alpha)$, $f_2=\frac{1}{2}(1+\alpha)$.

It should be noted that the time limited filters do not overlap in time, while the band limited filters

do not overlap in frequency even if we choose the minimal sub-carrier spacing that is equal to $1/T_0$. In an ideal channel they meet the generalized Nyquist criterion and introduce no ISI and no ICI.

Nyquist filters, and in particular sqrrc filters, do not introduce any ISI, however the condition of zero ICI is fulfilled only if the sub-carrier spacing is larger than $1/T_0$. In [34] it is shown that it is still possible to null the ISI and ICI components even with Nyquist filters and minimal sub-carrier spacing if an offset-QAM (OQAM) modulation technique is deployed.

The Gaussian shaped filters are not Nyquist. However, they have the interesting property of being practically limited in time and in frequency. Real asynchronous channels introduce a certain amount of time dispersion, of time misalignment, and of frequency misalignment, which translates into a loss of system orthogonality. That is, some degree of ISI and ICI is always present. To this respect Gaussian filters turn out to be an interesting choice that allows controlling the interference components [37]. The analytical evaluation of the interference components in such an environment is investigated in Chapter 8.

Other choices for the sub-channel filters are described in [20], [76], [80].

2.1.3 Notation

Herein, we summarize some useful notation that we will use throughout this work.

- M: Number of sub-channels.
- T: Transmission period.
- $W = 1/T$: Transmission rate.
- $T_0 = NT$: Sub-channel data period.
- $W_0 = 1/T_0$: Sub-channel data rate.
- $T_1 = MT$: Sub-channel transmission period with $M \le N$.
- $W_1 = 1/T_1$: Sub-channel transmission rate (nominal sub-channel bandwidth).
- $R = M/T_0$: Transmission data rate.
- f_k: Sub-carrier *k*.
- f_C: Carrier of bandpass modulator.
- $a^k(lT_0)$: Complex data symbol transmitted on sub-carrier *k* at time instant lT_0.
- $g_S^k(t)$: Interpolation filter of sub-channel *k*. Prototype filter when identical for all *k*.
- $g_T^k(t) = g_S^k(t)e^{j2\pi f_k t}$: Transmit filter of sub-channel *k*.
- $g_{TX}(t)$: Broadband transmit filter.

Since in the next chapters we deal with signals and quantities belonging to multiple users, we add a superscript (or subscript) to denote signals and quantities belonging to a given user *u*. For instance,

- $a^{u,k}(lT_0)$: Complex data symbol transmitted on sub-carrier *k* at time lT_0 by user *u*.
- $g_S^{u,k}(t)$: Interpolation filter of sub-channel *k* and user *u*.
- $g_T^{u,k}(t)$: Transmit filter of sub-channel *k* and user *u*.
- $f_{C,u}$: Carrier of bandpass modulator of user *u*.

2.2 Multitone Modulation

We are here interested on describing discrete-time implementations of a multicarrier modulator. These implementations are obtained under the assumption of having uniformly spaced carriers (*tones*) :

$$f_k = \frac{k}{T_1} \qquad k = 0,...,M-1 . \tag{2.13}$$

In principle, a discrete-time implementation of the multicarrier modulator is obtained by sampling (2.3) at rate $1/T$,

$$x(iT) = \sum_{l=-\infty}^{\infty} \sum_{k=0}^{M-1} a^k(lT_0) g_S^k(iT - lT_0)\, e^{j\frac{2\pi}{M}ik} . \tag{2.14}$$

To proceed we assume the interpolation filters to be identical, i.e., $g_S^k(t) = g(t)$. Then,

$$x(iT) = \sum_{l=-\infty}^{\infty} \sum_{k=0}^{M-1} \tilde{a}^k(lT_0) g_T^k(iT - lT_0) \tag{2.15}$$

with

$$\tilde{a}^k(lT_0) = a^k(lT_0) e^{j2\pi\frac{N}{M}lk} \tag{2.16}$$

$$g_T^k(nT) = g(nT) e^{j\frac{2\pi}{M}nk} . \tag{2.17}$$

In the next sections we show that efficient FFT based implementations are possible. In particular, when $N > M$ or $N = M$ the resulting schemes are respectively referred to as *non-critically sampled filtered multitone modulation*, and *critically sampled filtered multitone modulation* [21]. In the latter case the sub-carrier spacing is minimal.

2.2.1 Non-critically Sampled Filtered Multitone Modulation

A non-critically sampled filtered multitone modulation scheme (NCS-FMT) is obtained under the following assumptions:

1. $N > M$;
2. Tones spaced by $1/T_1$ (non minimal sub-carrier spacing);
3. Identical interpolation filters.

Let us define

$$i = mM + n \qquad m = -\infty,...,+\infty \qquad n = 0,...,M-1. \tag{2.18}$$

Then,

$$x(iT) = x(mT_1 + nT) = \sum_{l=-\infty}^{\infty} \sum_{k=0}^{M-1} a^k(lT_0) g(mT_1 + nT - lT_0)\, e^{j\frac{2\pi}{M}nk} . \tag{2.19}$$

Let $x^n(mT_1) = x(mT_1 + nT)$ and $g^n(mT_1 - lT_0) = g(mT_1 + nT - lT_0)$ be the polyphase decomposition[6] of $x(iT)$, and $g(iT - lT_0)$ respectively. Then, the *n-th* polyphase component of $x(iT)$ at time mT_1 is

$$x^n(mT_1) = \sum_{l=-\infty}^{\infty} \underbrace{\sum_{k=0}^{M-1} a^k(lT_0) e^{j\frac{2\pi}{M}nk}}_{A^n(lT_0)} g^n(mT_1 - lT_0) \ . \tag{2.20}$$

Note that (2.20) corresponds to an interpolation of the sequence $A^n(lT_0)$ by a factor of N followed by a decimation of a factor of M . $A^n(lT_0)$ is the IDFT of the data block $\{a^k(lT_0)\}$.

We can proceed following [9], [21] by defining the following index relations[7] (function of m).

$$p(m) = m \ \text{div} \ N \tag{2.21}$$

$$q(m) = m \ \text{mod} \ N \tag{2.22}$$

Then, $g^n\left(mT_1 - lT_0\right) = g^n\left(p(mM)T_0 - lT_0 + q(mM)T\right)$. With the change of variable $p - l \to l$ we get

$$x^n(mT_1) = \sum_{l=-\infty}^{\infty} A^n\left(p(mM)T_0 - lT_0\right) g^n\left(lT_0, mT_1\right) \tag{2.23}$$

where

---

[6] The polyphase decomposition is typically defined in the Z domain. Herein, is derived in the time domain as a serial to parallel conversion of a high rate signal $x(iT)$, $i = -\infty,...,+\infty$, into M low rate signals $x^n(mMT) = x(mMT + nT)$, $n = 0,...,M-1$, $m = -\infty,...,+\infty$. The M signals $x^n(mMT)$ are referred to as polyphase components of $x(iT)$.

[7] We denote with (a div b) and (a mod b) the integer division and the reminder of the integer division.

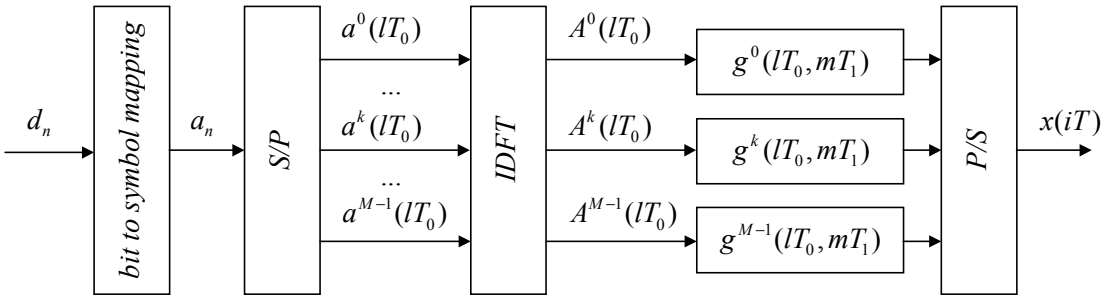

Fig. 2.6. Non-critically sampled FMT modulator.

$$g^n\left(lT_0, mT_1\right) = g^n\left(lT_0 + q(mM)T\right) \tag{2.24}$$

is a periodic time-variant filter. Therefore, the multitone signal is obtained as follows (Fig. 2.6).

1. Apply an M-point IDFT[8] on blocks of M data symbols $\{a^k(lT_0)\}$;
2. Filter the *n-th* IDFT output with the discrete-time time-variant filter $g^n(lT_0, mT_1)$ according to (2.23) and (2.24).
3. Parallel to serial convert the M output signals.

2.2.2 Critically Sampled Filtered Multitone Modulation

A critically sampled filtered multitone modulation scheme (CS-FMT) is obtained under the following assumptions:

1. $N = M$;
2. Tones spaced by $1/T_0$ (minimal sub-carrier spacing);
3. Identical interpolation filters.

The *n-th* polyphase component of $x(iT)$ at time mT_0 is

$$x^n(mT_0) = \sum_{l=-\infty}^{\infty} \underbrace{\sum_{k=0}^{N-1} a^k(lT_0) e^{j\frac{2\pi}{N}nk}}_{A^n(lT_0)} g^n((m-l)T_0) \ . \tag{2.25}$$

Therefore, the multitone signal is obtained as follows (Fig. 2.7).

---

[8] Let $\underline{a} = [a^0, ..., a^{M-1}]$ and $\underline{A} = [A^0, ..., A^{M-1}]$, the IDFT of the sequence $\underline{a}$ and the DFT of $\underline{A}$ are respectively defined as $A^n = \sum_{k=0}^{M-1} a^k e^{j\frac{2\pi}{M}nk}$, and $a^k = \frac{1}{M}\sum_{n=0}^{M-1} A^n e^{-j\frac{2\pi}{M}nk}$.

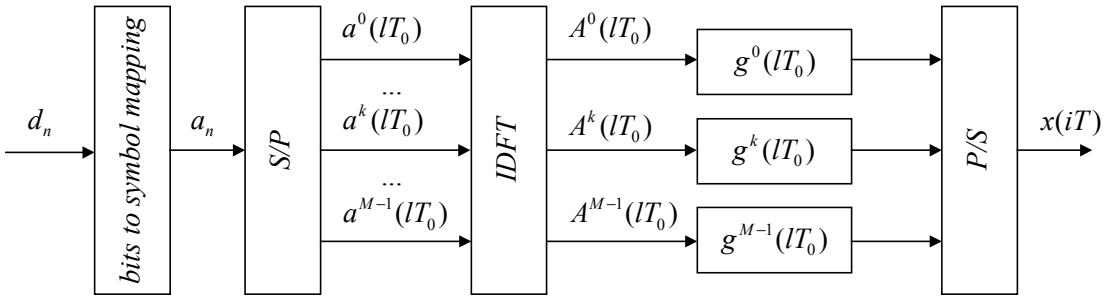

Fig. 2.7. Critically sampled FMT modulator.

1. Apply an N-point IDFT on blocks of N data symbols $\{a^k(lT_0)\}$;
2. Filter the *n-th* IDFT output with the discrete-time filter $g^n(lT_0)$;
3. Parallel to serial convert the N output signals.

Note that the *n-th* polyphase component of the multitone signal is obtained by filtering at low rate the IDFT outputs with $g^n(lT_0)$. Therefore, the system implementation is particularly efficient.

2.2.3 Discrete Multitone Modulation

The modulation scheme is referred to as discrete multitone modulation under the following assumptions.

1. $N = M$;
2. Tones spaced by $1/T_0$.
3. Prototype filters strictly time limited and defined as in (2.5).

It follows that the polyphase components of the multitone signal are

$$x^n(mT_0) = \frac{1}{\sqrt{T_0}} \sum_{k=0}^{N-1} a^k(mT_0) e^{j\frac{2\pi}{N}nk}. \tag{2.26}$$

Therefore no sub-channel filtering is required.

Note that some literature refers to this modulation scheme as OFDM, *orthogonal frequency division multiplexing*. We prefer to denote with OFDM a broader category of multitone modulation schemes that are based on the use of the DFT.

2.2.4 Discrete Multitone Modulation with Cyclic Prefix

Discrete multitone modulation is often deployed with the insertion of a cyclic prefix, which allows for simplified equalization in inter-symbol interference channels. It is interesting to note that similar, although not identical, discrete-time implementations are obtained by sampling of (2.3), or by defining it directly in the digital domain[9]. Let us start by deriving it from sampling of (2.3) under the following assumptions:

1. $N = M + \mu$;
2. Tones spaced by $1/T_1$;
3. Prototype filters strictly time limited and defined as (Fig. 2.8):

$$g(t) = \frac{1}{\sqrt{T_0}} e^{-j\frac{2\pi}{M}k\mu} \text{rect}(\frac{t - T_0/2}{T_0}). \tag{2.27}$$

Let us sample (2.3) at time iT. If we define

$$i = mN + n \qquad m = -\infty, ..., +\infty \qquad n = 0, ..., N-1, \tag{2.28}$$

the *n-th* polyphase component of $x(iT)$ at time mT_0 is

$$\begin{aligned} x^n(mT_0) &= \sum_{l=-\infty}^{\infty} \sum_{k=0}^{M-1} a^k(lT_0) e^{-j\frac{2\pi}{M}k\mu} e^{j\frac{2\pi}{M}k(mN+n)} g(nT + mT_0 - lT_0) \\ &= \frac{1}{\sqrt{T_0}} \sum_{k=0}^{M-1} \underbrace{a^k(mT_0) e^{j\frac{2\pi}{M}km\mu}}_{\tilde{a}^k(mT_0)} e^{j\frac{2\pi}{M}k(n+M-\mu)} \end{aligned}. \tag{2.29}$$

Therefore, the N polyphase components are obtained by applying an M-point IDFT to the rotated data block $\tilde{a}^k(mT_0) = a^k(mT_0) e^{j\frac{2\pi}{M}km\mu}$, $k = 0, ..., M-1$, and adding a prefix that equals the last μ IDFT outputs.

Typically [15], DMT with cyclic prefix is implemented by directly applying the IDFT on $a^k(mT_0)$, which corresponds to use sub-channel transmit filters

$$g_T^k(t) = \frac{1}{\sqrt{T_0}} e^{j\frac{2\pi}{T_1}k(t-\mu T)} \text{rect}(\frac{t - T_0/2}{T_0}) \tag{2.30}$$

in an architecture without oscillators.

---

[9] This is often called in literature OFDM with cyclic prefix.

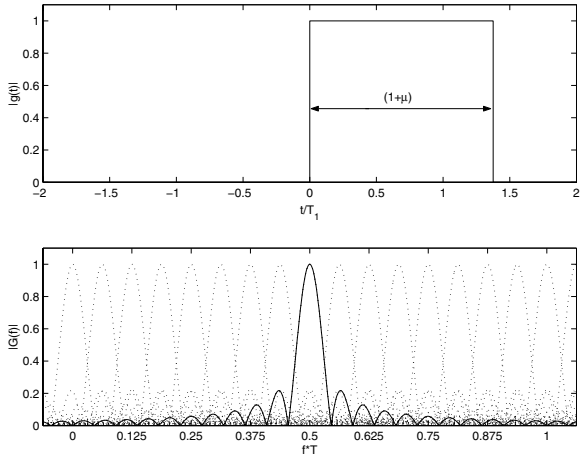

Fig. 2.8. Time limited prototype filter with guard time. M=16, μ=6.

In fact, the *n-th* polyphase component ($n = 0,..., N-1$) at time mT_0 can now be written as

$$\begin{aligned} x^n(mT_0) &= \sum_{l=-\infty}^{\infty} \sum_{k=0}^{M-1} a^k(lT_0) g_T^k(t - lT_0) \\ &= \sum_{l=-\infty}^{\infty} \sum_{k=0}^{M-1} a^k(lT_0) e^{j\frac{2\pi}{M}k(n+mN-\mu-lN)} \operatorname{rect}\left(\frac{nT + mT_0 - lT_0 - T_0/2}{T_0}\right). \\ &= \frac{1}{\sqrt{T_0}} \sum_{k=0}^{M-1} a^k(mT_0) e^{j\frac{2\pi}{M}k(n+M-\mu)} \end{aligned} \tag{2.31}$$

2.3 Remarks on the Digital Implementation

In the previous section the multitone modulator has been derived from the multicarrier modulator. It has been described as a discrete-time version of the latter. It should be noted that the two schemes are equivalent only in principle. In fact we have used a sampling rate equal to $1/T$ although the bandwidth of the multicarrier signal may be larger. In practice, the multicarrier transmitter is implemented by passing the sequence of multitone symbols through a digital-to-analog converter (DAC) and an analog transmit filter $g_{TX}(t)$ whose objective is to reduce the spectral components at the output of the bandwidth $1/T$. To simplify the design of the analog filters, and in particular of the receiver anti-aliasing filter, typically virtual carriers are added at the spectrum edges, i.e., we avoid transmission on a small percentage of the outermost carriers.

Multitone modulation can also be interpreted as a discrete-time multiple-input multiple-output (MIMO) transform. Let $\underline{a}(lT_0) = [a^0(lT_0),..., a^{M-1}(lT_0)]$ be the vector of data inputs at time lT_0. Then the vector of modulated symbols $\underline{x}(mT_1) = [x^0(mT_1),..., x^{M-1}(mT_1)]$ at time mT_1 is obtained by first

applying an M-point IDFT to the sequence of data vectors followed by MIMO filtering.

It is interesting to note that assuming an ideal channel the concatenation of the P/S converter and the S/P converter is irrelevant. The MIMO transform $\underline{a}(lT_0) \rightarrow \underline{x}(mT_1)$ may exhibit ISI and cross talks (ICI). Since the IDFT is invertible the reversibility of the overall transform requires the MIMO polyphase filter bank to be invertible.

Finally, we emphasize that the design of the sub-channel filters in FMT systems aims at avoiding spectral overlapping across adjacent sub-channels. This allows nulling out the ICI at the expense of an increase of ISI over each sub-channel (see Chapter 8). The design is simplified in non-critically sampled FMT systems since they deploy larger sub-carrier spacing. For instance we may choose to deploy sqrrc filters with appropriate (larger than $1/T_0$) sub-carrier spacing. Other filter options to be deployed in FMT architectures are reported in [20], while filters for OFDM-OQAM schemes are studied in [76], [80]. We point out that with time/frequency overlapping filters, e.g., Gaussian pulses, the system can be viewed as a sort of multichannel partial response transmission system. Partial response signaling [48] has found application in the GSM and EDGE (enhanced data rate for GSM evolution) systems [28]. The former deploys single carrier Gaussian minimum shift keying modulation (GMSK). The latter deploys also single carrier 8-PSK with Gaussian pulse shaping.

3 MULTICARRIER MULTIUSER SYSTEMS

In the previous chapter we have revised the multicarrier modulation concept and its digital implementation. We now consider the problem of sharing a common communication channel among multiple users that deploy some form of multicarrier modulation. In general several different ways are possible to access the common channel, such as a combination of TDMA, FDMA, CDMA with multicarrier modulation. A simple method referred to as multicarrier multiple access (MC-MA), is obtained by combining multicarrier modulation with frequency division multiplexing. First, a number of carriers are allocated inside the available spectrum. Then, subsets of carriers are assigned to distinct users and are used for multicarrier modulation. The transmitters can be efficiently implemented by digital architectures that are similar to the ones we described in Chapter 2. The system is then referred to as multitone multiple access (MT-MA). The key design issues are the choice of the transmit filters, the sub-carrier spacing, and the tone multiplexing algorithm across users.

3.1 Asynchronous Multicarrier Multiuser Communications

Let us consider a multiuser communication system where N_U users wish to communicate with a receive station, Fig. 3.1.

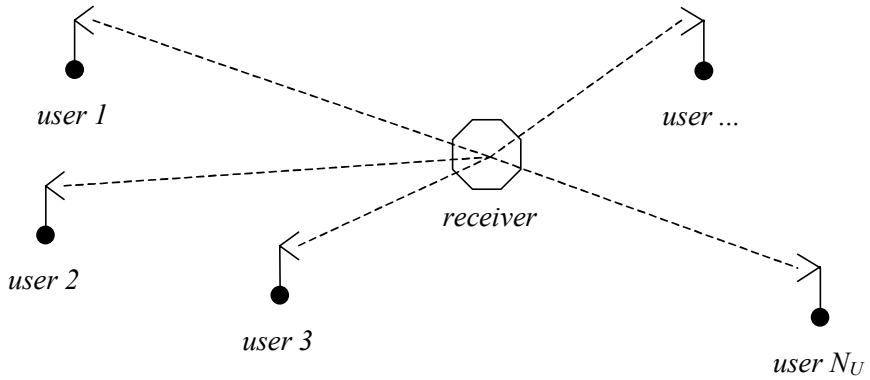

Fig. 3.1. Multiple access channel.

The common channel can be shared among the users in several ways. In this chapter we briefly

describe multiple access schemes that are based on combining multicarrier modulation with time division (TDMA), frequency division (FDMA), and code division (CDMA) multiple access. Then, we devise a method based on combining multicarrier modulation with sub-carrier multiplexing.

In general the received signals are asynchronous, meaning that they have a certain degree of time and carrier frequency misalignment with respect to the receiver temporal and carrier frequency reference. The description of the asynchronous multiple access channel model is reported in Chapter 4. We mostly focus on wireless mobile applications.

3.1.1 Multicarrier TDMA

In multicarrier TDMA a frame of duration T_F is subdivided into N_U time slots of duration $T_S = T_F / N_U$. Each user is assigned a given time slot for the duration of which it transmits its multicarrier signal. Therefore, the users share the same spectrum but access it at different time instants. The multicarrier signal of a given user can be obtained from a digital efficient implementation.

In such a system, demodulation is single user based. It requires slot, symbol, and carrier synchronization for just one user at the time. The only source of interference among signals of distinct users is due to the slot misalignments. Therefore, a guard time between slots is required to avoid overlapping of adjacent slots.

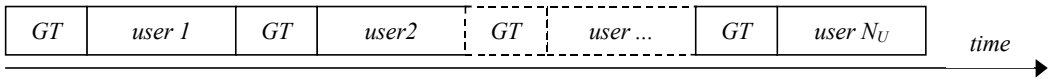

Fig. 3.2. Time division multiplexing of N_U multicarrier signals (users). *GT*: guard time.

3.1.2 Multicarrier FDMA

In multicarrier FDMA the overall spectrum W is subdivided into N_U frequency bands of width $W_B = W / N_U$. Each user is assigned a given frequency band inside which it transmits its multicarrier modulated signal. It follows that the users transmit their multicarrier signals at the same time but occupy distinct frequency bands.

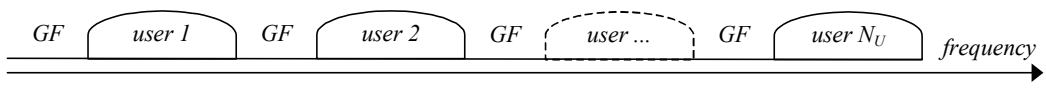

Fig. 3.3. Frequency division multiplexing of N_U multicarrier signals (users). *GF*: guard frequency.

Demodulation is single user based. It requires carrier and symbol synchronization for a given user at the time. No interference components arise from time misalignments, as well as from carrier frequency offsets among users provided that the adjacent bands do not overlap. For this purpose frequency guards may be deployed.

3.1.3 Multicarrier CDMA

The combination of multicarrier modulation and CDMA can be done in various forms. A fairly broad literature deals with it. Essentially, three approaches have been proposed. A first method, referred to as MC-CDMA [30], [31], consists of a concatenation of direct sequence spreading and multicarrier modulation. Distinct spreading codes are assigned to distinct users. In a second method, referred to as MC-DS-CDMA [18], [19], [51], [38], spreading is applied over each low rate sub-channel before sub-carrier modulation. In a third method, referred to as MT-CDMA [79], spreading takes place at the output of the multitone modulator. An overview of the various forms of multicarrier CDMA has been done in [57].

3.2 Multicarrier Multiple Access (MC-MA)

Another possible media access scheme can be derived generalizing the MC-FDMA idea. Let us assume that the users share the same spectrum with bandwidth W. A number of sub-carriers, say M, are distributed inside the spectrum. We assign a subset of the available sub-carriers to each user. Therefore, the available sub-channels are multiplexed across users (Fig. 3.4). The sub-carriers may be uniformly or non-uniformly spaced, and are assigned to users not necessarily in blocks.

This scheme is a generalization of frequency division multiplexing. We refer to it as *multicarrier multiple access*, MC-MA. Note that the sub-channels may overlap as a function of the sub-carrier spacing and the sub-band filter shape.

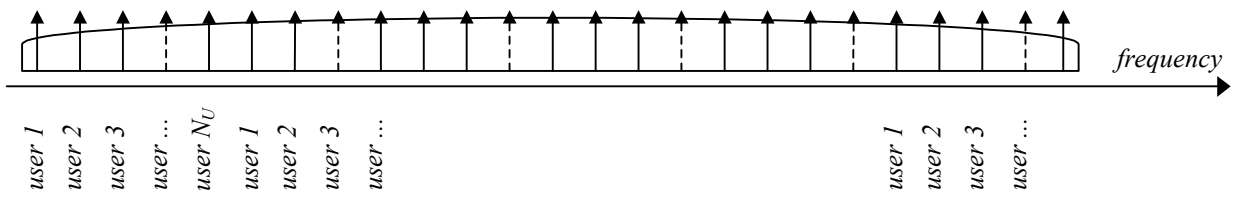

Fig. 3.4. Multicarrier multiplexing of N_U users.

An analog implementation of the *u-th* user transmitter is a straightforward extension of the multicarrier modulation scheme illustrated in Chapter 2. For clarity we depict a block diagram

scheme in Fig. 3.5. The transmitted multicarrier signal of user u, before broadband filtering and bandpass modulation, is

$$x^u(t) = \sum_{k=0}^{M-1} \sum_{l=-\infty}^{\infty} a^{u,k}(lT_0) g_S^{u,k}(t - lT_0) e^{j2\pi f_k t} \tag{3.1}$$

where $a^{u,k}(lT_0)$ is the sequence of data symbols belonging to user u and sub-channel k. Assuming that K_u sub-carriers are assigned to user u, only K_u sub-channel data streams differ from zero. That is, sub-carrier multiplexing is implemented by setting to zero $M - K_u$ sub-channels out of M total ones.

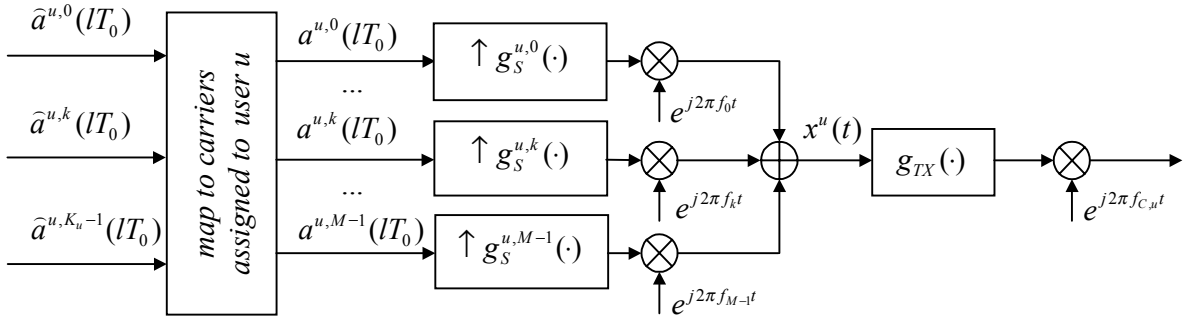

Fig. 3.5. Analog implementation of the MC-MA transmitter of user *u*.

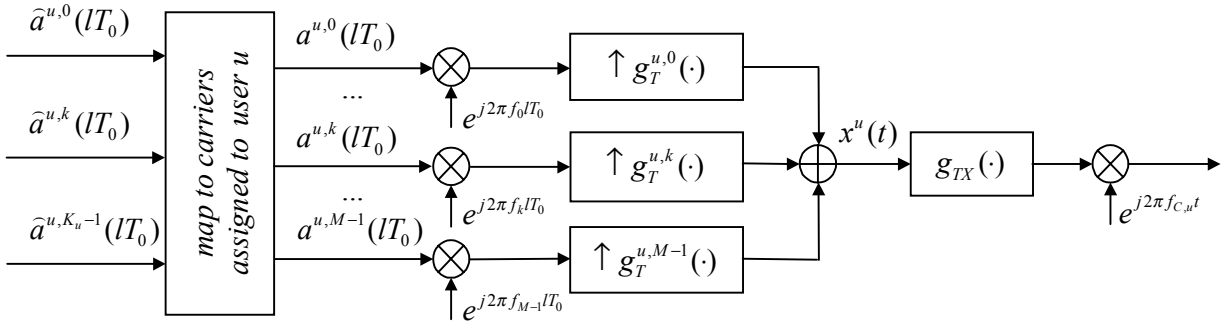

Fig. 3.6. MC-MA transmitter architecture without oscillators for user *u*.

An architecture without oscillators (Fig. 3.6) can be easily derived by defining

$$\tilde{a}^{u,k}(lT_0) = a^{u,k}(lT_0) e^{j2\pi f_k lT_0} \tag{3.2}$$

$$g_T^{u,k}(t) = g_S^{u,k}(t) e^{j2\pi f_k t} \tag{3.3}$$

such that

$$x^u(t) = \sum_{k=0}^{M-1} \sum_{l=-\infty}^{\infty} \tilde{a}^{u,k}(lT_0) g_T^{u,k}(t - lT_0)\,. \tag{3.4}$$

It should be noted that we assume that the carrier $f_{C,u}$ of the bandpass modulator may differ across the users. This is to take into account the effect of the precision and the instability of the oscillators, as well as the effect of Doppler shifts from the movement of the transmitters (see Chapter 4).

By extending the results of Chapter 2, a MC-MA transmitter can be efficiently implemented in the digital domain. This is illustrated in the next section.

3.3 Multitone Multiple Access (MT-MA)

A discrete-time implementation of the transmitter of user *u* in a MC-MA system can be obtained following the derivation in Chapter 2.

Efficient digital implementations are possible under the assumption of identical interpolation filters and uniform sub-carrier spacing. In such a case, if $N > M$ the system is referred to *as non-critically sampled filtered multitone multiple access* (NCS-FMT-MA) (Fig. 3.7). Otherwise, if $N = M$ the system is referred to as *critically sampled filtered multitone multiple access* (CS-FMT-MA). The *M* polyphase components of the multitone signal of user *u* are

$$x^{u,n}(mT_1) = \sum_{l=-\infty}^{\infty} \sum_{k=0}^{M-1} a^{u,k}(lT_0) e^{j\frac{2\pi}{M}nk} g^n(mT_1 - lT_0) \tag{3.5}$$

where the *n-th* sub-channel filter is $g^n(mT_1 - lT_0) = g(mT_1 - lT_0 + nT)$. If $N > M$ the filtering operation can be efficiently implemented by defining a periodically time-variant filter $g^n(lT_0, mT_1)$ as shown in Section 2.2.1. If $N = M$ filtering takes place at rate T_0, i.e., the filter is static.

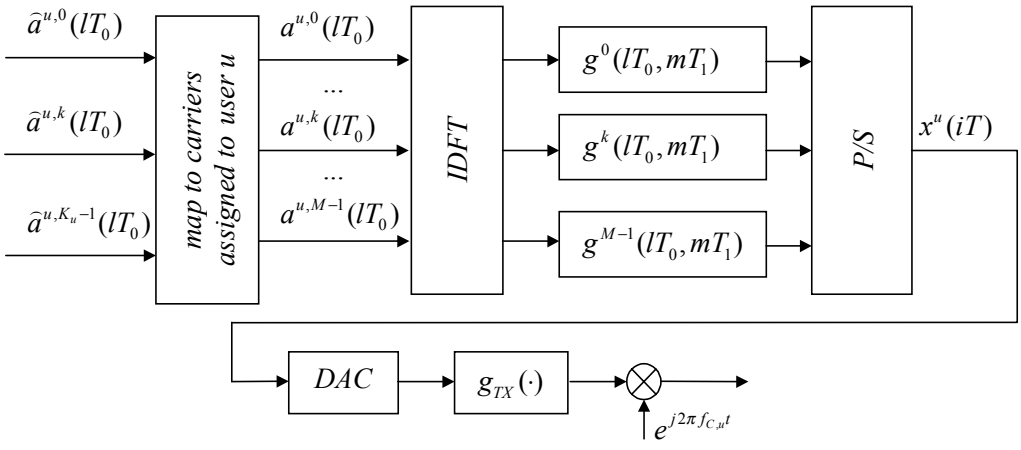

Fig. 3.7. NCS-FMT-MA modulator of user *u*.

3.4 Schemes for the Assignment of Tones to Users

In a multicarrier/multitone multiple access system multiplexing is obtained by assigning sub-sets of sub-carriers/tones to distinct users. The allocation scheme plays an important role for the optimization of the spectral efficiency, the exploitation of the frequency diversity, and the complexity of the detection algorithm (see Chapter 5). It can be static or dynamic, orthogonal or non-orthogonal.

To maximize the spectral efficiency we could allow for a non-orthogonal scheme where distinct users share some of the sub-carriers [57]. To exploit at best the channel frequency diversity, the tones should be distributed across the overall spectrum, or be dynamically allocated in accordance to the channel dynamic conditions [19].

In the next chapters we will show that the users' asynchronism and the channel frequency selectivity generate multiple access interference at the receiver side. In order to minimize the multiple access interference power levels and simplify the receiver complexity it is better to allocate trunks of tones that are as far as possible across users. In the following we outline some orthogonal allocation strategies.

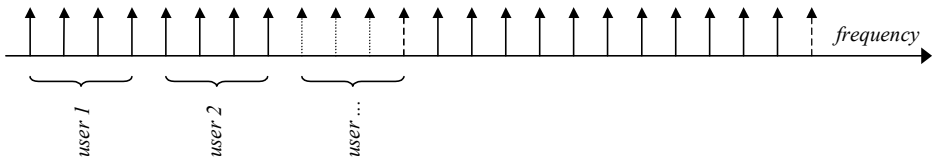

Fig. 3.8. Block tone multiplexing.

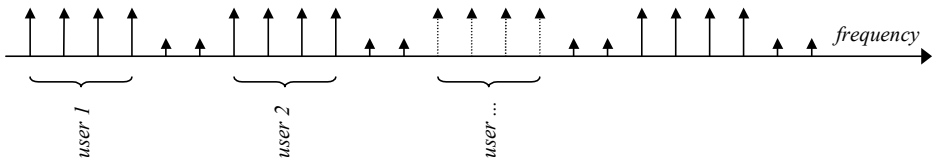

Fig. 3.9. Block tone multiplexing with frequency guards.

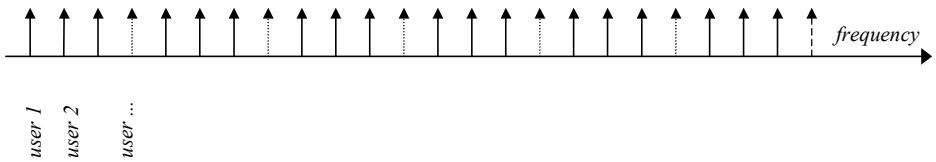

Fig. 3.10. Interleaved tone multiplexing.

A. *Block allocation*. Each user is assigned a block of K_u contiguous tones. Distinct users use distinct blocks (Fig. 3.8).

B. *Block allocation with frequency guards*. As Scheme A with the insertion of guard tones (virtual carriers) between adjacent blocks (Fig. 3.9).

C. *Interleaved allocation*. The tones of the users are regularly interleaved across the overall spectrum (Fig. 3.10).

D. *Random allocation*. The tones are randomly allocated with the only constraint of avoiding the carrier hits.

E. *Dynamic allocation*. The tones can be dynamically allocated according to a given pattern. Multiplexing of users becomes a sort of multitone frequency hopping [57], [45].

F. *Adaptive allocation*. The tones are allocated to users in an adaptive mode by changing the assignment according to the channel conditions and interference levels. It requires a feedback control loop from the receiver that monitors the received powers of all users (see Chapter 11).

We point out that the multicarrier multiple access scheme that we have described can be applied to both the uplink (terminals to base link) and the downlink (base to terminals link). However, we focus on the uplink since the asynchronism across users translates into a more critical scenario.

4 ASYNCHRONOUS MULTIPLE ACCESS CHANNEL

In this chapter we describe the asynchronous multiuser channel model that is used throughout the following chapters. The model is appropriate to describe the uplink of a multiuser wireless communications system such as the uplink of a satellite system, of a wireless LAN or of a mobile cellular system. In general we consider transmission over time-variant frequency selective fading channels. Users are asynchronous, i.e., they have a certain amount of temporal and carrier frequency misalignment with respect to a reference at the receiver. The time misalignments are due different propagation delays or different communication starting epochs. The carrier frequency misalignments are due to the drifts of the oscillators and to the Doppler shift from movements.

4.1 Time-Variant Broadband Channel

Let us consider a multicarrier multiple access system where N_U users wish to transmit their multicarrier (lowpass) signal $x^u(\tau)$ to a central receiver, e.g., base station. All MC signals occupy the same spectrum *W*. The complex transmission model[10] is depicted in Fig. 4.1. The signal $x^u(\tau)$ is passed through a broadband transmit filter $g_{TX}(\tau)$ whose output is $x_1^u(\tau_1)$. This filter may be deployed to shape the spectrum of the multicarrier signal. If we use a digital implementation of the multicarrier transmitter we assume $g_{TX}(\tau)$ to comprise the digital-to-analog converter. The filtered signal is quadrature modulated, e.g., to radio frequency, with carrier $f_{C,u}$ and transmitted through a linear time-variant channel whose complex bandpass impulse response is $\hat{g}_{ch}^u(\tau_1;\lambda)$. We assume each signal to experience a propagation delay or time misalignment given by Δt_u. Then, the composite bandpass received signal in the absence of thermal noise is obtained by the superposition of the N_U bandpass signals $x_4^u(\lambda)$ each belonging to a given user *u*: $x_4(\lambda) = \sum_{u=1}^{N_U} x_4^u(\lambda)$.

At the receiver side the received signal is down-converted and lowpass filtered in order to

[10] We assume the notation described in Appendix B for linear time-variant and time-invariant transforms.

accomplish quadrature demodulation. We assume the receiver oscillator to have frequency $f_C = \Delta f_u - f_{C,u}$ and phase $\varphi_C = \Delta\varphi_u - \varphi_{C,u}$. That is, it may differ from the *u-th* transmitter oscillator by a constant *frequency offset* Δf_u and *phase offset* $\Delta\varphi_u$. The frequency offset is generated by a misadjustment between the two oscillators, or by the presence of Doppler shifts due to the movement of the transmitters.

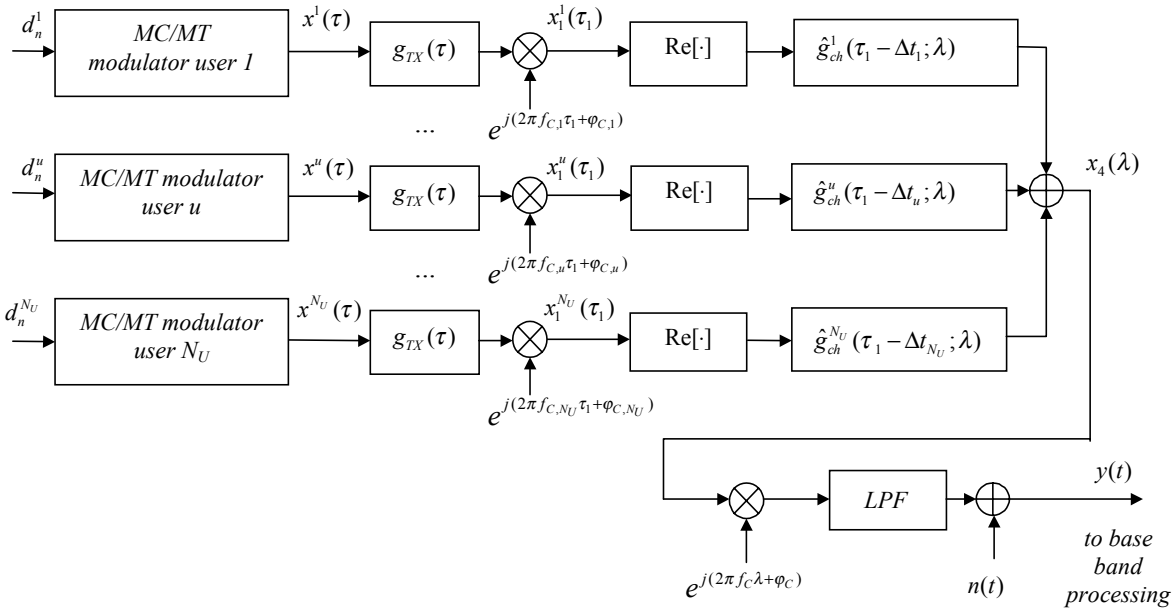

Fig. 4.1. Multicarrier/multitone multiuser asynchronous transmission model (complex representation).

It can be shown (see Appendix A) that the lowpass received signal component that belongs to user *u* in the absence of additive noise is

$$y^u(t) = e^{j(2\pi\Delta f_u t + \Delta\phi_u)} \int_R x^u(t-\tau) g_E^u(\tau - \Delta t_u; t) d\tau \tag{4.1}$$

where the *phase offset* is

$$\Delta\phi_u = \Delta\varphi_u - 2\pi\Delta t_u (f_C + \Delta f_u) \tag{4.2}$$

and the *equivalent lowpass channel impulse response* is

$$g_E^u(\tau - \Delta t_u; t) = \frac{1}{2} \int_R g_{TX}(\tau - \tau_1) g_{ch}^u(\tau_1 - \Delta t_u; t) d\tau_1 \tag{4.3}$$

with $g_{ch}^u(\tau_1; t)$ being the time-variant lowpass channel impulse response, i.e.,

$$g_{ch}^u(\tau_1; t) = e^{-j2\pi f_{C,u}\tau_1} \hat{g}_{ch}^u(\tau_1; t). \tag{4.4}$$

The composite received lowpass signal is then

$$y(t) = \sum_{u=1}^{N_U} y^u(t) + n(t) \tag{4.5}$$

where $n(t)$ is the thermal noise contribution. This model is depicted in Fig. 4.2. The complex noise process $n(t)$ is assumed to be stationary zero mean white Gaussian with spectral density $2N_0$ (in the signal bandwidth of interest). Note that this model comprises also the case of synchronous users with propagation through an identical channel for all of them, i.e., the downlink.

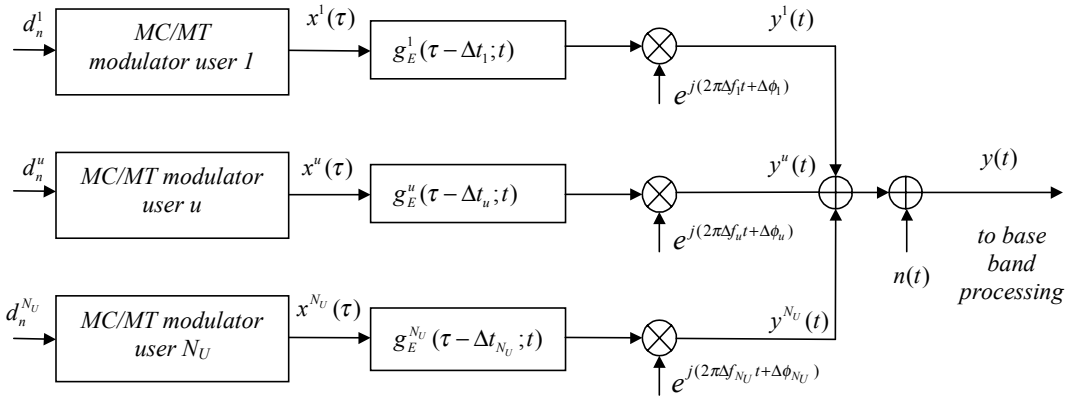

Fig. 4.2. Multicarrier/multitone multiuser asynchronous lowpass transmission model.

4.1.1 Equivalent Sub-channel Impulse Response

Let us consider a multicarrier system (analog implementation). The input to the broadband transmit filter of user u is $x^u(\tau) = \sum_{k=0}^{M-1} \sum_{l=-\infty}^{\infty} \tilde{a}^{u,k}(lT_0) g_T^{u,k}(\tau - lT_0)$, with $\tilde{a}^{u,k}(lT_0) = a^{u,k}(lT_0) e^{j2\pi f_k lT_0}$ and $g_T^{u,k}(\tau) = g^{u,k}(\tau) e^{j2\pi f_k \tau}$. Thus, if we define the *equivalent sub-channel impulse response* as

$$\begin{aligned} g_R^{u,k}(\tau;t) &= \int_R g_T^{u,k}(\tau-\tau') g_E^u(\tau';t) d\tau' = \int_R e^{j2\pi f_k(\tau-\tau')} g_S^{u,k}(\tau-\tau') g_E^u(\tau';t) d\tau' \\ &= e^{j2\pi f_k \tau} \int_R g_S^{u,k}(\tau-\tau') \underbrace{e^{-j2\pi f_k \tau'} g_E^u(\tau';t)}_{g_E^{u,k}(\tau';t)} d\tau' \end{aligned} \tag{4.6}$$

the received signal component of user u, and the composite received signal are respectively

$$y^u(t) = e^{j(2\pi\Delta f_u t+\Delta\phi_u)} \sum_{k=0}^{M-1} \sum_{l=-\infty}^{+\infty} a^{u,k}(lT_0) e^{j2\pi f_k lT_0} g_R^{u,k}(t - \Delta t_u - lT_0; t) \tag{4.7}$$

$$y(t) = \sum_{u=1}^{N_U} e^{j(2\pi\Delta f_u t+\Delta\phi_u)} \sum_{k=0}^{M-1} \sum_{l=-\infty}^{+\infty} a^{u,k}(lT_0) e^{j2\pi f_k lT_0} g_R^{u,k}(t - \Delta t_u - lT_0; t) + n(t). \tag{4.8}$$

Now, let us consider a multitone system (digital implementation). From Chapter 3 the input to the broadband transmit filter that is assumed to include the DAC is

$$x^u(t) = \sum_{i=-\infty}^{\infty} Tx^u(iT)\delta(t-iT) = \sum_{k=0}^{M-1}\sum_{i=-\infty}^{\infty}\sum_{l=-\infty}^{\infty} T\tilde{a}^{u,k}(lT_0)g_T^{u,k}(iT-lT_0)\delta(t-iT) \tag{4.9}$$

with $g_T^{u,k}(iT) = g_S^{u,k}(iT)e^{j2\pi f_k iT}$. Thus, the received signal component that belongs to user *u* is

$$\begin{aligned} y^u(t) &= e^{j(2\pi\Delta f_u t+\Delta\phi_u)}\sum_{k=0}^{M-1}\sum_{i=-\infty}^{\infty}\sum_{l=-\infty}^{\infty} T\tilde{a}^{u,k}(lT_0)g_T^{u,k}(iT-lT_0)\int_R \delta(t-\tau-iT)g_E^u(\tau-\Delta t_u;t)d\tau \\ &= e^{j(2\pi\Delta f_u t+\Delta\phi_u)}\sum_{k=0}^{M-1}\sum_{l=-\infty}^{\infty}\tilde{a}^{u,k}(lT_0)\sum_{i=-\infty}^{\infty} Tg_T^{u,k}(iT)g_E^u(t-iT-lT_0-\Delta t_u;t) \\ &= e^{j(2\pi\Delta f_u t+\Delta\phi_u)}\sum_{k=0}^{M-1}\sum_{l=-\infty}^{\infty}\tilde{a}^{u,k}(lT_0)\underbrace{\sum_{i=-\infty}^{\infty} Te^{j2\pi f_k iT}g_S^{u,k}(iT)g_E^u(t-iT-lT_0-\Delta t_u;t)}_{g_R^{u,k}(t-lT_0-\Delta t_u;t)} \end{aligned} \tag{4.10}$$

Therefore, the composite received signal can be written as in (4.8), provided that the *equivalent sub-channel impulse response* is defined as follows

$$g_R^{u,k}(\tau;t) = \sum_{i=-\infty}^{\infty} Te^{j2\pi f_k iT}g_S^{u,k}(iT)g_E^u(\tau-iT;t). \tag{4.11}$$

Based on the results of this section we can depict the link of user *u* and sub-carrier *k* as in Fig. 4.3.

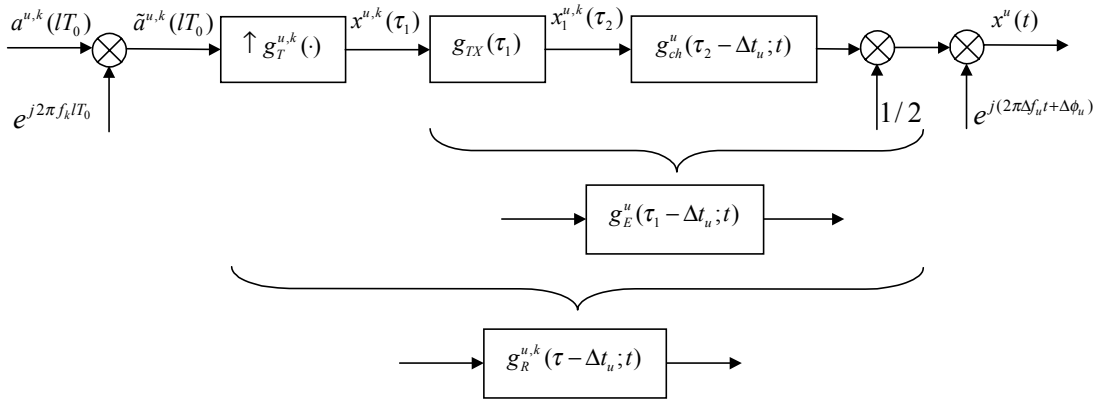

Fig. 4.3. Lowpass equivalent transmission model for the link of user *u* and sub-carrier *k*.

4.1.2 Frequency Offsets and Time Offsets at Sub-Channel Level

In the above channel model we have assumed that all sub-channels of a given user experience the same frequency offset, phase offset, and time offset. Clearly, a simple modification to the notation can include the case of sub-channels of a given user *u* having distinct frequency/phase/time offsets. If we make the substitutions $\Delta f_u \to \Delta f_{u,k}$, $\Delta\phi_u \to \Delta\phi_{u,k}$, $\Delta t_u \to \Delta t_{u,k}$ (u=1,...,N_U and k=0,...,M-1) we can rewrite in more general form that the composite received signal is

$$y(t) = \sum_{u=1}^{N_U}\sum_{k=0}^{M-1}\sum_{l=-\infty}^{+\infty} a^{u,k}(lT_0)e^{j2\pi f_k lT_0}e^{j(2\pi\Delta f_{u,k}t+\Delta\phi_{u,k})}g_R^{u,k}(t-\Delta t_{u,k}-lT_0;t)+n(t). \tag{4.8 b}$$

This notation may be appropriate in an analog implementation where for instance the oscillators of a given transmitter are unlocked. The original notation is particularly appropriate for systems where the transmitters are digitally implemented and is motivated by the interest to study the effects of asynchronism between distinct users. The more general assumption of distinct frequency offsets over the sub-channels of a given user can be used to model the effect of the sampling clock frequency offset [52]. It is also understood that the original notation includes (although in a little unnatural form) the more general one if we augment the index N_U to MN_U, i.e., we consider MN_U users each transmitting over one sub-channel.

4.1.3 Asynchronous Users

The multiple access channel model that we have described is based on the general assumption that signals belonging to distinct users propagate through distinct channels. At the receiver side temporal and frequency synchronization can be achieved only for a given signal at the time. After synchronization one of the two signals will be inevitably time and frequency misadjusted whenever the associated time/frequency offsets differ (Fig. 4.4-Fig. 4.5). Note in Fig. 4.5 that all sub-carriers are assumed to be shifted by the same amount. Further, we can assume that the time offsets and frequency offsets are constant for a given time interval and independent across users. The statistical distribution of the time offset can be assumed uniformly distributed between a minimum and maximum value, while the frequency offset can be assumed uniformly or Gaussian distributed.

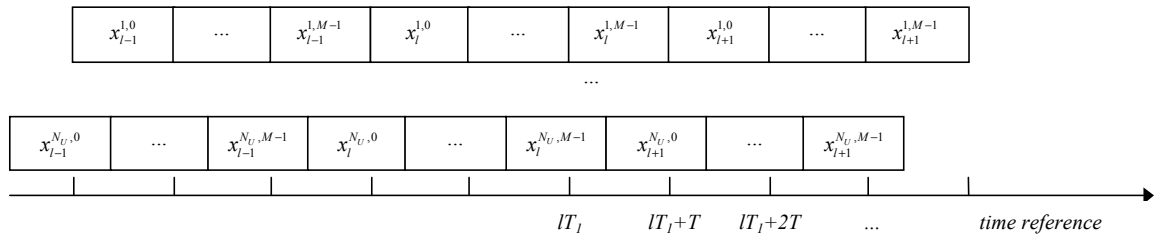

Fig. 4.4. Time misadjustment. $x_l^{u,n} = x^u(lT_1 + nT)$.

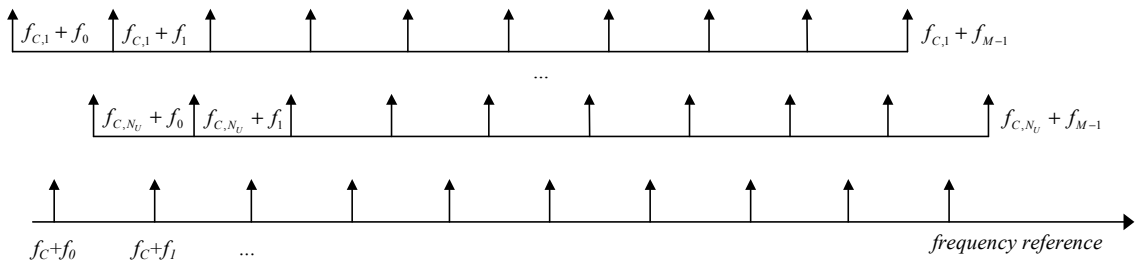

Fig. 4.5. Carrier misadjustment.

4.1.4 Time Offsets

As explained in the previous section we can assume to acquire perfect time synchronization with a given user. If transmission is fully asynchronous the other users will inevitably be time misadjusted as a result of a propagation delay or a different transmission starting epoch. However we can easily add some level of synchronization by assuming that each user deploys as transmission time reference the downlink frame. Therefore only the propagation delay gives rise to the time offsets. Let us assume two users at relative distance Δs, then the relative time offset due to propagation delay is

$$\Delta t = 2\frac{\Delta s}{c} \approx 0.67 \cdot 10^{-8} \cdot \Delta s . \tag{4.12}$$

If R is the maximum distance of a given user from the receiver (cell radius) then we can compute the maximum misadjustment in terms of number of chips[11] as a function of chip rate, see Table 4.1.

R	Δt	Chips @ 1 Mchip/s	Chips @ 10 Mchip/s	Chips @ 100 Mchip/s
10 m	0.067 μs	0.067	0.67	6.7
100 m	0.67 μs	0.67	6.7	67
1000 m	6.7 μs	6.7	67	670
10000 m	670 μs	67	670	6700

Table 4.1. Normalized time offset due to propagation delay.

4.1.5 Frequency Offsets

Assuming to acquire carrier synchronization with a given user, the others can be frequency non-synchronized due to the different oscillator frequency or to Doppler shifts from movements.

Let p_c be the oscillator precision in parts per million (p.p.m), then

$$\frac{M\Delta f_{oscill}}{W} = f_C 10^{-6} p_c \frac{M}{W} \tag{4.13}$$

is the normalized frequency offsets due to the oscillator precision with respect to the sub-carrier spacing (assuming M uniformly spaced sub-carriers in the bandwidth W). If we fix the overall bandwidth it increases with the carrier frequency, and the number of sub-carriers. This is reported in Table 4.2 assuming a radio frequency oscillator with precision of 1 p.p.m.

[11] Having in mind a digital implementation of the transmitter, we denote with *chip* the transmitted symbol of duration T.

f_{RF} GHz	$M\Delta f_{oscill}/W$								
	W=1 MHz			W=10 MHz			W=100 MHz		
	M=16	128	1024	16	128	1024	16	128	1024
1	0.016	0.128	1.024	0.0016	0.0128	0.1024	0.00016	0.00128	0.01024
10	0.16	1.28	10.24	0.016	0.128	1.024	0.0016	0.0128	0.1024
100	1.6	12.8	102.4	0.16	1.28	10.24	0.016	0.128	1.024

Table 4.2. Normalized frequency offset (fraction of sub-carrier spacing) with oscillator precision of 1 p.p.m.

Let v be the maximum user velocity (in the radial direction towards the receiver) then the maximum normalized frequency offset due to Doppler is calculated as

$$\frac{M\Delta f_{Doppler}}{W} = f_C \frac{v}{c}\frac{M}{W}. \tag{4.14}$$

If we fix the overall bandwidth it increases with the carrier frequency, the velocity and the number of sub-carriers.

$$\frac{\Delta f_{Doppler}}{\Delta f_{oscill}} = \frac{v}{c}\frac{10^6}{p_c} \approx 0.093\cdot 10^{-2}\frac{v\ [km/h]}{p_c\ [p.p.m]}. \tag{4.15}$$

Assuming $p_c \sim 1\ p.p.m$, and $v \sim 100$ km/h, we obtain $\Delta f_{Doppler}/\Delta f_{oscill} \approx 0.093$.

Clearly the maximum frequency offsets among to users is twice that reported in (4.13) and (4.14).

4.1.6 Time-Variant Multipath Fading Channels

In mobile wireless applications the transmission media is characterized by an equivalent lowpass impulse response $g_{ch}^{u}(\tau;t)$ that is in general time-variant and frequency selective.

A widely used model assumes a tapped delay line model with N_P+1 discrete rays each having a delay equal to $\tau(p)$ [43], i.e.,

$$g_{ch}^{u}(\tau;t) = \sum_{p=1}^{N_P}\alpha^{u}(p;t)\delta(\tau-\tau^{u}(p)). \tag{4.16}$$

The channel taps $\alpha^{u}(p;t)$ can be further modeled with wide sense stationary complex Gaussian processes. If their mean is zero their envelope is Rayleigh distributed otherwise is Ricean distributed. In the former case the channel is said to be a Rayleigh fading channel, in the latter a Ricean fading channel.

In terms of temporal statistics the Clarke's isotropic scattering model yields the following correlation function

$$E[g_{ch}^{u}(p;t)g_{ch}^{u}(p;t+\tau)^{*}] = J_0(2\pi\Delta f_{Doppler}\tau) \tag{4.17}$$

where $J_0(\tau)$ is the zero-order Bessel function of the first kind. The taps cross-correlation is assumed to be zero.

With this channel model the equivalent sub-channel impulse response (assuming analog sub-channel transmit filters and assuming to include the broadband transmit filter in the channel impulse response) is

$$g_R^{u,k}(\tau;t) = \sum_{p=0}^{N_P} \alpha^u(p;t) g_T^{u,k}(\tau - \tau_u(p)) = e^{j2\pi f_k \tau} \sum_{p=0}^{N_P} \alpha^u(p;t) e^{-j2\pi f_k \tau_u(p)} g_S^{u,k}(\tau - \tau_u(p)). \quad (4.18)$$

4.1.7 Static Multipath Fading

If the propagation media is static for the duration of the transmission interval, the channel impulse response is written as $g_{ch}^u(t)$. If we further assume a tapped delayed line model we have

$$g_{ch}^u(t) = \sum_{p=0}^{N_P} \alpha^u(p) \delta(t - \tau_u(p)). \quad (4.19)$$

4.1.8 Static Multipath Fading and Flat Sub-channel Frequency Response

It is interesting to note that for a high number of sub-carriers we can assume that the sub-channel has flat frequency response. Let $x^{u,k}(t)e^{j2\pi f_k t}$ be the signal transmitted through the *k-th* sub-channel, then

$$\begin{aligned} y^{u,k}(t) &= \int_{-\infty}^{+\infty} x^{u,k}(\tau) e^{j2\pi f_k \tau} g_E^u(t-\tau) d\tau = \int_{-\infty}^{+\infty} X^{u,k}(f - f_k) G_E^u(f) e^{j2\pi f t} df \\ &\approx G_E^u(f_k) \int_{f_k - \frac{1}{2T_0}}^{f_k + \frac{1}{2T_0}} X^{u,k}(f - f_k) e^{j2\pi f t} df \approx G_E^u(f_k) x^{u,k}(t) e^{j2\pi f_k t} \end{aligned}. \quad (4.20)$$

Therefore, the *k-th* received signal component equals the *k-th* sub-channel transmitted signal weighted by the frequency response of the channel at frequency f_k. Note that (4.20) is just an approximation obtained under the assumption of strictly frequency limited *k-th* transmitted signal. The overall received signal component belonging to user *u* in the absence of additive noise, time and frequency offsets, is then

$$y^u(t) \approx \sum_{k=0}^{M-1} G_E^u(f_k) x^{u,k}(t) e^{j2\pi f_k t}. \quad (4.21)$$

APPENDIX TO CHAPTER 4

A Lowpass Transmission Model

In this appendix we derive the equivalent lowpass transmission model that comprises the transmit filter, the quadrature modulator at frequency f_C, the time-variant channel, and the quadrature demodulator. A block diagram is depicted in Fig. 4.6 assuming a complex representation and the absence of thermal noise. We use some results and notation on linear time-variant systems of Appendix B.

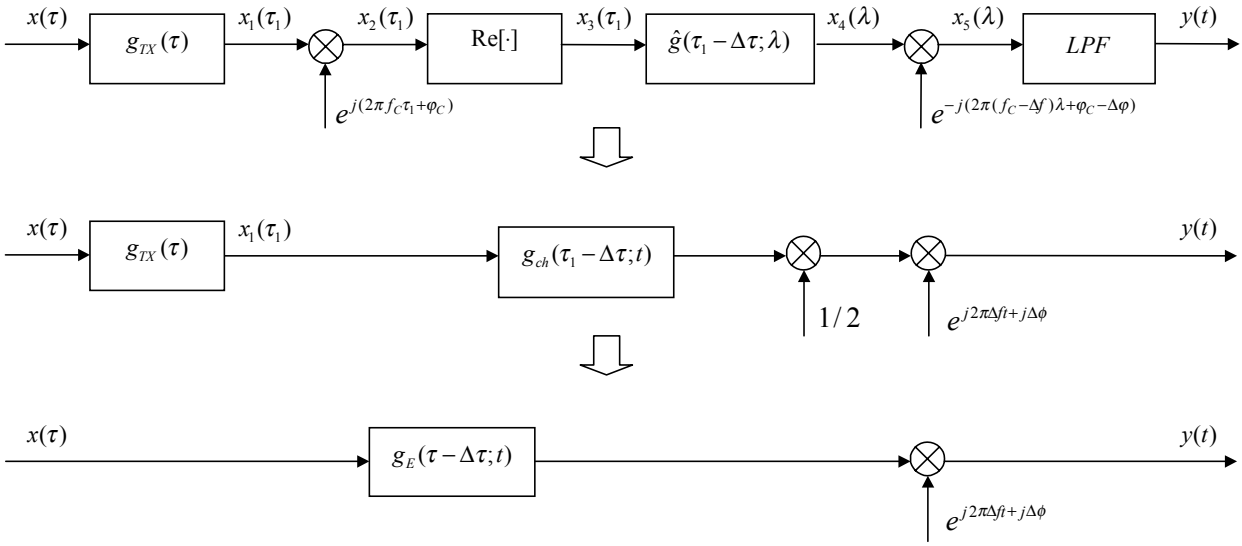

Fig. 4.6. Lowpass equivalent transmission model in the presence of time offset, frequency offset, phase offset, and time-variant channel (complex representation).

The lowpass complex signal $x(\tau)$ is passed through the transmit filter $g_{TX}(\tau)$. Then, it is bandpass modulated with carrier f_C, e.g., at radio frequency. The bandpass transmitted signal is $x_3(\tau_1) = \mathrm{Re}[x_1(\tau_1)e^{j(2\pi f_C\tau_1+\varphi_C)}]$. Let $\hat{g}_{ch}(\tau_1;\lambda)$ be the linear time-variant bandpass channel impulse response. Then, the bandpass received signal is

$$\begin{aligned} x_4(\lambda) &= \mathrm{Re}\left[\int_R x_1(\lambda-\tau_1)e^{j(2\pi f_C(\lambda-\tau_1)+\varphi_C)}\hat{g}_{ch}(\tau_1-\Delta\tau;\lambda)d\tau_1\right] \\ &= \mathrm{Re}\left[e^{j(2\pi f_C(\lambda-\Delta\tau)+\varphi_C)}\int_R x_1(\lambda-\tau_1)\underbrace{e^{-j2\pi f_C(\tau_1-\Delta\tau)}\hat{g}_{ch}(\tau_1-\Delta\tau;\lambda)}_{g_{ch}(\tau_1-\Delta\tau;\lambda)}d\tau_1\right] \end{aligned} \tag{A.1}$$

where $g_{ch}(\tau_1;\lambda) = \hat{g}_{ch}(\tau_1;\lambda)e^{-j2\pi f_C\tau_1}$ is the equivalent lowpass channel impulse response. Note that we have included a propagation delay and/or time misalignment in the transmission model.

Now, the received lowpass signal is obtained by quadrature demodulation and lowpass filtering (LPF). If we assume a local oscillator with frequency $f_{loc} = \Delta f - f_C$ and phase $\varphi_{loc} = \Delta\varphi - \varphi_C$ we obtain

$$\begin{aligned} x_5(\lambda) = &\frac{1}{2}e^{j2\pi\Delta f\lambda}e^{-j2\pi f_C\Delta\tau + j\Delta\varphi}\int_R x_1(\lambda-\tau_1)g_{ch}(\tau_1-\Delta\tau;\lambda)d\tau_1 + \\ &+\frac{1}{2}e^{-j2\pi f_C(2\lambda+\Delta\tau)+j(2\pi\Delta f\lambda+\Delta\varphi-2\varphi_C)}\int_R x_1^*(\lambda-\tau_1)g_{ch}^*(\tau_1-\Delta\tau;\lambda)d\tau_1 \end{aligned} . \quad (A.2)$$

At the output of the LPF the components around twice the carrier frequency are eliminated, which yields

$$y(t) = \frac{1}{2}e^{j2\pi\Delta ft + j\Delta\phi}\int_R x_1(t-\tau_1)g_{ch}(\tau_1-\Delta\tau;t)d\tau_1 \quad (A.3)$$

with $\Delta\phi = \Delta\varphi - 2\pi f_C\Delta\tau$.

Finally, using the results in Appendix B we can write

$$y(t) = e^{j2\pi\Delta ft + j\Delta\phi}\int_R x(t-\tau)g_E(\tau-\Delta\tau;t)d\tau \quad (A.4)$$

where the equivalent lowpass impulse response obtained by the concatenation of the broadband transmit filter with the time-variant channel is (including the factor 1/2)

$$g_E(\tau-\Delta\tau;t) = \frac{1}{2}\int_R g_{TX}(\tau-\tau_1)g_{ch}(\tau_1-\Delta\tau;t)d\tau_1 . \quad (A.5)$$

B Linear Time-Variant Transforms

The following input-output relation defines a linear time-variant transform

$$y(t) = \int_R x(t-\tau')g(\tau';t)d\tau' = \int_R x(\tau')g(t-\tau';t)d\tau' \tag{B.1}$$

where $g(\tau;t)$ with $t \in R$, $\tau \in R$ is the response at time t of an impulse applied at time $t-\tau$, i.e., the response to the signal $\delta(\tau'-t+\tau)$:

$$g(\tau;t) = \int_R \delta(\tau-\tau')g(\tau';t)d\tau'. \tag{B.2}$$

The transform is depicted in Fig. 4.7. When the transform is time invariant the input-output relation is given by the convolution of the input signal $x(\tau)$ with the impulse response $g(\tau)$. This conventional transform is a filter (Fig. 4.8).

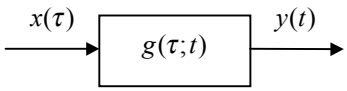

Fig. 4.7. Linear time-variant transform.

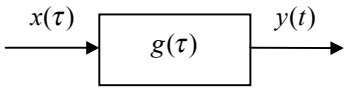

Fig. 4.8. Linear time-invariant transform (filter).

CASCADE OF A LINEAR TIME INVARIANT TRANSFORM WITH A LINEAR TIME-VARIANT TRANSFORM

Let us consider the system depicted in Fig. 4.9. The system comprises the concatenation of a linear time-invariant transform with a linear time-variant transform.

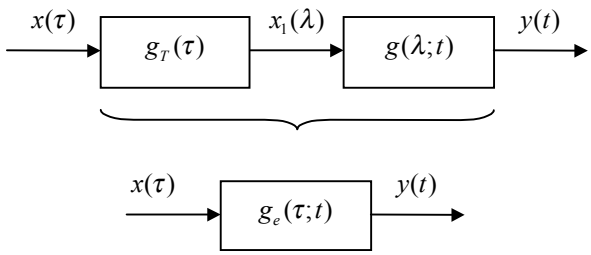

Fig. 4.9. Cascade of linear time-invariant with linear time-variant transform.

Proposition. The concatenation of a linear time-invariant transform $g_T(\tau)$ with a linear time-variant transform $g(\lambda;t)$ is equivalent to a linear time-variant transform with impulse response

$$g_e(\tau;t) = \int_R g_T(\tau-\lambda)g(\lambda;t)d\lambda \,. \tag{B.3}$$

Proof. By using the definition in (B.1) the output signal is obtained as follows.

$$y(t) = \int_R x_1(t-\lambda)g(\lambda;t)d\lambda = \int_R\int_R x(t-\lambda-\tau)g_T(\tau)g(\lambda;t)d\tau d\lambda \,.$$

If we substitute the integration variable $\tau \to \tau - \lambda$ we obtain

$$y(t) = \int_R x(t-\tau)\underbrace{\int_R g_T(\tau-\lambda)g(\lambda;t)d\lambda}_{g_e(\tau;t)}d\tau \,,$$

which proves the equivalence.

CASCADE OF A LINEAR TIME-VARIANT TRANSFORM WITH A LINEAR TIME-INVARIANT TRANSFORM

Let us consider the system depicted in Fig. 4.10. The system comprises the concatenation of a linear time-variant transform with a linear time-invariant transform.

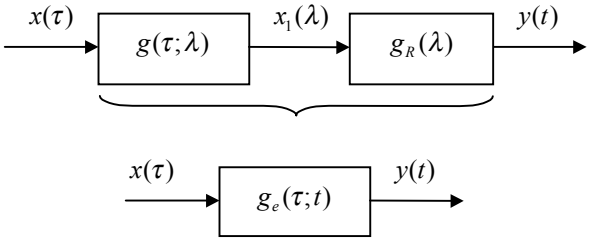

Fig. 4.10. Cascade of linear time-variant with linear time-invariant transform.

Proposition. The concatenation of a linear time-variant $g(\tau;\lambda)$ transform with a linear time-invariant transform $g_R(\lambda)$ is equivalent to a linear time-variant transform with impulse response

$$\begin{aligned} g_e(\tau;t) &= \int_R g_R(t-\lambda)g(\lambda+\tau-t;\lambda)d\lambda \\ &= \int_R g(\tau-\lambda;t-\lambda)g_R(\lambda)d\lambda \\ &= \int_R g_R(\tau-\lambda)g(\lambda;t-\tau+\lambda)d\lambda \end{aligned} \,. \tag{B.4}$$

Proof. The output signal is obtained as follows.

$$y(t) = \int_R x_1(\lambda)g_R(t-\lambda)d\lambda = \int_R\int_R x(\tau)g(\lambda-\tau;\lambda)g_R(t-\lambda)d\tau d\lambda \,.$$

If we substitute the integration variable $\tau \to t - \tau$ we obtain

$$y(t) = \int_R x(t-\tau) \underbrace{\int_R g_R(t-\lambda) g(\lambda + \tau - t; t) d\lambda}_{g_e(\tau;t)} d\tau ,$$

which proves that the overall transform equals a time-variant system with impulse response given by the first expression in (B.4). The other two expressions in (B.4) are obtained by the integration variable substitutions $\lambda \to t - \lambda$ and $\lambda \to t - \tau + \lambda$.

PERMUTING THE ORDER OF TRANSFORMS IN LINEAR TIME-VARIANT SYSTEMS

In general it is not possible to permute the order of the transforms in a system that is obtained by the concatenation of time-variant with time-invariant transforms. However we prove the following proposition.

Proposition. Let Φ_1 be a linear transform obtained by the concatenation of the linear time-invariant transform $g_1(\tau)$ with the linear time-variant transform $g(\tau;t)$. Let Φ_2 be a linear transform obtained by the concatenation of the linear time-variant transform $g(\tau;t)$ with the linear time-invariant transform $g_1(t)$. Then, Φ_1 and Φ_2 are equivalent if the time-variant impulse response is static for the duration of the pulse $g_1(t)$.

Proof. Consider the system in Fig. 4.9. We have already shown that it is equivalent to a linear time-variant system with impulse response $g_e(\tau;t)$. If $g(\tau - \lambda; t) = g(\tau - \lambda; t - \lambda)$ for $\lambda \in \Im[g_1(\lambda)]$, where $\Im[g_1(\lambda)]$ is the set that defines the duration of the pulse $g_1(\lambda)$, we can write

$$g_e(\tau;t) = \int_R g_1(\lambda) g(\tau - \lambda; t) d\lambda = \int_R g_1(\lambda) g(\tau - \lambda; t - \lambda) d\lambda .$$

Therefore, the equivalent impulse response is obtained by the concatenation of the time-variant transform $g(\tau;\lambda)$ with the time-invariant transform $g_1(\lambda)$.

Consider the system in Fig. 4.10. We have already shown that it is equivalent to a linear time-variant system with impulse response $g_e(\tau;t)$. If $g(\tau - \lambda; t - \lambda) = g(\tau - \lambda; t)$ for $\lambda \in \Im[g_1(\lambda)]$, where $\Im[g_1(\lambda)]$ is the set that defines the duration of the pulse $g_1(\lambda)$, we can write

$$g_e(\tau;t) = \int_R g(\tau - \lambda; t - \lambda) g_1(\lambda) d\lambda = \int_R g(\tau - \lambda; t) g_1(\lambda) d\lambda = \int_R g_R(\tau - \lambda) g(\lambda; t) d\lambda .$$

With the variable substitution $\lambda \to \tau - \lambda$ we obtain

$$g_e(\tau;t) = \int_R g_1(\tau - \lambda) g(\lambda; t) d\lambda$$

which proves that the equivalent impulse response is obtained by the concatenation of the time-invariant transform $g_1(\tau)$ with the time-variant transform $g(\lambda;t)$.

5 DEMODULATION IN MULTICARRIER AND MULTITONE MULTIUSER SYSTEMS

In this chapter we address the problem of devising the optimal demodulator for an asynchronous multiple access multicarrier system. We pursue the concept of optimum maximum a posteriori detection of multiple received signals. The resulting receiver comprises a front-end structure followed by a maximum a posteriori processor. The demodulator is optimal in the probabilistic sense and is capable of delivering optimum soft information on the transmitted bits/symbols of all users.

Since the complexity of the optimum demodulator grows exponentially with the number of users, the number of sub-channels, and the channel memory, we propose several simplified detection approaches. These are based on iterative detection schemes where soft/hard information is exchanged between sub-trellises that are obtained by partitioning the full hyper trellis that describes the hidden multiple-input multiple-output Markov model .

5.1 Optimal Demodulation of Multicarrier Multiuser Signals

The goal of the baseband demodulator (detector) is to reconstruct the sequence of transmitted bits/symbols of all users from the observation of the complex lowpass signal $y(t)$ at the output of the receiver front end (see (4.5)). This is a problem of jointly detecting multiple received signals.

Assuming to observe the received signal over a finite time window $t \in I$, with I sufficiently long such that border effects can be ignored, the optimal symbol detector decides in favor of a transmitted data sequence $\underline{\hat{a}} = \{\hat{a}^{u,k}(lT_0)\}$, $lT_0 \in I$, $u = 1,...,N_U$, $k = 0,...,M-1$, that maximizes the a posteriori probability

$$P\left(\underline{a} \mid y(t)\right) = \frac{p\left(y(t) \mid \underline{a}\right)}{p\left(y(t)\right)} P\left(\underline{a}\right). \tag{5.1}$$

In what follows we assume the transmitted symbols to be independent. If coding is applied, this is a reasonable assumption when the coded bits or symbols are interleaved (Chapter 9). If no side information is available the symbols can be considered equally likely, and the decision rule collapses to the maximum likelihood one.

Under the assumption of the additive thermal noise $n(t)$ to be white Gaussian with spectral density $2N_0$, the channel probability density function [12] (pdf) conditioned on a given data sequence $\underline{\hat{a}}$, the channel, the frequency offset, and the time offset of all users, is (apart from a constant factor)

$$p(y(t) \mid \underline{\hat{a}}) \sim e^{-\frac{1}{4N_0}\Omega(\underline{\hat{a}})} \tag{5.2}$$

$$\Omega(\underline{\hat{a}}) = \int_{t\in I} \mid y(t) - \sum_{u=1}^{N_U} \sum_{lT_0 \in I} \sum_{k=0}^{M-1} \hat{a}^{u,k}(lT_0) e^{j2\pi f_k lT_0} e^{j(2\pi\Delta f_u t + \Delta\phi_u)} g_R^{u,k}(t - \Delta t_u - lT_0; t) \mid^2 dt \,. \tag{5.3}$$

In the appendix to this chapter (Appendix C) we show that the *channel log-likelihood function* (5.3) can be decomposed, apart from constant additive terms, as

$$\Omega(\underline{\hat{a}}) \sim -\sum_{lT_0 \in I} \sum_{u=1}^{N_U} \sum_{k=0}^{M-1} \Omega^{u,k,l}(\underline{\hat{a}}) \tag{5.4}$$

$$\begin{aligned} \Omega^{u,k,l}(\underline{\hat{a}}) = \mathrm{Re}\Bigg\{ \hat{a}^{u,k^*}(lT_0) \Bigg(& 2z^{u,k}(lT_0) - \sum_{u'=1}^{N_U} \sum_{k'=0}^{M-1} \hat{a}^{u',k'}(lT_0) s^{u,u',k,k'}(lT_0, lT_0) + \\ & - 2\sum_{u'=1}^{N_U} \sum_{k'=0}^{M-1} \sum_{l'<l} \hat{a}^{u',k'}(l'T_0) s^{u,u',k,k'}(lT_0, l'T_0) \Bigg) \Bigg\} \end{aligned} \tag{5.5}$$

where the *z-parameters* and *s-parameters* [13] are defined respectively as

$$z^{u,k}(lT_0) = e^{-j(2\pi f_k lT_0 + \Delta\phi_u)} \int_I y(t) e^{-j2\pi\Delta f_u t} g_R^{u,k^*}(t - \Delta t_u - lT_0; t) dt \tag{5.6}$$

$$\begin{aligned} & s^{u,u',k,k'}(lT_0, l'T_0) = \\ & = e^{-j(2\pi(f_k lT_0 - f_{k'} l'T_0) + \Delta\phi_u - \Delta\phi_{u'})} \int_I e^{-j2\pi(\Delta f_u - \Delta f_{u'})t} g_R^{u,k^*}(t - lT_0 - \Delta t_u; t) g_R^{u',k'}(t - l'T_0 - \Delta t_{u'}; t) dt \,. \end{aligned} \tag{5.7}$$

From (5.6), $z^{u,k}(lT_0)$ corresponds to the matched filter output sample of the frequency de-rotated an phase compensated received signal. The filter is matched to the equivalent *k-th* sub-channel impulse response of user *u*, and samples are taken at rate $1/T_0$.

---

[12] The channel pdf (5.2) is obtained from a generalization of the one reported in [74] for single link (user) transmission and in [78] for multiple channel transmission systems. A generalization of the channel pdf was also used in [82] for the derivation of the MLSE receiver for asynchronous CDMA channels, and more recently in [63], [65] for the derivation of the MAP equalizer in space-time coded systems. Note that we here consider the thermal noise to be white Gaussian. The case of correlated noise could be included as shown in [74]. Further, the case of distinct time/frequency offsets at sub-channel level (Section 4.1.2) can also be included; the reader is referred to Section 5.3 at the end of this chapter.

[13] We borrow the terminology z-parameters and s-parameters from [11].

From (5.7), $s^{u,u',k,k'}(lT_0, l'T_0)$ is obtained by cross-correlating, with appropriate frequency offset and phase offset compensation, the equivalent *k-th* sub-channel impulse response of user *u*, with the equivalent *k′-th* sub-channel impulse response of user *u′*.

According to (5.5), cross-terms may be present. They are a function of two symbols transmitted on two given carriers during two signaling periods. These cross-terms are interference components that may be helpful, from a conceptual standpoint, to distinguish as follows:

1. *Intersymbol interference* on sub-carrier *k* assigned to user *u*. This is zero if $s^{u,u,k,k}(lT_0, l'T_0) = 0$, for all $l \neq l'$.
2. *Intercarrier interference* between sub-carriers *k* and *k′* assigned to user *u*. This is zero if $s^{u,u,k,k'}(lT_0, l'T_0) = 0$, for all $k \neq k'$ and any pair *l*, *l′*.
3. *Multiple-access interference* between sub-carriers *k* and *k′*, assigned respectively to user *u* and *u′*, over symbols transmitted at signaling periods lT_0 and $l'T_0$. This is zero if $s^{u,u',k,k'}(lT_0, l'T_0) = 0$ for any pair of distinct users.

These interference components are a function of the prototype filter shape, the sub-carrier spacing and allocation, the channel, and the time/frequency offsets (Chapter 8). In order to implement efficiently the multicarrier-user detector, it is desirable that the s-parameters have a duration that is limited in time, i.e., as a function of index *l′*, and in frequency, i.e., as a function of index *k′*. Clearly, this depends upon the system design and channel characteristics. For instance if the prototype filters are practically limited in time and frequency, and the sub-carriers are appropriately allocated to the users, then the condition of limited cross-correlations can be fulfilled. If this is the case, it is convenient to further partition (5.5) (see Appendix C) as follows:

$$\begin{aligned}\Omega^{u,k,l}(\underline{\hat{a}}) = \mathrm{Re}\Big\{\hat{a}^{u,k^*}(lT_0)\Big(\; & 2z^{u,k}(lT_0) - \hat{a}^{u,k}(lT_0)s^{u,u,k,k}(lT_0, lT_0) + \\ & -2\sum_{u'<u}\hat{a}^{u',k}(lT_0)s^{u,u',k,k}(lT_0, lT_0) + \\ & -2\sum_{u'=1}^{N_U}\sum_{k'<k}\hat{a}^{u',k'}(lT_0)s^{u,u',k,k'}(lT_0, lT_0) + \\ & -2\sum_{u'=1}^{N_U}\sum_{k'=1}^{N}\sum_{l'<l}\hat{a}^{u',k'}(l'T_0)s^{u,u',k,k'}(lT_0, l'T_0)\;\Big)\Big\}\end{aligned} \quad . \tag{5.8}$$

If we substitute (5.2) in (5.1), under the assumption of the data symbols to be independent, the a posteriori probability (5.1) can be factored as follows

$$P(\underline{\hat{a}} \mid y(t)) \sim \prod_{lT_0 \in I}\prod_{u=1}^{N_U}\prod_{k=0}^{M-1}\left(e^{-\frac{1}{4N_0}\Omega^{u,k,l}(\underline{\hat{a}})}P(\hat{a}^{u,k}(lT_0))\right). \tag{5.9}$$

To proceed, if we define the index relations,

$$M_1 = MN_U \tag{5.10}$$

$$m = u + kN_U + lM_1 - 1 \qquad u = 1,...,N_U \quad k = 0,...,M-1 \quad l = -\infty,...,\infty \tag{5.11}$$

$$l(m) = m \ \text{div} \ M_1 \tag{5.12}$$

$$k(m) = (m \bmod M_1) \ \text{div} \ N_U \tag{5.13}$$

$$u(m) = ((m \bmod M_1) \bmod N_U) + 1 \tag{5.14}$$

the sequence of data symbols and matched filter outputs can be ordered as follows

$$\hat{a}_m = \hat{a}^{u(m),k(m)}(l(m)T_0) \qquad m = -\infty,...,\infty \tag{5.15}$$

$$z_m = z^{u(m),k(m)}(l(m)T_0) \qquad m = -\infty,...,\infty . \tag{5.16}$$

It follows that the log-likelihood function (5.4), taking into account (5.8), is rewritten as follows

$$\Omega(\underline{\hat{a}}) = \sum_m \Omega_m(\underline{\hat{a}}) \tag{5.17}$$

$$\begin{aligned}\Omega_m(\underline{\hat{a}}) = \Omega^{u(m),k(m),l(m)}(\underline{\hat{a}}) = \mathrm{Re}\Big\{\hat{a}_m^* \Big(2z_m - \hat{a}_m s^{u(m),u(m),k(m),k(m)}(l(m)T_0, l(m)T_0) + \\ -2\sum_{n>0} \hat{a}_{m-n} s^{u(m),u(m-n),k(m),k(m-n)}(l(m)T_0, l(m-n)T_0) \Big)\Big\}.\end{aligned} \tag{5.18}$$

In other words the log-likelihood function is obtained as the sum of the *transition metrics* (5.18). Therefore, if we define the *state* as follows

$$S_{m-1} = \{\hat{a}_{m-1}, ..., \hat{a}_{m-L_m}\}, \tag{5.19}$$

for a finite L_m such that

$$s^{u(m),u(m-n),k(m),k(m-n)}(l(m)T_0, l(m-n)T_0) = 0 \qquad \text{for} \quad n > L_m \ , \tag{5.20}$$

and the *state transition probability* as follows

$$\gamma_m(S_m, z_m \mid S_{m-1}) \sim \underbrace{e^{-\frac{1}{4N_0}\Omega_m(\underline{\hat{a}})}}_{p(z_m|S_m,S_{m-1})} \underbrace{P(\hat{a}_m)}_{P(S_m|S_{m-1})} , \tag{5.21}$$

the factorization of the a posteriori probability in (5.9) becomes

$$P(\underline{\hat{a}} \mid y(t)) \sim \prod_m \gamma_m(S_m, z_m \mid S_{m-1}) . \tag{5.22}$$

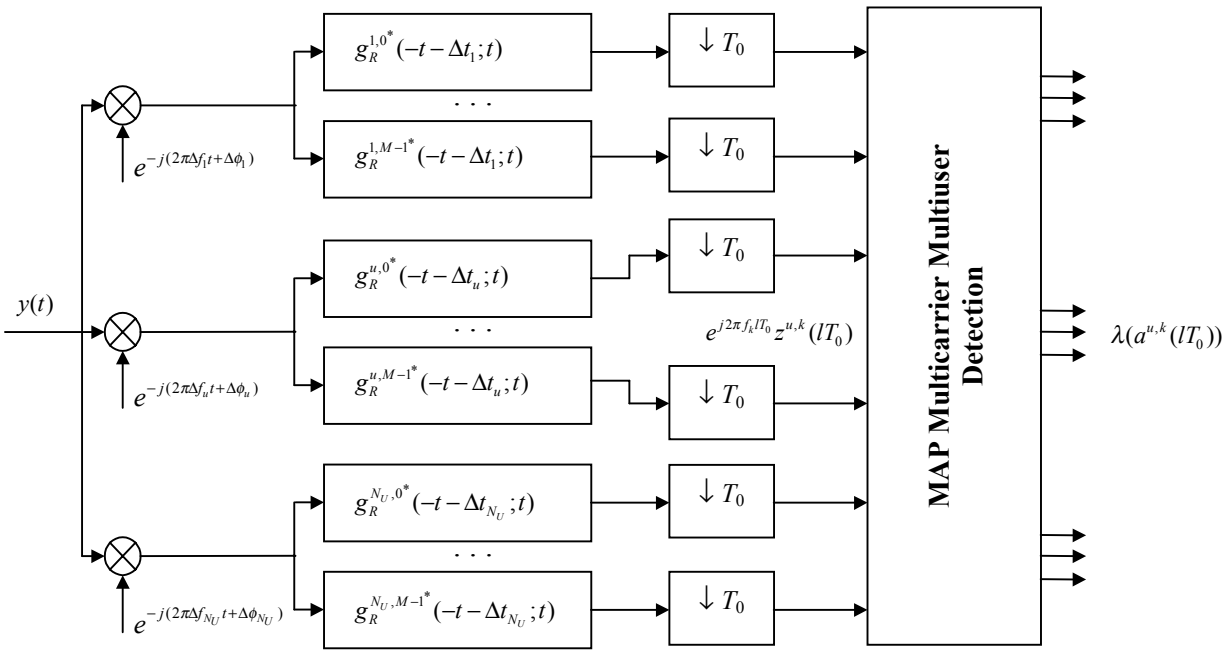

Fig. 5.1. Multicarrier-user baseband detector.

That is, the a posteriori probability is factored into the product of the state transition probabilities. In turn the state transition probability is obtained as the product of the *conditional channel pdf*,

$$p(z_m \mid S_m, S_{m-1}) = e^{-\frac{1}{4N_0}\Omega_m(\underline{\hat{a}})}, \tag{5.23}$$

with the *a priori transition probability* between state S_{m-1} and S_m

$$P(S_m \mid S_{m-1}) = P(\hat{a}_m). \tag{5.24}$$

Given the factorization in (5.22) we can use the maximum a posteriori/BCJR algorithm [5] to calculate the a posteriori probability of the data symbols, the a posteriori probability of the data bits, and the a posteriori probability of a data/bit sequence (see next sections). A block diagram of the baseband processing is depicted in Fig. 5.1.

5.1.1 3D Markov Chain Representation and Algorithm Complexity

The factorization in (5.22) implies that the evolution of the state defined in (5.19) observed at the sub-channel matched filter outputs can be represented with a Markov chain with transition probabilities defined in (5.21). It is interesting to note that when we move on the underlying trellis structure by one step we increase either the user index, or the sub-carrier index, or the time index:

$$S_{m+1} = S_{u(m+1)+N_U k(m+1)+M_1 l(m+1)} \rightarrow \begin{matrix} S_{u(m)+1+N_U k(m)+M_1 l(m)} \\ S_{u(m)+N_U (k(m)+1)+M_1 l(m)} \\ S_{u(m)+N_U k(m)+M_1 (l(m)+1)} \end{matrix} . \tag{5.25}$$

Therefore, the trellis can be imagined as a hyper trellis with a 3-D structure. The trellis has a number of states that is equal to $|\Sigma| = 2^{N_{bps} L_m}$, and a number of transitions to/from each state that is equal to $|\mathrm{T}| = 2^{N_{bps}}$ where N_{bps} is the number of bits per constellation symbol. Note that L_m satisfies the relation $1 \le L_m \le MN_U L_{ch}$ where L_{ch} is the channel temporal memory. The trellis structure essentially determines the complexity of the detection algorithm. Therefore the complexity grows exponentially with the number bits per constellation symbol, the number of users, the number of sub-carriers, and the channel memory.

5.1.2 Maximum a Posteriori Detection

The maximum a posteriori algorithm [5], [32], [83] can be used to compute:

1. The a posteriori probability of the data symbols[14], i.e.,

$$\lambda(a_m = a) = P(a_m = a \mid \underline{z}) = P\left(a^{u(m),k(m)}(l(m)T_0) = a \mid \underline{z}\right) \tag{5.26}$$

   with $a \in A$, and A being the set of all possible data symbols (constellation alphabet).

2. The *a posteriori probability of the data bits*, i.e.,

$$\lambda(d_i = d) = P(d_i = d \mid \underline{z}) \tag{5.27}$$

   with $d = \pm 1$, and $i = mN_{bps} + n$ with $n = 0, ..., N_{bps} - 1$.

3. The *a posteriori probability of a data sequence*, i.e.,

$$\lambda(\underline{a}) = P(\underline{a} \mid \underline{z}) \tag{5.28}$$

   with $\underline{a} \in \underline{A}$, and $\underline{A}$ being the set of all possible data sequences.

Deciding in favor of the symbol, bit, or sequence for which the a posteriori probability (*soft value*) is maximum makes hard symbol, bit, or sequence decisions, i.e.,

$$\hat{a}_m = \arg\max_{a \in A} \{\lambda(a_m = a)\} \tag{5.29}$$

$$\hat{d}_i = \arg\max_{d \in \{\pm 1\}} \{\lambda(d_i = d)\} \tag{5.30}$$

$$\underline{\hat{a}} = \arg\max_{\underline{a} \in \underline{A}} \{\lambda(\underline{a})\} = \prod_m \arg\max_{a \in A} \{\lambda(a_m = a)\} . \tag{5.31}$$

[14] We denote with $\underline{z}$ the sequence of matched filter outputs z_m.

The a posteriori probability of the data symbol and the data bit are respectively obtained as follows (ignoring a constant factor)

$$\lambda(a_m = a) \sim \sum_{(S_{m-1}, S_m) \in T(a)} \alpha_{m-1}(S_{m-1}) \gamma_m(S_m, z_m \mid S_{m-1}) \beta_m(S_m) \tag{5.32}$$

$$\lambda(d_i = d) \sim \sum_{(S_{m-1}, S_m) \in T(d)} \alpha_{m-1}(S_{m-1}) \gamma_m(S_m, z_m \mid S_{m-1}) \beta_m(S_m) \tag{5.33}$$

where the sum in (5.32) is computed over all state transitions that are determined by the symbol $a_m = a$, while the sum in (5.33) is computed over all state transitions that are determined by the bit $d_i = d$. Further, $\alpha_m(S_m)$ and $\beta_{m-1}(S_{m-1})$ are recursively computed as

$$\alpha_m(S_m) = \sum_{S_{m-1} \in \Sigma} \alpha_{m-1}(S_{m-1}) \gamma_m(S_m, z_m \mid S_{m-1}) \tag{5.34}$$

$$\beta_{m-1}(S_{m-1}) = \sum_{S_m \in \Sigma} \beta_m(S_m) \gamma_m(S_m, z_m \mid S_{m-1}) \tag{5.35}$$

with Σ being the set of all possible states. The cardinality of such a set, $|\Sigma|$, can be assumed finite with practically time-frequency limited sub-channel impulse responses.

We can now summarize the fundamental operations for computing the a posteriori probabilities:

1. Compute the z-parameters. These are obtained by convolving the received signal with a bank of time-variant filters matched to all sub-channel impulse responses of each user. The matched filter outputs are then sampled at rate $1/T_0$.
2. Compute the s-parameters. These parameters are obtained by cross-correlating any two sub-channel impulse responses of any two users.
3. Consider a block of matched filter outputs of finite length L that correspond to the finite time window *I*. Order the matched filter outputs and consequently the data symbols in accordance to the definitions (5.16), (5.15). Initialize $\alpha_0(S_0)$ and $\beta_L(S_L)$, setting them to 1 in correspondence to the known starting and ending states and to zero otherwise.
4. Recursively compute $\alpha_m(S_m)$ and $\beta_m(S_m)$ according to (5.34) and (5.35).
5. Once $\alpha_{m-1}(S_{m-1})$ and $\beta_m(S_m)$ have been computed, they can be multiplied with the appropriate $\gamma_m(S_m, z_m \mid S_{m-1})$ to obtain $\lambda(a_m)$ or $\lambda(d_i)$ according to (5.32), (5.33). The evaluation of the transition probability $\gamma_m(S_m, z_m \mid S_{m-1})$ requires the a priori probability of the symbols/bits that are associated with such a transition, i.e., $P(S_m \mid S_{m-1})$. Clearly, it can be set to a constant value if it is unknown, i.e., bits/symbols are considered equally likely. Assuming independent data bits such an a priori probability can be further factored as follows:

$$P(S_m \mid S_{m-1}) = \prod_{n=0}^{N_{bps}-1} P(d_{mN_{bps}+n}). \tag{5.36}$$

5.1.3 Some Remarks on Optimal MAP Detection

A. The algorithm is the optimal multicarrier multiuser detector in the probabilistic sense. It is applicable to both multicarrier and multitone multiple access systems.

B. The algorithm delivers soft outputs at bit level, symbol level, and sequence level. Therefore it is suited for application in concatenated systems with interleavers, e.g., when channel coding with interleaving is deployed (Chapter 9).

C. It is based on a coherent metric that requires estimation of the time offset, the frequency offset, and the time-variant impulse response of all sub-channels of all users.

D. If the channel is static, $g_{ch}^{u}(\tau;t) = g_{ch}^{u}(t)$, then the z-parameters and s-parameters are calculated as follows.

$$z^{u,k}(lT_0) = e^{-j(2\pi f_k lT_0 + \Delta\phi_u)} \int_I y(t) e^{-j2\pi\Delta f_u t} g_R^{u,k^*}(t - \Delta t_u - lT_0)dt \tag{5.37}$$

$$s^{u,u',k,k'}(lT_0, l'T_0) = e^{-j\left(2\pi(f_k lT_0 - f_{k'} l'T_0) + 2\pi(\Delta f_u - \Delta f_{u'})lT_0 + \Delta\phi_u - \Delta\phi_{u'}\right)} \cdot$$
$$\cdot \int_{t+lT_0 \in I} e^{-j2\pi(\Delta f_u - \Delta f_{u'})t} g_R^{u,k^*}(t - \Delta t_u) g_R^{u',k'}(t + lT_0 - l'T_0 - \Delta t_{u'})dt \,. \tag{5.38}$$

Under the hypothesis of constant time/frequency offsets, the integral can be calculated off-line once for all the transmission duration.

E. The transition probability can include the a priori information on the transmitted symbols/bits. The estimation of it can be performed iteratively in a coded system by exploiting the redundancy introduced by the channel encoders (Chapter 9). The resulting receiver implements a form of turbo detection and decoding [44], [60], [63], [65].

F. If no a priori information is included in the transition probability the algorithm delivers the maximum likelihood solution. Such a solution is efficiently obtained with a Viterbi algorithm over the 3-D trellis.

G. The implementation of the MAP algorithm requires the utilization of probabilities, and in particular the computation of the channel transition probability through exponential functions. A simplified implementation of the algorithm is possible by operating in the logarithm domain [83]. It is usually referred to as *log-MAP algorithm*.

H. In FMT-MA systems the receiver front-end (where the z-s-parameters are computed) has an efficient discrete-time implementation (Chapter 6).

5.2 Sub-optimal Multicarrier Multiuser Detection

In this section we devise methods to simplify the complexity of the detector of a multicarrier multiple access system.

5.2.1 Approaches for Simplified Detection

Optimal multicarrier multiuser detection might be too complex to be practical even for a small number of users, sub-carriers, and low modulation orders. Therefore, complexity reduction techniques/approaches have to be developed. We list some possible approaches.

A. Introduce some level of time and frequency synchronization among users. For instance a control loop from the base station can be deployed such that the terminals can adjust their local oscillators, and timing [77].

B. Lower the interference components by the appropriate choice of the sub-carrier spacing, the design of the prototype filters, the design the tone allocation strategy and the insertion of time and frequency guards.

C. Simplify the MLSE/MAP multicarrier multiuser detector through reduced state techniques.

In Chapter 8 we investigate the effect on complexity due to the prototype filters, and sub-carrier allocation strategies. In the sections below, we focus on reduced state algorithms.

5.2.2 Reduced-State MAP Detection

Let us consider the full state 3-D trellis with all possible transitions. Reducing the number of states implies that some of the branches in the full state 3-D trellis are cut. This is done dynamically as we move through the 3-D trellis by retaining only a certain amount of states. This is equivalent to force hard decisions on some of the past (in the user-frequency-time sense) transmitted data symbols.

It should be noted that the BCJR algorithm requires a forward and backward recursion on a full 3-D trellis. Nevertheless, it is possible to reduce the number of states by retaining for instance the forward direction reduced trellis also for the backward direction.

Since three dimensions are involved more freedom is left on how to choose the surviving states. We can for instance extend the M-algorithm [2] or the decision-feedback with set-partitioning algorithm [29] to the context that we are considering here. It is straightforward to extend the M-algorithm, by just retaining at each step the states with the best metric (highest probability).

With set-partitioning and decision feedback we can decide to reduce the states in the user, the frequency, or the time direction. Therefore, we can implement detectors with increasing complexity that range from the single carrier single user, to the full multicarrier multiuser detector. We want to

point out that they all are obtained as a simplification of the optimal detector.

5.2.3 Multicarrier Multiuser Detection with Decision Feedback

Multicarrier multiuser detection with decision feedback is implemented by forcing hard decisions as we proceed onto the 3-D trellis, such that at each step only few states/paths are retained. For instance, we can reduce the 3-D trellis into a 2-D trellis by decision feedback in either the user, or the temporal, or the frequency dimension.

Another way to proceed is to retain a 3-D trellis but reduce, through decision feedback, the memory in each dimension. In other words we can keep a lower amount of states on each dimension.

Note that when coding is applied soft information can be fed back from a soft-output decoder, and can be included in the metric transition (see Chapter 9). Therefore, multiple iterations can be run by concatenating the reduced-state multicarrier-user detector with the soft output channel decoder.

5.2.4 Iterative Sub-Trellis Detection

Instead of implementing the full state optimum detector we can approach the MAP solution by partitioning the full 3-D trellis into independent sub-trellises. Decisions made on each trellis can be exchanged among the trellises (Fig. 5.2-Fig. 5.5). Exchange of information can be done in parallel, or in serial mode.

If channel coding is deployed the detectors and the decoders can be concatenated in a parallel or serial fashion depending on how channel coding is done (Chapter 9). To limit error propagation it may be beneficial to use soft symbol decisions, whenever reliability information is available (for instance at the output of the soft output channel decoders). Soft decision feedback can be directly included in metric (5.8) by using instead of the hard symbols $a^{u,k}(lT_0)$ their average value, i.e.,

$$\overline{a}_m = \sum_{a \in A} aP[a_m = a]. \tag{5.39}$$

Special cases of iterative sub-trellis detection are per-user, per-carrier, and per-symbol detection.

5.2.5 Iterative Per-User Detection

Per-user detection is accomplished when splitting the 3-D trellis into a bank of N_U 2-D trellises. Each detector performs equalization in time and frequency for a given user, and takes into account the information on the MAI by feedback from the other detectors (Fig. 5.3). If the 2-D trellises are concatenated in parallel, the data decisions are reused in a new parallel detection stage after

detection from all trellises is completed. If they are serially concatenated, a given user detector can immediately use the decisions provided by the previous user detector. The similarity to parallel and serial interference cancellation in CDMA systems is clear [12], [46], [81]. Note that this approach basically consists on canceling the interfering terms using soft/hard decisions from other independent detection stages. Typically, cancellation is done in three steps: make decisions on the transmitted symbols, regenerate the individual received signals, and subtract them from the original received signal. However, regeneration is not necessary since decisions can be directly included in the metric (5.8).

5.2.6 Iterative Per-Carrier Detection

A further reduction in complexity is obtained by splitting the 3-D trellis into a bank of MN_U single carrier detectors. Each detector is single carrier based meaning that it just performs equalization in the temporal direction (Fig. 5.4) separately for each sub-carrier. Again exchanging of information can be done in a parallel or in a serial iterative mode.

5.2.7 Iterative Per-Symbol Detection

A more drastic reduction in complexity is achieved by making symbol by symbol decisions. That is, we make decisions on the transmitted data symbols by processing a single matched filter output at the time. The symbol by symbol detectors can still be iteratively concatenated. Once we have made soft/hard decisions on a given data symbol (of a given user and sub-carrier) this can be included in the metric that is used for the detection of a new symbol Fig. 5.5.

For instance, parallel iterative per-symbol detection can be implemented as follows.

A. At the first pass, make hard decisions on all data symbols of a given transmission block, i.e. compute for all $u = 1,...,N_U$, $k = 0,...,M-1$, $lT_0 \in I$:

$$\hat{a}^{u,k}(lT_0)_{it=0} = \arg\max_{a\in A} \mathrm{Re}\left\{a^*\left(2z^{u,k}(lT_0) - as^{u,u,k,k}(lT_0,lT_0)\right)\right\}. \tag{5.40}$$

B. Run a new per-symbol detection stage including the available decisions from the previous iteration, i.e., compute for all $u = 1,...,N_U$, $k = 0,...,M-1$, $lT_0 \in I$:

$$\hat{a}^{u,k}(lT_0)_{it=i} = \arg\max_{a\in A} \mathrm{Re}\left\{a^*\left(2z^{u,k}(lT_0) - as^{u,u,k,k}(lT_0,lT_0) - 2\sum_{\substack{(u',k',l')\\ \neq \\ (u,k,l)}} \hat{a}^{u',k'}(l'T_0)_{it=i-1} s^{u,u',k,k'}(lT_0,l'T_0)\right)\right\} \tag{5.41}$$

The sum is computed over all possible terns (u',k',l') that differ from the tern (u,k,l).

The decision metric above is obtained by isolating in (C.4) and (C.6) of Appendix C, the terms that depend upon the data symbol that we are detecting. Note that the metric requires knowledge of the s-parameters that in practice have to be estimated.

Clearly, detection can take place in serial mode by including in the metric the data decisions as soon as they come available. It can also be advantageous to start detection from the user/carrier that has the best signal power. That is, we run a sort of ordered (according to the power level) detection process.

Further, soft data decisions $\bar{a}^{u',k'}(l'T_0)$ (instead of hard data decisions $\hat{a}^{u',k'}(l'T_0)$) can be included in the metric and are calculated as shown in (5.39). The probabilities of the data symbols can be provided by an ad hoc channel decoder or by the detector itself [59]. In the latter case they can be approximated as follows (apart from a constant factor):

$$P[\hat{a}^{u,k}(lT_0)=a]_{it=i} \sim e^{-\frac{1}{4N_0}\mathrm{Re}\left\{a^*\left(2z^{u,k}(lT_0)-as^{u,u,k,k}(lT_0,lT_0)-2\sum_{\substack{(u',k',l')\\ \neq \\ (u,k,l)}}\hat{a}^{u',k'}(l'T_0)_{it=i-1}s^{u,u',k,k'}(lT_0,l'T_0)\right)\right\}}. \qquad (5.42)$$

Note that (5.42) requires knowledge of the noise variance.

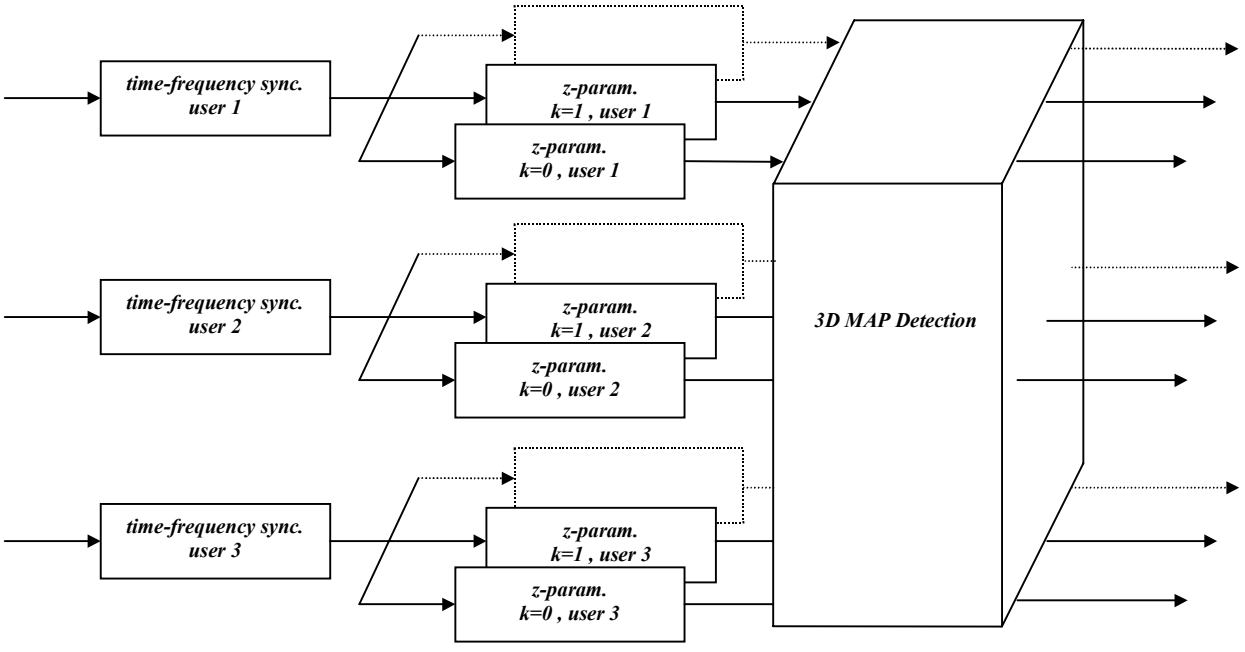

Fig. 5.2. Optimal MAP detection over a 3D trellis.

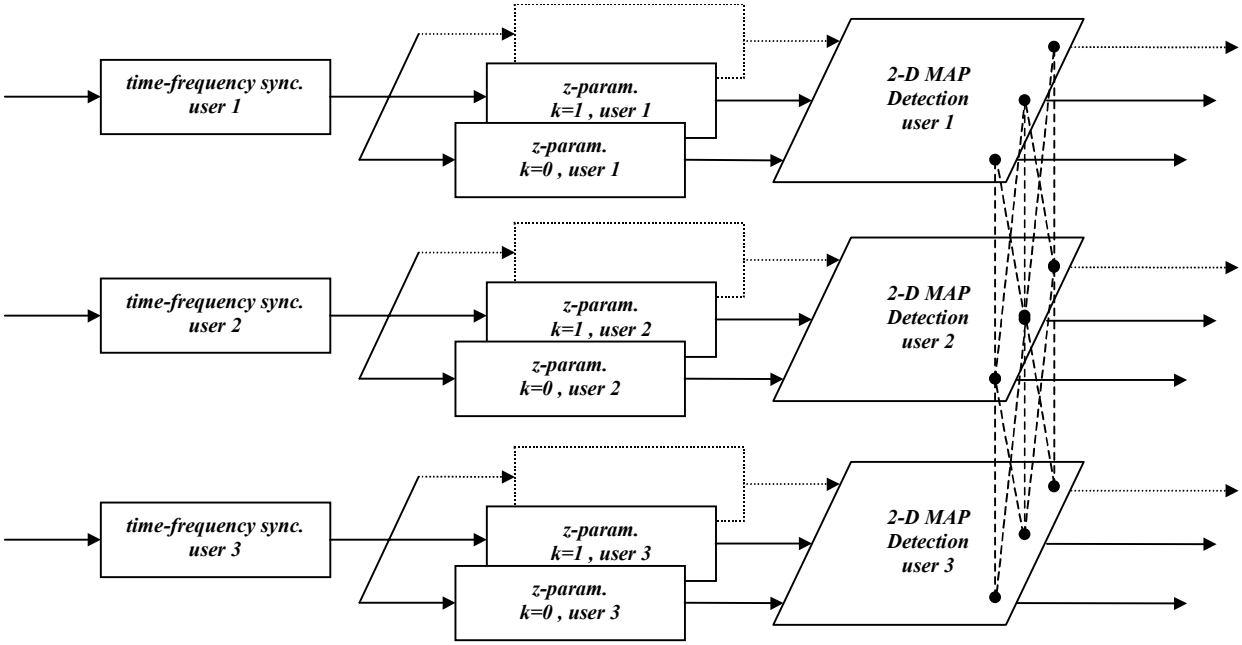

Fig. 5.3. Iterative per-user detection. Exchange of information takes place in the user direction.

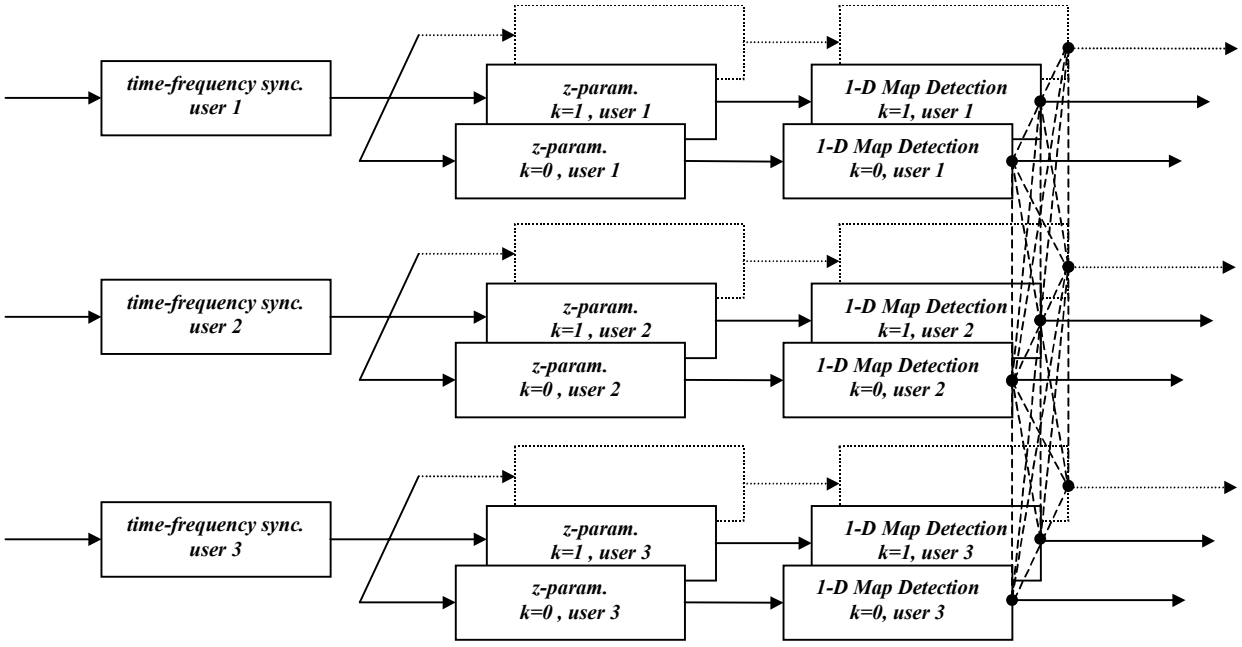

Fig. 5.4. Iterative per-carrier detection. Exchange of information takes place in the frequency and user direction.

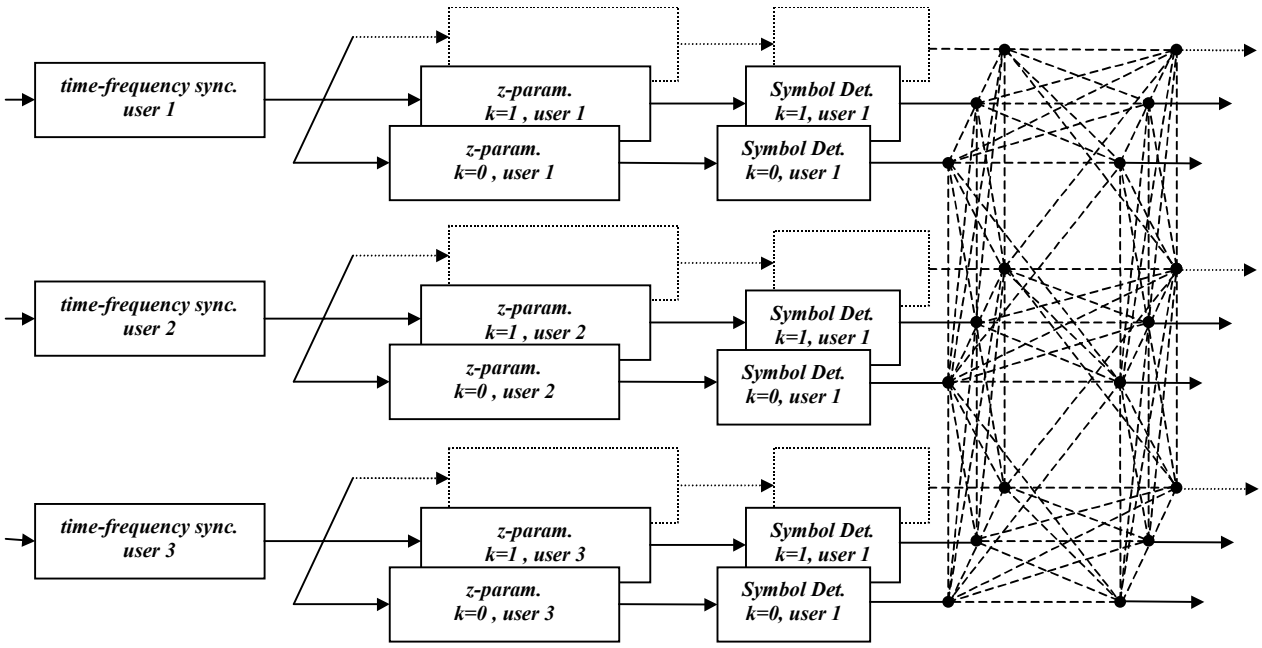

Fig. 5.5. Iterative per-symbol detection. Exchange of information takes place in the temporal, frequency, and user direction.

5.3 A Remark on the Asynchronism at Sub-channel Level

The optimal MAP multicarrier multiuser detector has been described by assuming that all sub-channels of a given user experience an identical frequency offset and time offset. Clearly, a simple modification to the notation can include the case of sub-channels of a given user having distinct frequency/time/phase offsets. This can be easily obtained by substituting Δf_u with $\Delta f_{u,k}$, $\Delta \phi_u$ with $\Delta \phi_{u,k}$, and Δt_u with $\Delta t_{u,k}$ (see Section 4.1.2). In such a case the derivation of the optimal detector is identical although it starts from the received signal model of equation (4.8 b). The algorithm and the metrics described in this chapter remain unchanged provided that the z-parameters and the s-parameters are written as follows:

$$z^{u,k}(lT_0) = e^{-j(2\pi f_k lT_0 + \Delta\phi_{u,k})} \int_I y(t) e^{-j2\pi \Delta f_{u,k} t} g_R^{u,k^*}(t - \Delta t_{u,k} - lT_0; t) dt \tag{5.6 b}$$

$$s^{u,u',k,k'}(lT_0, l'T_0) = \\ = e^{-j\left(2\pi (f_k lT_0 - f_{k'} l'T_0) + \Delta\phi_{u,k} - \Delta\phi_{u',k'}\right)} \int_I e^{-j2\pi(\Delta f_{u,k} - \Delta f_{u',k'})t} g_R^{u,k^*}(t - lT_0 - \Delta t_{u,k}; t) g_R^{u',k'}(t - l'T_0 - \Delta t_{u',k'}; t) dt \,. \tag{5.7 b}$$

We emphasize that our interest is to primarily investigate the asynchronism across users in discrete time implementations. It is also understood that the original notation does not exclude the case of asynchronism at both user and sub-channel level as explained in see Section 4.1.2.

APPENDIX TO CHAPTER 5

C Metric Derivation

We herein derive the metric in (5.5) and (5.8). We consider a static channel, which allows for simplified notation. The derivation for the more general time-variant channel is identical.

Let

$$Z(t) = \sum_{u=1}^{N_U} e^{j(2\pi\Delta f_u t + \Delta\phi_u)} \sum_{k=0}^{M-1} \sum_{l=-\infty}^{\infty} \hat{a}^{u,k}(lT_0) e^{j2\pi f_k lT_0} g_R^{u,k}(t - \Delta t_u - lT_0) \tag{C.1}$$

then the channel log-likelihood function (5.3) is decomposed as follows.

$$\Omega(\underline{\hat{a}}) = \int_I |y(t) - Z(t)|^2 \, dt = \int_I |y(t)|^2 \, dt - 2\,\mathrm{Re}\left\{ \int_I Z(t)^* y(t) dt \right\} + \int_I Z(t)^* Z(t) dt = A + B + C. \tag{C.2}$$

The terms A, B, C are defined as follows

$$A = \int_I |y(t)|^2 \, dt \tag{C.3}$$

$$\begin{aligned} B &= -2\,\mathrm{Re}\left\{ \sum_{lT_0 \in I} \sum_{u=1}^{N_U} \sum_{k=0}^{M-1} \hat{a}^{u,k}(lT_0)^* e^{-j2\pi f_k lT_0} e^{-j\Delta\phi_u} \int_I g_R^{u,k}(t - \Delta t_u - lT_0)^* e^{-j2\pi\Delta f_u t} y(t) dt \right\} \\ &= -2\,\mathrm{Re}\left\{ \sum_{lT_0 \in I} \sum_{u=1}^{N_U} \sum_{k=0}^{M-1} \hat{a}^{u,k}(lT_0)^* z^{u,k}(lT_0) \right\} \end{aligned} \tag{C.4}$$

with

$$z^{u,k}(lT_0) = e^{-j2\pi f_k lT_0} e^{-j\Delta\phi_u} \int_{-\infty}^{+\infty} y(t) e^{-j2\pi\Delta f_u t} g_R^{u,k}(t - \Delta t_u - lT_0)^* dt \tag{C.5}$$

$$\begin{aligned} C = \sum_{lT_0 \in I} \sum_{u=1}^{N_U} \sum_{k=0}^{M-1} \sum_{l'T_0 \in I} \sum_{u'=1}^{N_U} \sum_{k'=0}^{M-1} & (\hat{a}^{u,k}(lT_0)^* e^{-j2\pi f_k lT_0} e^{-j\Delta\phi_u} \hat{a}^{u',k'}(l'T_0) e^{j2\pi f_{k'} l'T_0} e^{j\Delta\phi_{u'}} \cdot \\ & \cdot \int_I e^{j2\pi(\Delta f_{u'} - \Delta f_u)t} g_R^{u,k}(t - \Delta t_u - lT_0)^* g_R^{u',k'}(t - \Delta t_{u'} - l'T_0) dt) \\ = \sum_{lT_0 \in I} \sum_{u=1}^{N_U} \sum_{k=0}^{M-1} \sum_{l'T_0 \in I} \sum_{u'=1}^{N_U} \sum_{k'=0}^{M-1} & \hat{a}^{u,k}(lT_0)^* \hat{a}^{u',k'}(l'T_0) s^{u,u',k,k'}(lT_0, l'T_0) \end{aligned} \tag{C.6}$$

with

$$\begin{aligned} & s^{u,u',k,k'}(lT_0, l'T_0) = \\ & = e^{-j2\pi(f_k lT_0 - f_{k'} l'T_0)} e^{-j(\Delta\phi_u - \Delta\phi_{u'})} \int_I e^{j2\pi(\Delta f_{u'} - \Delta f_u)t} g_R^{u,k}(t - \Delta t_u - lT_0)^* g_R^{u',k'}(t - \Delta t_{u'} - l'T_0) dt \cdot \end{aligned} \tag{C.7}$$

We can further partition C as follows

$$\begin{aligned} C = & \sum_{lT_0 \in I} \sum_{u=1}^{N_U} \sum_{k=0}^{M-1} \sum_{u'=1}^{N_U} \sum_{k'=0}^{M-1} \hat{a}^{u,k}(lT_0)^* \hat{a}^{u',k'}(lT_0) s^{u,u',k,k'}(lT_0, lT_0) + \\ & + \sum_{lT_0 \in I} \sum_{u=1}^{N_U} \sum_{k=0}^{M-1} \sum_{l'<l} \sum_{u'=1}^{N_U} \sum_{k'=0}^{M-1} \hat{a}^{u,k}(lT_0)^* \hat{a}^{u',k'}(l'T_0) s^{u,u',k,k'}(lT_0, l'T_0) + . \\ & + \sum_{lT_0 \in I} \sum_{u=1}^{N_U} \sum_{k=0}^{M-1} \sum_{l'<l} \sum_{u'=1}^{N_U} \sum_{k'=0}^{M-1} \hat{a}^{u,k}(l'T_0)^* \hat{a}^{u',k'}(lT_0) s^{u,u',k,k'}(l'T_0, lT_0) \end{aligned} \quad \text{(C.8)}$$

If we exchange u with u' and k with k' in the last term in (C.8), since $s^{u,u',k,k'}(lT_0, l'T_0) = s^{u',u,k',k^*}(l'T_0, lT_0)$, C becomes

$$\begin{aligned} C = & \sum_{lT_0 \in I} \sum_{u=1}^{N_U} \sum_{k=0}^{M-1} \sum_{u'=1}^{N_U} \sum_{k'=0}^{M-1} \hat{a}^{u,k}(lT_0)^* \hat{a}^{u',k'}(lT_0) s^{u,u',k,k'}(lT_0, lT_0) + \\ & + 2\,\mathrm{Re}\{ \sum_{lT_0 \in I} \sum_{u=1}^{N_U} \sum_{k=0}^{M-1} \sum_{l'<l} \sum_{u'=1}^{N_U} \sum_{k'=0}^{M-1} \hat{a}^{u,k}(lT_0)^* \hat{a}^{u',k'}(l'T_0) s^{u,u',k,k'}(lT_0, l'T_0) \} \end{aligned} . \quad \text{(C.9)}$$

Therefore, neglecting the constant term A, and summing up B and C, (5.4)-(5.5) follow.

To derive (5.8), we can further partition C as follows.

$$\begin{aligned} C = & \sum_{lT_0 \in I} \sum_{u=1}^{N_U} \sum_{k=0}^{M-1} \sum_{u'=1}^{N_U} \hat{a}^{u,k}(lT_0)^* \hat{a}^{u',k}(lT_0) s^{u,u',k,k}(lT_0, lT_0) + \\ & + \sum_{lT_0 \in I} \sum_{u=1}^{N_U} \sum_{k=0}^{M-1} \sum_{u'=1}^{N_U} \sum_{k'<k} (\hat{a}^{u,k}(lT_0)^* \hat{a}^{u',k'}(lT_0) s^{u,u',k,k'}(lT_0, lT_0) + \hat{a}^{u,k'}(lT_0)^* \hat{a}^{u',k}(lT_0) s^{u,u',k',k}(lT_0, lT_0)) \\ & + 2\,\mathrm{Re}\{ \sum_{lT_0 \in I} \sum_{u=1}^{N_U} \sum_{k=0}^{M-1} \sum_{l'<l} \sum_{u'=1}^{N_U} \sum_{k'=0}^{M-1} \hat{a}^{u,k}(lT_0)^* \hat{a}^{u',k'}(l'T_0) s^{u,u',k,k'}(lT_0, l'T_0) \} \end{aligned} \quad \text{(C.10)}$$

$$\begin{aligned} C = & \sum_{lT_0 \in I} \sum_{u=1}^{N_U} \sum_{k=0}^{M-1} \hat{a}^{u,k}(lT_0)^* \hat{a}^{u,k}(lT_0) s^{u,u,k,k}(lT_0, lT_0) + \\ & + \sum_{lT_0 \in I} \sum_{u=1}^{N_U} \sum_{k=0}^{M-1} \sum_{u'<u} (\hat{a}^{u,k}(lT_0)^* \hat{a}^{u',k}(lT_0) s^{u,u',k,k}(lT_0, lT_0) + \hat{a}^{u',k}(lT_0)^* \hat{a}^{u,k}(lT_0) s^{u',u,k,k}(lT_0, lT_0)) \\ & + \sum_{lT_0 \in I} \sum_{u=1}^{N_U} \sum_{k=0}^{M-1} \sum_{u'=1}^{N_U} \sum_{k'<k} (\hat{a}^{u,k}(lT_0)^* \hat{a}^{u',k'}(lT_0) s^{u,u',k,k'}(lT_0, lT_0) + \hat{a}^{u,k'}(lT_0)^* \hat{a}^{u',k}(lT_0) s^{u,u',k',k}(lT_0, lT_0)) \\ & + 2\,\mathrm{Re}\{ \sum_{lT_0 \in I} \sum_{u=1}^{N_U} \sum_{k=0}^{M-1} \sum_{l'<l} \sum_{u'=1}^{N_U} \sum_{k'=0}^{M-1} \hat{a}^{u,k}(lT_0)^* \hat{a}^{u',k'}(l'T_0) s^{u,u',k,k'}(lT_0, l'T_0) \} \end{aligned} \quad \text{(C.11)}$$

If we exchange u with u' in the third row in (C.11), and if we note that $s^{u,u',k,k}(lT_0, lT_0) = s^{u',u,k,k^*}(lT_0, lT_0)$, and $s^{u,u',k,k'}(lT_0, lT_0) = s^{u',u,k',k^*}(lT_0, lT_0)$, C becomes:

$$
\begin{aligned}
C = & \sum_{lT_0 \in I} \sum_{u=1}^{N_U} \sum_{k=0}^{M-1} \hat{a}^{u,k}(lT_0)^* \hat{a}^{u,k}(lT_0) s^{u,u,k,k}(lT_0, lT_0) + \\
& + 2\,\mathrm{Re}\{\sum_{lT_0 \in I} \sum_{u=1}^{N_U} \sum_{k=0}^{M-1} \sum_{u'<u} (\hat{a}^{u,k}(lT_0)^* \hat{a}^{u',k}(lT_0) s^{u,u',k,k}(lT_0, lT_0)\} \\
& + 2\,\mathrm{Re}\{\sum_{lT_0 \in I} \sum_{u=1}^{N_U} \sum_{k=0}^{M-1} \sum_{u'=1}^{N_U} \sum_{k'<k} (\hat{a}^{u,k}(lT_0)^* \hat{a}^{u',k'}(lT_0) s^{u,u',k,k'}(lT_0, lT_0)\} \\
& + 2\,\mathrm{Re}\{\sum_{lT_0 \in I} \sum_{u=1}^{N_U} \sum_{k=0}^{M-1} \sum_{l'<l} \sum_{u'=1}^{N_U} \sum_{k'=0}^{M-1} \hat{a}^{u,k}(lT_0)^* \hat{a}^{u',k'}(l'T_0) s^{u,u',k,k'}(lT_0, l'T_0)\}
\end{aligned}
\quad . \qquad \text{(C.12)}
$$

Equation (C.12) corresponds to (5.8).

6 IMPLEMENTATION OF THE FRONT-END RECEIVER FOR MULTICARRIER-USER DETECTION

We have shown that the optimal multicarrier-user detector comprises a front-end structure where the z-s-parameters are computed, followed by a maximum a posteriori processor. We herein investigate in more detail the front-end receiver part. We consider both analog and discrete-time implementations for both static and time-variant channels. It is shown that in FMT-MA systems the resulting front-end architecture is efficiently implemented through discrete-time polyphase filter banks followed by discrete Fourier transforms.

6.1 Computation of the z-parameters and s-parameters

In this chapter we focus on the calculation of the z and s parameters that are required for optimal multicarrier-user detection. Both static and time-variant channels are considered. We start from an analog implementation and then we address the discrete-time implementation that is suited for application in MT-MA systems. We assume that the time offsets, the frequency offsets, and the channel impulse responses are known.

6.2 Analog Implementation in Static Channels

In this section we consider a static channel impulse response and the deployment of analog filters.

6.2.1 Matched Filter Outputs

Assuming a static channel impulse response, the matched filter output (z-parameter) at time $t' \in R$ can be evaluated in several alternative forms as illustrated in Fig. 6.1. Recall that the equivalent sub-channel impulse response $g_R^{u,k}(t)$ is obtained by the concatenation of the sub-channel transmit filter, the broadband transmit filter, and the channel impulse response. The alternative forms are obtained by exchanging the order of the convolutions.

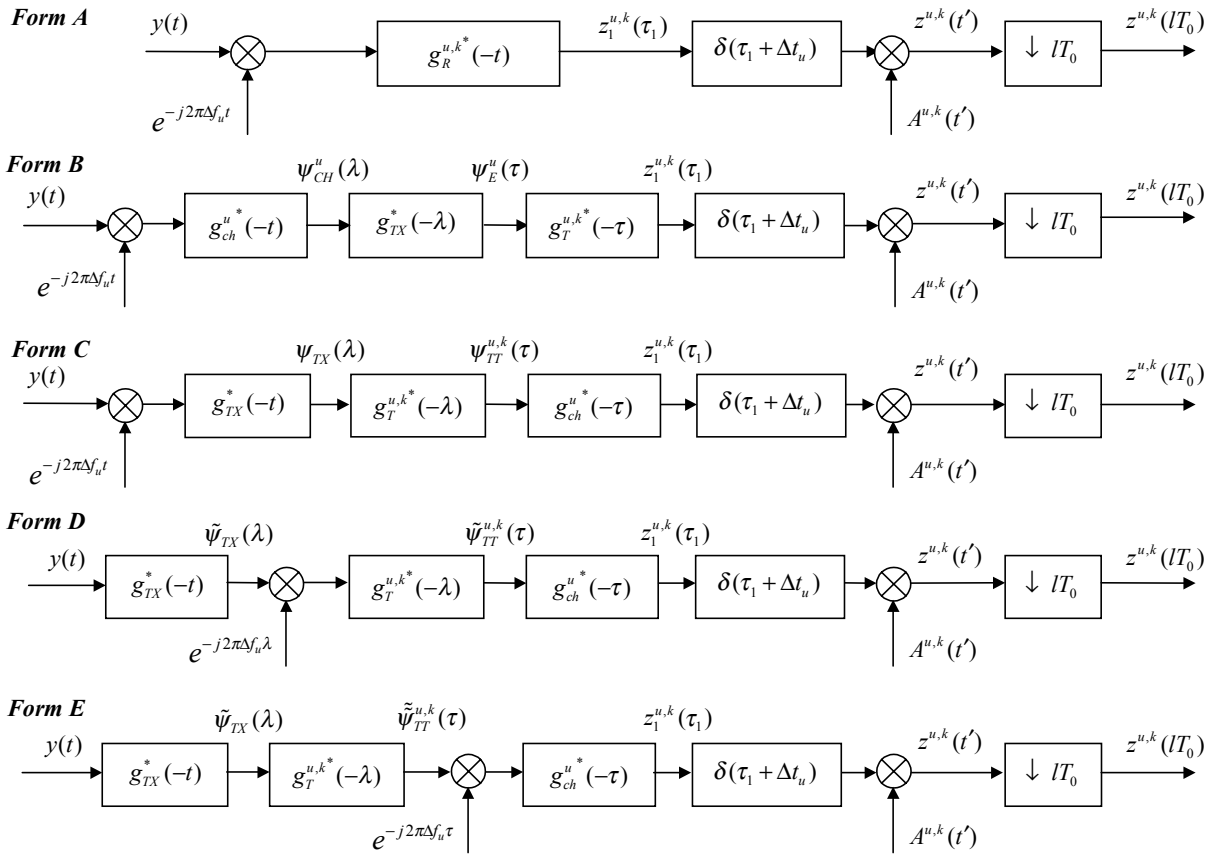

Fig. 6.1. Alternative front-end receiver structures. *Form D* and *E* hold for $\Delta f_u \ll 1/T$ and $\Delta f_u \ll 1/T_1$.

To start, let us define $A^{u,k}(t')$, with $t' \in R$, as follows[15]

$$A^{u,k}(t') = e^{-j(2\pi f_k \lfloor t'/T_0 \rceil T_0 + \Delta\phi_u)}. \tag{6.1}$$

Form A. Sub-channel impulse response matched filtering, i.e.,

$$z^{u,k}(t') = A^{u,k}(t') \int_{t\in I} y(t) e^{-j2\pi\Delta f_u t} g_R^{u,k^*}(t - \Delta t_u - t')dt. \tag{6.2}$$

That is, the z-parameter $z^{u,k}(t')$ is obtained by matched filtering the frequency offset compensated input signal, $y(t)e^{-j2\pi\Delta f_u t}$, with the equivalent *k-th* sub-channel impulse response of user *u*, followed by time offset compensation and multiplication with the factor $A^{u,k}(t')$.

Form B. Channel matched filtering, followed by broadband transmit pulse matched filtering and sub-channel transmit pulse matched filtering, i.e.,

$$z^{u,k}(t') = A^{u,k}(t') \int_{\tau\in R} g_T^{u,k^*}(\tau) \underbrace{\int_{\lambda\in R} g_{TX}^*(\lambda-\tau) \underbrace{\int_{t\in I} y(t) e^{-j2\pi\Delta f_u t} g_{ch}^{u^*}(t - \Delta t_u - t' - \lambda)dt}_{\psi_{CH}^u(\lambda+t'+\Delta t_u)} d\lambda}_{\psi_E^u(\tau+t'+\Delta t_u)} d\tau. \tag{6.3}$$

[15] We denote with $\lfloor t \rceil$ the closest integer to t.

This form is simply obtained by substituting in (6.2) the definition of $g_R^{u,k}(t)$.

Form C. Broadband transmit pulse matched filtering, followed by sub-channel transmit pulse matched filtering and channel matched filtering i.e.,

$$z^{u,k}(t') = A^{u,k}(t') \int_{\tau \in R} g_{ch}^{u\,*}(\tau) \underbrace{\int_{\lambda \in R} g_T^{u,k\,*}(\lambda - \tau) \underbrace{\int_{t \in I} y(t) e^{-j2\pi \Delta f_u t} g_{TX}^*(t - \Delta t_u - t' - \lambda) dt}_{\psi_{TX}(\lambda + t' + \Delta t_u)} d\lambda}_{\psi_{TT}^{u,k}(\tau + t' + \Delta t_u)} d\tau . \quad (6.4)$$

Form D. Under the assumption of frequency offsets much smaller than the bandwidth of the broadband transmit filter, i.e., $\Delta f_u \ll 1/T$ for all u, the frequency offset compensation can take place after filtering with a fixed pulse matched to the broadband transmit filter[16], i.e.,

$$z^{u,k}(t') \approx A^{u,k}(t') \int_{\tau \in R} g_{ch}^{u\,*}(\tau) \underbrace{\int_{\lambda \in R} g_T^{u,k\,*}(\lambda - \tau) e^{-j2\pi \Delta f_u (\lambda + t' + \Delta t_u)} \underbrace{\int_{t \in I} y(t) g_{TX}^*(t - \Delta t_u - t' - \lambda) dt}_{\tilde{\psi}_{TX}(\lambda + t' + \Delta t_u)} d\lambda}_{\tilde{\psi}_{TT}^{u,k}(\tau + t' + \Delta t_u)} d\tau . \quad (6.5)$$

Form E. Under the assumption of frequency offsets much smaller than the bandwidth of the sub-channel transmit filter, i.e., $\Delta f_u \ll 1/T_1$ for all u, the frequency offset compensation can take place after filtering with a fixed pulse matched to the concatenation of the broadband transmit filter with the sub-channel transmit filter, i.e.,

$$z^{u,k}(t') \approx A^{u,k}(t') \int_{\tau \in R} g_{ch}^{u\,*}(\tau) e^{-j2\pi \Delta f_u (\tau + t' + \Delta t_u)} \underbrace{\int_{\lambda \in R} g_T^{u,k\,*}(\lambda - \tau) \underbrace{\int_{t \in I} y(t) g_{TX}^*(t - \Delta t_u - t' - \lambda) dt}_{\tilde{\psi}_{TX}(\lambda + t' + \Delta t_u)} d\lambda}_{\tilde{\psi}_{TT}^{u,k}(\tau + t' + \Delta t_u)} d\tau . \quad (6.6)$$

It is clear that the assumption of $\Delta f_u \ll 1/T$ typically holds in a single user scenario where a coarse frequency synchronization stage, in the receiver front end, takes care of compensating large frequency offsets in the order or in excess of the transmission rate $1/T$. In a multiuser scenario this assumption requires more stringent requirements on the oscillators precision. Although the assumption of $\Delta f_u \ll 1/T_1$ may theoretically hold, it may be too heavy in practical scenarios.

To proceed let us assume a static tapped delay line channel model with taps spaced by multiples of $T_c = T/K$ with $K \geq 1$, i.e., $g_{ch}^u(\tau) = \sum_{p=0}^{N_P} \alpha^u(p) \delta(\tau - pT_c)$. Then, from Form C we obtain

[16] For $\Delta f_u T \ll 1$ we have $\int_{t \in I} y(t) e^{-j2\pi \Delta f_u t} g_{TX}^*(t - \gamma) dt = e^{-j2\pi \Delta f_u \gamma} \int_{t \in I} y(t) e^{-j2\pi \Delta f_u (t - \gamma)} g_{TX}^*(t - \gamma) dt \approx e^{-j2\pi \Delta f_u \gamma} \int_{t \in I} y(t) g_{TX}^*(t - \gamma) dt$.

$$z^{u,k}(t') = A^{u,k}(t')\sum_{p=0}^{N_P} \alpha^{u^*}(p)\psi_{TT}^{u,k}(t' + pT_c + \Delta t_u) \tag{6.7}$$

or equivalently

$$z^{u,k}(t') = A^{u,k}(t')\sum_{p=0}^{N_P} \alpha^{u^*}(p)\int_{\lambda\in R} g_T^{u,k^*}(\lambda)\psi_{TX}(\lambda + t' + pT_c + \Delta t_u)d\lambda \tag{6.8}$$

In the hypothesis of small frequency offsets, i.e., $\Delta f_u \ll 1/T$, we can write

$$z^{u,k}(t') = A^{u,k}(t')\sum_{p=0}^{N_P} \alpha^{u^*}(p)\int_{\lambda\in R} g_T^{u,k^*}(\lambda)e^{-j2\pi\Delta f_u(\lambda+t'+pT_c+\Delta t_u)}\tilde{\psi}_{TX}(\lambda + t' + pT_c + \Delta t_u)d\lambda\,. \tag{6.9}$$

The last expression is interesting because it says that we can first to matched filtering with a static pulse matched to the broadband transmit filter. Then, we perform frequency and time offset compensation. Finally, we do sub-channel transmit pulse matched filtering and ray combining.

6.2.2 Cross-Correlations

The cross-correlation between two sub-channels (s-parameter) can be evaluated in the following alternative forms. Let us define

$$B^{u,u',k,k'}(t',t'') = e^{-j\left(2\pi(f_k\lfloor t'/T_0\rfloor T_0 - f_{k'}\lfloor t''/T_0\rfloor T_0)+\Delta\phi_u-\Delta\phi_{u'}\right)} \tag{6.10}$$

with $t' \in R$, and $t'' \in R$.

Form A. Direct cross correlation, i.e.,

$$s^{u,u',k,k'}(t',t'') = B^{u,u',k,k'}(t',t'')\int_{t\in I} e^{-j2\pi(\Delta f_u-\Delta f_{u'})t} g_R^{u,k^*}(t-t'-\Delta t_u)g_R^{u',k'}(t-t''-\Delta t_{u'})dt\,. \tag{6.11}$$

The s-parameter is obtained by evaluating the cross correlation among two given sub-channel impulse responses $g_R^{u,k}(t)$ with appropriate frequency and time offset compensation. The evaluation of (6.11) requires the estimation of the equivalent sub-channel impulse responses.

Form B. Transmit filter cross-correlation followed by channel cross correlation, i.e.,

$$s^{u,u',k,k'}(t',t'') = B^{u,u',k,k'}(t',t'')\int_{t\in I} e^{-j2\pi(\Delta f_u-\Delta f_{u'})t}\int_{\tau\in R} g_T^{u,k^*}(t-t'-\Delta t_u-\tau)g_E^{u}(\tau)d\tau\int_{\tau'\in R} g_T^{u',k'}(t-t''-\Delta t_{u'}-\tau')g_E^{u'}(\tau')d\tau' dt$$

$$= B^{u,u',k,k'}(t',t'')\int_R g_E^{u}(\tau)\int_R g_E^{u'}(\tau')\underbrace{\int_I e^{-j2\pi(\Delta f_u-\Delta f_{u'})t} g_T^{u,k^*}(t-t'-\Delta t_u-\tau)g_T^{u',k'}(t-t''-\Delta t_{u'}-\tau')dt}_{\kappa_T^{u,u',k,k'}(t''+\Delta t_{u'}+\tau'-t'-\Delta t_u-\tau)} d\tau d\tau'\,. \tag{6.12}$$

The evaluation of (6.12) requires the estimation of the channel impulse responses, and the knowledge of the cross-correlation of the sub-channel transmit filters. Recall that $g_E^u(t)$ corresponds to the concatenation of the broadband transmit pulse with the channel impulse

response.

Form C. Channel cross correlation followed by transmit filter cross-correlation, i.e.,

$$s^{u,u',k,k'}(t',t'') = B^{u,u',k,k'}(t',t'') \int_{t\in I} e^{-j2\pi(\Delta f_u - \Delta f_{u'})t} \int_{\tau\in R} g_T^{u,k^*}(\tau) g_E^{u}(t-t'-\Delta t_u-\tau)d\tau \int_{\tau'\in R} g_T^{u',k'}(\tau') g_E^{u'}(t-t''-\Delta t_{u'}-\tau')d\tau' dt$$

$$= B^{u,u',k,k'}(t',t'') \int_R g_T^{u,k}(\tau) \int_R g_T^{u',k'}(\tau') \underbrace{\int_I e^{-j2\pi(\Delta f_u - \Delta f_{u'})t} g_E^{u^*}(t-t'-\Delta t_u-\tau) g_E^{u'}(t-t''-\Delta t_{u'}-\tau')dt}_{\kappa_E^{u,u'}(t''+\Delta t_{u'}+\tau'-t'-\Delta t_u-\tau)} d\tau d\tau' . \quad (6.13)$$

The above expressions can be further manipulated in the hypothesis of assuming a tapped delay line channel model and small frequency offsets.

6.3 Digital Implementation in Static Channels

So far we have considered signals defined in the real domain, i.e., continuous time signals. We are here interested on describing discrete-time processing. We implicitly assume to deal with a multitone multiple access system that deploys discrete-time transmit pulses $g_T^{u,k}(iT)$.

Let us assume at the receiver side an A/D converter with rate $1/T_c$, and $T_c=T/K$. Then, if we define the time delay as $\Delta t_u = p_u T_c + \varepsilon_u$, with p_u integer and ε_u a fraction of T_c, the discrete-time received signal component that belongs to user u is

$$y^u(nT_c) = e^{j(2\pi\Delta f_u nT_c + \Delta\phi_u)} \sum_{k=0}^{M-1} \sum_{l=-\infty}^{\infty} a^{u,k}(lT_0) e^{j2\pi f_k lT_0} g_R^{u,k}(nT_c - p_u T_c - \varepsilon_u - lT_0) \quad (6.14)$$

where the *k-th* sub-channel equivalent impulse response has been defined in (4.11).

Note that the choice of $K>1$ allows representing more accurately the continuos time channel impulse response and coping with fractional time delays.

6.3.1 Digital Computation of the z-parameters

The calculation of the z-parameters can be done digitally by extending the results of Section 6.2. For instance, Form A becomes

$$z^{u,k}(lT_0) = A^{u,k}(lT_0) \sum_{nT_c\in I} T_c y(nT_c) e^{-j2\pi\Delta f_u nT_c} g_R^{u,k^*}(nT_c - lT_0 - p_u T_c - \varepsilon_u) . \quad (6.15)$$

If we consider a tapped delay line channel model and we assume to include in it the fractional time delay, we can manipulate (6.8) to yield

$$z^{u,k}(lT_0) = A^{u,k}(lT_0) \sum_{p=0}^{N_P} \alpha^{u^*}(p) \sum_{iT\in R} T g_T^{u,k^*}(iT) \psi_{TX}(iT + lT_0 + pT_c + p_u T_c) . \quad (6.16)$$

Note that $\psi_{TX}(nT_c)$ can be obtained by filtering the frequency offset compensated input signal with an analog filter matched to the broadband transmit filter and sampling the output at rate $1/T_c$. If we assume small frequency offsets the temporal and frequency compensation can take place after matched filtering. This is illustrated in Fig. 6.2 and Fig. 6.3. Finally, discrete-time filtering with the sub-channel transmit filter takes place at rate $1/T$.

In FMT-MA the front-end can be more efficiently implemented as we will show.

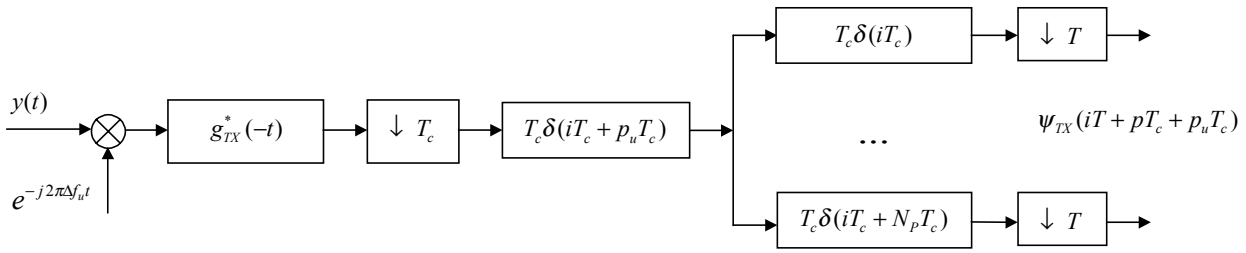

Fig. 6.2. Pre-filtering with pulse matched to the broadband transmit filter after frequency offset compensation.

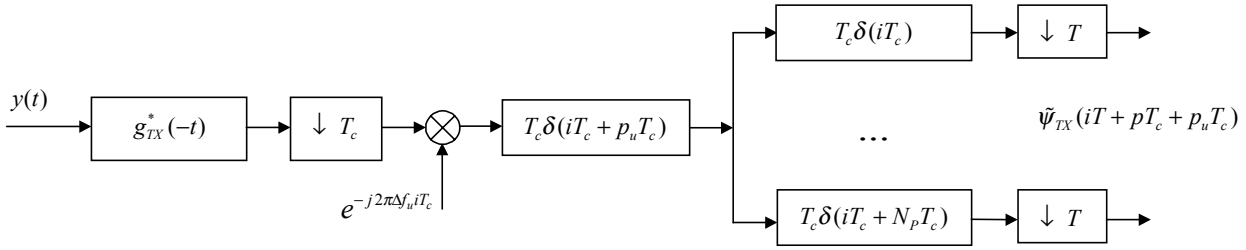

Fig. 6.3. Pre-filtering with pulse matched to the broadband transmit filter followed by frequency offset compensation in the presence of frequency offsets much smaller than $1/T$.

6.3.2 Digital Computation of the s-parameters

The digital computation of the s-parameters is simply obtained by the discrete-time implementation of (6.11)-(6.13). For instance (6.11) becomes

$$s^{u,u',k,k'}(lT_0, l'T_0) = \\ = B^{u,u',k,k'}(lT_0, l'T_0) \sum_{nT_c \in I} e^{-j2\pi(\Delta f_u - \Delta f_{u'})nT_c} g_R^{u,k^*}(nT_c - lT_0 - p_u T_c - \varepsilon_u) g_R^{u',k'}(nT_c - l'T_0 - p_{u'} T_c - \varepsilon_{u'}). \quad (6.17)$$

According to (6.17), we first compute (estimate) the equivalent sub-channel impulse responses. Then, we run the discrete-time cross correlation among a pair of equivalent sub-channel impulse responses. The evaluation is done at rate $1/T_c$.

6.3.3 Digital Computation of the z-parameters in FMT-MA

The front-end receiver architecture is greatly simplified in an FMT-MA system. In fact, if we assume uniformly spaced sub-carriers and identical transmit filters, the sub-channel transmit filter is $g_T^{u,k}(iT) = g(iT)e^{j2\pi/M ik}$ from (6.16) we obtain

$$z^{u,k}(lT_0) = e^{-j\Delta\phi_u}\sum_{p=0}^{N_P}\alpha^{u^*}(p)\sum_{iT\in R} Te^{-j\frac{2\pi}{M}ik} g^*(iT - lT_0)\psi_{TX}(iT + pT_c + p_uT_c) \tag{6.18}$$

$$z^{u,k}(lT_0) = e^{-j\Delta\phi_u}\sum_{p=0}^{N_P}\alpha^{u^*}(p)\sum_{n=0}^{M-1}\frac{1}{M}e^{-j\frac{2\pi}{M}nk}\sum_{m=-\infty}^{\infty} T_1 g^{n^*}(mT_1 - lT_0)\psi_{TX}^n(mT_1 + pT_c + p_uT_c) \tag{6.19}$$

where $g^n(mT_1 - lT_0) = g(mT_1 - lT_0 + nT)$ and $\psi_{TX}^n(mT_1 + pT_c + p_uT_c) = \psi_{TX}(mT_1 + pT_c + p_uT_c + nT)$. Let us define the index relations

$$\overline{p}(l) = l \text{ div } M \tag{6.20}$$

$$\overline{q}(l) = l \text{ mod } M\,. \tag{6.21}$$

Then, $g^n(mT_1 - lT_0) = g^n(mT_1 - \overline{p}(lN)T_1 - \overline{q}(lN)T)$. With the change of variable $m - \overline{p} \to m$ we get

$$z^{u,k}(lT_0) = e^{-j\Delta\phi_u}\sum_{p=0}^{N_P}\alpha^{u^*}(p)\sum_{n=0}^{M-1}\frac{1}{M}e^{-j\frac{2\pi}{M}nk}\underbrace{\sum_{m=-\infty}^{\infty} T_1 g^{n^*}(mT_1, lT_0)\psi_{TX}^n(mT_1 + \overline{p}(lN)T + pT_c + p_uT_c)}_{\psi_{TT}^{u,n}(\overline{p}(lN)T + pT_c + p_uT_c)} \tag{6.22}$$

where

$$g^n(mT_1, lT_0) = g^n(mT_1 - \overline{q}(lN)T) \tag{6.23}$$

is the (periodic) time-variant filter matched to the time-variant sub-channel transmit filter. The resulting front-end is depicted in Fig. 6.4. Note that the overall front-end structure is obtained by deploying N_U modules identical to the one shown in Fig. 6.4, i.e., one module per active user. Therefore, the total number of outputs can go up to MN_U. The front-end comprises a stage where the channel echoes are coherently combined, followed by a S/P conversion stage, then by a bank of time-variant transmit pulse matched filters, and finally by a DFT stage.

If we further consider a critically sampled FMT system, i.e., M=N and T_1=T_0, (6.22) simplifies to

$$z^{u,k}(lT_0) = e^{-j\Delta\phi_u}\sum_{p=0}^{N_P}\alpha^{u^*}(p)\sum_{n=0}^{N-1}\frac{1}{N}e^{-j\frac{2\pi}{N}nk}\sum_{m=-\infty}^{\infty} T_0 g^{n^*}(mT_0 - lT_0)\psi_{TX}^n(mT_0 + lT_0 + pT_c + p_uT_c)\,. \tag{6.24}$$

Several resulting receiver front-end structures are depicted in Fig. 6.5-Fig. 6.7. They have been obtained by exchanging the order of the summations. Although the implementation that corresponds to Fig. 6.7 is the more complex it has the advantage of requiring combining of the channel taps after

the DFT. This may be helpful when implementing the channel estimator.

It is interesting to note that the structures above resembles a CDMA RAKE receiver [48]. In fact the channel rays are coherently combined and then processed to generate M narrow band sub-channels.

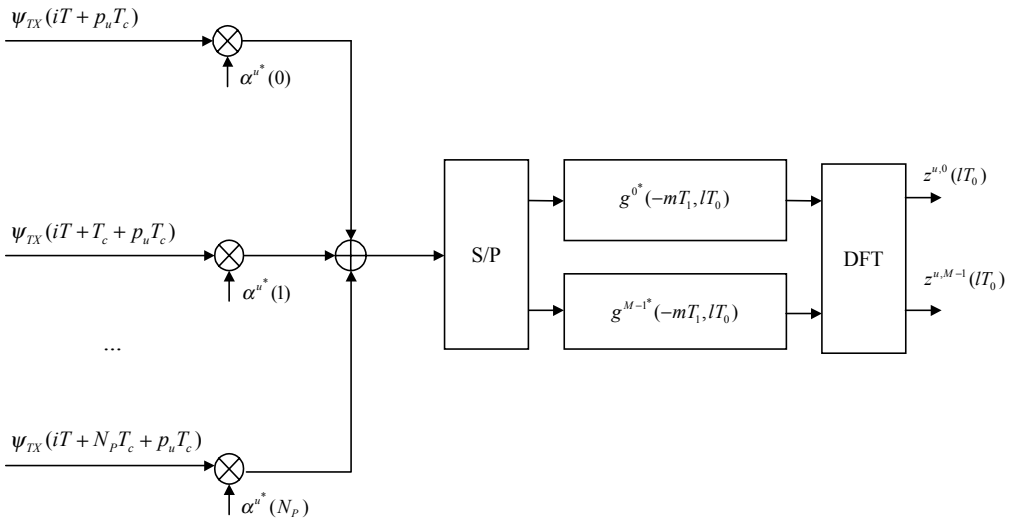

Fig. 6.4. Digital front-end receiver for NCS-FMT-MA. Only the portion relative to user u is shown. Ray combining, matched to transmit pulse filtering, and DFT.

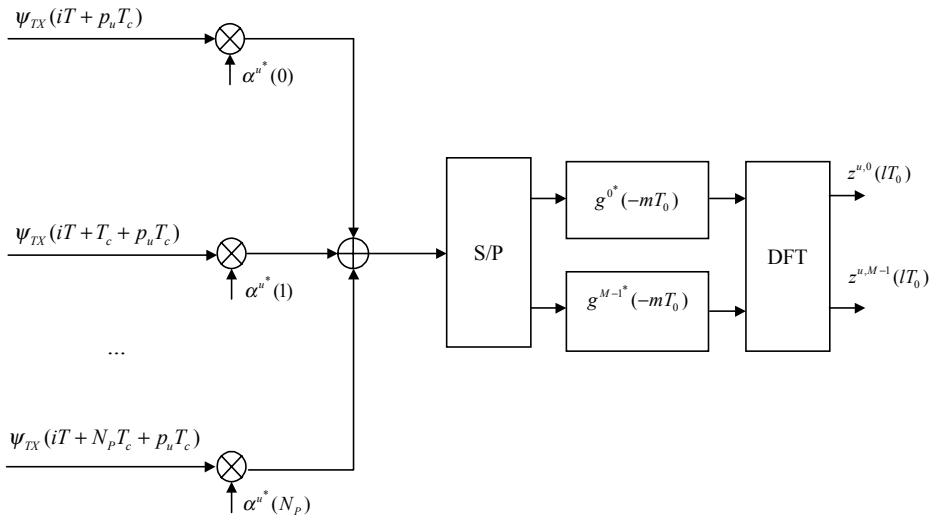

Fig. 6.5. Digital front-end receiver for CS-FMT-MA. Only the portion relative to user u is shown. Ray combining, matched to transmit pulse filtering, and DFT.

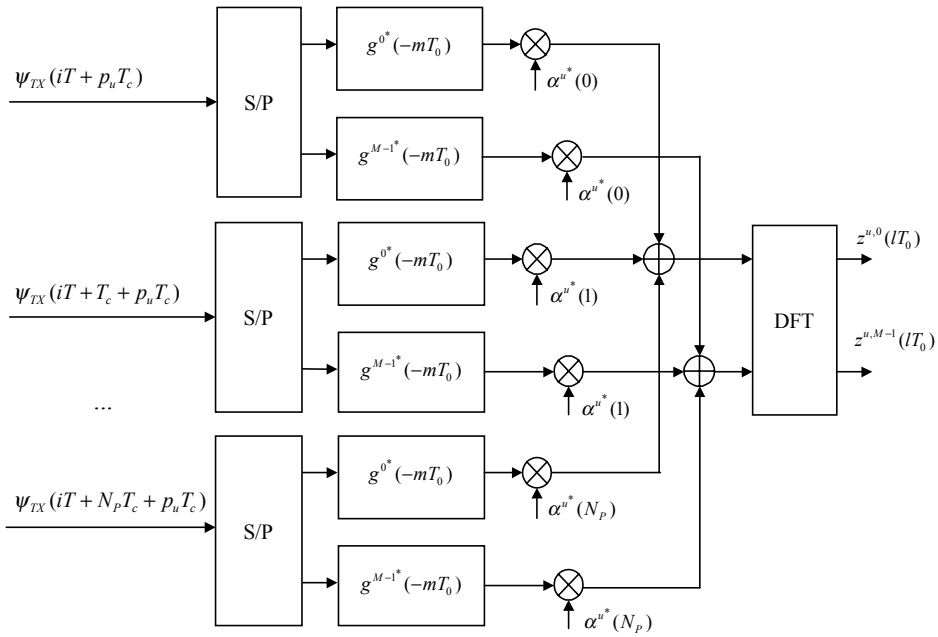

Fig. 6.6. Digital front-end receiver for CS-FMT-MA. Only the portion relative to user *u* is shown. Matched to transmit pulse filtering, ray combining, and DFT.

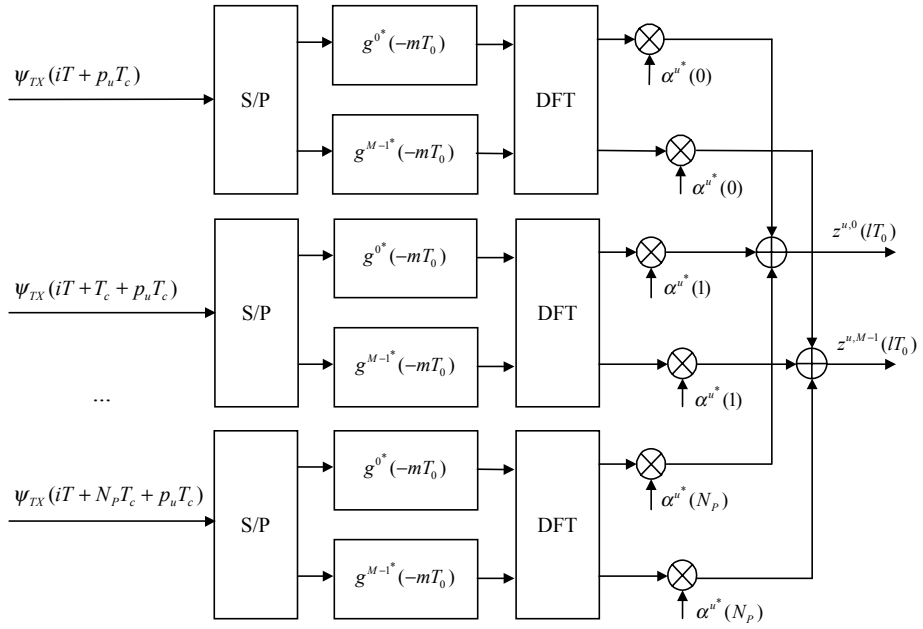

Fig. 6.7. Digital front-end receiver for CS-FMT-MA. Only the portion relative to user *u* is shown. Matched to transmit pulse filtering, DFT, and ray combining. One DFT per resolvable channel echo.

6.3.4 Digital Computation of the z-parameters in DMT-MA

Transmit sub-channel filtering does not take place when we deploy rectangular filters (DMT). For instance with reference to Fig. 6.5, the DFT follows immediately after ray combining.

6.3.5 Digital Computation of the s-parameters in FMT-MA

With reference to (6.17), with FMT-MA the s-parameter can be evaluated as follows.

$$s^{u,u',k,k'}(lT_0,l'T_0)=B^{u,u',k,k'}(lT_0,l'T_0)\sum_{n=0}^{M-1}\sum_{n'=0}^{M-1}e^{-j\frac{2\pi}{M}kn}e^{j\frac{2\pi}{M}k'n'}\cdot \\ \cdot\sum_{m=-\infty}^{\infty}\sum_{m'=-\infty}^{\infty}g^{n*}(mT_1)g^{n'}(m'T_1)\kappa_E^{u,u'}(mT_1+lT_0+nT;m'T_1+l'T_0+n'T) \tag{6.25}$$

$$\kappa_E^{u,u'}(mT;m'T)=\sum_{nT_c\in I}e^{-j2\pi(\Delta f_u-\Delta f_{u'})nT_c}g_E^{u*}(nT_c-p_uT_c-\varepsilon_u-mT)g_E^{u'}(nT_c-p_{u'}T_c-\varepsilon_{u'}-m'T)\,. \tag{6.26}$$

According to (6.26) we can first compute the channels cross-correlations at rate *1/T*$_c$. Then, we sample the channel cross-correlation at rate *1/T*. Finally we evaluate (6.25).

Further manipulations are possible when for instance we consider a tap delay line channel model.

6.4 Analog Implementation in Time-Variant Channels

6.4.1 Matched Filter Outputs

In the presence of a time-variant channel impulse response the matched filter output (z-parameter) at time *t′*, can be evaluated in several alternative forms. It should be noted that when dealing with time-variant channels we can't apply transmit pulse matched filtering before channel matched filtering. If the channel variation is small for the duration of the sub-channel transmit pulse, i.e. $g_E^u(\tau;t)\approx g_E^u(\tau;(k+1/2)T_0)$ for $kT_0\le\tau\le(k+1)T_0$, we can apply the results found in quasi-static channels, and permute the order of matched filtering.

Form A. Equivalent sub-channel matched filtering, i.e.,

$$z^{u,k}(t')=A^{u,k}(t')\int_I y(t)e^{-j2\pi\Delta f_u t}g_R^{u,k*}(t-\Delta t_u-t';t)dt\,. \tag{6.27}$$

That is, the z-parameter $z^{u,k}(t')$ is obtained by matched filtering the frequency offset compensated input signal, $y(t)e^{-j2\pi\Delta f_u t}$, with the equivalent *k-th* sub-channel time-variant impulse response of user *u*, $g_R^{u,k*}(-\tau-\Delta t_u;t)$, and multiplying it by the factor $A^{u,k}(t')$.

Form B. Channel matched filtering, followed by broadband pulse matched filtering and sub-channel pulse matched filtering, i.e.,

$$z^{u,k}(t') = A^{u,k}(t') \int_{\tau\in R} g_T^{u,k^*}(\tau) \underbrace{\int_{\lambda\in R} g_{TX}^*(\lambda-\tau) \underbrace{\int_{t\in I} y(t) e^{-j2\pi\Delta f_u t} g_{ch}^{u\,*}(t-\Delta t_u - t' - \lambda; t) dt}_{\psi_{CH}^u(\lambda+t'+\Delta t_u)} d\lambda}_{\psi_E^u(\tau+t'+\Delta t_u)} d\tau \,. \quad (6.28)$$

Form C. If we assume the channel to be static for the duration of the broadband transmit filter[17] we can revert the order of matched filtering between the channel and the broadband transmit filter, i.e.,

$$z^{u,k}(t') = A^{u,k}(t') \int_{\tau\in R} g_T^{u,k^*}(\tau) \int_{\lambda\in R} g_{ch}^{u\,*}(\lambda-\tau; \Delta t_u + t' + \lambda) \underbrace{\int_{t\in I} y(t) e^{-j2\pi\Delta f_u t} g_{TX}^*(t-\Delta t_u - t' - \lambda) dt}_{\psi_{TX}(\lambda+t'+\Delta t_u)} d\lambda d\tau \,. \quad (6.29)$$

Under the hypothesis of small frequency offsets the associated compensation can be done after broadband pulse matched filtering.

To proceed let us assume a time-variant tapped delay line channel model with taps spaced by multiples of $T_c = T/K$ with $K > 1$, i.e., $g_{ch}^u(\lambda; t) = \sum_{p=0}^{N_P} \alpha^u(p; t)\delta(\lambda - pT_c)$. Then, under the hypothesis of Form C we obtain

$$z^{u,k}(t') = A^{u,k}(t') \sum_{p=0}^{N_P} \int_{\tau\in R} g_T^{u,k^*}(\tau) \alpha_u^*(p; \tau + t' + \Delta t_u + pT_c) \psi_{TX}(\tau + t' + \Delta t_u + pT_c) d\tau \,. \quad (6.30)$$

6.4.2 Cross-correlations

Form A. Direct cross correlation, i.e.,

$$s^{u,u',k,k'}(t', t'') = B^{u,u',k,k'}(t', t'') \int_I e^{-j2\pi(\Delta f_u - \Delta f_{u'})t} g_R^{u,k^*}(t - t' - \Delta t_u; t) g_R^{u',k'}(t - t'' - \Delta t_{u'}; t) dt \,. \quad (6.31)$$

The s-parameter is obtained by evaluating the cross correlation among two given impulse responses $g_R^{u,k}(t)$ with appropriate frequency and time offset compensation. The evaluation of (6.31) requires the estimation of the equivalent sub-channel impulse responses.

Form B. Channels cross correlation followed by sub-channel transmit filter cross-correlation, i.e.,

$$s^{u,u',k,k'}(t', t'') = B^{u,u',k,k'}(t', t'') \int_{\tau\in R} g_T^{u,k}(\tau) \int_{\tau'\in R} g_T^{u',k'}(\tau') \underbrace{\int_I e^{-j2\pi(\Delta f_u - \Delta f_{u'})t} g_E^{u\,*}(t - t' - \Delta t_u - \tau; t) g_E^{u'}(t - t'' - \Delta t_{u'} - \tau'; t) dt}_{\kappa_E^{u,u'}(t'+\Delta t_u+\tau; t''+\Delta t_{u'}+\tau')} d\tau d\tau' \,. \quad (6.32)$$

[17] The duration of the broadband transmit filter can be assumed to be about *T*. However, here we assume the channel might change over the duration of the sub-channel transmit filters that is equal to or larger than *NT*.

6.5 Digital Implementation in Time-Variant Channels

We here consider the digital implementation of the front-end receiver in time-variant channels. The discrete-time received component that belongs to user *u* is

$$y(nT_c) = e^{j(2\pi\Delta f_u nT_c + \Delta\phi_u)} \sum_{k=0}^{M-1} \sum_{l=-\infty}^{\infty} a^{u,k}(lT_0) e^{j2\pi f_k lT_0} g_R^{u,k}(nT_c - p_u T_c - \varepsilon_u - lT_0; nT_c). \quad (6.33)$$

6.5.1 Digital Computation of the z-parameters

The z-parameter can be computed digitally, for instance, as follows,

$$z^{u,k}(lT_0) = A^{u,k}(lT_0) \sum_{nT_c \in I} T_c y(nT_c) e^{-j2\pi\Delta f_u nT_c} g_R^{u,k^*}(nT_c - p_u T_c - \varepsilon_u - lT_0; nT_c). \quad (6.34)$$

If we consider a tapped delay line channel model, time variations small over the duration of the broadband transmit pulse, and discrete-time sub-channel transmit pulses (MT-MA), the z-parameter can be written in the following form (from (6.30)):

$$z^{u,k}(lT_0) = A^{u,k}(lT_0) \sum_{p=0}^{N_P} \sum_{iT \in R} T g_T^{u,k^*}(iT) \alpha_u^*(p; iT + lT_0 + p_u T_c + pT_c) \psi_{TX}(iT + lT_0 + p_u T_c + pT_c). \quad (6.35)$$

Note that as for the static case, $\psi_{TX}(nT_c)$ can be obtained by filtering the frequency offset compensated input signal with an analog filter matched to the broadband transmit filter and sampling the output at rate $1/T_c$. If we assume small frequency offsets the temporal and frequency compensation can take place after this matched filter. Therefore, the pre-filtering structures in Fig. 6.2 and Fig. 6.3 can still be deployed in time-variant channels. Further, according to (6.35) a prediction of the channel is required. This might be difficult to be obtained in channel estimation schemes that rely on past symbol decisions. However, it is possible to minimize the channel prediction as illustrated in the next section.

6.5.2 Digital Computation of the s-parameters

The s-parameters can be digitally computed in various forms. For instance,

$$s^{u,u',k,k'}(lT_0, l'T_0) = \\ = B^{u,u',k,k'}(lT_0, l'T_0) \sum_{nT_c \in I} T_c e^{-j2\pi(\Delta f_u - \Delta f_{u'})nT_c} g_R^{u,k^*}(nT_c - lT_0 - p_u T_c - \varepsilon_u; nT_c) g_R^{u',k'}(nT_c - l'T_0 - p_{u'} T_c - \varepsilon_{u'}; nT_c). \quad (6.36)$$

According to (6.36), we first need to estimate the overall time-variant channel impulse response. Then we run the discrete-time cross correlation among the overall channel impulse responses. The evaluation is done at rate $1/T_c$. Note that the s-parameters are time-variant.

6.5.3 Digital Computation of the z-parameters in FMT-MA

Let us assume an FMT-MA system, i.e., uniformly spaced sub-carriers and equal transmit filters. Then, from (6.35) under the associated hypothesis,

$$z^{u,k}(lT_0) = A^{u,k}(lT_0)\sum_{p=0}^{N_P}\sum_{n=0}^{M-1}\frac{1}{M}e^{-j\frac{2\pi}{M}nk}\cdot \\ \cdot\sum_{m=-\infty}^{\infty}T_1 g^{n^*}(mT_1)\alpha^{u,n^*}(p;mT_1+lT_0+p_uT_c+pT_c)\psi_{TX}^{n}(mT_1+lT_0+p_uT_c+pT_c) \tag{6.37}$$

where $\alpha^{u,n}(p;mT_1+lT_0+p_uT_c+pT_c)=\alpha^{u}(p;mT_1+lT_0+p_uT_c+pT_c+nT)$.

Further, simplifications are possible by introducing appropriate index relations as shown for the static case. Here we consider the case of a critically sampled FMT-MA system. In this case (6.37) becomes

$$z^{u,k}(lT_0) = \\ =A^{u,k}(lT_0)\sum_{p=0}^{N_P}\sum_{n=0}^{N-1}\frac{1}{N}e^{-j\frac{2\pi}{N}nk}\sum_{m=-\infty}^{\infty}T_0 g^{n^*}(mT_0-lT_0)\alpha^{u,n^*}(p;mT_0+p_uT_c+pT_c)\psi_{TX}^{n}(mT_0+p_uT_c+pT_c) \tag{6.38}$$

The resulting front-end receiver structure for user *u* is shown in Fig. 6.8.

6.5.4 Digital Computation of the z-parameters in DMT-MA

When we deploy rectangular filters (DMT-MA) the filtering operation with $g(iT)$ does not take place.

$$z^{u,k}(lT_0)=A^{u,k}(lT_0)\sum_{n=0}^{N-1}\frac{1}{N}e^{-j\frac{2\pi}{N}nk}\sum_{p=0}^{N_P}\alpha^{u,n^*}(p;lT_0+p_uT_c+pT_c)\psi_{TX}^{n}(lT_0+p_uT_c+pT_c). \tag{6.39}$$

Note that the DFT is computed over a block of channel samples weighted with the time-variant channel taps.

6.5.5 Digital Computation of the s-parameters in FMT-MA

The evaluation of the s-parameters is obtained as follows.

$$s^{u,u',k,k'}(lT_0,l'T_0)=B^{u,u',k,k'}(lT_0,l'T_0)... \\ ...\sum_{n=0}^{M-1}\sum_{n'=0}^{M-1}e^{-j\frac{2\pi}{M}kn}e^{j\frac{2\pi}{M}k'n'}\sum_{m}\sum_{m'}g^{n^*}(mT_1)g^{n'}(m'T_1)\kappa_E^{u,u'}(mT_1+lT_0+nT;m'T_1+l'T_0+n'T) \tag{6.40}$$

$$\kappa_E^{u,u'}(mT;m'T)=\sum_{nT_c\in I}e^{-j2\pi(\Delta f_u-\Delta f_{u'})nT_c}g_E^{u^*}(nT_c-p_uT_c-\varepsilon_u-mT;nT_c)g_E^{u'}(nT_c-p_{u'}T_c-\varepsilon_{u'}-m'T;nT_c). \tag{6.41}$$

According to (6.41) we can first compute the channels cross-correlations at rate $1/T_c$. Then, we

sample the channel cross-correlation at rate *1/T*. Finally, we evaluate (6.40).

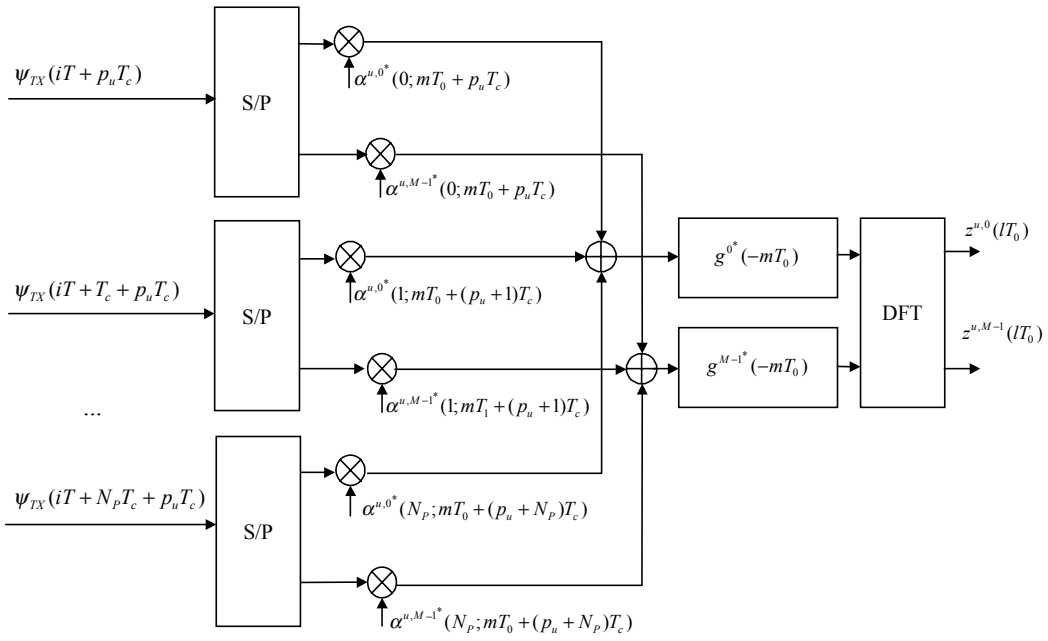

Fig. 6.8. Digital front-end receiver in CS-FMT-MA for time-variant channels.

6.6 Concluding Remarks

In this chapter we have focused on the baseband front-end receiver structure. It comprises a bank of MN_U sub-channel matched filters assuming N_U active users and M sub-carriers per user.

In static channels several alternative forms have been derived. These, exploit the permutation property of the convolution of concatenated pulses. In particular, for small frequency offsets the receiver front-end comprises first a filter matched to the transmit broadband pulse followed by sampling at rate $1/T_c$, and then by frequency offset and time offset compensation. Further, if we model the channel with a tap delay line and assume an FMT-MA system, the receiver front-end comprises a stage where the channel echoes are combined, a stage where matched to the sub-channel transmit pulse filtering takes place, and a final stage where a DFT is run. Therefore, the front-end resembles a DFT based rake receiver.

In time-variant channels it is not possible to permute the order of convolution. Therefore, we need to first filter the frequency compensated received signal with a filter matched to the time-variant channel, then with a filter matched to the broadband transmit pulse, and finally with a filter matched to the sub-channel transmit pulse. However, under the assumption of time variations small over the duration of the broadband transmit pulse, pre-filtering with a static filter matched to

broadband transmit pulse can be done similarly to the static case. In FMT-MA systems efficient digital implementations are possible. The front-end receiver comprises a stage where the time-variant channel echoes are combined, a stage where matched to the sub-channel transmit pulse filtering takes place, and a final stage where a DFT is run.

In both static and time-variant asynchronous channels the estimation of the time offset, the frequency offset, and the channel impulse response is required. It should be noted that in a multiuser environment the channel estimation task might be more challenging than that in a single user scenario. Channel estimation in single user DMT is studied in [25], [41]. The practical implementation can follow data aided estimation approaches. That is, a first estimation is obtained from the knowledge of pilot symbols that are inserted in the transmitted frame. Then, tracking of the channel variation in the frame can rely on decision aided adaptive techniques.

7 SINGLE CARRIER DETECTION IN DMT-MA WITH CYCLIC PREFIX

In this chapter we consider simplified detection in a MC-MA system that deploys rectangular filters with guard time, as well as in its discrete-time counterpart, namely DMT-MA with cyclic prefix. It consists of partial sub-channel matched filtering. The digital implementation simplifies to the well known technique based on FFT and one tap equalization per channel. The receiver can handle a channel time dispersion plus propagation delay that does not exceed the cyclic prefix duration. Otherwise, self-interference or MAI interference arises. If the channel is time-variant or a carrier frequency offset exists, inter-carrier interference is introduced at the partial matched filter outputs. We emphasize that this receiver is sub-optimal and does not allow the exploitation of frequency and temporal diversity if no channel coding is deployed.

7.1 Simplified Detection in MC-MA with Rectangular Filters

Let us consider a multicarrier multiple access system that deploys rectangular prototype filters with guard time. In particular, let us consider an analog implementation without oscillators (Section 2.2.4) that is obtained by using the transmit filters defined in (2.30).

Simple although sub-optimal demodulation is accomplished by using a bank of MN_U single carrier detectors. Each detector acquires time and frequency synchronization with the desired user/carrier and applies partial matched filtering with

$$g_{part}^{k}(t)=\frac{\sqrt{T_0}}{T_1}e^{j\frac{2\pi}{T_1}k(t-\frac{\mu T}{2})}\,\mathrm{rect}\left(\frac{t-T_0/2}{T_1}\right). \tag{7.1}$$

The *k-th* partial matched filter output of user u is

$$z_{part}^{u,k}(t')=e^{-j\Delta\phi_u}\int_{I} y(t)e^{-j2\pi\Delta f_u t}g_{part}^{k^*}(t-\Delta t_u-t')dt\,. \tag{7.2}$$

If we substitute $y(t)$ in (7.2) we obtain,

$$z_{part}^{u,k}(lT_0)=\sum_{u'=1}^{N_U}\sum_{k'=0}^{M-1}\sum_{l'=-\infty}^{\infty}a^{u',k'}(l'T_0)s_{part}^{u,u',k,k'}(lT_0,l'T_0)+w^{u,k}(lT_0) \tag{7.3}$$

with partial correlation factor (partial s-parameter) given by

$$s_{part}^{u,u',k,k'}(t',t'') = e^{j(\Delta\phi_{u'}-\Delta\phi_u)}\int_I e^{-j2\pi(\Delta f_u-\Delta f_{u'})t} g_R^{u',k'}(t-\Delta t_{u'}-t'';t) g_{part}^{k^*}(t-\Delta t_u-t')dt \qquad (7.4)$$

and

$$w^{u,k}(lT_0) = \int_I n(t)e^{-j(2\pi\Delta f_u t+\Delta\phi_u)} g_{part}^{k^*}(t-\Delta t_u-lT_0;t)dt\,. \qquad (7.5)$$

7.1.1 Static Tapped Delay Line Channel

To proceed, let us assume propagation through a tapped delay line static channel, i.e., $g_E^u(t) = \sum_{p=0}^{N_P}\alpha^u(p)\delta(t-\tau_u(p))$. Then, the partial s-parameters can be computed in closed form (see the appendix to this chapter, Appendix D). Let us define

$$\tau_p = t' + \Delta t_u - t'' - \Delta t_{u'} - \tau_{u'}(p) \qquad (7.6)$$

$$\nu = \frac{k}{T_1} + \Delta f_u - \frac{k'}{T_1} - \Delta f_{u'}\,. \qquad (7.7)$$

Then, if the define A_p as in Table 7.1, the partial s-parameters are

$$s_{part}^{u,u',k,k'}(t',t'') = \frac{1}{T_1}e^{j\left(2\pi(\Delta f_{u'}-\Delta f_u)(t'+\Delta t_u)+\Delta\phi_{u'}-\Delta\phi_u+\frac{\pi}{M}(k-k')\mu\right)}\sum_{p=0}^{N_P}e^{j\frac{2\pi}{T_1}k'\tau_p}A_p\,. \qquad (7.8)$$

$\lvert\tau_p\rvert \le \mu T/2$	(7.9)
$A_p = e^{-j\pi\nu T_0}T_1\alpha^{u'}(p)\operatorname{sinc}(\nu T_1)$	
$\lvert\tau_p - \mu T/2\rvert \le T_1$	(7.10)
$A_p = e^{-j\pi\nu(T_0+\lvert\tau_p-\mu\frac{T}{2}\rvert)}(T_0-\mu T/2-\lvert\tau_p\rvert)\alpha^{u'}(p)\operatorname{sinc}\left((T_0-\mu T/2-\lvert\tau_p\rvert)\nu\right)$	
$\lvert\tau_p - \mu T/2\rvert > T_1$	(7.11)
$A_p = 0$	

Table 7.1. Parameter A_p of equation (7.8) in AWGN.

Note that in the absence of frequency offsets, and with maximum time offset (that includes propagation delay and channel echoes delay) $\lvert\tau_{p,\max}\rvert \le \mu T/2$ the partial crosscorrelation are all

zero with the exception of [18]

$$s_{part}^{u,u,k,k}(t',t') = \sum_{p=0}^{N_P} \alpha^u(p) e^{-j\frac{2\pi}{T_1}k\tau_u(p)} . \tag{7.12}$$

It follows that the partial matched filter output of user u and sub-carrier k is given by

$$z_{part}^{u,k}(lT_0) = a^{u,k}(lT_0) s_{part}^{u,u,k,k}(lT_0, l'T_0) + w^{u,k}(lT_0) . \tag{7.13}$$

That is, the superposition of the weighted data symbol transmitted on that sub-channel, plus thermal noise. Therefore, in such a condition data detection simplifies to the following steps

1. Acquire time and frequency synchronization with each user/carrier.
2. Run partial matched filtering with a filter that is partially matched to the sub-channel transmit pulse.
3. Sample at rate $1/T_0$.
4. Send the samples to a decision device. The decision device requires knowledge of $s_{part}^{u,u,k,k}(lT_0, lT_0)$ and makes decisions similarly to the rule expressed by (5.40).

The presence of frequency offsets, and time delays in excess of the guard time introduce interference, as (7.9)-(7.10) show. Further, note that since the channel rays are non-coherently combined, as (7.12) shows, the detector cannot exploit any frequency diversity.

7.1.2 Time-Variant Channel

To understand the effect of a time-variant channel, let us assume it to be frequency non selective and defined as $g_E^u(\tau;t) = \alpha^u(t)\delta(\tau)$. It acts as a multiplicative distortion, which is typically used to model, for instance, a flat fast fading channel (see also Section 10.5). In the absence of time offsets and including the eventual frequency offsets in the channel impulse response, the partial s-parameters are

$$s^{u,u',k,k'}(lT_0, l'T_0) = \frac{1}{T_1}\int_I \alpha^{u'}(t+lT_0) e^{-j\frac{2\pi}{T_1}k(t-\mu T/2)} e^{j\frac{2\pi}{T_1}k'(t-l'T_0+lT_0-\mu T)} \operatorname{rect}\left(\frac{t-T_0/2}{T_1}\right) \operatorname{rect}\left(\frac{t-l'T_0+lT_0-T_0/2}{T_0}\right) dt$$

and differ from zero only for $l = l'$:

$$s^{u,u',k,k'}(lT_0, lT_0) = \frac{1}{T_1} e^{j\frac{2\pi}{M}\mu(k/2-k')} \int_I \alpha^{u'}(t+lT_0) e^{-j\frac{2\pi}{T_1}t(k-k')} \operatorname{rect}\left(\frac{t-T_0/2}{T_1}\right) dt . \tag{7.14}$$

Now (7.14) generally differs from zero for any u, u', and k, k'. Therefore, a time-variant channel

[18] If the channel taps are T spaced (7.12) is the DFT of the channel impulse response.

introduces inter-carrier interference. For instance, if we consider a channel that remains constant over an interval of duration T, i.e., $\alpha^u(t) = \sum_{p=-\infty}^{\infty} \alpha^u(p)\,\mathrm{rect}(\frac{t-pT-T/2}{T})$, then the evaluation of (7.14) yields

$$s^{u,u',k,k'}(lT_0, lT_0) = A\ \mathrm{sinc}(\frac{k-k'}{M})\ \sum_{p=0}^{M-1} \tilde{\alpha}^u(p+lN+\mu/2) e^{-j\frac{2\pi}{M}p(k-k')} \tag{7.15}$$

where A is a constant factor.

In Section 10.5 we will study in more detail the effects of fast fading assuming it to be characterized by a given temporal correlation.

7.2 Digital Implementation of Simplified Detection

We have shown that an efficient digital implementation of the transmitter is obtained by using a IDFT with (N-μ) points, and adding a prefix that is equal to the last μ IDFT outputs. At the receiver if we assume a sampling period $T_c = T$ we obtain from (7.2),

$$z_{part}^{u,k}(lT_0) = \frac{\sqrt{T_0}}{T_1} \sum_{nT \in I} T\ \tilde{y}(nT) e^{-j\frac{2\pi}{M}k(n-\mu/2)}\,\mathrm{rect}\left(\frac{nT - T_0/2}{T_1}\right) \tag{7.16}$$

where the frequency and time compensated input signal is

$$\tilde{y}(nT) = y(nT + \Delta t_u + lT_0) e^{-j2\pi\Delta f_u (nT+\Delta t_u+lT_0)} e^{-j\Delta\phi_u}\ . \tag{7.17}$$

Therefore,

$$z_{part}^{u,k}(lT_0) = \sqrt{T_0} \sum_{n=0}^{M-1} \frac{1}{M} \tilde{y}(nT + \frac{\mu T}{2}) e^{-j\frac{2\pi}{M}kn}\ . \tag{7.18}$$

It follows that the simplified detector in DMT with cyclic prefix comprises the following steps:

1. Acquire time and frequency synchronization with each user.
2. Sample the input signal at rate *1/T*.
3. S/P convert the stream of samples.
4. Disregard the first $\mu/2$ samples.
5. Apply a M-point DFT.
6. Send the samples to a decision device.

A detailed analysis and performance evaluation of single carrier detection in DMT-MA is reported in Chapter 10. In Chapter 11, we deal with the problem of determining the capacity region of DMT-MA.

APPENDIX TO CHAPTER 7

D Partial S-Parameters

Under the assumptions of Section 7.1.1, the partial s-parameters assuming analog filters are computed as follows.

$$s_{part}^{u,u',k,k'}(t',t'') = e^{j(\Delta\phi_{u'}-\Delta\phi_u)}\sum_{p=0}^{N_P}\alpha^{u'}(p)\int_I e^{-j2\pi(\Delta f_u-\Delta f_{u'})t}\, g_T^{u',k'}(t-\Delta t_{u'}-t''-\tau^{u'}(p))\, g_{part}^{u,k\,*}(t-\Delta t_u-t')dt$$

$$= \frac{e^{j(\Delta\phi_{u'}-\Delta\phi_u)}}{T_1}\sum_{p=0}^{N_P}\alpha^{u'}(p)\int_I e^{-j2\pi(\Delta f_u-\Delta f_{u'})(t+t'+\Delta t_u)} e^{-j\frac{2\pi}{T_1}k(t-\mu T/2)}\, e^{j\frac{2\pi}{T_1}k'(t-t''-\Delta t_{u'}-\tau^{u'}(p)+t'+\Delta t_u-\mu T)} \cdot$$
$$\cdot \mathrm{rect}\left(\frac{t-T_0/2}{T_1}\right)\mathrm{rect}\left(\frac{t-t''-\Delta t_{u'}-\tau_{u'}(p)+t'+\Delta t_u-T_0/2}{T_0}\right)dt$$

$$= \frac{e^{j(\Delta\phi_{u'}-\Delta\phi_u)}e^{-j2\pi(\Delta f_u-\Delta f_{u'})(t'+\Delta t_u)}e^{j\frac{\pi}{M}(k-k')\mu}}{T_1}\sum_{p=0}^{N_P}e^{j\frac{2\pi}{T_1}k'(t'+\Delta t_u-t''-\Delta t_{u'}-\tau_{u'}(p))}\alpha^{u'}(p)\int_I e^{-j2\pi\nu t}\,\mathrm{rect}\left(\frac{t-T_0/2}{T_1}\right)\mathrm{rect}\left(\frac{t-T_0/2+\tau_p}{T_0}\right)dt\,.$$

To proceed let us define A_p as follows, where we assume the observation interval sufficiently long.

If $|\tau_p| \le \mu\frac{T}{2}$

$$A_p = \alpha^{u'}(p)\int_{I\to R} e^{-j2\pi\nu t}\,\mathrm{rect}\left(\frac{t-T_0/2}{T_1}\right)dt = \alpha^{u'}(p)e^{-j\pi\nu T_0}T_1\,\mathrm{sinc}(\nu T_1)\,.$$

If $|\tau_p - \mu\frac{T}{2}| \le T_1$

$$A_p = \alpha^{u'}(p)\int_{I\to R} e^{-j2\pi\nu t}\,\mathrm{rect}\left(\frac{t-T_0/2-|\tau_p-\mu\frac{T}{2}|/2}{T_0-\mu\frac{T}{2}-|\tau_p|}\right)dt$$
$$= \alpha^{u'}(p)e^{-j\pi\nu(T_0+|\tau_p-\mu\frac{T}{2}|)}(T_0-\mu\frac{T}{2}-|\tau_p|)\,\mathrm{sinc}((T_0-\mu\frac{T}{2}-|\tau_p|)\nu)\,.$$

If $|\tau_p - \mu\frac{T}{2}| > T_1$, we obtain that $A_p = 0$.

Therefore,

$$s_{part}^{u,u',k,k'}(t',t'') = \frac{e^{j(\Delta\phi_{u'}-\Delta\phi_u)}e^{-j2\pi(\Delta f_u-\Delta f_{u'})(t'+\Delta t_u)}e^{j\frac{\pi}{M}(k-k')\mu}}{T_1}\sum_{p=0}^{N_P}e^{j\frac{2\pi}{T_1}k'\tau_p}A_p\,.$$

8 MULTICARRIER MULTIPLE ACCESS SYSTEM DESIGN AND PERFORMANCE

The complexity of multicarrier-user detection and its performance depend upon the channel characteristics, the time/frequency asynchronism, the choice of the sub-channel transmit filters, and the tone multiplexing across users. In this chapter we investigate the impact of several prototype filter options and tone allocation strategies on performance and complexity. We first analytically evaluate the interference components. Then, we report results from simulations. Based on the results we devise system design guidelines.

8.1 Multiple-Input Multiple-Output System Model

Let us consider the front-end receiver outputs (z-parameters) that are defined according to (5.6). If we substitute the definition (4.8) of $y(t)$ in (5.6) we obtain

$$z^{u,k}(lT_0) = \sum_{u'=1}^{N_U} \sum_{k'=0}^{M-1} \sum_{l'=-\infty}^{\infty} a^{u',k'}(l'T_0) s^{u,u',k,k'}(lT_0, l'T_0) + w^{u,k}(lT_0) \tag{8.1}$$

$$w^{u,k}(lT_0) = A^{u,k}(lT_0) \int_I n(t) e^{-j2\pi\Delta f_u t} g_R^{u,k^*}(t - \Delta t_u - lT_0; t) dt \tag{8.2}$$

for $u = 1,...,N_U$, $k = 0,...,M-1$, $l = -\infty,...,\infty$, $A^{u,k}(lT_0)$ is defined in (6.1).

Therefore, the overall communication system that comprises the concatenation of the multicarrier transmitters, channel, and front-end receiver can be modeled as a multiple-input multiple-output (MIMO) discrete-time system (Fig. 8.1). The model has MN_U inputs and MN_U outputs, assuming that each user may transmit over all sub-carriers. To proceed we can further partition (8.1) as follows.

$$z^{u,k}(lT_0) = a^{u,k}(lT_0) s^{u,u,k,k}(lT_0, lT_0) + \xi^{u,k}(lT_0) + w^{u,k}(lT_0) \tag{8.3}$$

$$\xi^{u,k}(lT_0) = \underbrace{\sum_{l' \neq l} a^{u,k}(l'T_0) s^{u,u,k,k}(lT_0, l'T_0)}_{ISI} + \underbrace{\sum_{k' \neq k} \sum_{l'=-\infty}^{\infty} a^{u,k'}(l'T_0) s^{u,u,k,k'}(lT_0, l'T_0)}_{ICI} + \\ + \underbrace{\sum_{u' \neq u} \sum_{l'=-\infty}^{\infty} a^{u',k}(l'T_0) s^{u,u',k,k}(lT_0, l'T_0)}_{MA-ISI} + \underbrace{\sum_{u' \neq u} \sum_{k' \neq k} \sum_{l'=-\infty}^{\infty} a^{u',k'}(l'T_0) s^{u,u',k,k'}(lT_0, l'T_0)}_{MA-ICI} . \tag{8.4}$$

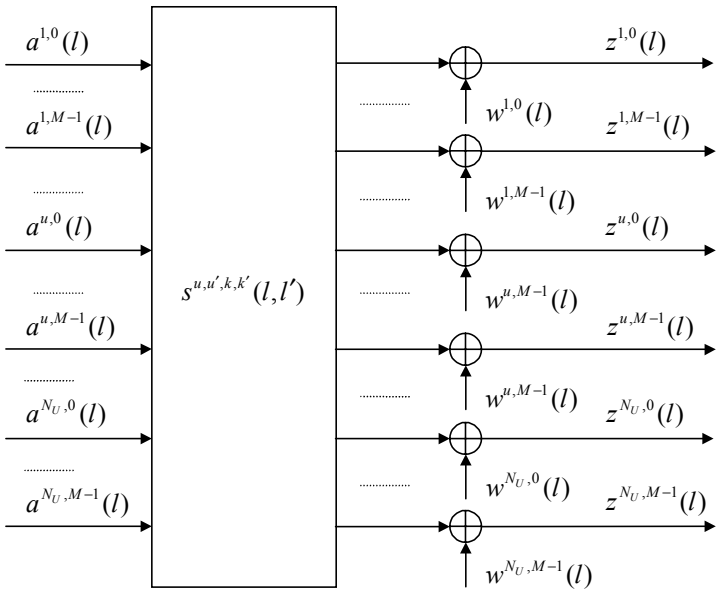

Fig. 8.1. Discrete-time MIMO model with MN_U inputs and MN_U outputs for MC-MA.

According to (8.3)-(8.4) the matched filter output of user u, sub-carrier k at time instant lT_0 is obtained by the superposition of the (weighted) data symbol that is transmitted by that user on that carrier and time instant, with interference components and thermal noise. Assuming $n(t)$ to be stationary zero mean white Gaussian with spectral density $2N_0$, the noise samples (8.2) are Gaussian with zero mean and autocorrelation

$$r_w^{u,u',k,k'}(lT_0, l'T_0) = E[w^{u,k}(lT_0)w^{u',k'}(l'T_0)^*] = 2N_0 s^{u,u',k,k'}(lT_0, l'T_0). \tag{8.5}$$

The interference components can be distinguished in self-interference and multiple access interference.

A given user on its sub-carriers generates the self-interference. If we consider a single user system then inter-carrier interference (ICI) and inter-symbol interference (ISI) may arise because of the presence of time/frequency offsets, channel frequency selectivity, or the non-orthogonal design of the prototype filters. The inter-carrier interference depends on the data symbols transmitted on different sub-carriers, while the inter-symbol interference is a function of the data symbols transmitted on the same sub-carrier but at different time instants.

In a multiuser system, the other users generate the multiple access interference. The multiple access inter-carrier interference (MA-ICI) depends on the symbols transmitted on different carriers by other users, while the multiple access inter-symbol interference (MA-ISI) is a function of the data symbols transmitted on the same sub-carrier. Note that we assume that a given sub-carrier may be shared among more than one user and we include such interference in the MA-ISI term.

8.2 Analysis of the Interference Components

The interference $\xi^{u,k}(lT_0)$ is a discrete-time process whose second order statistics can be computed in closed form once the s-parameters are known in closed form. In the next sections we assess the statistical characterization of the interference and the computation of the s-parameters for several prototype filter shapes.

8.2.1 Statistics of the Interference

Let us make the following assumptions:

1. Independent and identically distributed (i.i.d.) data symbols with zero mean and power $P_{u,k} = E[|a^{u,k}(lT_0)|^2]$;
2. Static channel impulse responses and constant time/frequency offsets.

Then, the interference seen by user u on sub-carrier k, $\xi^{u,k}(lT_0)$, is a wide sense discrete-time stationary process with mean, and power (computed with respect to the data symbols) respectively equal to

$$m_{\xi^{u,k}} = E[\xi^{u,k}(lT_0)] = 0 \tag{8.6}$$

$$P_{\xi^{u,k}} = E[|\xi^{u,k}(lT_0)|^2] = \sum_{u'=1}^{N_u}\sum_{k'=0}^{M-1}\sum_{l'=-\infty}^{\infty}\left(P_{u',k'}\,|s^{u,u',k,k'}(lT_0,l'T_0)|^2\right) - P_{u,k}\,|s^{u,u,k,k}(lT_0,lT_0)|^2. \tag{8.7}$$

Therefore, (8.7) is known when we know the s-parameters. Note that both the result of the sum in (8.7) and $|s^{u,u',k,k'}(lT_0,lT_0)|^2$ are independent of l and l'. However, the interference experienced by distinct sub-carriers may differ. The power in (8.7) corresponds to the interference power conditioned on the time and frequency offsets of all users. If the channel is time-variant the interference power is time-variant.

8.2.2 Gaussian Approximation

Since the alphabet of the data symbols is finite, the interference real and imaginary parts take values in a finite interval. Nevertheless, we may want to approximate its distribution with a Gaussian distribution as the number of users and sub-carriers increases. In Chapter 10 we will use the Gaussian approximation for the simplified evaluation of the error probability of single carrier detection in DMT-MA.

8.3 Closed Form S-parameters

Herein we investigate the impact on the interference components of different choices of the tone allocations and the sub-channel transmit filters. We assume the presence of time/frequency offsets, and we consider a static channel that is modeled with a tapped delay line including the broadband transmit filter, i.e., $g_E^u(t) = \sum_{p=0}^{N_P} \alpha^u(p)\delta(t-\tau_u(p))$. In particular we evaluate the s-parameters under the assumption of deploying time limited filters, time limited filters with guard time, frequency limited filters, and Gaussian shaped filters[19]. The filters are considered to be analog and identical for all sub-carriers (prototype filters).

In what follows it is useful to define the following quantities

$$\tau = t' + \Delta t_u - t'' - \Delta t_{u'} \qquad (8.8) \qquad\qquad \nu = f_k + \Delta f_u - f_{k'} - \Delta f_{u'} \qquad (8.9)$$

$$\tau_{p,p'} = t' + \Delta t_u + \tau_u(p) - t'' - \Delta t_{u'} - \tau_{u'}(p') . \qquad (8.10)$$

The s-parameter can be written in general form (see the appendix to this chapter, Appendix E) as

$$s^{u,u',k,k'}(t',t'') = \sum_{p=0}^{N_P}\left(\alpha^{u^*}(p)\sum_{p'=0}^{N_P}\alpha^{u'}(p')A_{p,p'}\right) \qquad (8.11)$$

where $A_{p,p'}$ is a function of the quantities in (8.8)-(8.10).

Let us assume t', Δt_u, Δf_u, $\tau_u(p)$ to be the sampling epoch, the time delay, the frequency offset and the echo delay of a given sub-channel u (or equivalently belonging to user u) that is associated to the sub-carrier f_k. Let t'', $\Delta t_{u'}$, $\Delta f_{u'}$, $\tau_{u'}(p)$ be the same quantities for a second sub-channel u' that is associated to the sub-carrier $f_{k'}$. Then, from the analysis of (8.11) we can determine the cross-correlation among two given sub-channels as a function of the associated sampling instants, time offsets, frequency offsets, and channel time dispersion. Note that τ is a function of the relative time misalignment and sampling instant difference; $\tau_{p,p'}$ is a function of the overall time misalignment (propagation delay plus echo delay); ν represents the spacing between the pair of sub-carriers associated to the pair of sub-channels including their relative frequency offset. Therefore, with this notation we can assume, in general, that the two sub-channels belong to distinct users as well as to just one user.

---

[19] With this choice of prototype filters, the efficient discrete-time counterpart corresponds to DMT-MA, DMT-MA with cyclic prefix, FMT-MA with ideal band-limited filters, and FMT-MA with Gaussian filters.

8.3.1 Time-Limited Prototype Filters

Let us consider a multicarrier system with prototype filters that are perfectly time-limited as defined in (2.7). In Appendix E we show that $A_{p,p'}$ fulfills the following relations[20].

If $|\tau_{p,p'}| \leq T_0$

$$A_{p,p'} = B^{u,u',k,k'}(t',t'')e^{j2\pi\left((\Delta f_{u'}-\Delta f_u)(t'+\Delta t_u+\tau_u(p))+f_{k'}\tau_{p,p'}-\nu(T_0-\tau_{p,p'})/2\right)}\frac{T_0-|\tau_{p,p'}|}{T_0}\mathrm{sinc}\left((T_0-|\tau_{p,p'}|)\nu\right) \quad (8.12)$$

If $|\tau_{p,p'}| > T_0$ $\qquad A_{p,p'} = 0.$ $\qquad (8.13)$

In order to get insight, we consider an ideal channel and we plot in Fig. 8.2-Fig. 8.3 the magnitude of the s-parameter, as a function of the sub-carrier spacing (normalized to $1/T_0$) when the two sub-channels experience a given time misalignment and/or a given frequency offset. In the figures the star/circle marks correspond to $f_1 - f_2 = f_k - f_{k'} = (k-k')/T_0$, i.e., to minimal sub-carrier spacing. Further we assume no sampling errors, thus we set $t' = l_1 T_0$ and $t'' = l_2 T_0$ with $l_2 = \{l_1,\ l_1+1\}$.

Let us fix the transmission bandwidth to $1/T$, and consider the deployment of N=16 and N=64 sub-carriers. Then, for a fixed value of frequency offset ($0.125/16/T$ in the figures) and of time offset ($8T$ in the figures), we see that by increasing the number of sub-carriers we can diminish the interference level from the time misalignment, but we increase the one due to the frequency offset.

Now, let us assume a multiple access scenario with an ideal channel that has no time dispersion and where the users have distinct frequency offsets and time offsets (smaller than $T_0/2$). Let us assume to acquire perfect temporal and frequency synchronization with a given user at the time, then the analysis of (8.11) together with (8.12)-(8.13) reveals that the system exhibits:

A. MA-ISI and MA-ICI that are due to time misaligned users. The MA-ISI on a given sub-carrier spans only the previous and the following data symbols, i.e., $a^{u',k}(l'T_0)$ with $l' = \{l-1,\ l,\ l+1\}$.

B. MA-ICI that is due to frequency misaligned users.

The considerations above can be extended to a time dispersive channel. Its effect is to introduce both self and multiple access ISI and ICI. The ISI spans only two adjacent data symbols (assuming a maximum echo delay plus time misalignment smaller than $T_0/2$).

Whenever we are not perfectly time aligned, e.g., for a sampling error, with a given user we introduce ISI and ICI. Whenever we are not frequency aligned we introduce ICI.

---

[20] The parameter $B^{u,u',k,k'}(t',t'')$ has been defined in (6.10).

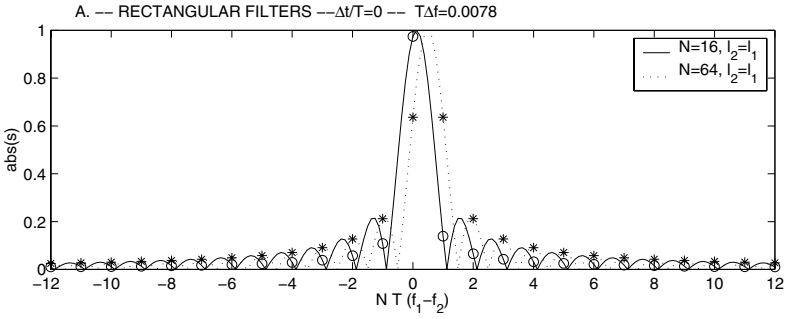

Fig. 8.2. Magnitude of cross correlation as a function of normalized sub-carrier spacing. Rectangular filters with duration NT with N=16 and N=64. No time misalignment, and frequency offset Δf=0.125/16/T.

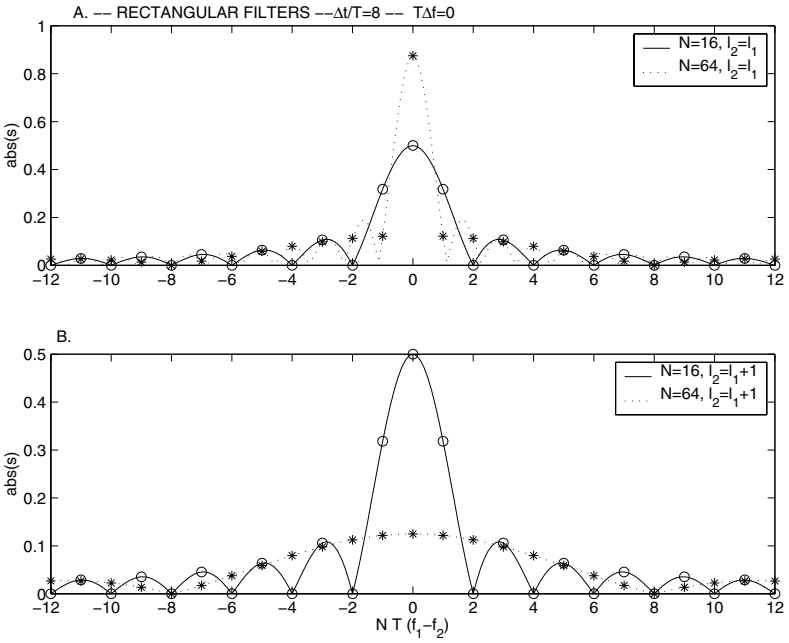

Fig. 8.3. Magnitude of cross correlation as a function of sub-carrier spacing. Rectangular filters with duration NT with N=16 and N=64. Time misalignment Δt=8T, and no frequency offset.

8.3.2 Time-Limited Prototype Filters with Guard Interval

We have described simplified detection for MC-MA with rectangular filters and guard interval (cyclic prefix) in Chapter 7. The redundancy introduced by the guard interval allows for simplified demodulation based on partial matched filtering. The system is robust against time misalignments, and consequently ISI channels. However, it has to be said that the system presents some drawbacks. First, the spectral efficiency of the system can drastically diminish since it requires the deployment of guard intervals that are as long as the sum of the maximum echo delay with the time offset.

Second, partial matched filtering does not allow the exploitation of the frequency diversity on each individual sub-channel. Finally, we are still required to counteract the inter-carrier interference that is present with fast time-variant channels or with carrier frequency offsets.

8.3.3 Frequency-Limited Prototype Filters

Here we consider a special case of a multicarrier multiple access system where the prototype filters are frequency limited and defined as in (2.7).

Let us assume a static multipath channel response. In Appendix E we show that $A_{p,p'}$ fulfills the following relations.

If $|\nu| \leq 1/T_0$

$$A_{p,p'} = B^{u,u',k,k'}(t',t'')e^{j2\pi\left((\Delta f_{u'}-\Delta f_u)(t'+\Delta t_u+\tau_u(p))+f_{k'}\tau_{p,p'}+\nu\tau_{p,p'}/2\right)}(1-\frac{|\nu|}{T_0})\mathrm{sinc}\left(\tau_{p,p'}(\frac{1}{T_0}-|\nu|)\right) \quad (8.14)$$

If $|\nu| > 1/T_0$ $$A_{p,p'} = 0. \quad (8.15)$$

To get insight, let us assume an ideal channel, perfect sampling, and minimal sub-carrier spacing. Then, from the analysis of (8.11) together with (8.14)-(8.15) we see that a multiple access system exhibits:

A. MA-ICI due to frequency misaligned users. The ICI contribution on a given sub-carrier is due only to the left-right adjacent sub-carriers (assuming users with distinct sub-carriers and frequency offsets smaller than $1/(2T_0)$).

B. MA-ISI is present on a given sub-carrier only if the same sub-carrier is assigned to other users that are time misaligned.

Clearly, if we increase the sub-carrier spacing we can diminish the ICI. If the channel is frequency selective and introduces resolvable echoes, then a given user does not experience any self-ICI, however each of its sub-carriers experiences self-ISI. Sampling errors introduce only self-ISI, while self-ICI is present only in the presence of (self) frequency offsets.

Clearly, the deployment of frequency limited filters is impractical and some excess bandwidth will always be present. However, filters with small excess bandwidth can be designed. For instance, we can deploy square-root-raised-cosine filters with small roll-off factor (see (2.11)). In the next section we consider Gaussian shaped filters that have the advantage of being, practically, time and frequency limited.

8.3.4 Gaussian Prototype Filters

An interesting choice is to deploy Gaussian prototype filters (2.9). In Appendix E we show that $A_{p,p'}$ is given by

$$A_{p,p'} = B^{u,u',k,k'}(t',t'')e^{j\pi\left((f_k+f_{k'})\tau_{p,p'}+(\Delta f_{u'}-\Delta f_u)(\tau_{p,p'}+2t''+2\Delta t_{u'}+2\tau_{u'}(p'))\right)}e^{-(\frac{\alpha}{\sqrt{2}T_0}\tau_{p,p'})^2}e^{-(\frac{\pi T_0}{\sqrt{2}\alpha}v)^2}. \quad (8.16)$$

In Fig. 8.5-Fig. 8.6, we plot the magnitude of the s-parameter with Gaussian shaped filters that have $f_{3dB}T_0$=0.33 as a function of the normalized sub-carrier spacing. The N=16 and N=64 curves overlap. Note that in the absence of both time and frequency offset a certain amount of ICI and ISI is always present (Fig. 8.4). However, diminishing f_{3dB} can reduce the ICI at the expense of the ISI. The ISI (Fig. 8.4) essentially spans two adjacent symbols, and the ICI two adjacent sub-carriers. Fig. 8.5 shows that in the presence of a frequency offset the ICI increases with respect to Fig. 8.4. In the presence of a time offset (Fig. 8.6) the ICI is not significantly altered with respect to Fig. 8.4, but the ISI increases.

Thus, by the appropriate choice of the Gaussian filters shape and sub-carrier spacing we can control the interference components and potentially simplify the task of the optimum multicarrier-user detector.

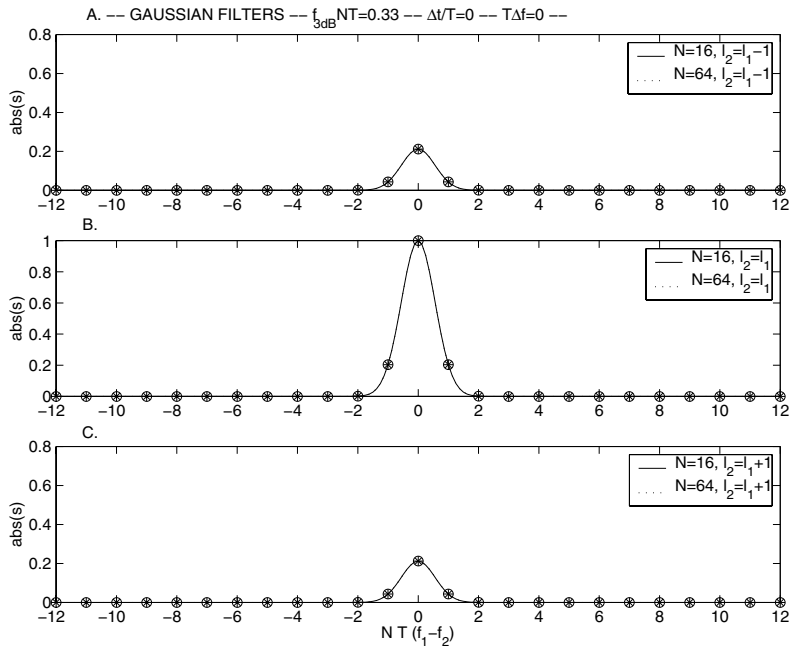

Fig. 8.4. Magnitude of cross correlation as a function of sub-carrier spacing. Gaussian filters with $f_{3dB}NT$=0.33, and N=16 and N=64. No time misalignment and no frequency offset.

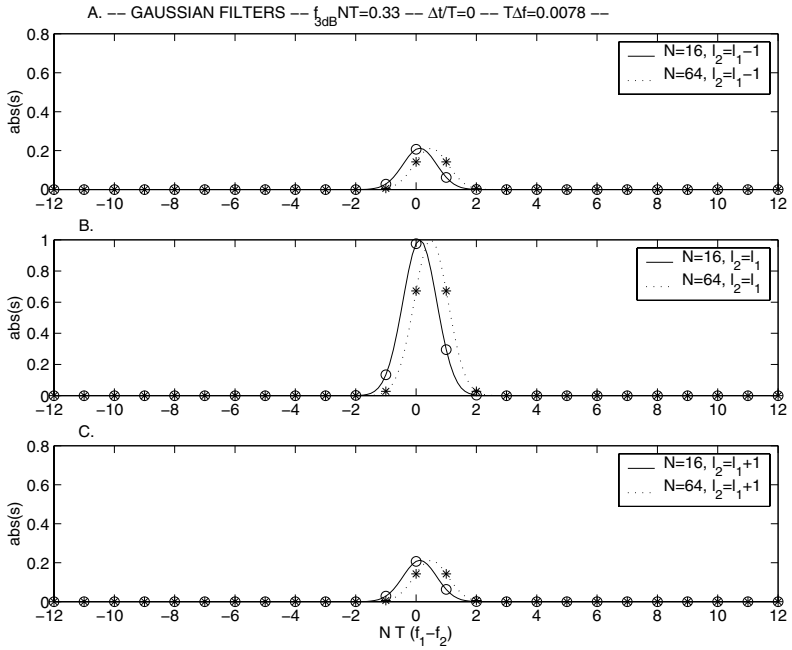

Fig. 8.5. Magnitude of cross correlation as a function of sub-carrier spacing. Gaussian filters with $f_{3dB}NT$=0.33, and N=16 and N=64. No time misalignment, and frequency offset Δf=0.125/16/T.

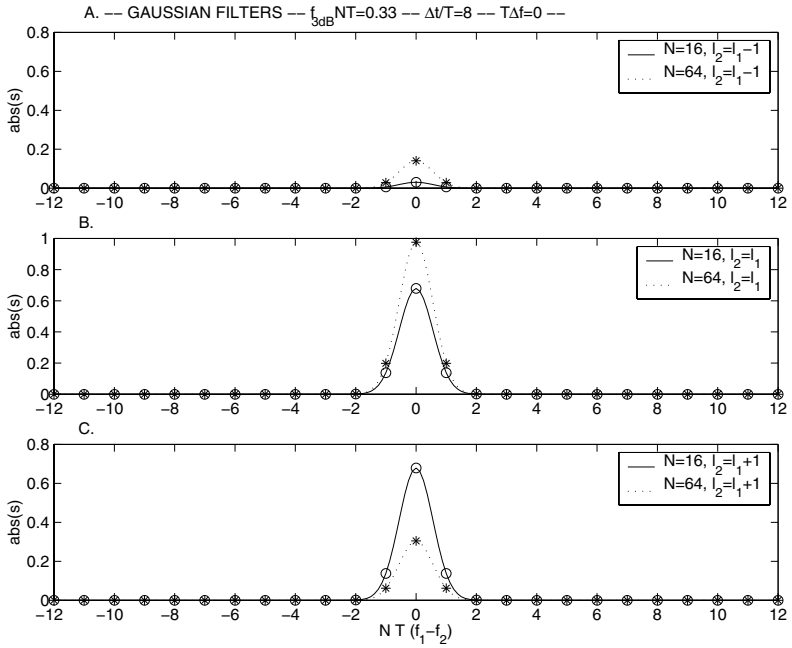

Fig. 8.6. Magnitude of cross correlation as a function of sub-carrier spacing. Gaussian filters with $f_{3dB}NT$=0.33, and N=16 and N=64 carriers. Time misalignment Δt=8T, and no frequency offset.

8.4 Bit-Error-Rate Performance Evaluation

To illustrate the main advantages and potentiality of the proposed multicarrier-user detection approach, we report performance curves that have been obtained by computer simulations. We consider several FMT/DMT system scenarios (with minimal sub-carrier spacing) to test:

A. Performance of single carrier detection in the presence of time and frequency offsets.
B. Performance of iterative per-symbol detection in the presence of time and frequency offsets.
C. Performance of DMT in frequency selective static and fast Rayleigh fading.

The performance of optimal (full complexity) multicarrier-user detection is assumed to approach the "genie" bound that is obtained with perfect extrinsic knowledge, i.e., with ideal knowledge of all interfering data symbols and perfect interference cancellation.

8.4.1 Uncoded Multiuser System Scenario

We consider an uncoded system with a total number of sub-carriers M=16 that are uniformly spaced. The system is critically sampled, i.e., N=M. Two users are multiplexed by assigning 8 sub-carriers each. The allocation scheme is either block or interleaved with equal power tones.

We assume the users to experience a time misalignment that is uniformly distributed between [$-T_0/2$, $T_0/2$], and a frequency offset that is uniformly distributed between [$-0.125/T_0$, $0.125/T_0$], relatively to a fixed reference point at the receiver.

We consider both the case where the prototype filters are rectangular in time (DMT-MA) with no cyclic prefix, and the case where the filters are Gaussian shaped with $f_{3dB}T_0 = 0.33$ (FMT-MA).

No channel coding is considered. Each user transmits a frame of 160 information bits that are mapped to 4-PSK symbols with Gray coding. These frames of information symbols correspond to 10 FMT/DMT symbols over which the time/frequency offset is constant, and changes randomly over the next 10 DMT/FMT symbols.

The simulation is implemented at chip level T_c=T, i.e., with no over sampling. Propagation is through an AWGN channel with no fading.

First consider single carrier detection. That is, detection on each sub-carrier is symbol by symbol based (according to (5.40)) and neglects the interference components. In Fig. 8.7 we report bit error rate performance collected over 5000 frames. The reference curve is represented by the BER achieved when all users are synchronous (Bound), or identically when interference cancellation takes place with perfect knowledge of all extrinsic information, i.e., all symbols transmitted by the other user.

As it can be seen all single carrier detection curves exhibit an error floor that is significantly high for DMT with interleaved tone multiplexing. With FMT there is an improvement although not significant. Only DMT with block tone multiplexing yields acceptable performance. In general better performance is obtained with the block tone allocation strategy, since less MAI is introduced.

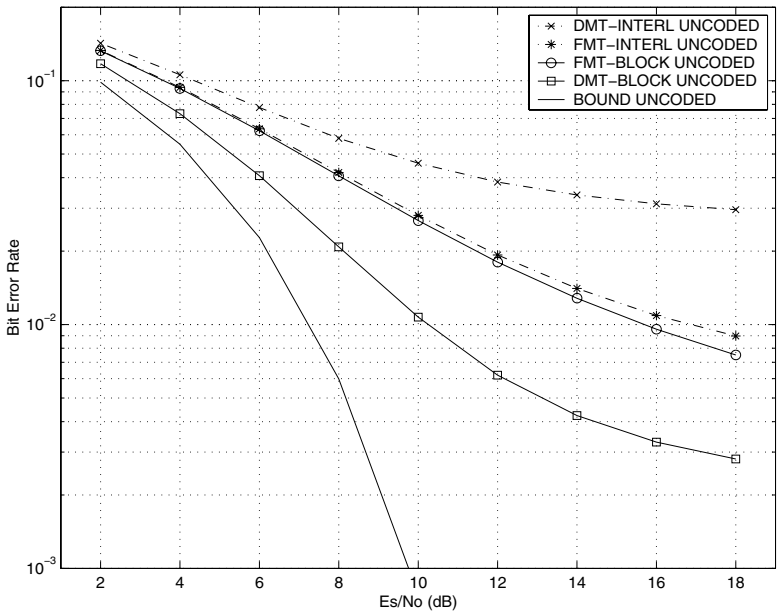

Fig. 8.7. Average bit-errror-rate performance of single carrier detection in uncoded critically sampled MT-MA with Gaussian Filters (FMT) and rectangular filters (DMT). Two users, 8 carriers/user. AWGN channel, with Δt_u uniformly distributed in [-8T, 8T] and Δf_u uniformly distributed in [-0.125/T_0, 0.125/T_0].

Now consider iterative per-symbol detection (Fig. 8.8-Fig. 8.9). This simplified detection algorithm has been described in Section 5.2.6. Perfect knowledge of the time and frequency offsets is assumed. A significant performance improvement is found with few detection iterations[21]. Looking at Fig. 8.8 where the users' tones are interleaved the error floor is considerably lowered for DMT at the 8-th iteration. Further, FMT is less than 1 dB from the error rate bound. Iterative per-symbol detection of DMT yields good performance if the tones are block allocated as Fig. 8.9 shows. Negligible improvements are found with more than 8 iterations.

These results illustrate that iterative per-symbol detection can yield performance results that are near to the error rate bounds. This is especially through if the filters and the tone multiplexing are appropriately chosen. Optimal multicarrier detection is assumed to converge to the error rate bound curves although its high complexity may not justify the performance gain over per-symbol detection.

[21] Single carrier detection is identical to per-symbol detection at the first pass.

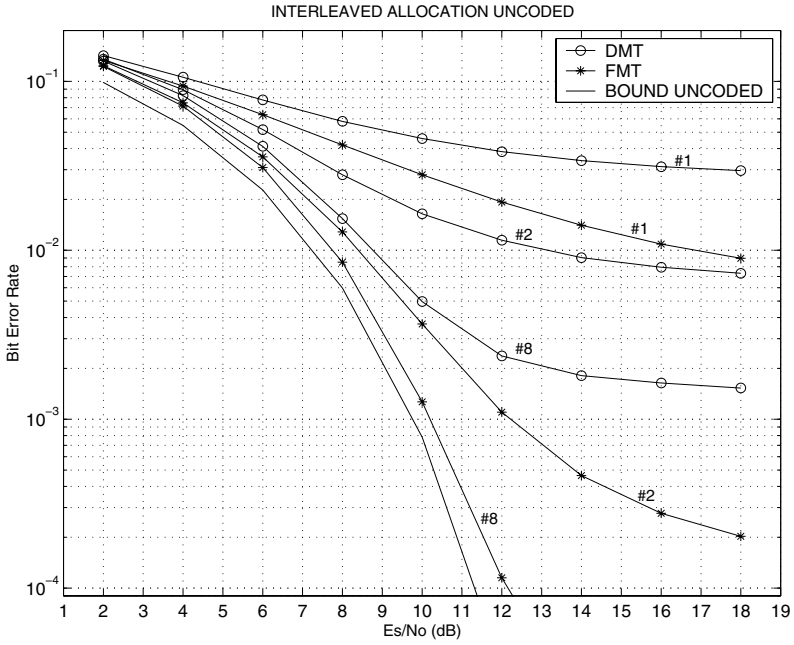

Fig. 8.8. Average bit-errror-rate performance of iterative per-symbol detection in uncoded critically sampled MT-MA with Gaussian Filters (FMT) and rectangular filters (DMT). Two users, 8 carriers/user. Δt_u uniformly distributed in [-8T, 8T] and Δf_u uniformly distributed in [-0.125/T_0, 0.125/T_0]. AWGN channel. Interleaved tone multiplexing.

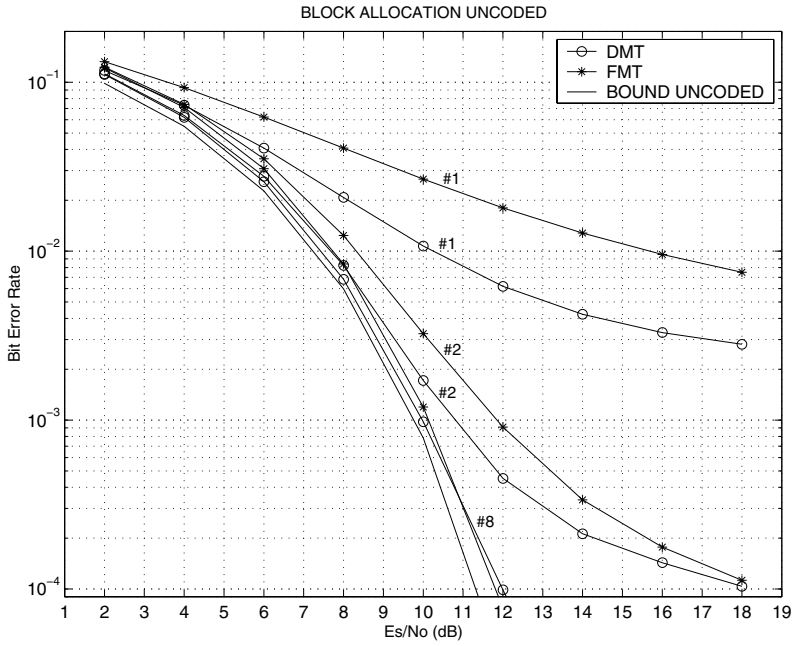

Fig. 8.9. Average bit-errror-rate performance of iterative per-symbol detection in uncoded critically sampled MT-MA with Gaussian Filters (FMT) and rectangular filters (DMT). Two users, 8 carriers/user. Δt_u uniformly distributed in [-8T, 8T] and Δf_u uniformly distributed in [-0.125/T_0, 0.125/T_0]. AWGN channel. Block tone multiplexing.

8.4.2 Single User System with Fast Time-Variant Fading

We now consider an uncoded system where a single user transmits its information with DMT with 8 sub-carriers and 4-PSK modulation. No cyclic prefix is added. Propagation is through a fading channel. In more detail we consider the following channel scenarios:

a) Flat Rayleigh fading that is static for the DMT block duration;
b) 2-rays channel with independent and Rayleigh faded rays that are static for the DMT block duration. The second ray is delayed by $3T$.
c) Flat Rayleigh fading channel, fully temporally de-correlated, i.e., fast fading.

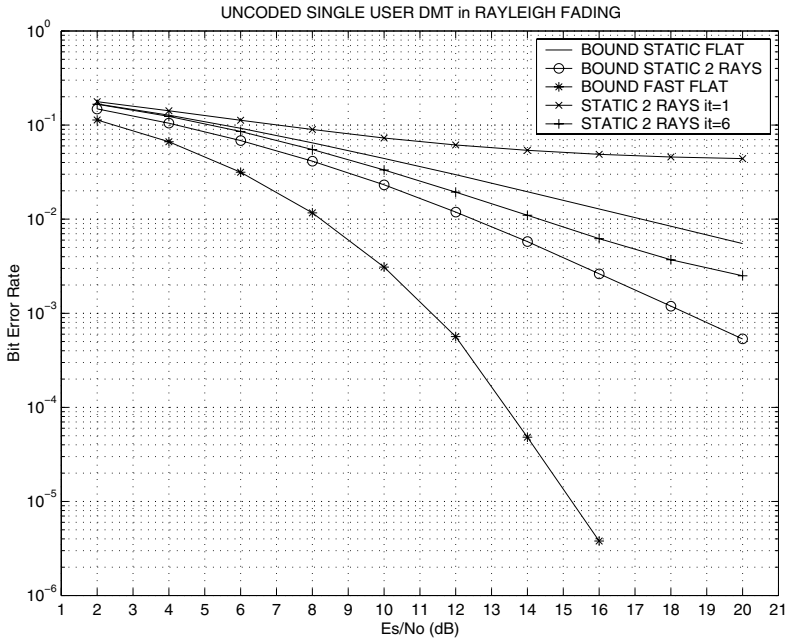

Fig. 8.10. Average bit-error-rate performance of uncoded DMT with 4-PSK. One user, 8 carriers. Flat static fading, 2-Rays static fading with relative delay $3T$, flat fast fading.

In Fig. 8.10 we report the performance of optimal multicarrier detection under the assumption of knowing the channel and all interfering data symbols, i.e., with perfect cancellation of all interfering data symbols. We refer to these error-rate curves as bound. Practical multicarrier detection shall converge to these bounds. This is to illustrate that with optimal detection an uncoded DMT system can exploit the frequency diversity of a frequency selective fading channel and the temporal diversity of a fast fading channel. In fact, observe that the performance in scenario b) and c) is much better than in a) (the slope of the curves shows that full diversity is exploited).

Note that if we inserted a cyclic prefix and we did conventional DMT detection the performance

in b) would be identical to a), i.e. no frequency diversity exploitation. Further, the performance in fast fading would be dramatically poor due to the fact that conventional FFT based demodulation with one tap equalization does not cope with the intercarrier interference introduced by the channel temporal variations.

We also report the performance obtained in 2 rays fading with practical iterative per-symbol detection. Note that although the time dispersion is significantly high at the sixth iteration a significant fraction of the diversity gain is exploited.

8.5 System Design Guidelines and Remarks

From the analysis above, we have shown that in a MC-MA system (self) ICI, (self) ISI, and MAI components can be present at the outputs of the matched filter bank. These components are a function of the prototype filter shape, the sub-carrier spacing, the tone allocation strategy, the time/frequency offsets among users, the sampling errors, and the channel characteristics. Low interference levels require filters that are limited in time and in frequency, with sub-carriers that are allocated as far as possible among users. In particular:

A. With time limited filters, a frequency selective channel is responsible for ICI, ISI, and MAI. Time offsets and frequency offsets among users yield a MAI contribution.

B. With time limited filters and cyclic prefix, it is possible to counteract the time misalignments across users as well as the echoes from a frequency selective channel.

C. With frequency limited filters it is possible to counteract the ICI from time misalignments and channel echoes at the expense of ISI. The frequency offsets may yield ICI contributions.

D. With filters that are practically limited in time and in frequency it is possible to reduce the ICI, ISI, and MAI. For instance, Gaussian filters are a reasonable choice.

E. Lower MAI is generated when the tones are allocated to users in disjoint blocks. With the block allocation of tones we can insert frequency guards in order to further separate the spectrum of distinct users.

F. Some degree of time and frequency synchronization among users is beneficial. However, it requires a feedback control from the receiver whose practicality and reliability has to be investigated [77].

G. Optimal multicarrier-user detection should be deployed in an asynchronous multicarrier multiple access channel. It is capable of coping with time/frequency asynchronism and time-variant dispersive channels. It allows to optimally demodulating DMT signals without requiring the insertion of the cyclic prefix, which translates in increased spectral efficiency.

H. Optimal detection is capable of exploiting temporal and frequency diversity. It is interesting to note that multitone modulation with optimal multitone detection can be interpreted as a diversity transform for fading channels [49].

I. Iterative per-symbol detection turns out to be a very simple detection approach that is capable of yielding performance close to optimal detection.

J. The other forms of iterative detection, namely, iterative per-carrier detection and iterative per-user detection, are expected to yield improved performance in severely interference-limited channels. The choice of what reduced complexity technique has to be deployed depends on the system. For instance, in an FMT-MA system with minimal spectral overlapping filters, and block-multiplexed users, detection can be per-carrier based. In other words we just need to perform equalization independently on each sub-carrier. If the multiplexing of users introduces significant MAI we can choose to deploy an iterative per-user detection scheme.

As a final remark on the system design for mobile wireless environments, we point out that once we fix the operating bandwidth the choice of the number of sub-carriers to be deployed has to tradeoff between the requirement of flat sub-channel frequency response and static channel over the multitone block duration.

APPENDIX TO CHAPTER 8

E S-Parameters in ISI Channel

If we consider a tapped delay line static channel model with impulse response $g_E^u(t) = \sum_p \alpha^u(p)\delta(t-\tau_u(p))$, the s-parameter is related to the s-parameter computed in an ideal channel as shown in what follows.

$$s^{u,u',k,k'}(t',t'') = B^{u,u',k,k'}(t',t'')\sum_p \alpha^{u^*}(p)\sum_{p'}\alpha^{u'}(p')\int_I e^{-j2\pi(\Delta f_u-\Delta f_{u'})t} g_T^{u,k^*}(t-t'-\Delta t_u-\tau_u(p))g_T^{u',k'}(t-t''-\Delta t_{u'}-\tau_{u'}(p'))dt$$

$$= B^{u,u',k,k'}(t',t'')\sum_p \alpha^{u^*}(p)\sum_{p'}\alpha^{u'}(p')\int_I \Big(e^{-j2\pi(\Delta f_u-\Delta f_{u'})(t+t'+\Delta t_u+\tau_u(p))} e^{-j2\pi f_k t} e^{j2\pi f_{k'}(t-t''-\Delta t_{u'}-\tau_{u'}(p')+t'+\Delta t_u+\tau_u(p))} \cdot$$

$$\cdot g^{u,k^*}(t) g^{u',k'}(t-t''-\Delta t_{u'}-\tau_{u'}(p')+t'+\Delta t_u+\tau_u(p))\Big)dt$$

$$= \sum_p \alpha^{u^*}(p)\sum_{p'}\alpha^{u'}(p')\Big(\underbrace{B^{u,u',k,k'}(t',t'')e^{-j2\pi(\Delta f_u-\Delta f_{u'})(t'+\Delta t_u+\tau_u(p))} e^{j2\pi f_k\tau_{p,p'}} \int_I e^{-j2\pi\nu t} g^{u,k^*}(t) g^{u',k'}(t+\tau_{p,p'})dt}_{A_{p,p'}=s^{u,u',k,k'}(t',t'') \text{ for } \tau=\tau_{p,p'}} \Big)$$

where we have used the definitions in (8.8)-(8.10). $A_{p,p'}$ is the s-parameter computed in an ideal channel with overall time offset $\tau = \tau_{p,p'}$. Therefore (8.11) follows.

To the limit $I \to R$, the integral is the Fourier transform of the product of two functions. Therefore, we can evaluate it by convolving the Fourier transforms of the two functions, i.e.,

$$A_{p,p'} = B^{u,u',k,k'}(t',t'')e^{-j2\pi(\Delta f_u-\Delta f_{u'})(t'+\Delta t_u+\tau_u(p))} e^{j2\pi f_k\tau_{p,p'}} \int_R G^{u,k^*}(f-\nu)G^{u',k'}(f)e^{j2\pi f\tau_{p,p'}}df \,. \qquad \text{(E.1)}$$

RECTANGULAR FILTERS

Let the prototype filters be rectangular and defined as in (2.5). The computation of $A_{p,p'}$ yields:

If $|\tau_{p,p'}| \le T_0$

$$A_{p,p'} = \frac{1}{T_0} B^{u,u',k,k'}(t',t'')e^{-j2\pi(\Delta f_u-\Delta f_{u'})(t'+\Delta t_u+\tau_u(p))} e^{j2\pi f_k\tau_{p,p'}} \int_{I\to R} e^{-j2\pi\nu t} \operatorname{rect}\left(\frac{t-T_0/2+\tau_{p,p'}/2}{T_0-|\tau_{p,p'}|}\right)dt$$

$$= B^{u,u',k,k'}(t',t'')e^{-j2\pi(\Delta f_u-\Delta f_{u'})(t'+\Delta t_u+\tau_u(p))} e^{j2\pi f_k\tau_{p,p'}} e^{-j\pi\nu(T_0-\tau_{p,p'})}(T_0-|\tau_{p,p'}|)/T_0 \operatorname{sinc}\left((T_0-|\tau_{p,p'}|)\nu\right).$$

Otherwise, if $|\tau_{p,p'}| > T_0$, $A_{p,p'} = 0$.

FREQUENCY LIMITED FILTERS

Let the prototype filters be defined according to (2.7). Then, using (E.1) we get:

$$A_{p,p'} = B^{u,u',k,k'}(t',t'')e^{-j2\pi(\Delta f_u - \Delta f_{u'})(t'+\Delta t_u+\tau_u(p))}e^{j2\pi f_{k'}\tau_{p,p'}}T_0\int_R \mathrm{rect}(T_0(f-\nu))\,\mathrm{rect}(T_0 f)e^{j2\pi f\tau_{p,p'}}df$$

$$= B^{u,u',k,k'}(t',t'')e^{-j2\pi(\Delta f_u - \Delta f_{u'})(t'+\Delta t_u+\tau_u(p))}e^{j2\pi f_{k'}\tau_{p,p'}}T_0\int_{-\infty}^{\infty} \mathrm{rect}\left(\frac{f-\nu/2}{\frac{1}{T_0}-|\nu|}\right)e^{j2\pi f\tau_{p,p'}}df\ .$$

If $|\nu| \le 1/T_0$

$$A_{p,p'} = B^{u,u',k,k'}(t',t'')e^{-j2\pi(\Delta f_u - \Delta f_{u'})(t'+\Delta t_u+\tau_u(p))}e^{j2\pi f_{k'}\tau_{p,p'}}e^{j\pi\tau_{p,p'}\nu}T_0\left(\frac{1}{T_0}-|\nu|\right)\mathrm{sinc}\left(\tau_{p,p'}\left(\frac{1}{T_0}-|\nu|\right)\right).$$

Else if $|\nu| > 1/T_0$, $A_{p,p'} = 0$.

GAUSSIAN FILTERS

Let us consider Gaussian filters as defined in (2.9). Then the computation of the s-parameters in an ideal channel yields

$$A_{p,p'} = \frac{B^{u,u',k,k'}(t',t'')\alpha}{\sqrt{\pi/2}T_0}\int_I e^{-j2\pi(\Delta f_u-\Delta f_{u'})t}e^{-j2\pi f_k(t-t'-\Delta t_u-\tau_u(p))}e^{j2\pi f_{k'}(t-t''-\Delta t_{u'}-\tau_{u'}(p'))}\cdot$$

$$\cdot e^{-(\frac{\alpha}{T_0}(t-t'-\Delta t_u-\tau_u(p)))^2}e^{-(\frac{\alpha}{T_0}(t-t''-\Delta t_{u'}-\tau_{u'}(p')))^2}dt$$

$$= \frac{B^{u,u',k,k'}(t',t'')\alpha}{\sqrt{\pi/2}T_0}e^{-j(2\pi f_k(-t'-\Delta t_u-\tau_u(p))-2\pi f_{k'}(-t''-\Delta t_{u'}-\tau_{u'}(p')))}e^{-\pi(\frac{\sqrt{2}\alpha}{\sqrt{\pi}T_0}(\frac{t'+\Delta t_u+\tau_u(p)-t''-\Delta t_{u'}-\tau_{u'}(p')}{2}))^2}\cdot$$

$$\cdot\int_I e^{-j2\pi(\Delta f_u-\Delta f_{u'}+f_k-f_{k'})t}e^{-\pi(\frac{\sqrt{2}\alpha}{\sqrt{\pi}T_0}(t-\frac{t'+\Delta t_u+\tau_u(p)+t''+\Delta t_{u'}+\tau_{u'}(p')}{2}))^2}dt$$

$$= \frac{B^{u,u',k,k'}(t',t'')\alpha}{\sqrt{\pi/2}T_0}\frac{\sqrt{\pi}T_0}{\sqrt{2}\alpha}e^{-j2\pi(f_k(-t'-\Delta t_u-\tau_u(p))-f_{k'}(-t''-\Delta t_{u'}-\tau_{u'}(p')))}\cdot$$

$$\cdot e^{-\pi(\frac{\sqrt{2}\alpha}{\sqrt{\pi}T_0}\tau_{p,p'}/2)^2}e^{-\pi(\frac{\sqrt{\pi}T_0}{\sqrt{2}\alpha}\nu)^2}e^{-j2\pi\nu(\frac{t'+\Delta t_u+\tau_u(p)+t''+\Delta t_{u'}+\tau_{u'}(p')}{2})}$$

$$= B^{u,u',k,k'}(t',t'')e^{j\pi(f_k+f_{k'})\tau_{p,p'}}e^{-j\pi(\Delta f_u-\Delta f_{u'})(t'+\Delta t_u+\tau_u(p)+t''+\Delta t_{u'}+\tau_{u'}(p'))}e^{-(\frac{\alpha}{\sqrt{2}T_0}\tau_{p,p'})^2}e^{-(\frac{\pi T_0}{\sqrt{2}\alpha}\nu)^2}$$

$$= B^{u,u',k,k'}(t',t'')e^{j\pi(f_k+f_{k'})\tau_{p,p'}}e^{-j\pi(\Delta f_u-\Delta f_{u'})(\tau_{p,p'}+2t''+2\Delta t_{u'}+2\tau_{u'}(p'))}e^{-(\frac{\alpha}{\sqrt{2}T_0}\tau_{p,p'})^2}e^{-(\frac{\pi T_0}{\sqrt{2}\alpha}\nu)^2}\ .$$

9 CHANNEL CODING AND TURBO MULTICARRIER-USER DECODING

So far we have considered the transmission of uncoded signals. In this chapter we address the channel coding and decoding problem. In particular we propose the deployment of bit interleaved codes. Decoding can be practically implemented through an iterative (turbo like) method where multicarrier detection and channel decoding are iteratively concatenated.

9.1 Channel Coding

It is interesting to note that with multicarrier modulation the channel coding problem is intrinsically a problem of coding for multiple-input multiple-output channels. Different coding approaches are possible such as deploy trellis codes where coding and modulation are jointly performed [75], or interleaved codes where coding and modulation are separately done [14]. Furthermore, excluding cooperation among users, for obvious practical reasons, coding for a given user can be done independently on each sub-carrier, or across sub-carriers. Coding across sub-carriers allows for the exploitation of the temporal and frequency diversity provided by time-variant frequency selective fading channels [1]. Here we consider the deployment of bit interleaved codes. The constituent encoders can be block, convolutional, or turbo encoders. Essentially two strategies are possible: sub-carrier interleaved coding and inter-carrier interleaved coding.

9.1.1 Sub-Carrier Interleaved Coding

In sub-carrier interleaved coding distinct information bits streams are transmitted over distinct sub-carriers, and are independently encoded (Fig. 9.1). In other words, each stream is encoded, interleaved, and mapped to complex data symbols. Finally, the parallel symbol streams are multicarrier modulated.

9.1.2 Inter-Carrier Interleaved Coding

In inter-carrier interleaved coding (Fig. 9.2), the original information bit stream is encoded and interleaved. Then, the encoded bit stream is parsed into a number of sub-streams equal to the

number of assigned sub-carriers. Each sub-stream of bits is mapped into complex data symbols. Finally, multicarrier modulation takes place.

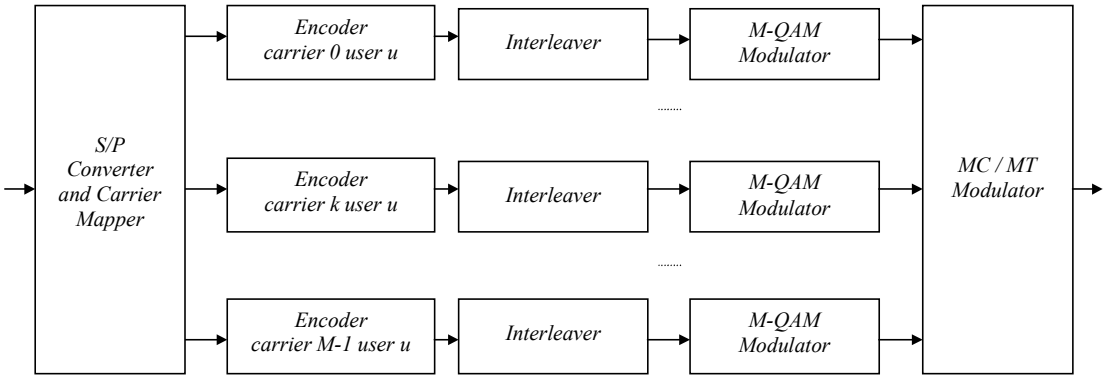

Fig. 9.1. Sub-carrier channel coding for user u.

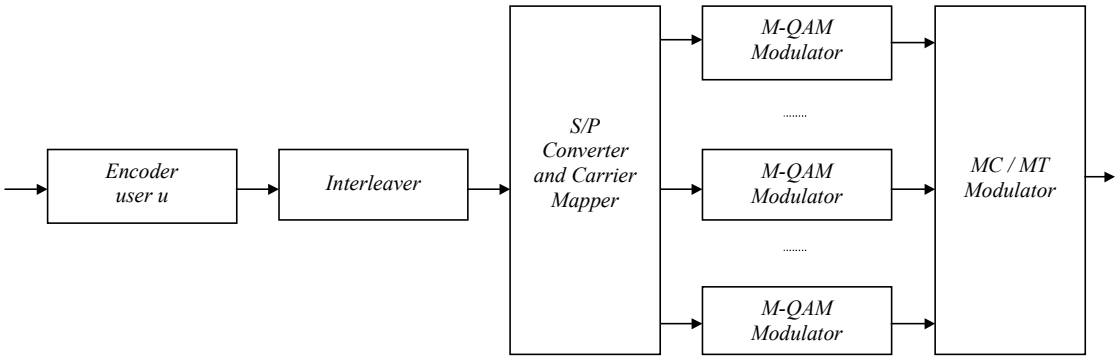

Fig. 9.2. Inter-carrier channel coding for user u.

9.2 Turbo Multicarrier-user Decoding

When interleaved codes are deployed optimal maximum likelihood decoding requires jointly taking into account the structure of the encoder, the interleaver, the modulator, and the channel. Practical and simplified decoding is accomplished through the turbo decoding approach by treating the system as a concatenated coded system [6]. Essentially, we run multicarrier-user detection, then after de-interleaving we run channel decoding (Fig. 9.3). Further, we can iteratively concatenate demodulation and decoding by passing feedback information from the decoders.

The turbo decoding approach has found many applications since it was deployed for decoding of turbo codes [10]. It has been proposed for turbo equalization of coded B-PSK signals in [24], for iterative demapping of coded M-PSK/M-QAM signals in [40], [56], for turbo decoding of differentially encoded M-PSK signals in [58], [60], [50], and for turbo multiuser decoding of coded

CDMA signals in [44]. Recently, it has been investigated as an effective technique in coded space-time architectures with multiple antennas [4], [61]-[66]. We point out that the coding problem for multicarrier systems has some analogies with the coded problem for multiple transmit-receive antenna systems. However, coding in multicarrier systems takes place in the frequency-time domain while coding in multiple transmit antenna systems takes place in the space-time domain. That is, the sub-channels in space-time coded systems entirely overlap in frequency while the sub-channels in a multicarrier system have a degree of overlapping that depends upon the design of the sub-carrier spacing and the transmit filters shape. From a diversity point of view, the resource to be exploited in space-time coded system is the spatial diversity of rich scattering environments, while in multicarrier systems is the frequency diversity of frequency selective fading channels. Clearly, a combination of space-time coding and multicarrier modulation is possible.

The multicarrier-user detector has now to provide the a posteriori probabilities of the coded bits, which are then de-interleaved and passed to the decoders. The decoders can be implemented with a soft-in soft-out algorithm (e.g., MAP decoder for convolutional codes [5], [83]) and are capable to deliver new a posteriori probabilities of the coded bits. These are interleaved and passed back to the multicarrier detector where are used as an estimate of the a priori transition probabilities, see (5.36). To minimize the correlation with previously computed soft information, extrinsic information has to be exchanged [32], [63], [65].

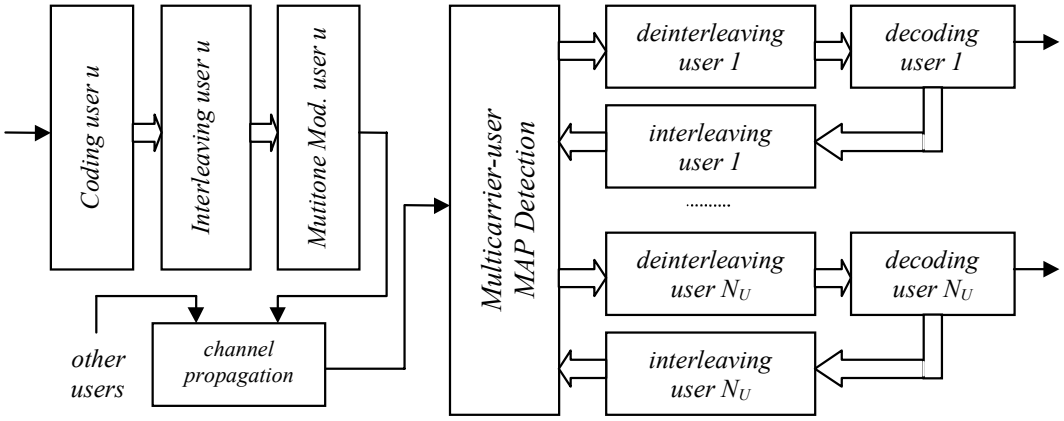

Fig. 9.3. Turbo multicarrier-user decoding.

9.3 Simplified Turbo Multicarrier-user Decoding

Simplified turbo multicarrier-user decoding can be implemented by concatenating simplified detectors with simplified decoders. For instance, we can use the simplified detection methods that we have described in Section 5.2.4. Further, we can pass hard feedback information, which requires conventional hard output decoders.

A drastic simplification is obtained by using a simple per-symbol based detector. At the first decoding stage we generate soft outputs by neglecting the presence of interference components. Then, we apply channel decoding and we feed back soft or hard information on the data symbols of all users. Now we can re-run detection including in the metric calculation the soft/hard knowledge of all interfering data symbols. We refer to this approach as *simplified turbo per-symbol decoding*. The computation of the logarithm of the a posteriori probability of a given coded bit (transmitted by user u on sub-carrier k) can be simplified at the detection stage as follows:

$$\ln \lambda(d_m = d)_{it=i} \sim \max_{a \in A(d_m=d)} \left\{ \mathrm{Re}\left\{ a^* \left(2z^{u,k}(lT_0) - as^{u,u,k,k}(lT_0, lT_0) - 2 \sum_{\substack{(u',k',l') \\ \neq \\ (u,k,l)}} \hat{a}^{u',k'}(l'T_0)_{it=i-1} s^{u,u',k,k'}(lT_0, l'T_0) \right) \right\} \right\} \quad (9.1)$$

where $\hat{a}^{u,k}(lT_0)$ are the soft/hard data symbols provided by the decoders at the previous iteration, while $A(d_m = d)$ is the set of data symbols $a^{u,k}(lT_0)$ (of user u, sub-carrier k, instant lT_0) that are labeled with bit $d_m = d$. Such a set has cardinality 2^{Nbps-1} with N_{bps} number of bits per data symbol. The above result is obtained by approximating the logarithm of the sum of exponentials with the highest exponent [59].

The performance of turbo per-symbol decoding is investigated in the next section.

9.4 Performance Evaluation

To illustrate the potentiality of the bit-interleaved coding and decoding approach we consider a system scenario identical to the one of Section 8.4.1. However, we add channel coding. Two users are independently coded. Frames of 80 information bits are encoded with a rate 1/2 convolutional code with memory 2. The resulting 160 coded bits are randomly interleaved, mapped to 4-PSK symbols according to the Gray rule, and assigned to the sub-carriers. Carrier spacing is minimal. We deploy simplified turbo per-symbol decoding. The feedback from the two decoders to the detector is hard. Note that this requires the deployment of conventional hard output Viterbi decoders.

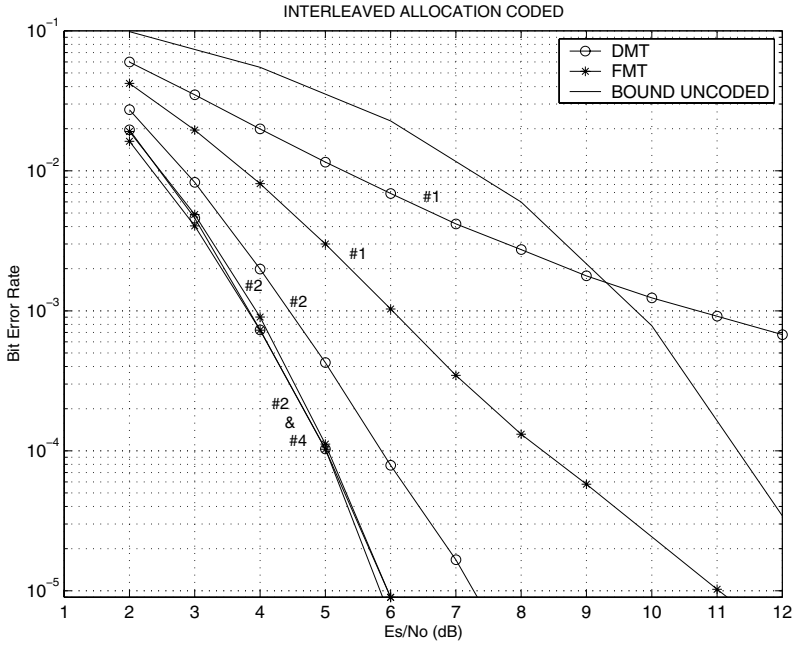

Fig. 9.4. BER performance of turbo per-symbol decoding of convolutionally coded critically sampled MT-MA with Gaussian Filters (FMT) and rectangular filters (DMT). Two users, 8 carriers/user. AWGN channel. Δt_u uniformly distributed in [-8T, 8T], and Δf_u uniformly distributed in [-0.125/T_0, 0.125/T_0]. Interleaved tone multiplexing.

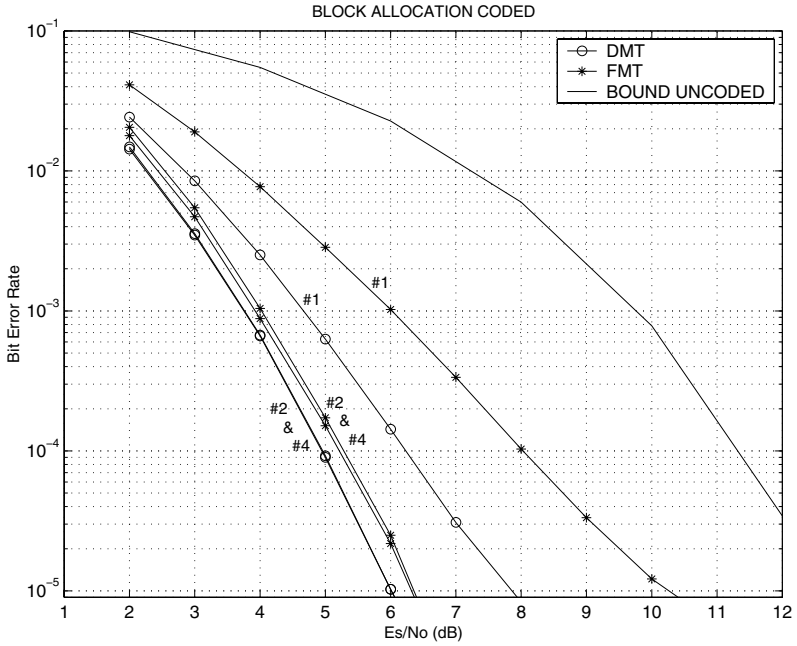

Fig. 9.5. BER performance of turbo per-symbol decoding of convolutionally coded critically sampled MT-MA with Gaussian Filters (FMT) and rectangular filters (DMT). Two users, 8 carriers/user. AWGN channel. Δt_u uniformly distributed in [-8T, 8T], Δf_u uniformly distributed in [-0.125/T_0, 0.125/T_0]. Block tone multiplexing.

Looking at Fig. 9.4 we can see that at the first decoding pass only FMT yields acceptable performance. However, with the block tone allocation DMT outperforms FMT as Fig. 9.5 shows.
At the fourth decoding pass, Fig. 9.4 shows that DMT and FMT with the interleaved tone allocation have similar performance, while DMT is better than FMT when the block tone allocation is deployed, Fig. 9.5.

In general we have found that, with coding, the interleaved multiplexing scheme is capable of yielding better performance than the block scheme as the number of iterations increases. Finally, observe that with coding and simplified turbo per-symbol decoding the performance enhancement, with respect to the uncoded system, is significant. At BER 10^{-4}, the SNR improvement is about 6.5 dB.

Further improvements are possible by increasing the complexity of the multicarrier-user detector and deploying optimal soft output MAP convolutional decoders [83].

10 PERFORMANCE ANALYSIS OF SINGLE USER DETECTION IN DMT-MA

In this chapter we assess the performance analysis of single user[22] detection in a DMT multiple access system. The analysis is based on a discrete-time system model. Performance is determined in terms of signal-to-noise-plus-interference ratio, and symbol/bit error rate. The performance is a function of many system parameters such as the amount of time offset and frequency offset, the channel characteristics, the tone multiplexing algorithm. To simplify the understanding of the impact of such parameters we consider first an AWGN channel, then a quasi-static multipath fading channel. Finally, we investigate the effect on performance when DMT communications take place over a fast fading channel with typical Bessel correlation function.

10.1 Discrete-Time System Model

We first revise some of the key concepts and notation used to describe a DMT-MA system assuming a discrete-time model.

10.1.1 Transmitter

Let us consider N_U users that share the medium with a DMT-MA scheme. The information bit stream of the *u-th* user is first mapped to complex data symbols with a spectrally efficient modulation scheme (e.g. M-PSK, M-QAM). Then, multiplexing and DMT modulation take place as shown in Fig. 10.1 and discussed in Chapter 3.

We assume that K_u tones are assigned to user *u*. After S/P conversion, the *i-th* block of K_u complex data symbols $\underline{c}^u(iT_0) = [c^{u,0}(iT_0),...,c^{u,K_u-1}(iT_0)]^T$ is transformed into a block of *M* symbols $\underline{a}^u(iT_0) = \underline{P}(u)\underline{c}^u(iT_0)$ by the excitation matrix $\underline{P}(u)$ of size *M* by K_u. The excitation matrix is unitary, and is constructed according to a given tone assignment algorithm [57]. Basically, the

[22] In this chapter we prefer to denote the demodulation algorithm with *single user detection* instead of *single carrier detection* (see Chapter 7). This is because time/carrier synchronization is on a per user basis.

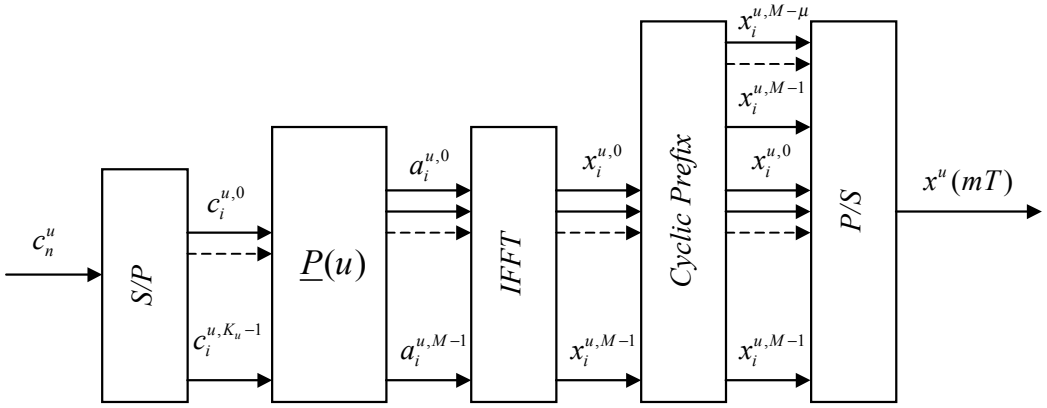

Fig. 10.1. Baseband DMT-MA transmitter for user *u*.

excitation matrix permutes the elements of $\underline{c}^u(iT_0)$ into the elements of $\underline{a}^u(iT_0)$ whose indices correspond to assigned tones, and inserts zeros in correspondence of unassigned tones. Hence, an *M*-point IFFT is applied and a cyclic prefix (guard time) of $\mu = \mu_1 + \mu_2$ data symbols is inserted.

As we have seen, the cyclic prefix is used to reduce the MAI in the presence of asynchronous users and to compensate for the effect of a frequency selective channel. The distinction between μ_1 and μ_2 is made by imagining that μ_1 counteracts the time misalignments (propagation delay) of the terminals while μ_2 the delayed echoes of the multipath channel.

Therefore, the *i-th* block of DMT symbols that are transmitted by user *u* is defined as follows (Section 2.2.4)

$$x_i^{u,k} = x^u(kT + iT_0) \qquad i = -\infty, ..., \infty \quad k = 0, ..., N-1 \tag{10.1}$$

$$x_i^{u,k} = \sum_{n=0}^{M-1} a^{u,n}(iT_0) e^{j\frac{2\pi}{M}n(k-\mu)} . \tag{10.2}$$

Finally, after P/S conversion the *u-th* user transmits the DMT symbol stream, at rate $W = 1/T$, below

$$x^u(mT) = x^u(mT = kT + iT_0) . \tag{10.3}$$

10.1.2 Discrete-Time Channel

We here assume a discrete-time channel model (Fig. 10.2) as a result of the following assumptions:

1. Ideal sampling at rate $1/T$;
2. Discrete-time tapped delay line channel model $g_E^u(mT) = \sum_{p=0}^{N_P} \alpha^u(p; mT)\delta(mT - pT)$ with taps spaced by T;

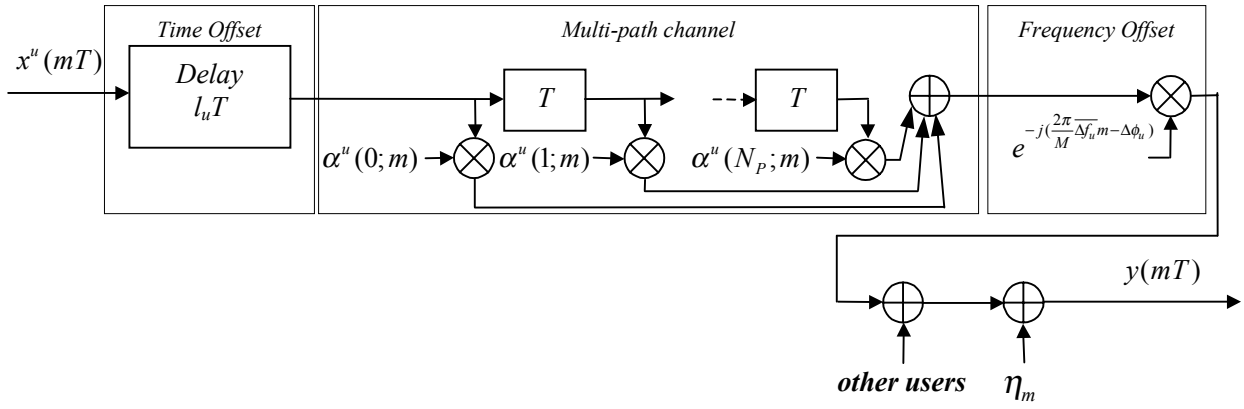

Fig. 10.2. Baseband equivalent channel model for user *u*.

3. Normalized to the sub-carrier spacing frequency offset $\overline{\Delta f_u} = -T_1 \Delta f_u$;
4. Time offset $\Delta t_u = l_u T$, with $l_u = -\infty, ..., \infty$.

From (4.1), the received sequence of samples at rate *W* is given by

$$y(mT) = \sum_{u=1}^{N_U} e^{j(2\pi \Delta f_u mT + \Delta\phi_u)} \sum_{p=0}^{N_P} \alpha^u(p;mT) x^u(mT - l_u T - pT) + \eta(mT) \tag{10.4}$$

with $\Delta\phi_u = -2\pi l_u T(f_C + \Delta f_u)$ and $\eta(mT)$ being the thermal noise contribution.

10.1.3 Single User Detection

In order to reconstruct the transmitted information data stream of all users, we adopt a bank of N_U single user detectors identical to the one shown in Fig. 10.3.

Demodulation for the *u-th* user is accomplished by first acquiring time and frequency synchronization with user *u* (that is equivalent to setting $l_u=0$ and $\Delta f_u=0$). Then, blocks of N samples are extracted. A window of *M* samples is set starting from the middle of the cyclic prefix of length μ_1. Finally, an *M*-point FFT is applied. From the FFT output we extract blocks of K_u decision variables, based on which the transmitted information bit stream is reconstructed.

It follows that the simplified detector in DMT-MA comprises the following steps:

1. Sample the input signal at rate *1/T*;
2. Acquire time and frequency synchronization with each user;
3. Get synchronization with the beginning of the cyclic prefix;
4. S/P convert the input stream into blocks of *N* of samples;
5. Disregard the first $\mu_2 + \mu_1/2$ samples and the last $\mu_1/2$;
6. Apply an M-point DFT and send the outputs to a decision device.

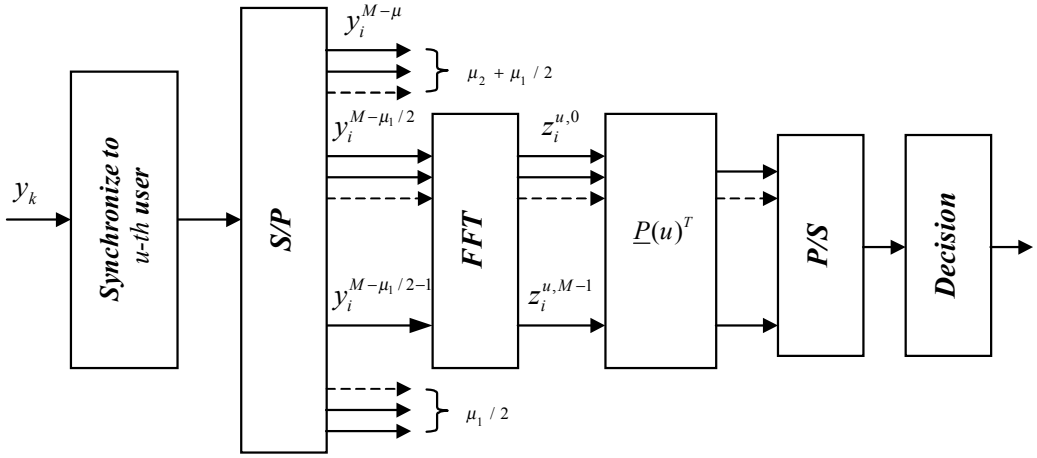

Fig. 10.3. Baseband DMT-MA receiver synchronized to user *u*.

Now, consider the symbols in (10.1), and let X_i^{u,k,l_u} be the *k-th* element of the *M*-point window shifted by l_u that is defined as follows

$$X_i^{u,k,l_u} = x^u((k+\mu-\frac{\mu_1}{2})T - l_u T + iT_0) \quad i=-\infty,...,\infty \quad k=0,...,M-1. \tag{10.5}$$

For clarity, the window can be depicted as follows

$$x_{i-1}^{u,M-\mu}...\,x_{i-1}^{u,0}...\,x_{i-1}^{u,M-1}x_i^{u,M-\mu}...\underbrace{\left[x_i^{u,M-\frac{\mu_1}{2}}...\,x_i^{u,M-1}x_i^{u,0}...\,x_i^{u,M-\frac{\mu_1}{2}-1}\right]}_{\overleftarrow{-|l_u|}\quad\overrightarrow{+|l_u|}}...\,x_i^{u,M-1}x_{i+1}^{u,M-\mu}...\,x_{i+1}^{u,0}...\,x_{i+1}^{u,M-1} \tag{10.6}$$

Then, the *k-th* sample of the *i-th* received block at the output of the synchronization window of user *u* is

$$y_i^k = y(kT+(\mu-\frac{\mu_1}{2})T+iT_0) = \sum_{u=1}^{N_U} e^{-j(\frac{2\pi}{M}\overline{\Delta f}_u k - \overline{\Delta\phi_{u,i}})} \sum_{p=0}^{N_P} \alpha^u(p;iT_0+(k+\mu-\frac{\mu_1}{2})T) X_{k-p}^{u,i,l_u} + \eta_i^k \tag{10.7}$$

with $i=-\infty,...,\infty$, $k=0,...,M-1$, and $\overline{\Delta\phi_{u,i}} = \Delta\phi_u - \frac{2\pi}{M}\overline{\Delta f}_u(iN+(\mu-\frac{\mu_1}{2}))$.

To proceed we make the following assumptions:

1. We assign disjoint sets of tones to distinct users. Thus, we denote the set of K_u tone indices univocally assigned to user *u* with $\Gamma_u = \{n_0^{u,i}...\ n_{K_u-1}^{u,i}\} \subset \{0\ ...\ M-1\}$;
2. The fading is slow, i.e. $\alpha^u(p;kT+iT_0) = \alpha^u(p;iT_0)$ is constant over the sampling window length;
3. The maximum delay of the channel rays is assumed smaller than the cyclic prefix μ_2, i.e., $N_P \le \mu_2$.

Therefore, the set of decision variables that allows recovering the transmitted symbols $a^{u,n}(iT_0)$ of

user u is

$$z^{u,n}(iT_0) = \frac{1}{M}\sum_{k=0}^{M-1} y_i^k e^{-j\frac{2\pi}{M}nk} = a^{u,n}(iT_0)H^{u,n}(iT_0) + \sum_{u'\neq u}\hat{\xi}^{u',n}(iT_0) + w^{u,n}(iT_0) \tag{10.8}$$

where $n \in \Gamma_u$ and

$$H^{u,n}(iT_0) = \sum_{p=0}^{N_P}\alpha^u(p;iT_0)e^{-j\frac{2\pi}{M}np} \tag{10.9}$$

$$\hat{\xi}^{u',n}(iT_0) = e^{j\overline{\Delta\phi_{u',i}}}\frac{1}{M}\sum_{k=0}^{M-1}\sum_{p=0}^{N_P}\alpha^{u'}(p;iT_0)X_{k-p}^{u',i,l_{u'}}e^{-j\frac{2\pi}{M}(n+\overline{\Delta f_{u'}})k} \tag{10.10}$$

$$w^{u,n}(iT_0) = \frac{1}{M}\sum_{k=0}^{M-1}\eta_i^k e^{-j\frac{2\pi}{M}nk}\,. \tag{10.11}$$

It follows that each sub-channel output is the sum of the data symbol $a^{u,n}(iT_0)$ weighted by the complex factor $H^{u,n}(iT_0)$, a noisy term $w^{u,n}(iT_0)$, and a multiple access interference (MAI) term $\xi^{u,n}(iT_0) = \sum_{u'\neq u}\hat{\xi}^{u',n}(iT_0)$. Note that $\xi^{u,n}(iT_0)$ is the overall interference seen by user u on its sub-carrier n, while $\hat{\xi}^{u',n}(iT_0)$ is the interference contribution due to user u'.

The *u′-th* user interference contribution on the *n-th* sub-carrier is given by (10.10). The MAI term differs from zero whenever at least one of the other users has a frequency offset $\Delta f_u \neq 0$, and/or a time delay such that $l_u < N_P - \mu_1/2 - \mu_2$ or $l_u > \mu_1/2$. Note that no self ISI and self ICI is present because we assume to acquire perfect time and frequency synchronization with the user that we are demodulating and the cyclic prefix handles the time dispersion of the channel.

Therefore, a simple way of counteracting the joint effect of multipath fading and time misalignments is to insert a guard time whose length is larger than the maximum time misalignment plus the maximum delay of the echoes. Since the time delay is a function of distance, this is a practical solution for systems with limited cell radius. However, we could always think of having some degree of centralized control that confines the time offset within the guard time length [77]. Vice versa the frequency offset detrimental effect can be lowered, but not completely eliminated, by the insertion of frequency guards.

In the next sections we evaluate the MAI second order statistics.

10.2 MAI Second Order Statistics

The second order statistics of the MAI are evaluated under the following assumptions.

1. Independent identically distributed data symbols with zero mean and power:
   $E[|a^{u,n}(iT_0)|^2] = P_{u,n}\delta_{n\in\Gamma_u}$, with $\delta_{n\in\Gamma_u} = 1$ if $n \in \Gamma_u$, and $\delta_{n\in\Gamma_u} = 0$ otherwise;
2. Independent channel rays with zero mean and power $E[|\alpha^u(p;iT_0)|^2] = \Omega_{u,p}$.

10.2.1 MAI Correlation

Under the above assumptions the MAI seen by user u has zero mean and conditional (on the time and frequency offsets) autocorrelation:

$$R^u_{\xi\xi}(n,n+p,iT_0,mT_0 \mid \underline{l},\underline{\Delta f}) = E[\xi^{u,n}(iT_0)\xi^{u,n+p^*}(mT_0) \mid \underline{l},\underline{\Delta f}] = \sum_{u'\neq u} R_{\hat{\xi}\hat{\xi}}(u',n,n+p,iT_0,mT_0 \mid l_{u'},\Delta f_{u'}) \quad (10.12)$$

$$R_{\hat{\xi}\hat{\xi}}(u',n,n+p,iT_0,mT_0 \mid l_{u'},\Delta f_{u'}) = E[\hat{\xi}^{u',n}(iT_0)\hat{\xi}^{u',n+p^*}(mT_0) \mid l_{u'},\Delta f_{u'}]. \quad (10.13)$$

Note that the expectation in (10.13) is evaluated over the data symbols and the channel taps[23] and represents the autocorrelation of just the interferer u'. The computation of such an autocorrelation is particularly laborious. Some details are summarized in the appendix to this chapter, Appendix F. In particular, the autocorrelation of the interference generated by a given user evaluated across sub-carriers n and $n+p$ during a given observation block is:

$$R_{\hat{\xi}\hat{\xi}}(u,n,n+p,iT_0,iT_0 \mid l_u,\Delta f_u) = \frac{1}{M^2}\sum_{k\in\Gamma_u} P_{u,k}\frac{A(n,p,k,l_u,\Delta f_u)}{(1-e^{-j\frac{2\pi}{M}(n+\overline{\Delta f_u}-k)})(1-e^{j\frac{2\pi}{M}(n+p+\overline{\Delta f_u}-k)})}. \quad (10.14)$$

The term $A(n,p,k,l_u,\Delta f_u)$ is a function of the sub-carrier indices n, $n+p$, k, and the time/frequency offsets. Closed expressions are reported in Table 10.5 of the Appendix F, and in [67].

10.2.2 MAI Power

The MAI power generated by user u (interferer) on sub-carrier n when it experiences a given time and frequency offset is obtained by setting $p = 0$ in (10.14),

$$M(u,n \mid l_u,\Delta f_u) = E[\hat{\xi}^{u,n}(iT_0)\hat{\xi}^{u,n^*}(iT_0) \mid l_u,\Delta f_u] = \frac{1}{M^2}\sum_{k\in\Gamma_u} P_{u,k}\frac{A(n,p=0,k,l_u,\Delta f_u)}{\sin^2\left(\frac{\pi}{M}(n+\overline{\Delta f_u}-k\right)} \quad (10.15)$$

where $A = A(n,p=0,k,l_u,\Delta f_u)$ is reported in the table below.

$-\frac{\mu_1}{2}-\mu_2 > l_u \geq -M+\frac{\mu_1}{2}$	(10.16)
$A=\sum_{t=0}^{N_P}\Omega_{u,t}\left\{\sin^2\left(\frac{\pi}{M}(t-l_u-\frac{\mu_1}{2}-\mu_2)(\overline{\Delta f_u}+n-k)\right)+\sin^2\left(\frac{\pi}{M}(t-l_u-\frac{\mu_1}{2}-\mu_2-M)(\overline{\Delta f_u}+n-k)\right)\right\}$	
$N_P-\frac{\mu_1}{2}-\mu_2 > l_u \geq -\frac{\mu_1}{2}-\mu_2$	(10.17)
$A=\sin^2(\pi\overline{\Delta f_u})\sum_{t=0}^{\mu-\frac{\mu_1}{2}+l_u}\Omega_{u,t}+\sum_{t=\mu-\frac{\mu_1}{2}+l_u+1}^{N_P}\Omega_{u,t}\left\{\sin^2\left(\frac{\pi}{M}(t-l_u-\frac{\mu_1}{2}-\mu_2)(\overline{\Delta f_u}+n-k)\right)+\sin^2\left(\frac{\pi}{M}(t-l_u-\frac{\mu_1}{2}-\mu_2-M)(\overline{\Delta f_u}+n-k)\right)\right\}$	
$\frac{\mu_1}{2} \geq l_u \geq N_P-\frac{\mu_1}{2}-\mu_2$	(10.18)
$A=\sin^2(\pi\overline{\Delta f_u})\sum_{t=0}^{N_P}\Omega_{u,t}$	
$N_P+\frac{\mu_1}{2} \geq l_u > \frac{\mu_1}{2}$	(10.19)
$A=\sin^2(\pi\overline{\Delta f_u})\sum_{t=l_u-\frac{\mu_1}{2}+1}^{N_P}\Omega_{u,t}+\sum_{t=0}^{l_u-\frac{\mu_1}{2}}\Omega_{u,t}\left\{\sin^2\left(\frac{\pi}{M}(t-l_u+\frac{\mu_1}{2})(\overline{\Delta f_u}+n-k)\right)+\sin^2\left(\frac{\pi}{M}(t-l_u+\frac{\mu_1}{2}+M)(\overline{\Delta f_u}+n-k)\right)\right\}$	
$M+\frac{\mu_1}{2} \geq l_u > N_P+\frac{\mu_1}{2}$	(10.20)
$A=\sum_{t=0}^{N_P}\Omega_{u,t}\left\{\sin^2\left(\frac{\pi}{M}(t-l_u+\frac{\mu_1}{2})(\overline{\Delta f_u}+n-k)\right)+\sin^2\left(\frac{\pi}{M}(t-l_u+\frac{\mu_1}{2}+M)(\overline{\Delta f_u}+n-k)\right)\right\}$	

Table 10.1. Parameter A of equation (10.15).

10.2.3 Average Signal-to-Noise-plus-Interference Power Ratio

We define the overall (conditional) signal-to-interference power ratio on the *n-th* sub-carrier belonging to the *u-th* user, as

$$SIR(u,n\,|\,\underline{l},\underline{\Delta f})=\frac{P_{u,n}}{\sum_{u'\neq u}M(u',n\,|\,l_{u'},\Delta f_{u'})}. \tag{10.21}$$

Similarly, the signal-to-noise-plus-interference power ratio is defined as

$$SINR(u,n\,|\,\underline{l},\underline{\Delta f})=\frac{P_{u,n}}{\sigma^2+\sum_{u'\neq u}M(u',n\,|\,l_{u'},\Delta f_{u'})} \tag{10.22}$$

[23] The cross-correlation between distinct users is zero under the assumption of independent zero mean data symbols.

where the noise power is $E[|w^{u,n}(iT_0)|^2]=\sigma^2$. Averaging over the set of tones assigned to user *u*, we get the average SIR and SINR seen by the *u-th* user

$$\overline{SIR}(u,n\,|\,\underline{l},\underline{\Delta f})=\frac{1}{K_u}\sum_{n\in\Gamma_u}\frac{P_{u,n}}{\sum_{u'\neq u}M(u',n\,|\,l_{u'},\Delta f_{u'})} \tag{10.23}$$

$$\overline{SINR}(u,n\,|\,\underline{l},\underline{\Delta f})=\frac{1}{K_u}\sum_{n\in\Gamma_u}\frac{P_{u,n}}{\sigma^2+\sum_{u'\neq u}M(u',n\,|\,l_{u'},\Delta f_{u'})}. \tag{10.24}$$

10.3 Performance in AWGN

Let us assume an AWGN channel (no multipath fading), and let us assume to set the starting point of the demodulation window of each user in the middle of the cyclic prefix. Then, the conditional interference power generated by interferer *u* on sub-carrier *n* is obtained from (10.15) setting $N_P=0$, $\Omega_{u,0}=1$, $\mu_2=0$, and $\mu=\mu_1$. Therefore, $A(n,0,k,l_u,\Delta f_u)$ can be written as in Table 10.2.

$\lvert l_u\rvert\leq\mu/2$	(10.25)
$A(n,0,k,l_u,\Delta f_u)=\sin^2(\pi\overline{\Delta f_u})$	
$\lvert l_u\rvert>\mu/2$	(10.26)
$A(n,0,k,l_u,\Delta f_u)=1-\cos\left(\pi(n+\overline{\Delta f_u}-k)\right)\cos\left(\frac{\pi}{M}(2\,\lvert l_u\rvert-\mu-M)(n+\overline{\Delta f_u}-k)\right)$	

Table 10.2. Parameter *A* of equation (10.15) in AWGN.

Under the hypothesis of zero frequency offset, (10.25)-(10.26) can be rewritten as follows.

$\lvert l_u\rvert\leq\mu/2$	(10.27)
$A(n,0,k,l_u,\Delta f_u)=0$	
$\lvert l_u\rvert>\mu/2$	(10.28)
$A(n,0,k,l_u,\Delta f_u)=2\sin^2\left(\frac{\pi}{M}(\lvert l_u\rvert-\frac{\mu}{2})(n-k)\right)$	

Table 10.3. Parameter *A* of equation (10.15) in AWGN and no frequency offset.

10.3.1 Comments on Performance

It should be noted that the MAI power is a function of the particular tone assignment criterion. We herein consider two particular cases.

In the first case we deploy interleaved tone multiplexing (Fig. 3.10). In the second case we assign disjoint blocks of K_u contiguous tones to each user (Fig. 3.8). Assuming $K_u = K$, $N_U = M/K$ (i.e. users with equal number of tones), the set of tone indices assigned to user $u = 0,...,N_U - 1$ in the above schemes can be expressed respectively as

$$\textit{Interleaved:} \quad k_{u,i} = u + \frac{M}{K} i \qquad i = 0,...,K-1 \tag{10.29}$$

$$\textit{Block:} \quad k_{u,i} = uK + i \qquad i = 0,...,K-1. \tag{10.30}$$

In order to quantify the MAI power or equivalently the SIR, we consider a system characterized by *M=1024* and *K=64*. We are interested on evaluating the power of the MAI generated by one active user on all the sub-carriers except the ones assigned to it. Basically this user acts as an interferer on all the sub-carriers that do not belong to its set of tones. We further consider both cases when this single interferer uses the set of tones defined in (10.29) or (10.30) (with *u=1*). In general, when this interferer has both a time and a frequency offset relatively to the user that we are demodulating, equations of Table 10.2 apply.

First, in Fig. 10.4 we plot the SIR (with $P_{u,n} = P_u = 1$ for all *n*) on the *n-th* sub-carrier as a function of the frequency offset when the time offset is smaller than half the guard time. Dashed curves are for the interleaved tone assignment, while solid curves are for the block tone assignment.

Note that when $|l_u| \leq \mu/2$, the interferer has equal power tones ($P_u = P_{u,n}$) and we consider the interleaved tone assignment of (10.29), the MAI power can be evaluated in closed form, yielding

$$M(u,n \mid l_u, \Delta f_u) = \frac{P_u}{N_U{}^2} \frac{\sin^2(\pi(n - k_{u,0} + \overline{\Delta f}_u))}{\sin^2(\frac{\pi}{N_U}(n - k_{u,0} + \overline{\Delta f}_u))}. \tag{10.31}$$

The worst case in terms of SIR occurs on the sub-carrier *n* that is adjacent to a sub-carrier belonging to the interfering set of tones (as Fig. 10.4 also confirms).

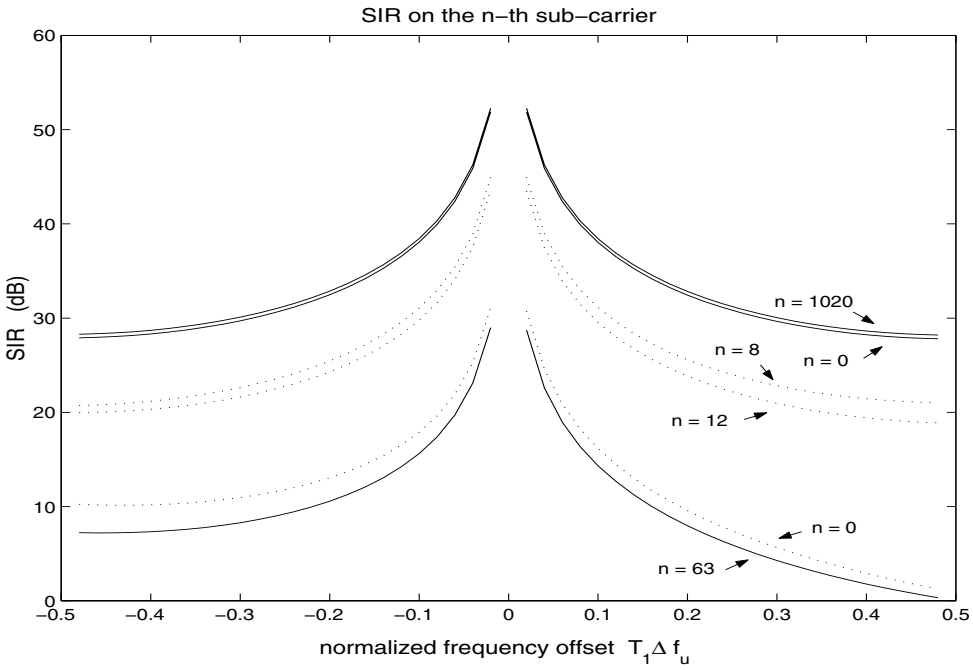

Fig. 10.4. SIR by a single user on the *n-th* sub-carrier as a function of the normalized to the sub-carrier spacing frequency offset. Time offset smaller than the guard interval. Solid lines: block tone assignment scheme. Dashed lines: interleaved tone assignment. M=1024, K=64.

Considering the block tone assignment, we report in Fig. 10.5 the MAI as a function of the sub-carrier for several values of the normalized frequency offset.

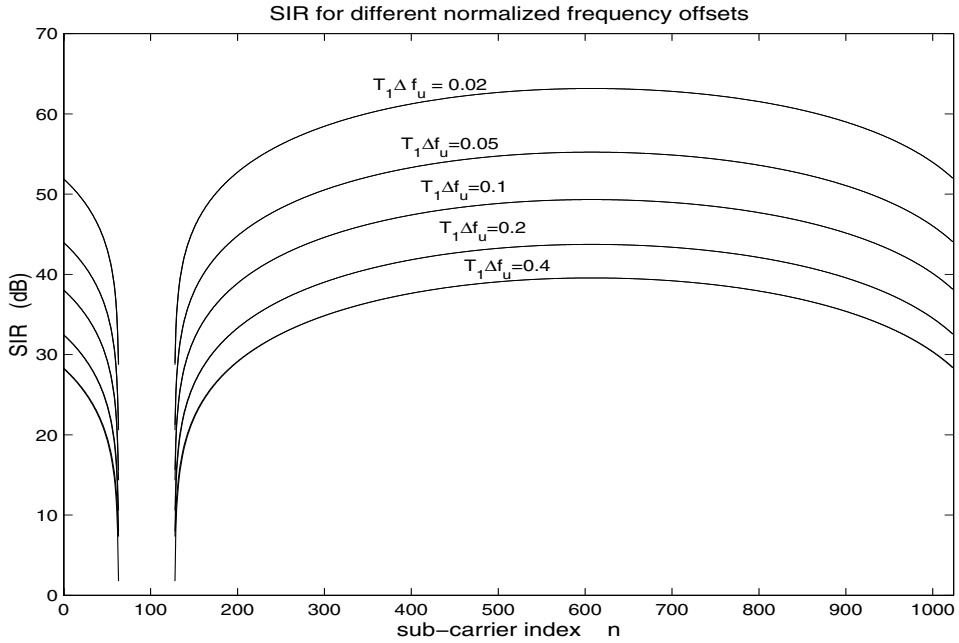

Fig. 10.5. SIR by a single user for a given normalized frequency offset as a function of the sub-carrier. Time offset smaller than the guard interval. Block tone assignment scheme with M=1024, K=64.

Now, assuming no frequency offset, the equations of Table 10.3 apply. In Fig. 10.6 we plot the SIR evaluated on different sub-carriers as a function of the excess time offset. Again the worst case in terms of SIR is seen to occur on an adjacent sub-carrier *n*.

It is interesting to observe that for the interleaved tone assignment case, as long as $|l_u|-\mu/2 \le K_u$, the MAI power in the absence of frequency offset is linearly increasing with the time delay and does not depend on the sub-carrier index *n*, as expressed by

$$M(u,n\,|\,l_u,\Delta f_u=0)=2P_uK_u(|\,l_u\,|-\mu/2)/M^2\,. \tag{10.32}$$

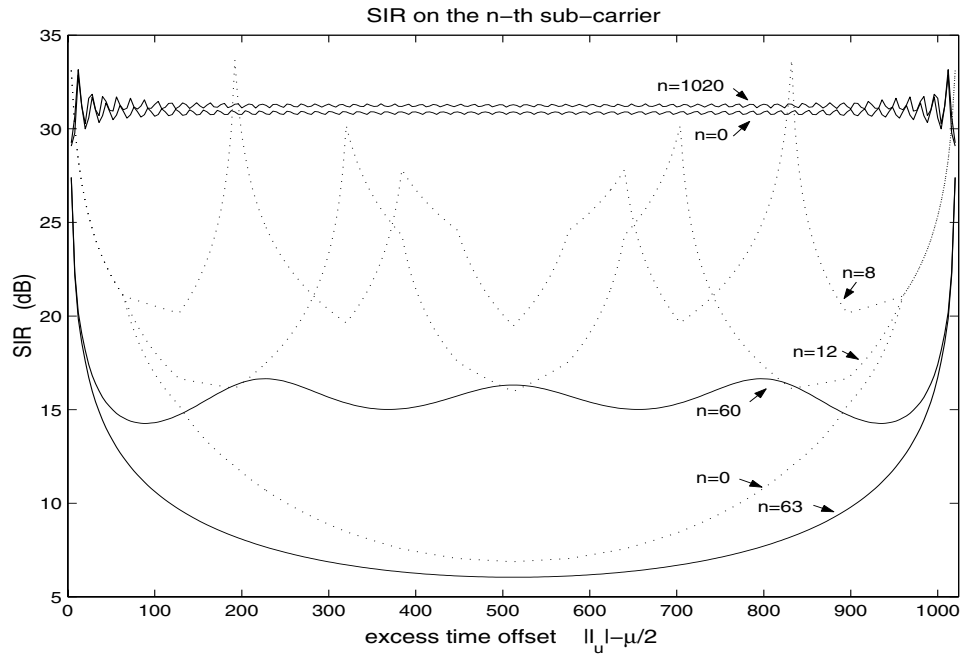

Fig. 10.6. SIR by a single user on the *n-th* sub-carrier as a function of the time offset exceeding the guard interval when there is no frequency offset. Solid lines: block tone assignment scheme. Dashed lines: interleaved tone assignment with M=1024, K=64.

Finally, consider Fig. 10.7 and Fig. 10.8 where we examine the joint effect, on an adjacent sub-carrier (worst case), of non-zero frequency offset and time offset larger than the guard time. Looking at Fig. 10.7 and Fig. 10.8, both assignment strategies exhibit strong penalties on the SIR, with a slight advantage for the interleaved case. On the other hand if the block strategy is deployed the SIR can be greatly bettered by turning off just the first tone in each block (see Fig. 10.9).

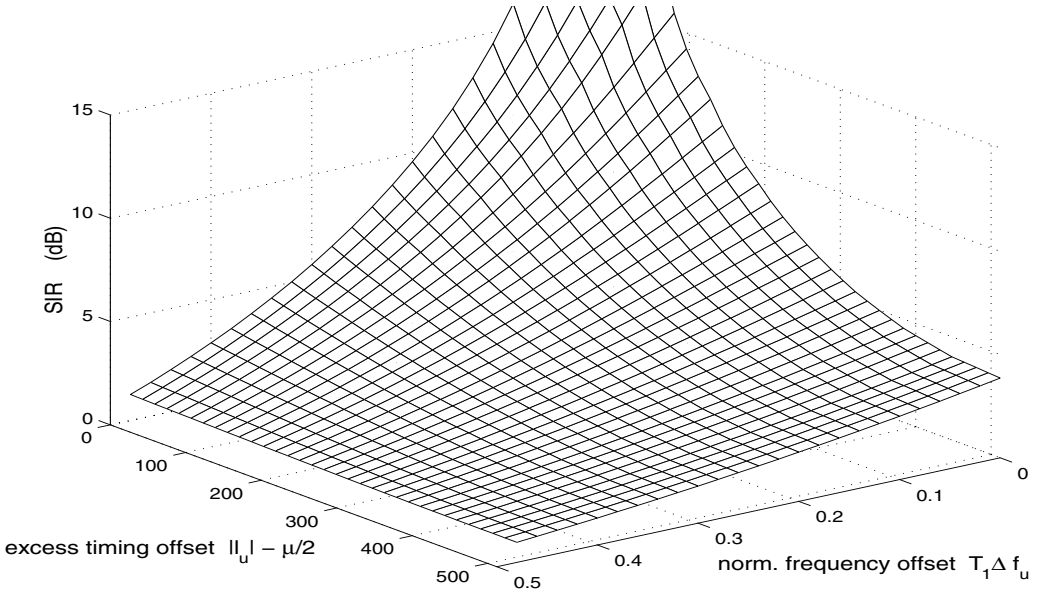

Fig. 10.7. SIR by a single user on an adjacent sub-carrier (worst case) as a function of the time offset exceeding the guard interval and the normalized frequency offset. Interleaved tone assignment scheme with M=1024, K=64.

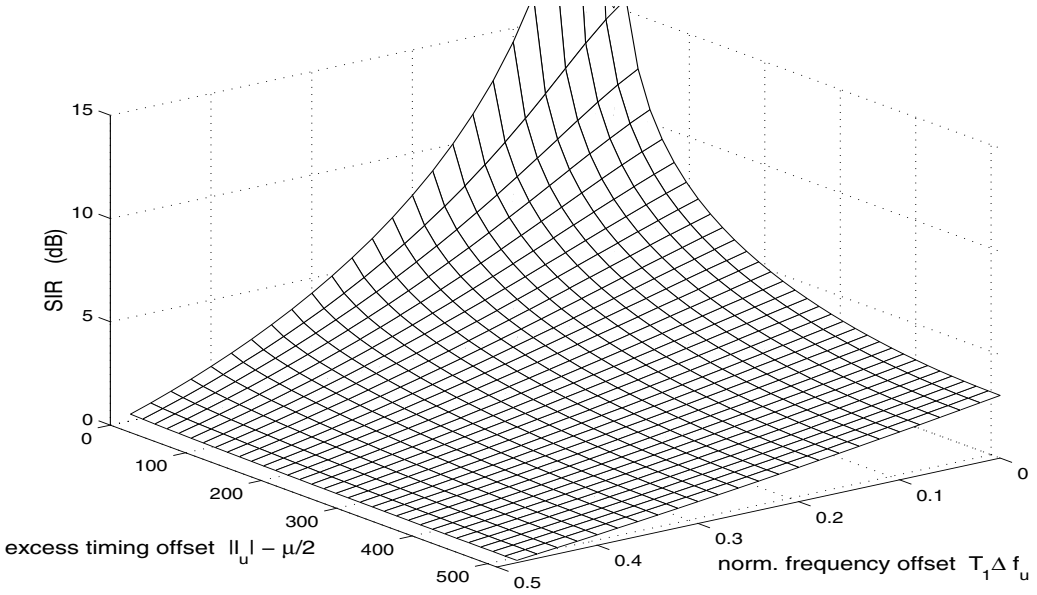

Fig. 10.8. SIR by a single user on an adjacent sub-carrier (worst case) as a function of the time offset exceeding the guard interval and the normalized frequency offset. Block tone assignment scheme with M=1024, K=64.

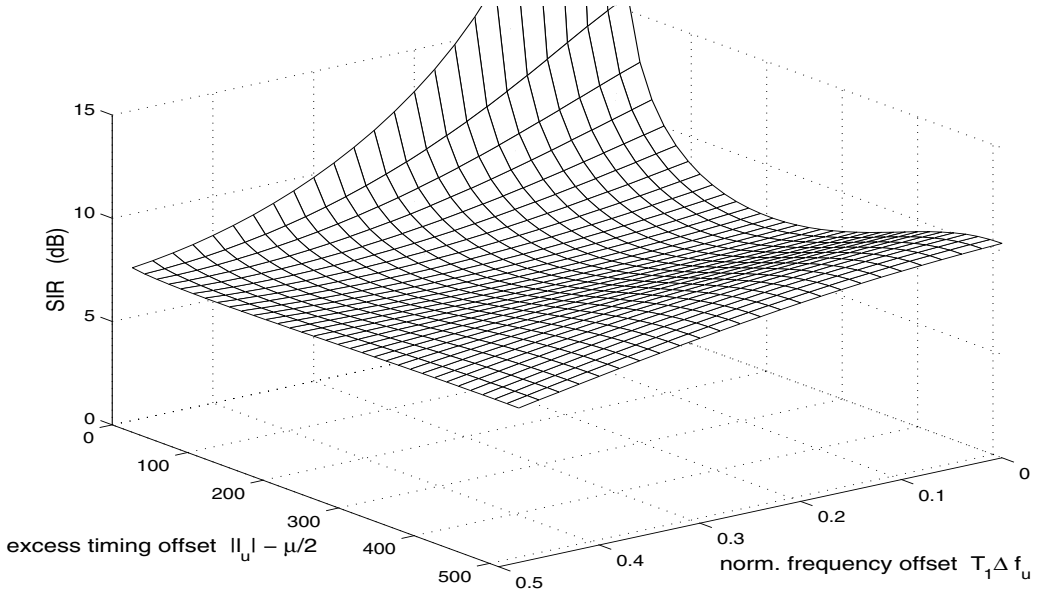

Fig. 10.9. SIR by a single user on an adjacent sub-carrier (worst case) as a function of the time offset exceeding the guard interval and the normalized frequency offset. Block tone assignment scheme with frequency guard, M=1024, K=64. The interferer does not transmit on the first tone (i.e. tone index 64).

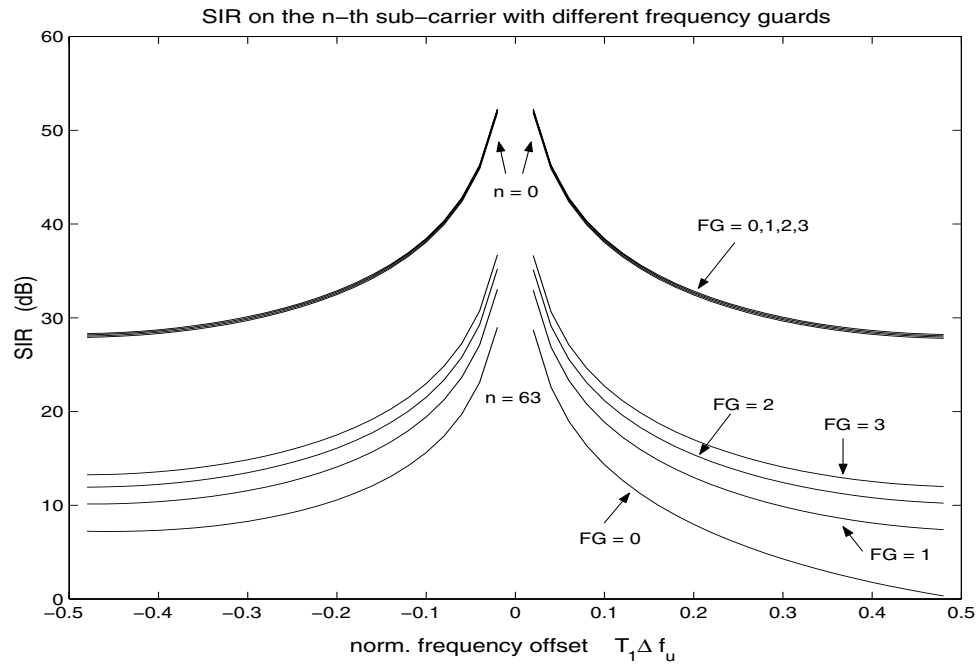

Fig. 10.10. SIR by a single user on the *n-th* sub-carrier as a function of the normalized frequency offset, with time offset smaller than the guard interval. Block tone assignment scheme, M=1024, K=64, and different number of unused tones at the lower end of each block.

From the above analysis, it follows that while we can suppress the detrimental effects of the time offset by an appropriate guard-time, the frequency offset effect can not be entirely suppressed. However, if we deploy a block tone assignment algorithm, the insertion of a frequency-guard between blocks belonging to distinct users can significantly lower the interference. Equivalently we can turn off some of the tones at the beginning of each block. In this way trading off with the spectral efficiency can optimize the system performance. The SIR gain with such an approach is shown, for instance, in Fig. 10.10.

10.4 Performance in Multipath Fading

In this section we evaluate the symbol error rate performance through a simple Gaussian approximation. The channel is assumed to be a slow, i.e., static for the duration of the DMT block, multipath Rayleigh fading channel.

10.4.1 Symbol Error Rate Performance

Under the hypothesis of the MAI being Gaussian distributed, the probability of symbol error is here approximated as follows.

Let us define $\mathrm{H}^u = E[|H^{u,n}(iT_0)|^2] = \sum_{p=0}^{N_P} \Omega_{u,p}$ and let $\gamma_s = |H^{u,n}(iT_0)|^2 \; SINR(u,n \mid \underline{l}, \underline{\Delta f}) / \mathrm{H}^u$ be the conditional average SINR, i.e. conditioned on the channel profile of user u and on the time/frequency offsets of all interferers. Let $P_{e,s}(n \mid \gamma_s)$ be the conditional probability of symbol error on the *n-th* sub-channel that is achieved with a given γ_s. Then, averaging over the distribution of γ_s yields the average symbol error rate of the *n-th* sub-channel, $P_{e,s}(n)$.

To exemplify the procedure, consider M-PSK modulation coherently detected. Since $|H^{u,n}(iT_0)|$ is Rayleigh distributed, then the result of first averaging over the distribution of $|H^{u,n}(iT_0)|$ is from [48] equation (14-4-39):

$$P_{e,s}(n \mid \underline{l}, \underline{\Delta f}) \approx \frac{(M-1)}{(M \log_2 M) \sin^2(\pi / M) \overline{\gamma}_s / 2} \tag{10.33}$$

where $\overline{\gamma}_s = SINR(n \mid \underline{l}, \underline{\Delta f})$.

A final integration over each $p_l(l_{u'})$, i.e. pdf of the delay of user u', and $p_f(\Delta f_{u'})$, i.e. pdf of the frequency offset of user u', yields the result.

Note that the time and frequency offsets are considered independent. Further, averaging of (10.33) is done only on the time and frequency offsets of the interferers and not on their channel

profile. The channel profile of the interferers concurs to the calculation of the average SINR in (10.22). Finally, observe that $P_{e,s}(n)$ is in general not the same for all sub-channels. The global performance of the *u-th* user link is then

$$P_{e,s}^{u} = \frac{1}{K_u} \sum_{n \in \Gamma_u} P_{e,s}(n) . \tag{10.34}$$

The evaluation of (10.34) is carried out numerically, and reported in the next section for several system scenarios.

10.4.2 Performance Results for Several System Scenarios

From the discussion in the previous sections it is clear that many system parameters determine the ultimate effect. As an example, we consider a hypothetical system whose main parameters are summarized in Table 10.4. The cyclic prefix allows fully compensating the multipath channel as long as the round trip propagation delay is smaller than 5.36 μs, that is for cells with radius up to 0.8 Km. The channel power profile is exponential and identical for all users, i.e. $\Omega_p^u = (1-e^{-\beta})(1-e^{-\beta N_P})^{-1} e^{-\beta p}$ with N_P=*42*, $\beta = \ln(1.1)$. The system is fully loaded.

W=4.096 MHz	**modulation** : 4-PSK	**max echo delay:** 10 μs
M=192 - μ=64	**total net bit-rate** : 6.144 Mb/s	exponential channel power profile
T=0.24 μs	**num. of users** : N_U=16	
μ_1=22 (5.36 μs) μ_2=42 (10μs)	**num. of tone/user** : K_u=12 equal power tones	

Table 10.4. System parameters.

First we show the average SIR performance (i.e. $\sigma^2 = 0$) as a function of the sub-carrier index $k = 0,...,K_u - 1$, in the presence of only frequency offsets (Fig. 10.11) and only time offsets (Fig. 10.12). Note that the indices *k* are mapped to the carriers $n_k^u \in \Gamma_u$ according to the tone assignment scheme (e.g. block, interleaved). The worst case that is here considered has all users with identical time and frequency offsets. Since the system is fully loaded, the tones have equal power and are assigned with symmetric rules, the average SIR performance does not differ among users.

The interleaved scheme yields a worse SIR compared to the block scheme. The SIR for the block scheme can be further improved by assigning a frequency guard at the beginning and/or end of each block. Basically this is equivalent to no symbol transmission on some of the tones at the lower or upper end of each block (e.g. FG=1 no symbols transmitted on the first tone, FG=2 no symbols transmitted on the first and last tone of each block).

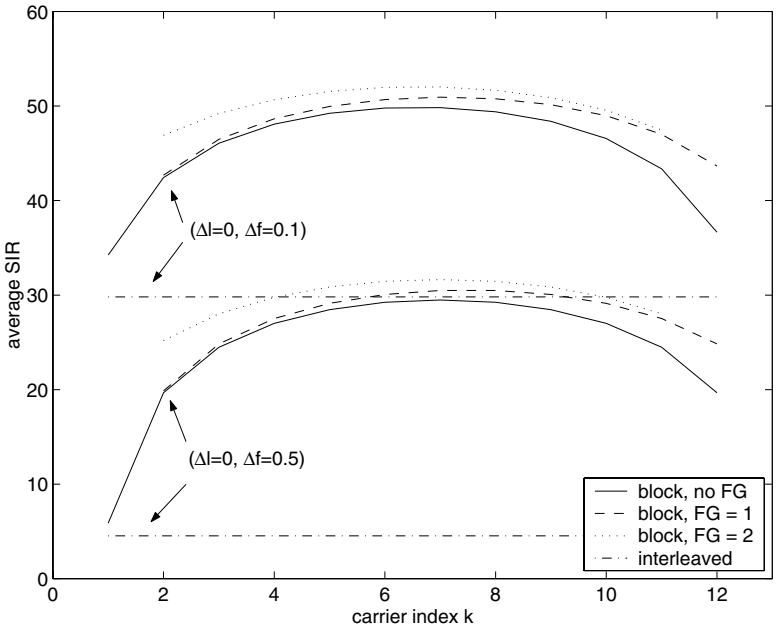

Fig. 10.11. Average SIR on each of the 12 sub-carriers assigned to user u when all the remaining users have no excess time offset but all have identical normalized frequency offset relatively to user u (i.e. worst case). Further, all users have equal power tones. The different curves are obtained for $T_l\Delta f_u$=0.1 and $T_l\Delta f_u$ =0.5 with block, block with frequency guards, and interleaved tone assignments.

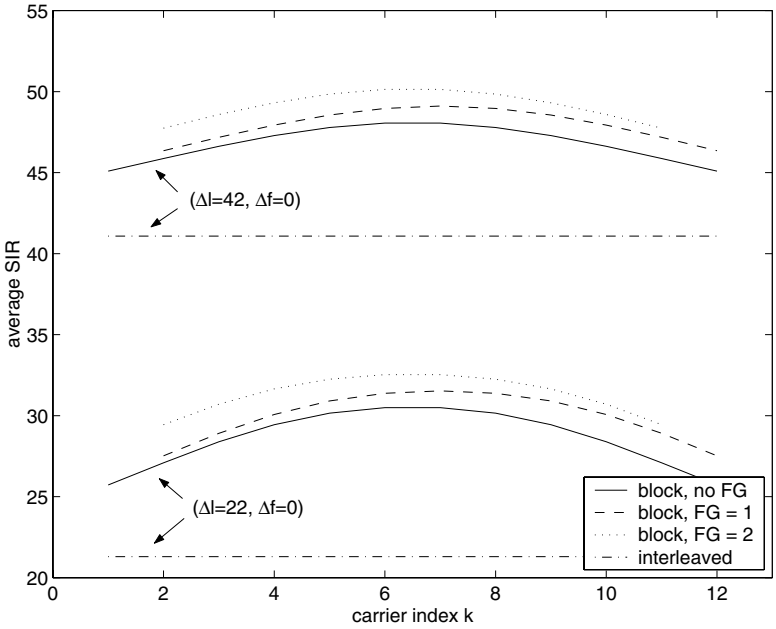

Fig. 10.12. Average SIR on each of the 12 sub-carriers assigned to user u when all the remaining users have no frequency offset but all have identical excess time offset relatively to user u (i.e. worst case). Further, all users have equal power tones. The different curves are obtained for Δt_u=22T and Δt_u=42T with block, block with frequency guards, and interleaved tone assignments.

Now consider the user link SER performance. Averaging of (10.33) is numerically done under the assumption of time offsets and frequency offsets uniformly distributed and independent among users. Each user has the same average SER performance. Comparing Fig. 10.13 with Fig. 10.14 the superiority of the block tone assignment scheme is clear. Further SER improvements are possible with the insertion of frequency guards as shown in Fig. 10.15, where the error floor due to the MAI significantly drops by just deploying one frequency guard. However, this goes together with some loss of bandwidth or net bit rate.

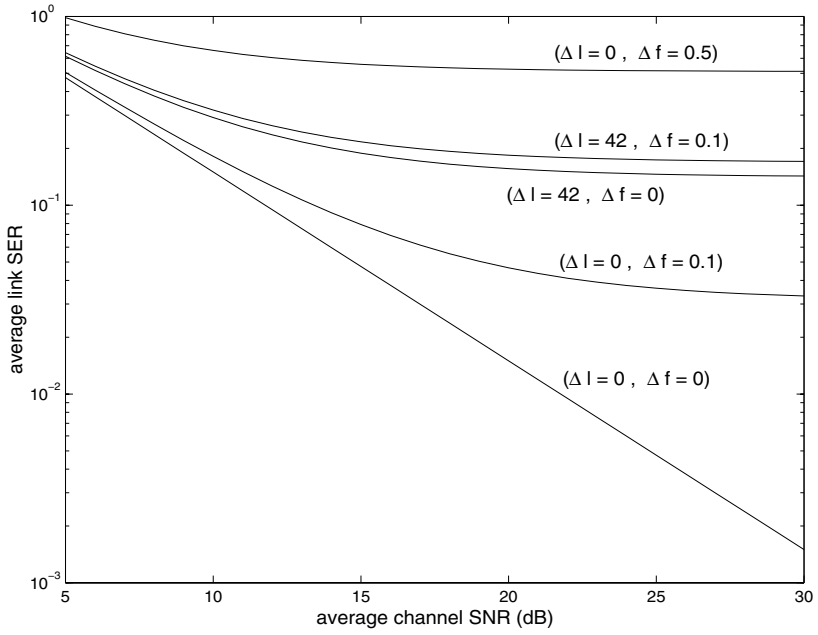

Fig. 10.13. User link average symbol error rate versus SNR for several values of maximum normalized frequency offset and maximum time offset. Time offsets and frequency offsets are uniformly distributed respectively in $[-T\Delta l\ ,\ T\Delta l]$ and in $[-\Delta f/T_1\ ,\ \Delta f/T_1]$. Interleaved tone assignment. Equal power tones.

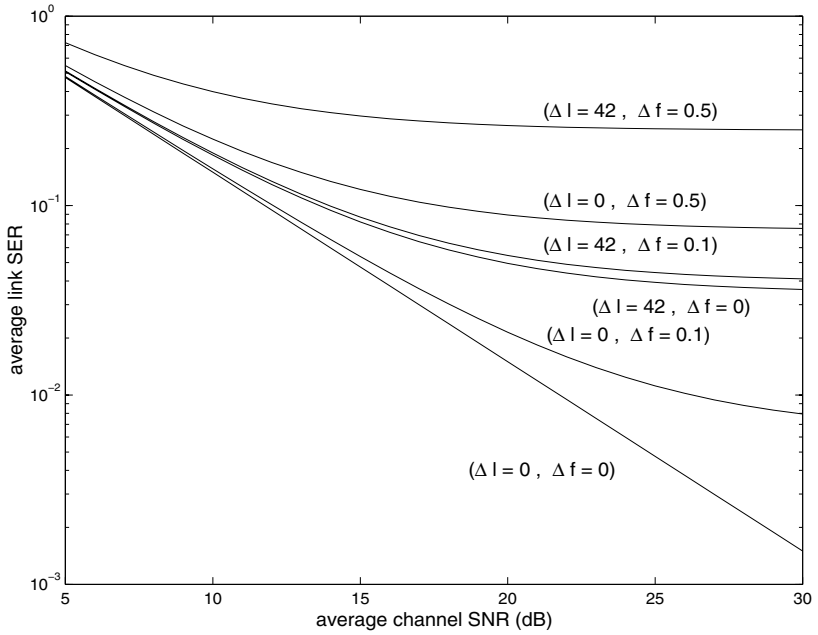

Fig. 10.14. User link average symbol error rate versus SNR for several values of maximum normalized frequency offset and maximum time offset. Time offsets and frequency offsets are uniformly distributed respectively in [$-T\Delta l$, $T\Delta l$] and in [$-\Delta f/T_1$, $\Delta f/T_1$]. Block tone assignment. Equal power tones

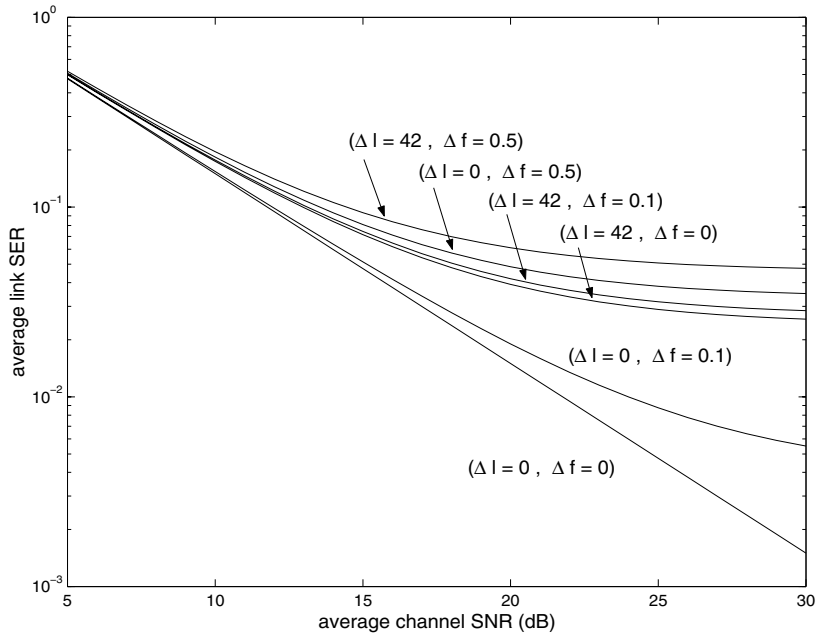

Fig. 10.15. User link average symbol error rate versus SNR for several values of maximum normalized frequency offset and maximum time offset. Time offsets and frequency offsets are uniformly distributed respectively in [$-T\Delta l$, $T\Delta l$] and in [$-\Delta f/T_1$, $\Delta f/T_1$]. Block tone assignment with one frequency guard. Equal power tones.

10.5 Performance in Fast Fading

The analysis of the previous sections is based on the assumption of quasi static fading channels, i.e. the channel does not vary over an observation block of *M* samples. This is a reasonable assumption for many broadband applications with relatively low mobility requirements. Nevertheless, it is interesting to investigate the effect of fast fading in a DMT system with a simple FFT based receiver (see also Chapter 7).

Let us assume to transmit the DMT modulated symbols (with no cyclic prefix) over a flat fading noisy channel. The sampled received signal (at rate *1/T*) is here modeled as follows:

$$y_i^k = \alpha_i^k x_i^k + \eta_i^k \tag{10.35}$$

where $\alpha_i^k = \alpha(0; kT + iT_0)$ represents the multiplicative distortion introduced by the fading channel, and η_i^k is an AWGN term. The conventional DMT receiver applies a DFT to blocks of *N=M* received samples:

$$z^n(iT_0) = \frac{1}{N}\sum_{k=0}^{N-1} y_i^k e^{-j\frac{2\pi}{N}nk} \qquad n = 0,...,N-1. \tag{10.36}$$

We can rewrite (10.36) as follows:

$$\begin{aligned} z^n(iT_0) &= \frac{1}{N}\sum_{m=0}^{N-1} a^m(iT_0) \underbrace{\sum_{k=0}^{N-1} \alpha_i^k e^{j\frac{2\pi}{N}(m-n)k}}_{H_{m-n}(iT_0)} + \underbrace{\sum_{k=0}^{N-1} \eta_i^k e^{-j\frac{2\pi}{N}nk}}_{w_i^n} \\ &= \frac{1}{N} H_0(iT_0) a^n(iT_0) + \frac{1}{N}\sum_{m\neq n} a^m(iT_0) H_{m-n}(iT_0) + w_i^n \end{aligned} . \tag{10.37}$$

The first term represents the transmitted symbol multiplied by $H_0(iT_0)/N$, while the second term is the inter-carrier interference (ICI) introduced, in general, by a time varying channel coefficient α_i^k that is not constant over a transmitted block. The last term is simply an additive Gaussian noise contribution to the received signal. If the channel is constant over the length of a DMT block, i.e. $\alpha_i^k = \alpha_i$, then no ICI is introduced and (10.37) becomes $z^n(iT_0) = \alpha_i a^n(iT_0) + w_i^n$.

10.5.1 Intercarrier Interference Second Order Statistics

We are here interested on evaluating the second order statistics of the ICI term in equation (10.37). A similar analysis is reported in [38]. Assuming a channel that is wide sense stationary we can drop the index *i* and rewrite the ICI term:

$$\xi^n = \frac{1}{N}\sum_{m\neq n} a^m \sum_{k=0}^{N-1} \alpha^k e^{j\frac{2\pi}{N}(m-n)k} \quad . \tag{10.38}$$

The ICI term can be considered Gaussian distributed when a large number of sub-carriers is deployed. Considering independent, zero mean, transmitted symbols a^m with power $E[|\, a^m\,|^2] = P_a$, the mean of the ICI term is $E\left[\xi^n\right] = 0$ while the autocorrelation can be computed as follows:

$$\begin{aligned} r_\xi(l) &= E\left[\xi^n \xi^{n+l^*}\right] = E\left[\left(\frac{1}{N}\sum_{m\neq n} a^m H_{m-n}\right)\left(\frac{1}{N}\sum_{p\neq n+l} a^p H_{p-n-l}\right)^*\right] \\ &= \frac{1}{N^2}\sum_{\substack{m\neq n \\ m\neq n+l}} E\left[|\, a^m\,|^2\right] E\left[H_{m-n} H^*_{m-n-l}\right] = \frac{P_a}{N^2}\sum_{\substack{m\neq n \\ m\neq n+l}} E\left[H_{m-n} H^*_{m-n-l}\right] \\ &= \frac{P_a}{N^2}\sum_{\substack{m\neq n \\ m\neq n+l}} E\left[\sum_{k=0}^{N-1}\alpha^k e^{j\frac{2\pi}{N}(m-n)k} \sum_{p=0}^{N-1}\alpha^{p^*} e^{-j\frac{2\pi}{N}(m-n-l)p}\right] \\ &= \frac{P_a}{N^2}\sum_{\substack{m\neq n \\ m\neq n+l}} \sum_{k=0}^{N-1}\sum_{p=0}^{N-1} E\left[\alpha^k \alpha^{p^*}\right] e^{j\frac{2\pi}{N}(m-n)k} e^{-j\frac{2\pi}{N}(m-n-l)p} \end{aligned} \quad .$$

Let $r_\alpha(p-k) = E\left[\alpha^p \alpha^{k^*}\right]$ then,

$$\begin{aligned} r_\xi(l) &= \frac{P_a}{N^2}\sum_{\substack{m\neq n \\ m\neq n+l}} \sum_{k=0}^{N-1}\sum_{p=0}^{N-1} r_\alpha(p-k) e^{j\frac{2\pi}{N}(m-n)k} e^{-j\frac{2\pi}{N}(m-n-l)p} \\ &= \frac{P_a}{N^2}\sum_{m=0}^{N-1}\sum_{k=0}^{N-1}\sum_{p=0}^{N-1} r_\alpha(p-k) e^{j\frac{2\pi}{N}(k-p)m} e^{j\frac{2\pi}{N}(lp+np-nk)} - \frac{P_a}{N^2}\sum_{k=0}^{N-1}\sum_{p=0}^{N-1} r_\alpha(p-k)\left(e^{j\frac{2\pi}{N}lk} + e^{j\frac{2\pi}{N}lp} - e^{j\frac{2\pi}{N}lp}\delta(l)\right) \\ &= \frac{P_a}{N^2}\sum_{k=0}^{N-1}\sum_{p=0}^{N-1} r_\alpha(p-k)\delta(k-p) e^{j\frac{2\pi}{N}(lp+np-nk)} - \frac{P_a}{N^2}\sum_{k=0}^{N-1}\sum_{p=0}^{N-1} r_\alpha(p-k)\left(e^{j\frac{2\pi}{N}lk} + e^{j\frac{2\pi}{N}lp}\left(1-\delta(l)\right)\right) \\ &= \frac{P_a}{N^2}\sum_{k=0}^{N-1} r_\alpha(0)\delta(0) e^{j\frac{2\pi}{N}(kl)} - \frac{P_a}{N^2}\sum_{k=0}^{N-1}\sum_{p=0}^{N-1} r_\alpha(p-k)\left(e^{j\frac{2\pi}{N}lk} + e^{j\frac{2\pi}{N}lp}\left(1-\delta(l)\right)\right) \\ &= \frac{P_a}{N^2} r_\alpha(0) N\sum_{k=0}^{N-1} e^{j\frac{2\pi}{N}(kl)} - \frac{P_a}{N^2}\sum_{k=0}^{N-1}\sum_{p=0}^{N-1} r_\alpha(p-k)\left(e^{j\frac{2\pi}{N}lk} + e^{j\frac{2\pi}{N}lp}\left(1-\delta(l)\right)\right) \end{aligned} \quad .$$

Finally, we obtain:

$$r_\xi(l) = \frac{P_a}{N} r_\alpha(0)\delta(l) - \frac{P_a}{N^2}\sum_{k=0}^{N-1}\sum_{p=0}^{N-1} r_\alpha(p-k)\left(e^{j\frac{2\pi}{N}lk} + e^{j\frac{2\pi}{N}lp}\left(1-\delta(l)\right)\right). \tag{10.39}$$

It follows that the autocorrelation of the ICI is completely specified by the statistics of the channel tap α^k. To proceed we assume the Clarke's isotropic scattering model for the channel α^k. Thus, α^k is a complex Gaussian process with zero mean, power one, and autocorrelation:

$$r_\alpha(l) = E\left[\alpha^n \alpha^{n+l^*}\right] = J_0\left(2\pi l f_d T\right) \tag{10.40}$$

where $J_0(.)$ is the zero-order Bessel function of the first kind, and f_d is the maximum Doppler spread. Equation (10.39) can now be particularized into:

$$r_\xi(l) = \frac{P_a}{N}\delta(l) - \frac{P_a}{N^2}\sum_{k=0}^{N-1}\sum_{p=0}^{N-1} J_0\left(2\pi f_d T(p-k)\right)\left(e^{j\frac{2\pi}{N}lk} + e^{j\frac{2\pi}{N}lp}\left(1-\delta(l)\right)\right). \tag{10.41}$$

The power of the ICI is then:

$$\begin{aligned} r_\xi(0) &= P_a - \frac{P_a}{N^2}\sum_{k=0}^{N-1}\sum_{p=0}^{N-1} J_0\left(2\pi f_d T(p-k)\right) = P_a - \frac{P_a}{N^2}\sum_{k=0}^{N-1}\sum_{m=k}^{k-N+1} J_0\left(2\pi f_d T m\right) \\ &= P_a - \frac{P_a}{N^2}\left(N + \sum_{k=1}^{N-1} 2(N-k) J_0\left(2\pi f_d T k\right)\right) \end{aligned}. \tag{10.42}$$

Now we define the signal-to-interference ratio as:

$$SIR = E\left[|a^n|^2\right] / E\left[|\xi^n|^2\right] = P_a / \sigma^2 . \tag{10.43}$$

We plot in Fig. 10.16 the SIR as a function of the normalized Doppler spread, $f_d T$ for a number of sub-carriers equal to *N*=8, 64, 128, 256, 512, 1024. Fig. 10.16 shows that the SIR decreases as the number of carriers and/or the Doppler spread increases. Further, the SIR exhibits a floor equal to:

$$SIR_{f_d T=\infty} = \lim_{f_d T \to \infty}\left(SIR(f_d T)\right) = \left(1 - \frac{1}{N}\right)^{-1} . \tag{10.44}$$

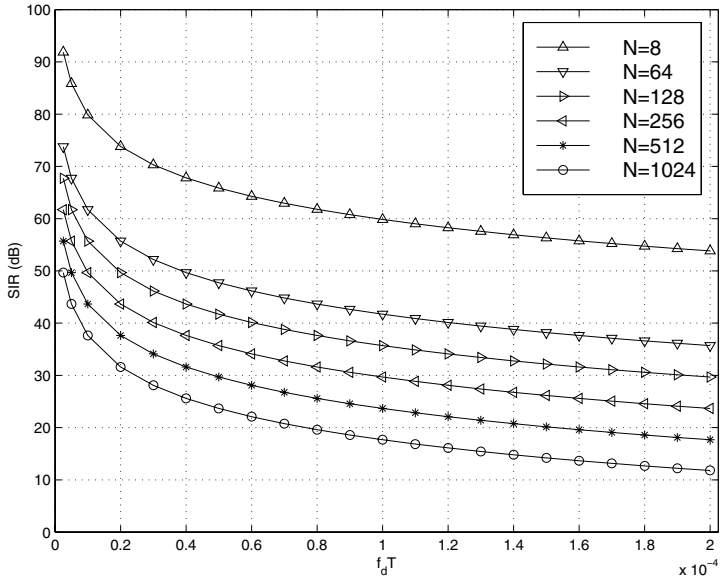

Fig. 10.16. SIR as a function of the normalized Doppler spread in DMT for several numbers of carriers *N*.

APPENDIX TO CHAPTER 10

F Interference Correlation

The computation of the interference correlation is particularly cumbersome. In this appendix we report the main points, while all details can be found in [67]. The calculation yields for the parameter A in equation (10.14) the expressions shown in Table 10.5.

$-\mu+\frac{\mu_1}{2}>l_u\geq -M+\frac{\mu_1}{2}$	(F.1)
$A(n,p,k,l_u,\Delta f_u)=\sum_{t=0}^{N_P}\Omega_{u,t}\{\ 2+2e^{j\frac{2\pi}{M}(t-l_u+\frac{\mu_1}{2}-\mu)p}-e^{j\frac{2\pi}{M}(t-l_u+\frac{\mu_1}{2}-\mu)(\overline{\Delta f_u}+n+p-k)}+$ $-e^{j\frac{2\pi}{M}(t-l_u+\frac{\mu_1}{2}-\mu)(-\overline{\Delta f_u}-n+k)}-e^{j\frac{2\pi}{M}(t-l_u+\frac{\mu_1}{2}-\mu-M)(-\overline{\Delta f_u}-n+k)}-e^{j\frac{2\pi}{M}(t-l_u+\frac{\mu_1}{2}-\mu-M)(\overline{\Delta f_u}+n+p-k)}\ \}$	
$N_P-\mu+\frac{\mu_1}{2}>l_u\geq -\mu+\frac{\mu_1}{2}$	(F.2)
$A(n,p,k,l_u,\Delta f_u)=2\sum_{t=0}^{N_P}\Omega_{u,t}-(e^{j2\pi\overline{\Delta f_u}}+e^{-j2\pi\overline{\Delta f_u}})\sum_{t=0}^{\mu-\frac{\mu_1}{2}+l_u}\Omega_{u,t}+\sum_{t=\mu-\frac{\mu_1}{2}+l_u+1}^{N_P}\Omega_{u,t}\{\ 2e^{j\frac{2\pi}{M}(-\mu+\frac{\mu_1}{2}-l_u+t)p}-e^{-j\frac{2\pi}{M}(-\mu+\frac{\mu_1}{2}-l_u+t)(n+\overline{\Delta f_u}-k)}+$ $-e^{-j\frac{2\pi}{M}(-\mu+\frac{\mu_1}{2}-l_u-M+t)(n+\overline{\Delta f_u}-k)}-e^{j\frac{2\pi}{M}(-\mu+\frac{\mu_1}{2}-l_u+t)(n+\overline{\Delta f_u}+p-k)}-e^{j\frac{2\pi}{M}(-\mu+\frac{\mu_1}{2}-l_u-M+t)(n+\overline{\Delta f_u}+p-k)}\ \}$	
$\frac{\mu_1}{2}\geq l_u\geq N_P-\mu+\frac{\mu_1}{2}$	(F.3)
$A(n,p,k,l_u,\Delta f_u)=(2-e^{j2\pi\overline{\Delta f_u}}-e^{-j2\pi\overline{\Delta f_u}})\sum_{t=0}^{N_P}\Omega_{u,t}$	
$N_P+\frac{\mu_1}{2}\geq l_u>\frac{\mu_1}{2}$	(F.4)
$A(n,p,k,l_u,\Delta f_u)=2\sum_{t=0}^{N_P}\Omega_{u,t}-(e^{j2\pi\overline{\Delta f_u}}+e^{-j2\pi\overline{\Delta f_u}})\sum_{t=l_u-\frac{\mu_1}{2}+1}^{N_P}\Omega_{u,t}+\sum_{t=0}^{l_u-\frac{\mu_1}{2}}\Omega_{u,t}\{\ 2e^{-j\frac{2\pi}{M}(l_u-\frac{\mu_1}{2}-t)p}-e^{j\frac{2\pi}{M}(l_u-\frac{\mu_1}{2}-t)(n+\overline{\Delta f_u}-k)}+$ $-e^{-j\frac{2\pi}{M}(M-l_u+\frac{\mu_1}{2}+t)(n+\overline{\Delta f_u}-k)}-e^{-j\frac{2\pi}{M}(l_u-\frac{\mu_1}{2}-t)(n+p+\overline{\Delta f_u}-k)}-e^{j\frac{2\pi}{M}(M-l_u+\frac{\mu_1}{2}+t)(n+p+\overline{\Delta f_u}-k)}\ \}$	
$M+\frac{\mu_1}{2}-1\geq l_u>N_P+\frac{\mu_1}{2}$	(F.5)
$A(n,p,k,l_u,\Delta f)=\sum_{t=0}^{N_P}\Omega_{u,t}\{\ 2+2e^{j\frac{2\pi}{M}(M-l_u+\frac{\mu_1}{2}+t)p}-e^{j\frac{2\pi}{M}(t-l_u+\frac{\mu_1}{2})(-\overline{\Delta f_u}-n+k)}-e^{j\frac{2\pi}{M}(t-l_u+\frac{\mu_1}{2})(\overline{\Delta f_u}+n+p-k)}+$ $-e^{j\frac{2\pi}{M}(M-l_u+\frac{\mu_1}{2}+t)(-\overline{\Delta f_u}-n+k)}-e^{j\frac{2\pi}{M}(t+M-l_u+\frac{\mu_1}{2})(\overline{\Delta f_u}+n+p-k)}\ \}$	

Table 10.5. Parameter A of equation (10.14).

First we summarize some relations and properties that turn out to be useful in the evaluation of the correlation. Under the assumptions of Section 10.2 the following relations apply.

$$E[a^{u',n}(iT_0)a^{u'',l}(mT_0)^*]=0 \quad \text{for } n\neq l \ \vee\ i\neq m \ \vee\ u'\neq u'' \tag{F.6}$$

$$E[x_i^{u,m}(x_i^{u,l})^*]=\sum_{n\in\Gamma_u}P_{u,n}e^{j\frac{2\pi}{M}n(m-l)} \qquad E[x_i^{u',m}(x_j^{u'',l})^*]=0 \quad \text{for } i\neq j \ \vee\ u'\neq u''. \tag{F.7}$$

Let the channel taps be redefined as follows:

$$h_i^{u,k,p}=e^{j(\overline{\Delta\phi_{u,i}}+\mu\frac{\pi}{M}\overline{\Delta f_u})}e^{-j\frac{2\pi}{M}\overline{\Delta f_u}k}\alpha^u(p;iT_0+(\mu+k)T). \tag{F.8}$$

Then, under the hypothesis of Section 10.2 we have

$$E[h_i^{u,m,p'}h_i^{u,l,p''*}]=0 \quad p'\neq p'' \qquad E[h_i^{u,m,p}h_i^{u,l,p^*}]=e^{-j\frac{2\pi}{M}\overline{\Delta f_u}(m-l)}\Omega_{u,p}. \tag{F.9}$$

In the calculation of the MAI autocorellation the following relations are extensively deployed.

$$\sum_{k=0}^{A}\sum_{l=0}^{k}f(l)g(k)=\sum_{l=0}^{A}\sum_{k=l}^{A}f(l)g(k) \tag{F.10}$$

$$\sum_{k=0}^{A}\sum_{l=k}^{A}f(l)g(k)=\sum_{l=0}^{A}\sum_{k=0}^{l}f(l)g(k) \tag{F.11}$$

$$\sum_{k=0}^{A}\sum_{l=0}^{k+B}f(l)g(k)=\sum_{l=0}^{B}\sum_{k=0}^{A}f(l)g(k)+\sum_{l=B+1}^{B+A}\sum_{k=l-B}^{A}f(l)g(k) \tag{F.12}$$

$$\sum_{k=0}^{A}\sum_{l=k}^{B}f(l)g(k)=\sum_{l=0}^{A}\sum_{k=0}^{l}f(l)g(k)+\sum_{l=A+1}^{B}\sum_{k=0}^{A}f(l)g(k) \tag{F.13}$$

$$\sum_{k=0}^{A}\sum_{l=0}^{B}f(l,k)+\sum_{k=0}^{A}\sum_{l=B+1}^{C}f(l,k)=\sum_{k=0}^{A}\sum_{l=0}^{C}f(l,k) \tag{F.14}$$

$$\sum_{k=A}^{B}e^{j\frac{2\pi}{M}k\alpha}=\frac{e^{j\frac{2\pi}{M}A\alpha}-e^{j\frac{2\pi}{M}(B+1)\alpha}}{1-e^{j\frac{2\pi}{M}\alpha}}. \tag{F.15}$$

To proceed we need to distinguish among distinct cases that are defined according to the time interval to which l_u belongs to. We set the starting point of the observation window at the end of the cyclic prefix.

Case 1a: $0 \geq -\mu - 1 \geq l_u \geq N_P - M + 1$

The M-point observation window is associated to *M* transmitted DMT symbols as illustrated below.

$$\underbrace{x_{i-1}^{u,M-N_P-|l_u|+\mu},\ldots,x_{i-1}^{u,M-|l_u|+\mu-1}}_{N_P},\underbrace{\left[\underbrace{x_{i-1}^{u,M-|l_u|+\mu},\ldots,x_{i-1}^{u,M-1}}_{|l_u|-\mu},\underbrace{x_i^{u,M-\mu},\ldots,x_i^{u,M-1}}_{\mu},\underbrace{x_i^{u,0},\ldots,x_i^{u,M-|l_u|-1}}_{M-|l_u|}\right]}_{\underline{X}^{u,i,l_u}}.$$

The received signal component that belongs to user *u* is defined as follows.

$$\begin{aligned}
&0 \leq k \leq |l_u| - \mu - 1 && \Rightarrow y_i^{u,k} = \sum_{t=0}^{N_P} h_i^{u,k,t} x_{i-1}^{u,M+\mu-|l_u|+k-t} \\
&|l_u| - \mu \leq k \leq N_P + |l_u| - \mu - 1 && \Rightarrow y_i^{u,k} = \sum_{t=0}^{k+\mu-|l_u|} h_k^{u,i,t} x_i^{u,M-|l_u|+k-t} + \sum_{t=k+\mu-|l_u|+1}^{N_P} h_i^{u,k,t} x_{i-1}^{u,M+\mu-|l_u|+k-t} \\
&N_P + |l_u| - \mu \leq k \leq |l_u| - 1 && \Rightarrow y_i^{u,k} = \sum_{t=0}^{N_P} h_i^{u,k,t} x_i^{u,M-|l_u|+k-t} \\
&|l_u| \leq k \leq N_P + |l_u| - 1 && \Rightarrow y_i^{u,k} = \sum_{t=0}^{k-|l_u|} h_i^{u,k,t} x_i^{u,-|l_u|+k-t} + \sum_{t=k-|l_u|+1}^{N_P} h_i^{u,k,t} x_i^{u,M-|l_u|+k-t} \\
&N_P + |l_u| \leq k \leq M - 1 && \Rightarrow y_i^{u,k} = \sum_{t=0}^{N_P} h_i^{u,k,t} x_i^{u,-|l_u|+k-t}
\end{aligned} .$$

The *n-th* FFT output component that belongs to user *u*, i.e., neglecting all other users' signals and thermal noise, during the *i-th* demodulation block, is

$$\begin{aligned}
\hat{\xi}^{u,n}(iT_0) = &\sum_{k=0}^{|l_u|-\mu-1} \sum_{t=0}^{N_P} h_i^{u,k,t} x_{i-1}^{u,M+\mu-|l_u|+k-t} \quad e^{-j\frac{2\pi}{M}kn} \quad + \\
+ &\sum_{k=|l_u|-\mu}^{N_P+|l_u|-\mu-1} \sum_{t=0}^{k+\mu-|l_u|} h_i^{u,k,t} x_i^{u,M-|l_u|+k-t} e^{-j\frac{2\pi}{M}kn} + \sum_{k=|l_u|-\mu}^{N_P+|l_u|-\mu-1} \sum_{t=k+\mu-|l_u|+1}^{N_P} h_i^{u,k,t} x_{i-1}^{u,M+\mu-|l_u|+k-t} e^{-j\frac{2\pi}{M}kn} \\
+ &\sum_{k=N_P+|l_u|-\mu}^{|l_u|-1} \sum_{t=0}^{N_P} h_i^{u,k,t} x_i^{u,M-|l_u|+k-t} e^{-j\frac{2\pi}{M}kn} \qquad . \quad \text{(F.16)} \\
+ &\sum_{k=|l_u|}^{N_P+|l_u|-1} \sum_{t=0}^{k-|l_u|} h_i^{u,k,t} x_i^{u,-|l_u|+k-t} e^{-j\frac{2\pi}{M}kn} + \sum_{k=|l_u|}^{N_P+|l_u|-1} \sum_{t=k-|l_u|+1}^{N_P} h_i^{u,k,t} x_i^{u,M-|l_u|+k-t} e^{-j\frac{2\pi}{M}kn} \\
+ &\sum_{k=N_P+|l_u|}^{M-1} \sum_{t=0}^{N_P} h_i^{u,k,t} x_i^{u,-|l_u|+k-t} e^{-j\frac{2\pi}{M}kn}
\end{aligned}$$

Now the autocorrelation of (F.16) is computed as follows.

$$R_{\hat{\xi}\hat{\xi}}(u,n,n+p,iT_0,iT_0 \mid l_u,\Delta f_u) = E[\hat{\xi}^{u,n}(iT_0)\hat{\xi}^{n,n+p}(iT_0)^* \mid l_u,\Delta f_u] =$$

$$= \frac{1}{M^2}\sum_{k'=0}^{|l_u|-\mu-1}\sum_{t'=0}^{N_P}\sum_{k''=0}^{|l_u|-\mu-1}\sum_{t''=0}^{N_P} E[h_i^{u,k',t'}(h_i^{u,k'',t''})^* x_{i-1}^{u,M+\mu-|l_u|+k'-t'}(x_{i-1}^{u,M+\mu-|l_u|+k''-t''})^*]e^{-j\frac{2\pi}{M}k'n}e^{j\frac{2\pi}{M}k''(n+p)}$$

$$+\frac{1}{M^2}\sum_{k'=0}^{|l_u|-\mu-1}\sum_{t'=0}^{N_P}\sum_{k''=|l_u|-\mu}^{N_P+|l_u|-\mu-1}\sum_{t''=k''+\mu-|l_u|+1}^{N_P} E[h_{k'}^{u,i,t'}(h_i^{u,k'',t''})^* x_{i-1}^{u,M+\mu-|l_u|+k'-t'}(x_{i-1}^{u,M+\mu-|l_u|+k''-t''})^*]e^{-j\frac{2\pi}{M}k'n}e^{j\frac{2\pi}{M}k''(n+p)}$$

$$+\frac{1}{M^2}\sum_{k'=|l_u|-\mu}^{N_P+|l_u|-\mu-1}\sum_{t'=k'+\mu-|l_u|+1}^{N_P}\sum_{k''=0}^{|l_u|-\mu-1}\sum_{t''=0}^{N_P} E[h_i^{u,k',t'}(h_i^{u,k'',t''})^* x_{i-1}^{u,M+\mu-|l_u|+k'-t'}(x_{i-1}^{u,M+\mu-|l_u|+k''-t''})^*]e^{-j\frac{2\pi}{M}k'n}e^{j\frac{2\pi}{M}k''(n+p)}$$

$$+\frac{1}{M^2}\sum_{k'=|l_u|-\mu}^{N_P+|l_u|-\mu-1}\sum_{t'=k'+\mu-|l_u|+1}^{N_P}\sum_{k''=|l_u|-\mu}^{N_P+|l_u|-\mu-1}\sum_{t''=k''+\mu-|l_u|+1}^{N_P} E[h_i^{u,k',t'}(h_i^{u,k'',t''})^* x_{i-1}^{u,M+\mu-|l_u|+k'-t'}(x_{i-1}^{u,M+\mu-|l_u|+k''-t''})^*]e^{-j\frac{2\pi}{M}k'n}e^{j\frac{2\pi}{M}k''(n+p)}$$

$$+\frac{1}{M^2}\sum_{k'=|l_u|-\mu}^{N_P+|l_u|-\mu-1}\sum_{t'=0}^{k+\mu-|l_u|}\sum_{k''=|l_u|-\mu}^{N_P+|l_u|-\mu-1}\sum_{t''=0}^{k+\mu-|l_u|} E[h_i^{u,k',t'}(h_i^{u,k'',t''})^* x_i^{u,M-|l_u|+k'-t'}(x_i^{u,M-|l_u|+k''-t''})^*]e^{-j\frac{2\pi}{M}k'n}e^{j\frac{2\pi}{M}k''(n+p)}$$

$$+\frac{1}{M^2}\sum_{k'=|l_u|-\mu}^{N_P+|l_u|-\mu-1}\sum_{t'=0}^{k+\mu-|l_u|}\sum_{k''=N_{t_u}+|l_u|-\mu-1}^{|l_u|-1}\sum_{t''=0}^{N_P} E[h_i^{u,k',t'}(h_i^{u,k'',t''})^* x_i^{u,M-|l_u|+k'-t'}(x_i^{u,M-|l_u|+k''-t''})^*]e^{-j\frac{2\pi}{M}k'n}e^{j\frac{2\pi}{M}k''(n+p)}$$

$$+\frac{1}{M^2}\sum_{k'=|l_u|-\mu}^{N_P+|l_u|-\mu-1}\sum_{t'=0}^{k+\mu-|l_u|}\sum_{k''=|l_u|}^{N_P+|l_u|-1}\sum_{t''=0}^{k-|l_u|} E[h_i^{u,k',t'}(h_i^{u,k'',t''})^* x_i^{u,M-|l_u|+k'-t'}(x_i^{u,-|l_u|+k''-t''})^*]e^{-j\frac{2\pi}{M}k'n}e^{j\frac{2\pi}{M}k''(n+p)}$$

$$+\frac{1}{M^2}\sum_{k'=|l_u|-\mu}^{N_P+|l_u|-\mu-1}\sum_{t'=0}^{k+\mu-|l_u|}\sum_{k''=|l_u|}^{N_P+|l_u|-1}\sum_{t''=k-|l_u|+1}^{N_P} E[h_i^{u,k',t'}(h_i^{u,k'',t''})^* x_i^{u,M-|l_u|+k'-t'}(x_i^{u,M-|l_u|+k''-t''})^*]e^{-j\frac{2\pi}{M}k'n}e^{j\frac{2\pi}{M}k''(n+p)}$$

$$+\frac{1}{M^2}\sum_{k'=|l_u|-\mu}^{N_P+|l_u|-\mu-1}\sum_{t'=0}^{k+\mu-|l_u|}\sum_{k''=N_P+|l_u|-1}^{M-1}\sum_{t''=0}^{N_P} E[h_i^{u,k',t'}(h_i^{u,k'',t''})^* x_i^{u,M-|l_u|+k'-t'}(x_i^{u,-|l_u|+k''-t''})^*]e^{-j\frac{2\pi}{M}k'n}e^{j\frac{2\pi}{M}k''(n+p)}$$

$$+\frac{1}{M^2}\sum_{k'=N_P+|l_u|-\mu}^{|l_u|-1}\sum_{t'=0}^{N_P}\sum_{k''=|l_u|-\mu}^{N_P+|l_u|-\mu-1}\sum_{t''=0}^{k+\mu-|l_u|} E[h_i^{u,k',t'}(h_i^{u,k'',t''})^* x_i^{u,M-|l_u|+k'-t'}(x_i^{u,M-|l_u|+k''-t''})^*]e^{-j\frac{2\pi}{M}k'n}e^{j\frac{2\pi}{M}k''(n+p)}$$

$$+\frac{1}{M^2}\sum_{k'=N_P+|l_u|-\mu}^{|l_u|-1}\sum_{t'=0}^{N_{t_u}-1}\sum_{k''=N_P+|l_u|-\mu}^{|l_u|-1}\sum_{t''=0}^{N_P} E[h_i^{u,k',t'}(h_i^{u,k'',t''})^* x_i^{u,M-|l_u|+k'-t'}(x_i^{u,M-|l_u|+k''-t''})^*]e^{-j\frac{2\pi}{M}k'n}e^{j\frac{2\pi}{M}k''(n+p)}$$

$$+\frac{1}{M^2}\sum_{k'=N_P+|l_u|-\mu}^{|l_u|-1}\sum_{t'=0}^{N_P}\sum_{k''=|l_u|}^{N_P+|l_u|-1}\sum_{t''=0}^{k-|l_u|} E[h_i^{u,k',t'}(h_i^{u,k'',t''})^* x_i^{u,M-|l_u|+k'-t'}(x_i^{u,-|l_u|+k''-t''})^*]e^{-j\frac{2\pi}{M}k'n}e^{j\frac{2\pi}{M}k''(n+p)}$$

$$+\frac{1}{M^2}\sum_{k'=N_P+|l_u|-\mu}^{|l_u|-1}\sum_{t'=0}^{N_P}\sum_{k''=|l_u|}^{N_P+|l_u|-1}\sum_{t''=k-|l_u|+1}^{N_P} E[h_i^{u,k',t'}(h_i^{u,k'',t''})^* x_i^{u,M-|l_u|+k'-t'}(x_i^{u,M-|l_u|+k''-t''})^*]e^{-j\frac{2\pi}{M}k'n}e^{j\frac{2\pi}{M}k''(n+p)}$$

$$+\frac{1}{M^2}\sum_{k'=N_P+|l_u|-\mu}^{|l_u|-1}\sum_{t'=0}^{N_P}\sum_{k''=N_P+|l_u|}^{N-1}\sum_{t''=0}^{N_P} E[h_i^{u,k',t'}(h_i^{u,k'',t''})^* x_i^{u,M-|l_u|+k'-t'}(x_i^{u,-|l_u|+k''-t''})^*]e^{-j\frac{2\pi}{M}k'n}e^{j\frac{2\pi}{M}k''(n+p)}$$

$$+\frac{1}{M^2}\sum_{k'=|l_u|}^{N_P+|l_u|-1}\sum_{t'=0}^{k-|l_u|}\sum_{k''=|l_u|-\mu}^{N_P+|l_u|-\mu-1}\sum_{t''=0}^{k+\mu-|l_u|}E[h_i^{u,k',t'}(h_i^{u,k'',t''})^*x_i^{u,-|l_u|+k'-t'}(x_i^{u,M-|l_u|+k''-t''})^*]e^{-j\frac{2\pi}{M}k'n}e^{j\frac{2\pi}{M}k''(n+p)}$$

$$+\frac{1}{M^2}\sum_{k'=|l_u|}^{N_P+|l_u|-1}\sum_{t'=0}^{k-|l_u|}\sum_{k''=N_P+|l_u|-\mu}^{|l_u|-1}\sum_{t''=0}^{N_P}E[h_i^{u,k',t'}(h_i^{u,k'',t''})^*x_i^{u,-|l_u|+k'-t'}(x_i^{u,M-|l_u|+k''-t''})^*]e^{-j\frac{2\pi}{M}k'n}e^{j\frac{2\pi}{M}k''(n+p)}$$

$$+\frac{1}{M^2}\sum_{k'=|l_u|}^{N_P+|l_u|-1}\sum_{t'=0}^{k-|l_u|}\sum_{k''=|l_u|}^{N_P+|l_u|-1}\sum_{t''=0}^{k-|l_u|}E[h_i^{u,k',t'}(h_i^{u,k'',t''})^*x_i^{u,-|l_u|+k'-t'}(x_i^{u,-|l_u|+k''-t''})^*]e^{-j\frac{2\pi}{M}k'n}e^{j\frac{2\pi}{M}k''(n+p)}$$

$$+\frac{1}{M^2}\sum_{k'=|l_u|}^{N_P+|l_u|-1}\sum_{t'=0}^{k-|l_u|}\sum_{k''=|l_u|}^{N_P+|l_u|-1}\sum_{t''=k-|l_u|+1}^{N_P}E[h_i^{u,k',t'}(h_i^{u,k'',t''})^*x_i^{u,-|l_u|+k'-t'}(x_i^{u,M-|l_u|+k''-t''})^*]e^{-j\frac{2\pi}{M}k'n}e^{j\frac{2\pi}{M}k''(n+p)}$$

$$+\frac{1}{M^2}\sum_{k'=|l_u|}^{N_P+|l_u|-1}\sum_{t'=0}^{k-|l_u|}\sum_{k''=N_P+|l_u|}^{M-1}\sum_{t''=0}^{N_P}E[h_i^{u,k',t'}(h_i^{u,k'',t''})^*x_i^{u,-|l_u|+k'-t'}(x_i^{u,-|l_u|+k''-t''})^*]e^{-j\frac{2\pi}{M}k'n}e^{j\frac{2\pi}{M}k''(n+p)}$$

$$+\frac{1}{M^2}\sum_{k'=|l_u|}^{N_P+|l_u|-1}\sum_{t'=k-|l_u|+1}^{N_P}\sum_{k''=|l_u|-\mu}^{N_P+|l_u|-\mu-1}\sum_{t''=0}^{k+\mu-|l_u|}E[h_i^{u,k',t'}(h_i^{u,k'',t''})^*x_i^{u,M-|l_u|+k'-t'}(x_i^{u,M-|l_u|+k''-t''})^*]e^{-j\frac{2\pi}{M}k'n}e^{j\frac{2\pi}{M}k''(n+p)}$$

$$+\frac{1}{M^2}\sum_{k'=|l_u|}^{N_P+|l_u|-1}\sum_{t'_u=k-|l_u|+1}^{N_P}\sum_{k''=N_P+|l_u|-\mu}^{|l_u|-1}\sum_{t''=0}^{N_P}E[h_i^{u,k',t'}(h_i^{u,k'',t''})^*x_i^{u,M-|l_u|+k'-t'}(x_i^{u,M-|l_u|+k''-t''})^*]e^{-j\frac{2\pi}{M}k'n}e^{j\frac{2\pi}{M}k''(n+p)}$$

$$+\frac{1}{M^2}\sum_{k'=|l_u|}^{N_P+|l_u|-1}\sum_{t'=k-|l_u|+1}^{N_P}\sum_{k''=|l_u|}^{N_P+|l_u|-1}\sum_{t''=0}^{k-|l_u|}E[h_i^{u,k',t'}(h_i^{u,k'',t''})^*x_i^{u,M-|l_u|+k'-t'}(x_i^{u,-|l_u|+k''-t''})^*]e^{-j\frac{2\pi}{M}k'n}e^{j\frac{2\pi}{M}k''(n+p)}$$

$$+\frac{1}{M^2}\sum_{k'=|l_u|}^{N_P+|l_u|-1}\sum_{t'=k-|l_u|+1}^{N_P}\sum_{k''=|l_u|}^{N_P+|l_u|-1}\sum_{t''=k-|l_u|+1}^{N_P}E[h_i^{u,k',t'}(h_i^{u,k'',t''})^*x_i^{u,M-|l_u|+k'-t'}(x_i^{u,M-|l_u|+k''-t''})^*]e^{-j\frac{2\pi}{M}k'n}e^{j\frac{2\pi}{M}k''(n+p)}$$

$$+\frac{1}{M^2}\sum_{k'=|l_u|}^{N_P+|l_u|-1}\sum_{t'=k-|l_u|+1}^{N_P}\sum_{k''=N_P+|l_u|}^{M-1}\sum_{t''=0}^{N_P}E[h_i^{u,k',t'}(h_i^{u,k'',t''})^*x_i^{u,M-|l_u|+k'-t'}(x_i^{u,-|l_u|+k''-t''})^*]e^{-j\frac{2\pi}{M}k'n}e^{j\frac{2\pi}{M}k''(n+p)}$$

$$+\frac{1}{M^2}\sum_{k'=N_P+|l_u|}^{M-1}\sum_{t'=0}^{N_P}\sum_{k''=|l_u|-\mu}^{N_P+|l_u|-\mu-1}\sum_{t''=0}^{k+\mu-|l_u|}E[h_i^{u,k',t'}(h_i^{u,k'',t''})^*x_i^{u,-|l_u|+k'-t'}(x_i^{u,M-|l_u|+k''-t''})^*]e^{-j\frac{2\pi}{M}k'n}e^{j\frac{2\pi}{M}k''(n+p)}$$

$$+\frac{1}{M^2}\sum_{k'=N_P+|l_u|}^{M-1}\sum_{t'=0}^{N_P}\sum_{k''=N_P+|l_u|-\mu}^{|l_u|-1}\sum_{t''=0}^{N_P}E[h_i^{u,k',t'}(h_i^{u,k'',t''})^*x_i^{u,-|l_u|+k'-t'}(x_i^{u,M-|l_u|+k''-t''})^*]e^{-j\frac{2\pi}{M}k'n}e^{j\frac{2\pi}{M}k''(n+p)}$$

$$+\frac{1}{M^2}\sum_{k'=N_P+|l_u|}^{M-1}\sum_{t'=0}^{N_P}\sum_{k''=|l_u|}^{N_P+|l_u|-1}\sum_{t''=0}^{k-|l_u|}E[h_i^{u,k',t'}(h_i^{u,k'',t''})^*x_i^{u,-|l_u|+k'-t'}(x_i^{u,-|l_u|+k''-t''})^*]e^{-j\frac{2\pi}{M}k'n}e^{j\frac{2\pi}{M}k''(n+p)}$$

$$+\frac{1}{M^2}\sum_{k'=N_P+|l_u|}^{M-1}\sum_{t'=0}^{N_P}\sum_{k''=|l_u|}^{N_P+|l_u|-1}\sum_{t''=k-|l_u|+1}^{N_P}E[h_i^{u,k',t'}(h_i^{u,k'',t''})^*x_i^{u,-|l_u|+k'-t'}(x_i^{u,M-|l_u|+k''-t''})^*]e^{-j\frac{2\pi}{M}k'n}e^{j\frac{2\pi}{M}k''(n+p)}$$

$$+\frac{1}{M^2}\sum_{k'=N_P+|l_u|}^{M-1}\sum_{t'=0}^{N_P}\sum_{k''=N_P+|l_u|}^{M-1}\sum_{t''=0}^{N_P}E[h_i^{u,k',t'}(h_i^{u,k'',t''})^*x_i^{u,-|l_u|+k'-t'}(x_i^{u,-|l_u|+k''-t''})^*]e^{-j\frac{2\pi}{M}k'n}e^{j\frac{2\pi}{M}k''(n+p)}$$

Using (F.9) the *u-th* interferer autocorrelation is[24]

$$R_{\hat{\xi}\hat{\xi}}(u,n,n+p,iT_0,iT_0 \mid l_u,\Delta f_u) =$$

$$= \frac{1}{M^2}\sum_{k\in\Gamma_u} P_{u,k} \sum_{k'=0}^{|l_u|-\mu-1}\sum_{t'=0}^{N_P}\sum_{k''=0}^{|l_u|-\mu-1}\sum_{t''=0}^{N_P} \Omega_{u,t'}\delta_{t't''} e^{-j\frac{2\pi}{M}\overline{\Delta f_u}(k'-k'')} e^{j\frac{2\pi}{M}k(k'-t'-k''+t'')} e^{-j\frac{2\pi}{M}k'n} e^{j\frac{2\pi}{M}k''(n+p)} +$$

$$+\frac{1}{M^2}\sum_{k\in\Gamma_u} P_{u,k} \sum_{k'=0}^{|l_u|-\mu-1}\sum_{t'=0}^{N_P}\sum_{k''=|l_u|-\mu}^{N_P+|l_u|-\mu-1}\sum_{t''=k''+\mu-|l_u|+1}^{N_P} \Omega_{u,t'}\delta_{t't''} e^{-j\frac{2\pi}{M}\overline{\Delta f_u}(k'-k'')} e^{j\frac{2\pi}{M}k(k'-t'-k''+t'')} e^{-j\frac{2\pi}{M}k'n} e^{j\frac{2\pi}{M}k''(n+p)}$$

$$+\frac{1}{M^2}\sum_{k\in\Gamma_u} P_{u,k} \sum_{k'=|l_u|-\mu}^{N_P+|l_u|-\mu-1}\sum_{t'=k'+\mu-|l_u|+1}^{N_P}\sum_{k''=0}^{|l_u|-\mu-1}\sum_{t''=0}^{N_P} \Omega_{u,t'}\delta_{t't''} e^{-j\frac{2\pi}{M}\overline{\Delta f_u}(k'-k'')} e^{j\frac{2\pi}{M}k(k'-t'-k''+t'')} e^{-j\frac{2\pi}{M}k'n} e^{j\frac{2\pi}{M}k''(n+p)}$$

$$+\frac{1}{M^2}\sum_{k\in\Gamma_u} P_{u,k} \sum_{k'=|l_u|-\mu}^{N_P+|l_u|-\mu-1}\sum_{t'=k'+\mu-|l_u|+1}^{N_P}\sum_{k''=|l_u|-\mu}^{N_P+|l_u|-\mu-1}\sum_{t''=k''+\mu-|l_u|+1}^{N_P} \Omega_{u,t'}\delta_{t't''} e^{-j\frac{2\pi}{M}\overline{\Delta f_u}(k'-k'')} e^{j\frac{2\pi}{M}k(k'-t'-k''+t'')} e^{-j\frac{2\pi}{M}k'n} e^{j\frac{2\pi}{M}k''(n+p)}$$

$$+\frac{1}{M^2}\sum_{k\in\Gamma_u} P_{u,k} \sum_{k'=|l_u|-\mu}^{N_P+|l_u|-\mu-1}\sum_{t'=0}^{k+\mu-|l_u|}\sum_{k''=|l_u|-\mu}^{N_P+|l_u|-\mu-1}\sum_{t''=0}^{k+\mu-|l_u|} \Omega_{u,t'}\delta_{t't''} e^{-j\frac{2\pi}{M}\overline{\Delta f_u}(k'-k'')} e^{j\frac{2\pi}{M}k(k'-t'-k''+t'')} e^{-j\frac{2\pi}{M}k'n} e^{j\frac{2\pi}{M}k''(n+p)}$$

$$+\frac{1}{M^2}\sum_{k\in\Gamma_u} P_{u,k} \sum_{k'=|l_u|-\mu}^{N_P+|l_u|-\mu-1}\sum_{t'=0}^{k+\mu-|l_u|}\sum_{k''=N_{t_u}+|l_u|-\mu-1}^{|l_u|-1}\sum_{t''=0}^{N_P} \Omega_{u,t'}\delta_{t't''} e^{-j\frac{2\pi}{M}\overline{\Delta f_u}(k'-k'')} e^{j\frac{2\pi}{M}k(k'-t'-k''+t'')} e^{-j\frac{2\pi}{M}k'n} e^{j\frac{2\pi}{M}k''(n+p)}$$

$$+\frac{1}{M^2}\sum_{k\in\Gamma_u} P_{u,k} \sum_{k'=|l_u|-\mu}^{N_P+|l_u|-\mu-1}\sum_{t'=0}^{k+\mu-|l_u|}\sum_{k''=|l_u|}^{N_P+|l_u|-1}\sum_{t''=0}^{k-|l_u|} \Omega_{u,t'}\delta_{t't''} e^{-j\frac{2\pi}{M}\overline{\Delta f_u}(k'-k'')} e^{j\frac{2\pi}{M}k(k'-t'-k''+t'')} e^{-j\frac{2\pi}{M}k'n} e^{j\frac{2\pi}{M}k''(n+p)}$$

$$+\frac{1}{M^2}\sum_{k\in\Gamma_u} P_{u,k} \sum_{k'=|l_u|-\mu}^{N_P+|l_u|-\mu-1}\sum_{t'=0}^{k+\mu-|l_u|}\sum_{k''=|l_u|}^{N_P+|l_u|-1}\sum_{t''=k-|l_u|+1}^{N_P} \Omega_{u,t'}\delta_{t't''} e^{-j\frac{2\pi}{M}\overline{\Delta f_u}(k'-k'')} e^{j\frac{2\pi}{M}k(k'-t'-k''+t'')} e^{-j\frac{2\pi}{M}k'n} e^{j\frac{2\pi}{M}k''(n+p)}$$

$$+\frac{1}{M^2}\sum_{k\in\Gamma_u} P_{u,k} \sum_{k'=|l_u|-\mu}^{N_P+|l_u|-\mu-1}\sum_{t'=0}^{k+\mu-|l_u|}\sum_{k''=N_{t_u}+|l_u|-1}^{M-1}\sum_{t''=0}^{N_P} \Omega_{u,t'}\delta_{t't''} e^{-j\frac{2\pi}{M}\overline{\Delta f_u}(k'-k'')} e^{j\frac{2\pi}{M}k(k'-t'-k''+t'')} e^{-j\frac{2\pi}{M}k'n} e^{j\frac{2\pi}{M}k''(n+p)}$$

$$+\frac{1}{M^2}\sum_{k\in\Gamma_u} P_{u,k} \sum_{k'=N_P+|l_u|-\mu}^{|l_u|-1}\sum_{t'=0}^{N_P}\sum_{k''=|l_u|-\mu}^{N_P+|l_u|-\mu-1}\sum_{t''=0}^{k+\mu-|l_u|} \Omega_{u,t'}\delta_{t't''} e^{-j\frac{2\pi}{M}\overline{\Delta f_u}(k'-k'')} e^{j\frac{2\pi}{M}k(k'-t'-k''+t'')} e^{-j\frac{2\pi}{M}k'n} e^{j\frac{2\pi}{M}k''(n+p)}$$

$$+\frac{1}{M^2}\sum_{k\in\Gamma_u} P_{u,k} \sum_{k'=N_P+|l_u|-\mu}^{|l_u|-1}\sum_{t'=0}^{N_{t_u}-1}\sum_{k''=N_P+|l_u|-\mu}^{|l_u|-1}\sum_{t''=0}^{N_P} \Omega_{u,t'}\delta_{t't''} e^{-j\frac{2\pi}{M}\overline{\Delta f_u}(k'-k'')} e^{j\frac{2\pi}{M}k(k'-t'-k''+t'')} e^{-j\frac{2\pi}{M}k'n} e^{j\frac{2\pi}{M}k''(n+p)}$$

$$+\frac{1}{M^2}\sum_{k\in\Gamma_u} P_{u,k} \sum_{k'=N_P+|l_u|-\mu}^{|l_u|-1}\sum_{t'=0}^{N_P}\sum_{k''=|l_u|}^{N_P+|l_u|-1}\sum_{t''=0}^{k-|l_u|} \Omega_{u,t'}\delta_{t't''} e^{-j\frac{2\pi}{M}\overline{\Delta f_u}(k'-k'')} e^{j\frac{2\pi}{M}k(k'-t'-k''+t'')} e^{-j\frac{2\pi}{M}k'n} e^{j\frac{2\pi}{M}k''(n+p)}$$

$$+\frac{1}{M^2}\sum_{k\in\Gamma_u} P_{u,k} \sum_{k'=N_P+|l_u|-\mu}^{|l_u|-1}\sum_{t'=0}^{N_P}\sum_{k''=|l_u|}^{N_P+|l_u|-1}\sum_{t''=k-|l_u|+1}^{N_P} \Omega_{u,t'}\delta_{t't''} e^{-j\frac{2\pi}{M}\overline{\Delta f_u}(k'-k'')} e^{j\frac{2\pi}{M}k(k'-t'-k''+t'')} e^{-j\frac{2\pi}{M}k'n} e^{j\frac{2\pi}{M}k''(n+p)}$$

$$+\frac{1}{M^2}\sum_{k\in\Gamma_u} P_{u,k} \sum_{k'=N_P+|l_u|-\mu}^{|l_u|-1}\sum_{t'=0}^{N_P}\sum_{k''=N_P+|l_u|}^{N-1}\sum_{t''=0}^{N_P} \Omega_{u,t'}\delta_{t't''} e^{-j\frac{2\pi}{M}\overline{\Delta f_u}(k'-k'')} e^{j\frac{2\pi}{M}k(k'-t'-k''+t'')} e^{-j\frac{2\pi}{M}k'n} e^{j\frac{2\pi}{M}k''(n+p)}$$

[24] $\delta_{t't''} = \begin{cases} 1 & t' = t'' \\ 0 & t' \neq t'' \end{cases}$.

$$+\frac{1}{M^2}\sum_{k\in\Gamma_u}P_{u,k}\sum_{k'=|l_u|}^{N_P+|l_u|-1}\sum_{t'=0}^{k-|l_u|}\sum_{k''=|l_u|-\mu}^{N_P+|l_u|-\mu-1}\sum_{t''=0}^{k+\mu-|l_u|}\Omega_{u,t'}\delta_{t't''}e^{-j\frac{2\pi}{M}\overline{\Delta f_u}(k'-k'')}e^{j\frac{2\pi}{M}k(k'-t'-k''+t'')}e^{-j\frac{2\pi}{M}k'n}e^{j\frac{2\pi}{M}k''(n+p)}$$

$$+\frac{1}{M^2}\sum_{k\in\Gamma_u}P_{u,k}\sum_{k'=|l_u|}^{N_P+|l_u|-1}\sum_{t'=0}^{k-|l_u|}\sum_{k''=N_P+|l_u|-\mu}^{|l_u|-1}\sum_{t''=0}^{N_P}\Omega_{u,t'}\delta_{t't''}e^{-j\frac{2\pi}{M}\overline{\Delta f_u}(k'-k'')}e^{j\frac{2\pi}{M}k(k'-t'-k''+t'')}e^{-j\frac{2\pi}{M}k'n}e^{j\frac{2\pi}{M}k''(n+p)}$$

$$+\frac{1}{M^2}\sum_{k\in\Gamma_u}P_{u,k}\sum_{k'=|l_u|}^{N_P+|l_u|-1}\sum_{t'=0}^{k-|l_u|}\sum_{k''=|l_u|}^{N_P+|l_u|-1}\sum_{t''=0}^{k-|l_u|}\Omega_{u,t'}\delta_{t't''}e^{-j\frac{2\pi}{M}\overline{\Delta f_u}(k'-k'')}e^{j\frac{2\pi}{M}k(k'-t'-k''+t'')}e^{-j\frac{2\pi}{M}k'n}e^{j\frac{2\pi}{M}k''(n+p)}$$

$$+\frac{1}{M^2}\sum_{k\in\Gamma_u}P_{u,k}\sum_{k'=|l_u|}^{N_P+|l_u|-1}\sum_{t'=0}^{k-|l_u|}\sum_{k''=|l_u|}^{N_P+|l_u|-1}\sum_{t''=k-|l_u|+1}^{N_P}\Omega_{u,t'}\delta_{t't''}e^{-j\frac{2\pi}{M}\overline{\Delta f_u}(k'-k'')}e^{j\frac{2\pi}{M}k(k'-t'-k''+t'')}e^{-j\frac{2\pi}{M}k'n}e^{j\frac{2\pi}{M}k''(n+p)}$$

$$+\frac{1}{M^2}\sum_{k\in\Gamma_u}P_{u,k}\sum_{k'=|l_u|}^{N_P+|l_u|-1}\sum_{t'=0}^{k-|l_u|}\sum_{k''=N_P+|l_u|}^{M-1}\sum_{t''=0}^{N_P}\Omega_{u,t'}\delta_{t't''}e^{-j\frac{2\pi}{M}\overline{\Delta f_u}(k'-k'')}e^{j\frac{2\pi}{M}k(k'-t'-k''+t'')}e^{-j\frac{2\pi}{M}k'n}e^{j\frac{2\pi}{M}k''(n+p)}$$

$$+\frac{1}{M^2}\sum_{k\in\Gamma_u}P_{u,k}\sum_{k'=|l_u|}^{N_P+|l_u|-1}\sum_{t'=k-|l_u|+1}^{N_P}\sum_{k''=|l_u|-\mu}^{N_P+|l_u|-\mu-1}\sum_{t''=0}^{k+\mu-|l_u|}\Omega_{u,t'}\delta_{t't''}e^{-j\frac{2\pi}{M}\overline{\Delta f_u}(k'-k'')}e^{j\frac{2\pi}{M}k(k'-t'-k''+t'')}e^{-j\frac{2\pi}{M}k'n}e^{j\frac{2\pi}{M}k''(n+p)}$$

$$+\frac{1}{M^2}\sum_{k\in\Gamma_u}P_{u,k}\sum_{k'=|l_u|}^{N_P+|l_u|-1}\sum_{t'=k-|l_u|+1}^{N_P}\sum_{k''=N_P+|l_u|-\mu}^{|l_u|-1}\sum_{t''=0}^{N_P}\Omega_{u,t'}\delta_{t't''}e^{-j\frac{2\pi}{M}\overline{\Delta f_u}(k'-k'')}e^{j\frac{2\pi}{M}k(k'-t'-k''+t'')}e^{-j\frac{2\pi}{M}k'n}e^{j\frac{2\pi}{M}k''(n+p)}$$

$$+\frac{1}{M^2}\sum_{k\in\Gamma_u}P_{u,k}\sum_{k'=|l_u|}^{N_P+|l_u|-1}\sum_{t'=k-|l_u|+1}^{N_P}\sum_{k''=|l_u|}^{N_P+|l_u|-1}\sum_{t''=0}^{k-|l_u|}\Omega_{u,t'}\delta_{t't''}e^{-j\frac{2\pi}{M}\overline{\Delta f_u}(k'-k'')}e^{j\frac{2\pi}{M}k(k'-t'-k''+t'')}e^{-j\frac{2\pi}{M}k'n}e^{j\frac{2\pi}{M}k''(n+p)}$$

$$+\frac{1}{M^2}\sum_{k\in\Gamma_u}P_{u,k}\sum_{k'=|l_u|}^{N_P+|l_u|-1}\sum_{t'=k-|l_u|+1}^{N_P}\sum_{k''=|l_u|}^{N_P+|l_u|-1}\sum_{t''=k-|l_u|+1}^{N_P}\Omega_{u,t'}\delta_{t't''}e^{-j\frac{2\pi}{M}\overline{\Delta f_u}(k'-k'')}e^{j\frac{2\pi}{M}k(k'-t'-k''+t'')}e^{-j\frac{2\pi}{M}k'n}e^{j\frac{2\pi}{M}k''(n+p)}$$

$$+\frac{1}{M^2}\sum_{k\in\Gamma_u}P_{u,k}\sum_{k'=|l_u|}^{N_P+|l_u|-1}\sum_{t'=k-|l_u|+1}^{N_P}\sum_{k''=N_P+|l_u|}^{M-1}\sum_{t''=0}^{N_P}\Omega_{u,t'}\delta_{t't''}e^{-j\frac{2\pi}{M}\overline{\Delta f_u}(k'-k'')}e^{j\frac{2\pi}{M}k(k'-t'-k''+t'')}e^{-j\frac{2\pi}{M}k'n}e^{j\frac{2\pi}{M}k''(n+p)}$$

$$+\frac{1}{M^2}\sum_{k\in\Gamma_u}P_{u,k}\sum_{k'=N_P+|l_u|}^{M-1}\sum_{t'=0}^{N_P}\sum_{k''=|l_u|-\mu}^{N_P+|l_u|-\mu-1}\sum_{t''=0}^{k+\mu-|l_u|}\Omega_{u,t'}\delta_{t't''}e^{-j\frac{2\pi}{M}\overline{\Delta f_u}(k'-k'')}e^{j\frac{2\pi}{M}k(k'-t'-k''+t'')}e^{-j\frac{2\pi}{M}k'n}e^{j\frac{2\pi}{M}k''(n+p)}$$

$$+\frac{1}{M^2}\sum_{k\in\Gamma_u}P_{u,k}\sum_{k'=N_P+|l_u|}^{M-1}\sum_{t'=0}^{N_P}\sum_{k''=N_P+|l_u|-\mu}^{|l_u|-1}\sum_{t''=0}^{N_P}\Omega_{u,t'}\delta_{t't''}e^{-j\frac{2\pi}{M}\overline{\Delta f_u}(k'-k'')}e^{j\frac{2\pi}{M}k(k'-t'-k''+t'')}e^{-j\frac{2\pi}{M}k'n}e^{j\frac{2\pi}{M}k''(n+p)}$$

$$+\frac{1}{M^2}\sum_{k\in\Gamma_u}P_{u,k}\sum_{k'=N_P+|l_u|}^{M-1}\sum_{t'=0}^{N_P}\sum_{k''=|l_u|}^{N_P+|l_u|-1}\sum_{t''=0}^{k-|l_u|}\Omega_{u,t'}\delta_{t't''}e^{-j\frac{2\pi}{M}\overline{\Delta f_u}(k'-k'')}e^{j\frac{2\pi}{M}k(k'-t'-k''+t'')}e^{-j\frac{2\pi}{M}k'n}e^{j\frac{2\pi}{M}k''(n+p)}$$

$$+\frac{1}{M^2}\sum_{k\in\Gamma_u}P_{u,k}\sum_{k'=N_P+|l_u|}^{M-1}\sum_{t'=0}^{N_P}\sum_{k''=|l_u|}^{N_P+|l_u|-1}\sum_{t''=k-|l_u|+1}^{N_P}\Omega_{u,t'}\delta_{t't''}e^{-j\frac{2\pi}{M}\overline{\Delta f_u}(k'-k'')}e^{j\frac{2\pi}{M}k(k'-t'-k''+t'')}e^{-j\frac{2\pi}{M}k'n}e^{j\frac{2\pi}{M}k''(n+p)}$$

$$+\frac{1}{M^2}\sum_{k\in\Gamma_u}P_{u,k}\sum_{k'=N_P+|l_u|}^{M-1}\sum_{t'=0}^{N_P}\sum_{k''=N_P+|l_u|}^{M-1}\sum_{t''=0}^{N_P}\Omega_{u,t'}\delta_{t't''}e^{-j\frac{2\pi}{M}\overline{\Delta f_u}(k'-k'')}e^{j\frac{2\pi}{M}k(k'-t'-k''+t'')}e^{-j\frac{2\pi}{M}k'n}e^{j\frac{2\pi}{M}k''(n+p)}.$$

With some algebra and relations (F.10)-(F.14) we obtain

$$R_{\hat{\xi}\hat{\xi}}(u,n,n+p,iT_0,iT_0 \mid l_u,\Delta f_u)=\frac{1}{M^2}\sum_{k\in\Gamma_u}P_{u,k}\sum_{k'=0}^{|l_u|-\mu-1}\sum_{t'=0}^{N_P}\sum_{k''=0}^{|l_u|-\mu-1}\Omega_{u,t'}e^{j\frac{2\pi}{M}k'(-\overline{\Delta f_u}-n+k)}e^{j\frac{2\pi}{M}k''(\overline{\Delta f_u}+n+p-k)}+$$

$$+\frac{1}{M^2}\sum_{k\in\Gamma_u}P_{u,k}\sum_{k'=0}^{|l_u|-\mu-1}\sum_{t'=0}^{N_P}\sum_{k''=0}^{t'-1}\Omega_{u,t'}e^{j\frac{2\pi}{M}(|l_u|-\mu)(\overline{\Delta f_u}+n+p-k)}e^{j\frac{2\pi}{M}k'(-\overline{\Delta f_u}-n+k)}e^{j\frac{2\pi}{M}k''(\overline{\Delta f_u}+n+p-k)}$$

$$+\frac{1}{M^2}\sum_{k\in\Gamma_u}P_{u,k}\sum_{t'=0}^{N_P}\sum_{k'=0}^{t'-1}\sum_{k''=0}^{|l_u|-\mu-1}\Omega_{u,t'}e^{j\frac{2\pi}{M}(|l_u|-\mu)(-\overline{\Delta f_u}-n+k)}e^{j\frac{2\pi}{M}k'(-\overline{\Delta f_u}-n+k)}e^{j\frac{2\pi}{M}k''(\overline{\Delta f_u}+n+p-k)}$$

$$+\frac{1}{M^2}\sum_{k\in\Gamma_u}P_{u,k}\sum_{t'=0}^{N_P}\sum_{k'=0}^{t'-1}\sum_{k''=0}^{t'-1}\Omega_{u,t'}e^{j\frac{2\pi}{M}(|l_u|-\mu)p}e^{j\frac{2\pi}{M}k'(-\overline{\Delta f_u}-n+k)}e^{j\frac{2\pi}{M}k''(\overline{\Delta f_u}+n+p-k)}$$

$$+\frac{1}{M^2}\sum_{k\in\Gamma_u}P_{u,k}\sum_{t'=0}^{N_P-1}\sum_{k'=t'}^{N_P}\sum_{k''=t'}^{M-1}\Omega_{u,t'}e^{j\frac{2\pi}{M}(|l_u|-\mu)p}e^{j\frac{2\pi}{M}k'(-\overline{\Delta f_u}-n+k)}e^{j\frac{2\pi}{M}k''(\overline{\Delta f_u}+n+p-k)}$$

$$+\frac{1}{M^2}\sum_{k\in\Gamma_u}P_{u,k}\sum_{k'=N_P}^{M-1-|l_u|+\mu}\sum_{t'=0}^{N_P}\sum_{k''=t'}^{M-1-|l_u|+\mu}\Omega_{u,t'}e^{j\frac{2\pi}{M}(|l_u|-\mu)p}e^{j\frac{2\pi}{M}k'(-\overline{\Delta f_u}-n+k)}e^{j\frac{2\pi}{M}k''(\overline{\Delta f_u}+n+p-k)}$$

Using (F.15) we obtain

$$R_{\hat{\xi}\hat{\xi}}(u,n,n+p,iT_0,iT_0 \mid l_u,\Delta f_u)=\frac{1}{M^2}\sum_{t'=0}^{N_P}\sum_{k\in\Gamma_u}P_{u,k}\frac{1-e^{j\frac{2\pi}{M}(|l_u|-\mu)(-\overline{\Delta f_u}-n+k)}}{1-e^{j\frac{2\pi}{M}(-\overline{\Delta f_u}-n+k)}}\frac{1-e^{j\frac{2\pi}{M}(|l_u|-\mu)(\overline{\Delta f_u}+n+p-k)}}{1-e^{j\frac{2\pi}{M}(\overline{\Delta f_u}+n+p-k)}}$$

$$+\frac{1}{M^2}\sum_{k\in\Gamma_u}P_{u,k}e^{j\frac{2\pi}{M}(|l_u|-\mu)(\overline{\Delta f_u}+n+p-c)}\frac{1-e^{j\frac{2\pi}{M}(|l_u|-\mu)(-\overline{\Delta f_u}-n+k)}}{1-e^{j\frac{2\pi}{M}(-\overline{\Delta f_u}-n+k)}}\sum_{t'=0}^{N_P}P_{h^{t'}u}\frac{1-e^{j\frac{2\pi}{M}t'(\overline{\Delta f_u}+n+p-k)}}{1-e^{j\frac{2\pi}{M}(\overline{\Delta f_u}+n+p-k)}}$$

$$+\frac{1}{M^2}\sum_{k\in\Gamma_u}P_{u,k}e^{j\frac{2\pi}{M}(-\overline{\Delta f_u}-n+c)(|l_u|-\mu)}\sum_{t'=0}^{N_P}\Omega_{u,t'}\frac{1-e^{j\frac{2\pi}{M}t'(-\overline{\Delta f_u}-n+k)}}{1-e^{j\frac{2\pi}{M}(-\overline{\Delta f_u}-n+k)}}\frac{1-e^{j\frac{2\pi}{M}(|l_u|-\mu)(\overline{\Delta f_u}+n+p-k)}}{1-e^{j\frac{2\pi}{M}(\overline{\Delta f_u}+n+p-k)}}$$

$$+\frac{1}{M^2}\sum_{k\in\Gamma_u}P_{u,k}e^{j\frac{2\pi}{M}(|l_u|-\mu)p}\sum_{t'=0}^{N_P}\Omega_{u,t'}\frac{1-e^{j\frac{2\pi}{M}t'(-\overline{\Delta f_u}-n+k)}}{1-e^{j\frac{2\pi}{M}(-\overline{\Delta f_u}-n+k)}}\frac{1-e^{j\frac{2\pi}{M}t''(\overline{\Delta f_u}+n+p-k)}}{1-e^{j\frac{2\pi}{M}(\overline{\Delta f_u}+n+p-k)}}$$

$$+\frac{1}{M^2}\sum_{k\in\Gamma_u}P_{u,k}e^{j\frac{2\pi}{M}(|l_u|-\mu)p}\sum_{t'=0}^{N_P}\Omega_{u,t'}\Bigg\{\frac{e^{j\frac{2\pi}{M}t'(-\overline{\Delta f_u}-n+k)}-e^{j\frac{2\pi}{M}N_P(-\overline{\Delta f_u}-n+k)}}{1-e^{j\frac{2\pi}{M}(-\overline{\Delta f_u}-n+k)}}\frac{e^{j\frac{2\pi}{M}t'(\overline{\Delta f_u}+n+p-k)}-e^{j\frac{2\pi}{M}(M-|l_u|+\mu)(\overline{\Delta f_u}+n+p-k)}}{1-e^{j\frac{2\pi}{M}(\overline{\Delta f_u}+n+p-k)}}$$

$$+\frac{e^{j\frac{2\pi}{M}N_P(-\overline{\Delta f_u}-n+k)}-e^{j\frac{2\pi}{M}(M-|l_u|+\mu)(-\overline{\Delta f_u}-n+k)}}{1-e^{j\frac{2\pi}{M}(-\overline{\Delta f_u}-n+k)}}\frac{e^{j\frac{2\pi}{M}t'(\overline{\Delta f_u}+n+p-k)}-e^{j\frac{2\pi}{M}(M-|l_u|+\mu)(\overline{\Delta f_u}+n+p-k)}}{1-e^{j\frac{2\pi}{M}(\overline{\Delta f_u}+n+p-k)}}\Bigg\}$$

Rearranging the terms finally yields,

$$R_{\hat{\xi}\hat{\xi}}(u,n,n+p,iT_0,iT_0 \mid l_u,\Delta f_u)=\frac{1}{M^2}\sum_{k\in\Gamma_u}\sum_{t=0}^{N_P}\Omega_{u,t}\frac{1}{(1-e^{j\frac{2\pi}{N}(-\overline{\Delta f_u}-n+k)})(1-e^{j\frac{2\pi}{N}(\overline{\Delta f_u}+n+p-k)})}\{2+2e^{j\frac{2\pi}{M}(t+|l_u|-\mu)p}+$$

$$-e^{j\frac{2\pi}{M}(t+|l_u|-\mu)(\Delta f_u+n+p-k)}-e^{j\frac{2\pi}{M}(t+|l_u|-\mu)(-\overline{\Delta f_u}-n+k)}-e^{j\frac{2\pi}{M}(t-M-|l_u|+\mu)(-\overline{\Delta f_u}-n+k)}-e^{j\frac{2\pi}{M}(M-|l_u|+\mu-t)(-\overline{\Delta f_u}-n-p+k)}\}$$

from which the term *A* in (F.1) is obtained by a shift of $\mu_1/2$, i.e., $l_u \to l_u-\mu_1/2$.

Case 1b: $0\geq -\mu-1\geq N_P-M\geq l_u$

The observation window is defined below.

$$\underbrace{x_{i-1}^{u,M-N_P-|l_u|+\mu},\ldots,x_{i-1}^{u,M-|l_u|+\mu-1}}_{N_P},\underbrace{\left[\underbrace{x_{i-1}^{u,M-|l_u|+\mu},\ldots,x_{i-1}^{u,M-1}}_{|l_u|-\mu},\underbrace{x_i^{u,M-\mu},\ldots,x_i^{u,M-1}}_{\mu},\underbrace{x_i^{u,0},\ldots,x_i^{u,M-|l_u|-1}}_{M-|l_u|}\right]}_{\underline{X}^{u,i,l_u}}.$$

The received signal component that belongs to user *u* is defined as follows:

$$\begin{aligned}
&0\leq k\leq|l_u|-\mu-1 && \Rightarrow\ y_i^{u,k}=\sum_{t=0}^{N_P}h_i^{u,k,t}x_{i-1}^{u,M+\mu-|l_u|+k-t}\\
&|l_u|-\mu\leq k\leq N_P+|l_u|-\mu-1 && \Rightarrow\ y_i^{u,k}=\sum_{t=0}^{k+\mu-|l_u|}h_i^{u,k,t}x_i^{u,M-|l_u|+k-t}+\sum_{t=k+\mu-|l_u|+1}^{N_P}h_i^{u,k,t}x_{i-1}^{u,M+\mu-|l_u|+k-t}\\
&N_P+|l_u|-\mu\leq k\leq|l_u|-1 && \Rightarrow\ y_i^{u,k}=\sum_{t=0}^{N_P}h_i^{u,k,t}x_i^{u,M-|l_u|+k-t}\\
&|l_u|\leq k\leq M-1 && \Rightarrow\ y_i^{u,k}=\sum_{t=0}^{k-|l_u|}h_i^{u,k,t}x_i^{u,-|l_u|+k-t}+\sum_{t=k-|l_u|+1}^{N_P}h_i^{u,k,t}x_i^{u,M-|l_u|+k-t}
\end{aligned}.$$

We can now compute the *n-th* FFT output component that belongs to user *u*. Then following similar steps to Case 1a we obtain the interference autocorrelation. This yields a result identical to Case 1a.

Case 2: $0\geq N_P-1-\mu\geq l_u\geq -\mu\geq N_P-M+1$

The observation window is defined below.

$$\underbrace{x_{i-1}^{u,M-N_P+\mu-|l_u|},\ldots,x_{i-1}^{u,M-1}}_{N_P-\mu+|l_u|},\underbrace{x_i^{u,M-\mu},\ldots,x_i^{u,M-|l_u|-1}}_{\mu-|l_u|}\underbrace{\left[\underbrace{x_i^{u,M-|l_u|},\ldots,x_i^{u,M-1}}_{|l_u|},\underbrace{x_i^{u,0},\ldots,x_i^{u,M-|l_u|-1}}_{M-|l_u|}\right]}_{\underline{X}^{u,i,l_u}}.$$

The received signal component that belongs to user *u* is defined as follows:

$$0 \le k \le N_P - \mu + |l_u| - 1 \quad \Rightarrow y_i^{u,k} = \sum_{t=0}^{k+\mu-|l_u|} h_i^{u,k,t} x_i^{u,M-|l_u|+k-t} + \sum_{t=k+\mu-|l_u|+1}^{N_P} h_i^{u,k,t} x_{i-1}^{u,M+\mu-|l_u|+k-t}$$

$$N_P - \mu + |l_u| \le k \le |l_u| - 1 \quad \Rightarrow y_i^{u,k} = \sum_{t=0}^{N_P} h_i^{u,k,t} x_i^{u,M-|l_u|+k-t}$$

$$|l_u| \le k \le N_P + |l_u| - 1 \quad \Rightarrow y_i^{u,k} = \sum_{t=0}^{k-|l_u|} h_i^{u,k,t} x_i^{u,-|l_u|+k-t} + \sum_{t=k-|l_u|+1}^{N_P} h_i^{u,k,t} x_i^{u,M-|l_u|+k-t}$$

$$N_P + |l_u| \le k \le M - 1 \quad \Rightarrow y_i^{u,k} = \sum_{t=0}^{N_P} h_i^{u,k,t} x_i^{u,-|l_u|+k-t}$$

We can now compute the *n-th* FFT output component that belongs to user *u*. Then following similar steps to Case 1a we obtain the interference autocorrelation. This yields

$$R_{\hat{\xi}\hat{\xi}}(u,n,n+p,iT_0,iT_0 \mid l_u,\Delta f_u) = \frac{1}{M^2} \sum_{k \in \Gamma_u} P_{u,k} \frac{1}{(1-e^{-j\frac{2\pi}{M}(n+\overline{\Delta f_u}-k)})(1-e^{j\frac{2\pi}{M}(n+\overline{\Delta f_u}+p-k)})} \{ \; 2\sum_{t=0}^{N_P} \Omega_{u,t} +$$

$$-(e^{j2\pi\overline{\Delta f_u}} + e^{-j2\pi\overline{\Delta f_u}}) \sum_{t=0}^{\mu-|l_u|} \Omega_{u,t} + \sum_{t=\mu-|l_u|+1}^{N_P} \Omega_{u,t} (2e^{j\frac{2\pi}{M}(-\mu+|l_u|+t)p} - e^{-j\frac{2\pi}{M}(-\mu+|l_u|+t)(n+\overline{\Delta f_u}-k)} +$$

$$-e^{-j\frac{2\pi}{M}(-\mu+|l_u|-M+t)(n+\overline{\Delta f_u}-k)} - e^{j\frac{2\pi}{M}(-\mu+|l_u|+t)(n+\overline{\Delta f_u}+p-k)} - e^{j\frac{2\pi}{M}(-\mu+|l_u|-M+t)(n+\overline{\Delta f_u}+p-k)}) \; \}$$

from which *A* in (F.2) is obtained by a shift of $\mu_1/2$, i.e., $l_u \to l_u - \mu_1/2$.

Case 3: $0 \ge l_u \ge N_P - \mu \ge -\mu \ge N_P + 1 - M$

The observation window is defined below.

$$\underbrace{x_i^{u,M-N_P-|l_u|},\ldots,x_i^{u,M-|l_u|-1}}_{N_P} \underbrace{\left[\underbrace{x_i^{u,M-|l_u|},\ldots,x_i^{u,M-1}}_{|l_u|}, \underbrace{x_i^{u,0},\ldots,x_i^{u,M-|l_u|-1}}_{M-|l_u|} \right]}_{\underline{X}^{u,i,l_u}}.$$

The received signal component that belongs to user *u* is defined as follows:

$$0 \le k \le |l_u| - 1 \quad \Rightarrow y_i^{u,k} = \sum_{t=0}^{N_P} h_i^{u,k,t} x_i^{u,M-|l_u|+k-t}$$

$$|l_u| \le k \le N_P + |l_u| - 1 \quad \Rightarrow y_i^{u,k} = \sum_{t=0}^{k-|l_u|} h_i^{u,k,t} x_i^{u,k-|l_u|-t} + \sum_{t=k-|l_u|+1}^{N_P} h_i^{u,k,t_u} x_i^{u,M-|l_u|+k-t}$$

$$N_P + |l_u| \le k \le M - 1 \quad \Rightarrow y_i^{u,k} = \sum_{t=0}^{N_P} h_i^{u,k,t} x_i^{u,k-|l_u|-t}$$

We can now compute the *n-th* FFT output component that belongs to user *u*. Then following similar steps to Case 1a we obtain the interferer autocorrelation. This yields

$$R_{\hat{\xi}\hat{\xi}}(u,n,n+p,iT_0,iT_0 \mid l_u,\Delta f_u)=\frac{1}{M^2}\sum_{k\in\Gamma_u}P_{u,k}\frac{(2-e^{j2\pi\overline{\Delta f_u}}-e^{-j2\pi\overline{\Delta f_u}})\sum_{t=0}^{N_P}\Omega_{u,t}}{(1-e^{-j\frac{2\pi}{M}(n+\overline{\Delta f_u}-k)})(1-e^{j\frac{2\pi}{M}(n+p+\overline{\Delta f_u}-k)})}$$

from which the term *A* in (F.3) is obtained by a shift of $\mu_1/2$, i.e., $l_u \to l_u-\mu_1/2$.

Case 4: $\mu \ge N_P \ge l_u \ge 0$

The observation window is defined below.

$$\underbrace{x_i^{u,M-N_P+|l_u|},\ldots,x_i^{u,M-1}}_{N_P-|l_u|},\underbrace{x_i^{u,0}\ldots,x_i^{u,|l_u|-1}}_{|l_u|},\underbrace{\left[\underbrace{x_i^{u,|l_u|},\ldots,x_i^{u,M-1}}_{M-|l_u|},\underbrace{x_{i+1}^{u,M-\mu},\ldots,x_{i+1}^{u,M-\mu+|l_u|-1}}_{|l_u|}\right]}_{\underline{X}^{u,i,l_u}}.$$

The received signal component that belongs to user *u* is defined as follows:

$$\begin{aligned}
&0\le k\le N_P-|l_u|-1 &&\Rightarrow\ y_i^{u,k}=\sum_{t_u=0}^{k+|l_u|}h_i^{u,k,t}x_i^{u,|l_u|+k-t}+\sum_{t_u=k+|l_u|+1}^{N_{t_u}-1}h_i^{u,k,t_u}x_i^{u,M+|l_u|+k-t}\\
&N_P-|l_u|\le k\le M-|l_u|-1 &&\Rightarrow\ y_i^{u,k}=\sum_{t=0}^{N_P}h_i^{u,k,t}x_i^{u,|l_u|+k-t}\\
&M-|l_u|\le k\le M-1 &&\Rightarrow\ y_i^{u,k}=\sum_{t=0}^{k-M+|l_u|}h_i^{u,k,t}x_{i+1}^{u,|l_u|-\mu+k-t}+\sum_{t=k-M+|l_u|+1}^{N_P}h_i^{u,k,t}x_i^{u,|l_u|+k-t}
\end{aligned}.$$

We can now compute the *n-th* FFT output component that belongs to user *u*. Then following similar steps to case 1a we obtain the interferer autocorrelation. This yields

$$\begin{aligned}
R_{\hat{\xi}\hat{\xi}}(u,n,n+p,iT_0,iT_0 \mid l_u,\Delta f_u)=&\frac{1}{M^2}\sum_{k\in\Gamma_u}P_{u,k}\frac{1}{(1-e^{-j\frac{2\pi}{M}(n+\overline{\Delta f_u}-k)})(1-e^{j\frac{2\pi}{M}(n+p+\overline{\Delta f_u}-k)})}\{\\
&2\sum_{t=0}^{N_P}\Omega_{u,t}-(e^{j2\pi\overline{\Delta f_u}}+e^{-j2\pi\overline{\Delta f_u}})\sum_{t=|l_u|+1}^{N_P}\Omega_{u,t}+\sum_{t=0}^{|l_u|}\Omega_{u,t}(2e^{-j\frac{2\pi}{M}(|l_u|-t)p}-e^{j\frac{2\pi}{M}(|l_u|-t)(n+\overline{\Delta f_u}-k)}+\\
&-e^{-j\frac{2\pi}{M}(M-|l_u|+t)(n+\overline{\Delta f_u}-k)}-e^{-j\frac{2\pi}{M}(|l_u|-t)(n+p+\overline{\Delta f_u}-k)}-e^{j\frac{2\pi}{M}(M-|l_u|+t)(n+p+\overline{\Delta f_u}-k)})\ \}
\end{aligned}$$

from which the term *A* in (F.4) is obtained by a translation of $\mu_1/2$, i.e., $l_u \to l_u-\mu_1/2$.

Case 5a: $\mu \ge l_u \ge N_P+1 \ge 0$

The observation window is defined below.

$$\underbrace{x_{|l_u|-N_P}^{u,i},\ldots,x_{|l_u|-1}^{u,i}}_{N_P},\underbrace{\left[\underbrace{x_{|l_u|}^{u,i},\ldots,x_{M-1}^{u,i}}_{M-|l_u|},\underbrace{x_{M-\mu}^{u,i+1},\ldots,x_{M-\mu+|l_u|-1}^{u,i+1}}_{|l_u|}\right]}_{\underline{X}^{u,i,l_u}}.$$

The received signal component that belongs to user u is defined as follows:

$$\begin{aligned}
&0 \le k \le M-|l_u|-1 && \Rightarrow\ y_i^{u,k} = \sum_{t=0}^{N_P} h_i^{u,k,t} x_i^{u,|l_u|+k-t} \\
&M-|l_u| \le k \le M+N_P-|l_u|-1 && \Rightarrow\ y_i^{u,k} = \sum_{t=0}^{k-M+|l_u|} h_i^{u,k,t} x_{i+1}^{u,|l_u|-\mu+k-t} + \sum_{t=k-M+|l_u|+1}^{N_P} h_i^{u,k,t} x_i^{u,|l_u|+k-t} \\
&M+N_P-|l_u| \le k \le M-1 && \Rightarrow\ y_i^{u,k} = \sum_{t=0}^{N_P} h_i^{u,k,t} x_{i+1}^{u,|l_u|-\mu+k-t}
\end{aligned}.$$

We can now compute the *n-th* FFT output component that belongs to user u. Then following similar steps to case 1a we obtain the interferer autocorrelation. This yields

$$\begin{aligned}
R_{\hat{\xi}\hat{\xi}}(u,n,n+p,iT_0,iT_0 \mid l_u,\Delta f_u) = \frac{1}{M^2}\sum_{k\in\Gamma_u} P_{u,k} \frac{1}{(1-e^{-j\frac{2\pi}{N}(n+\overline{\Delta f_u}-k)})(1-e^{j\frac{2\pi}{N}(n+p+\overline{\Delta f_u}-k)})}\{\ 2\sum_{t=0}^{N_P}\Omega_{u,t} + \\
+\sum_{t=0}^{N_P}\Omega_{u,t}(2e^{-j\frac{2\pi}{M}p(|l_u|-t)} - e^{j\frac{2\pi}{M}(n+p+\overline{\Delta f_u}-k)(M-|l_u|+t)} - e^{-j\frac{2\pi}{M}(n+p+\overline{\Delta f_u}-k)(|l_u|-t)} - e^{-j\frac{2\pi}{M}(n+\overline{\Delta f_u}-k)(M-|l_u|+t)} + \\
-e^{j\frac{2\pi}{M}(n+\overline{\Delta f_u}-k)(|l_u|-t)})\ \}
\end{aligned}$$

from which the term A in (F.5) is obtained by a shift of $\mu_1/2$, i.e., $l_u \to l_u - \mu_1/2$.

Case 5b: $N_P+\mu \ge l_u \ge \mu \ge N_P \ge 0$

The observation window is defined below.

$$\underbrace{x_i^{u,|l_u|-N_P},\ldots,x_i^{u,|l_u|-1}}_{N_P},\underbrace{\left[\underbrace{x_i^{u,|l_u|},\ldots,x_i^{u,M-1}}_{-|l_u|},\underbrace{x_{i+1}^{u,M-\mu},\ldots,x_{i+1}^{u,M-1}}_{\mu},\underbrace{x_{i+1}^{u,0},\ldots,x_{i+1}^{u,|l_u|-\mu-1}}_{|l_u|-\mu}\right]}_{\underline{X}^{u,i,l_u}}.$$

The received signal component that belongs to user u is defined as follows:

$$\begin{aligned}
&0 \le k \le M-|l_u|-1 && \Rightarrow\ y_i^{u,k} = \sum_{t=0}^{N_P} h_i^{u,k,t} x_i^{u,|l_u|+k-t} \\
&M-|l_u| \le k \le M+N_P-|l_u|-1 && \Rightarrow\ y_i^{u,k} = \sum_{t=0}^{k-M+|l_u|} h_i^{u,k,t} x_{i+1}^{u,|l_u|-\mu+k-t} + \sum_{t=k-M+|l_u|+1}^{N_P} h_i^{u,k,t} x_i^{u,|l_u|+k-t} \\
&M+N_P-|l_u| \le k \le M-|l_u|+\mu-1 && \Rightarrow\ y_i^{u,k} = \sum_{t=0}^{N_P} h_i^{u,k,t} x_{i+1}^{u,|l_u|-\mu+k-t} \\
&M-|l_u|+\mu \le k \le M-1 && \Rightarrow\ y_i^{u,k} = \sum_{t=0}^{k-M+|l_u|-\mu} h_i^{u,k,t} x_{i+1}^{u,-M+|l_u|-\mu+k-t} + \sum_{t=k-M+|l_u|-\mu+1}^{N_P} h_i^{u,k,t} x_{i+1}^{u,|l_u|-\mu+k-t}
\end{aligned}$$

The computation of the interference autocorrelation yields identical results to case 5a.

Case 5c: $l_u \geq N_P + \mu + 1 \geq \mu \geq N_P \geq 0$

The observation window is defined below.

$$\underbrace{x_i^{u,|l_u|-N_P},\ldots,x_i^{u,|l_u|-1}}_{N_P},\underbrace{\left[\underbrace{x_i^{u,|l_u|},\ldots,x_i^{u,M-1}}_{M-|l_u|},\underbrace{x_{i+1}^{u,M-\mu},\ldots,x_{i+1}^{u,M-1}}_{\mu},\underbrace{x_{i+1}^{u,0},\ldots,x_{i+1}^{u,|l_u|-\mu-1}}_{|l_u|-\mu}\right]}_{\underline{X}^{u,i,l_u}}.$$

The received signal component that belongs to user *u* is defined as follows:

$$\begin{aligned}
&0 \leq k \leq M-|l_u|-1 && \Rightarrow y_i^{u,k} = \sum_{t=0}^{N_P} h_k^{u,i,t} X_{|l_u|+k-t}^{u,i} \\
&M-|l_u| \leq k \leq M+N_P-|l_u|-1 && \Rightarrow y_i^{u,k} = \sum_{t=0}^{k-M+|l_u|} h_i^{u,k,t} x_{i+1}^{u,|l_u|-\mu+k-t} + \sum_{t=k-M+|l_u|+1}^{N_P} h_i^{u,k,t} x_i^{u,|l_u|+k-t} \\
&M+N_P-|l_u| \leq k \leq M-|l_u|+\mu-1 && \Rightarrow y_i^{u,k} = \sum_{t=0}^{N_P} h_i^{u,k,t} x_{i+1}^{u,l_u|-\mu+k-t} \\
&M-|l_u|+\mu \leq k \leq M-|l_u|+\mu+N_P-1 && \Rightarrow y_i^{u,k} = \sum_{t=0}^{k-M+|l_u|-\mu} h_i^{u,k,t} x_{i+1}^{u,-M+|l_u|-\mu+k-t} + \sum_{t=k-M+|l_u|-\mu+1}^{N_P} h_i^{u,k,t} x_{i+1}^{u,|l_u|-\mu+k-t} \\
&M-|l_u|+\mu+N_P \leq k \leq M-1 && \Rightarrow y_i^{u,k} = \sum_{t=0}^{N_P} h_i^{u,k,t} x_{i+1}^{u,-M+|l_u|-\mu+k-t}
\end{aligned}.$$

The computation of the autocorrelation yields identical results to Case 5a.

11 CAPACITY OF THE ASYNCHRONOUS DMT MULTIPLE ACCESS GAUSSIAN CHANNEL

In this chapter we study the capacity of an asynchronous DMT based communication system. Multiple users share a Gaussian channel through DMT modulation and tone multiplexing. We consider a bank of single user detectors at the output of which multiple access interference arises whenever time misalignments and frequency offsets exist among users. Consequently, we determine an inner bound to both the capacity of a given user link and the region of achievable information rates for joint reliable communications (i.e., capacity region). Such capacity inner bounds are random variables and function of several system parameters. The associated complementary cumulative distribution functions are defined and are evaluated for several system scenarios characterized by different tone assignment schemes and strategies of power allotment to sub-carriers. As a result, a pragmatic approach for enlarging the capacity region is devised. The approach is based on the appropriate insertion of a guard time, the partition of tones to users, and the choice of the power profile to be assigned to the sets of tones.

11.1 Preliminaries

In this chapter we address the problem of defining the *achievable information rates* for reliable communications (i.e. with arbitrarily small probability of error) of a set of time and frequency asynchronous users that share a Gaussian channel with a DMT multiple access scheme. In particular, demodulation is accomplished with a bank of parallel single user detectors, each perfectly time and frequency synchronized to a given user (Chapter 10).

Considering N_U users, the determination of the *capacity region*, which is the closure of the set of all achievable rate N_U-tuples, of such a scenario, is in general a formidable task [16], [23]. We determine an *inner bound*, i.e. a subset of the capacity region that can be achieved when deploying the proposed receiver. A trivial *outer bound* is found by considering the perfectly time and frequency synchronous system.

We emphasize that in this scenario the capacity region is determined as a function of several system parameters. Once we have constrained the total number of sub-carriers, and the total power

per user, the capacity region still depends on the number of users, the number of sub-carriers per user, the sub-carrier allocation scheme to users, the power allotment to sub-carriers, the deployment of time and frequency guards. Finally, there is a dependency on the time and frequency offsets of each user, which are random variables.

To proceed into the analysis we take the approach of treating the maximum rate for reliable communications of a given user link (link capacity) as a random variable. We fix a maximum time and frequency offset within the system, and then we compute the complementary cumulative distribution functions (ccdf) of the link capacity. These curves show the probability that a user link has a larger capacity than the corresponding abscissa, over all system realizations. The dependency on the tone allocation and power allotment scheme is illustrated by numerically computing, through Monte Carlo simulations, the ccdf for several assignment schemes in a fully loaded system. Among these, a promising dynamic tone allocation scheme yields increased capacity compared to the conventional block and interleaved tone allocations.

We further consider the joint ccdf of a set of users, from which it possible to determine, for instance, the N_U-tuples of achievable rates with a given probability.

11.2 Multiple Access Interference Channel Representation

In the presence of time and frequency asynchronous users the link of user u can be modeled as shown in Fig. 11.1, where the tone indices n_l, $l = 0,...,K_u - 1$, belong to the set Γ_u assigned to user u.

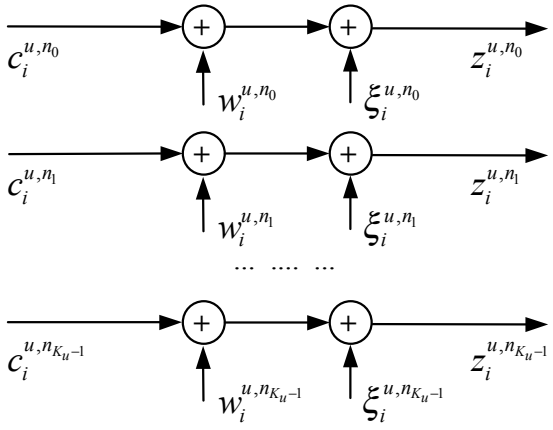

Fig. 11.1. MAI channel model for the link of user u.

The *u-th* user transmits its information through K_u parallel channels that experience additive multiple user interference and thermal noise. The thermal noise vector $\underline{w}^{u,i} = [w_i^{u,n_0},...,w_i^{u,n_{K_u-1}}]^T$ is

Gaussian distributed with zero mean and covariance $\underline{K}_{ww}^{u} = E[\underline{w}_i^u (\underline{w}_i^u)^H] = N_0 \underline{I}$, where $\underline{I}$ is the K_u by K_u identity matrix. In general the MAI is correlated in time (along index *i*) and in frequency (along the sub-carriers). However, we make the assumption of temporal uncorrelation, based on the fact that this is true for time offsets $|l_{u'}| \leq \mu/2$, $u' = 1,...,N_U$, and is a valid approximation for small time offsets exceeding the guard interval.

Now, for a capacity evaluation standpoint, we constrain to consider input signals with Gaussian distribution that have zero mean and covariance $\underline{K}_{cc}^{u} = E[\underline{c}_i^u (\underline{c}_i^u)^H]$. Inputs signals of distinct users are considered independent. It follows that the overall MAI is Gaussian distributed since each user generates a MAI contribution that is Gaussian. The mean of the MAI is zero and the covariance is $\underline{K}_{\xi\xi}^{u} = E[\underline{\xi}_i^u (\underline{\xi}_i^u)^H]$. In conclusion, the link of user *u* can be modeled as K_u additive Gaussian noise channels that are correlated. The time index *i* can be omitted and we can write in vector notation

$$\underline{Z}^u = \underline{C}^u + \underline{\Psi}^u + \underline{W}^u \tag{11.1}$$

$$\underline{\Psi}^u = \sum_{u'=1,\ u' \neq u}^{N_U} \underline{A}(u',u)\underline{C}^{u'} \tag{11.2}$$

with $\underline{Z}^u = [z^{u,n_0},...,z^{u,n_{K_u-1}}]^T$, $\underline{C}^u = [c^{u,n_0},...,c^{u,n_{K_u-1}}]^T$, $\underline{\Psi}^u = [\xi^{u,n_0},...,\xi^{u,n_{K_u-1}}]^T$, $\underline{W}^u = [w^{u,n_0},...,w^{u,n_{K_u-1}}]^T$ being respectively the output vector, the input vector, the interference vector, and the noise vector. $\underline{A}(u,u')$ is the interference matrix of user u' on user u. The interference matrix is a function of the system parameters and in particular of the relative time and frequency offset of user u' with respect to user *u*.

If we assume that the input covariance of each user is equal to $\underline{K}_{cc}^{u'} = diag(P_{u',n_0},...,P_{u',n_{K_{u'}-1}})$, and that all users have a time delay $|l_{u'}| \leq \mu/2$ relatively to user *u*, then the interference covariance seen by user *u* computed over sub-carrier indices *n* and *n*+*p* (belonging to Γ_u) has been evaluated in Section 10.2.1. The interference covariance matrix elements are:

$$K_{\xi\xi}^{u}(n,n+p) = \frac{1}{M^2} \sum_{\substack{u'=1 \\ u' \neq u}}^{N_U} \sum_{k \in \Gamma_{u'}} P_{u',k} \frac{2 - e^{j2\pi\overline{\Delta f_{u'}}} - e^{-j2\pi\overline{\Delta f}_{u'}}}{1 - e^{j\frac{2\pi}{M}(n+p+\overline{\Delta f_{u'}}-k)} - e^{-j\frac{2\pi}{M}(n+\overline{\Delta f_{u'}}-k)} + e^{j\frac{2\pi}{M}p}}. \tag{11.3}$$

The result in (11.3) will be used in the next section for the link capacity evaluation. Recall that $\overline{\Delta f_u}$ is the frequency offset normalized with respect to the sub-carrier spacing. Note that there is no dependency on the time offset since we have considered delays satisfying $|l_{u'}| \leq \mu/2$. It has to be

said that more general expressions can be calculated to include delays $|l_{u'}| > \mu/2$ (see Chapter 10).

11.3 Capacity Evaluation

The presence of asynchronous users (interferers) induces some degradation on the performance of the single user receiver. The problem we are dealing with is to quantify such degradation as a function of the system parameters. In Chapter 10 we have used the signal energy over noise plus interference ratio as a figure for the performance degradation. Now we aim to evaluate the capacity of the *u-th* link, and more in general the capacity region where jointly reliable communications are possible.

Within the model in the previous section, the capacity of the *u-th* user link is evaluated by maximizing the mutual input-output information $I(\underline{Z}^u; \underline{C}^u \mid \underline{C}^0, ..., \underline{C}^{u-1}, \underline{C}^{u+1} ...)$, over all possible input covariance matrices $\underline{K}^u_{cc}$ subject to the trace constraint $trace(\underline{K}^u_{cc}) = \sum_{n \in \Gamma_u} P_{u,n} \le P$. Since we consider Gaussian inputs, the capacity [25] in bit/s/Hz is obtained as shown below [23]:

$$C(u \mid \underline{K}^u_{\xi\xi}) = \frac{1}{K_u} \max_{\underline{K}^u_{cc}} \left\{ \log_2 \left(\frac{|\underline{K}^u_{cc} + \underline{K}^u_{ww} + \underline{K}^u_{\xi\xi}|}{|\underline{K}^u_{ww} + \underline{K}^u_{\xi\xi}|} \right) \right\} \tag{11.4}$$

where $|\underline{A}|$ is the determinant of the matrix $\underline{A}$, and K_u is the number of tones assigned to user *u*. Note that (11.4) is conditioned on the covariance of the interference, which in turn is a function of the input covariance of the interferers, their time/frequency offsets, and their set of assigned tones. For a particular system realization these parameters can be considered constant.

All information rates $R_u \le C(u \mid \underline{K}^u_{\xi\xi})$ allow communications with arbitrarily small probability of error over the *u-th* user link. Further, we do not consider the case where cooperation among decoders of distinct users exists. In this case a way to proceed would be to augment the dimensions of the model in (11.1)-(11.2).

To get insight, we constrain the input covariance to be diagonal for all users. With this hypothesis, knowing the frequency offset, and the set of assigned tones of each user, (11.3) gives the covariance matrix of the interference (when $|l_{u'}| \le \mu/2$ for all u'). Thus, (11.4) can be computed, yielding an achievable rate for a given user link. In this case, suppose to assign an equal number of tones to all users, and to distribute equally the power among tones, then the individual link capacities can in general differ. This is due to the fact that each of the links sees on its set of

[25] The standard capacity formula for real vectors is *(1/2)log$_2$[.]*. Since we are dealing with Gaussian complex vectors it can be shown that the factor (1/2) vanishes out.

tones a different MAI contribution. In this scenario, the conditional capacity region, which is the closure of the set of all rate vectors $\underline{R} = [R_1, ..., R_{N_U}]$ that satisfy $R_{u'} \leq C(u' \mid \underline{K}_{\xi\xi}^{u'})$ for $u' = 1, ..., N_U$, can be thought to be an hyper-parallelepiped. This capacity region (*inner bound*) is contained into the capacity region (*outer bound*) defined by all rate vectors whose components satisfy $R_{u'} \leq (1/K_{u'}) \log_2 \prod_{n \in \Gamma_{u'}} (1 + P_{u',n}/N_0)$ for $u' = 1, ..., N_U$. This outer bound is certainly achieved by the synchronous system where the MAI detrimental effect disappears.

11.4 Capacity as a Random Variable

In general, even if we constrain the input covariance matrices to be the same for all users, simple meaningful closed expressions that define the conditional capacity region (i.e. conditioned on the time and frequency offsets) cannot be found. This is because the interference covariance in (11.3) still has a dependency on how we assign the tones to the users. Furthermore, the time and frequency offsets are random parameters. Thus, to proceed we follow the approach of treating the link capacity (i.e. rate that grants reliable communications over a user link) a random variable. We consider the time and frequency offsets of all users independent and equally distributed. Then, we fix the tone assignment scheme together with the power allotment to sub-carriers, and we constrain the input covariance matrices of all users to be diagonal.

Our aim is now to compute the complementary cumulative distribution function (ccdf) of the link capacity. This is defined as the probability that the capacity of a given user is greater than a fixed value for all possible system realizations where all users have a time and frequency offset independently distributed

$$ccdf_u(\bar{C}) = P[C(u) > \bar{C}]. \tag{11.5}$$

If the tone assignment scheme of each user satisfies symmetry rules, the power allotment is also the same, and the system is fully loaded, then the ccdfs in (11.5) are the same for all users. Thus, rate $R_u = \bar{C}$ is achievable by the *u-th* link with probability given by (11.5), and the same applies to the other links, individually considered.

Following the same approach it is possible to define the joint link capacities ccdf

$$ccdf_U(\bar{C}_1, ..., \bar{C}_{N_U}) = P[C(u=1) > \bar{C}_1, ..., C(u=N_U) > \bar{C}_{N_U}]. \tag{11.6}$$

Now, the capacity region takes on a probabilistic significance. It can be interpreted as the region determined by all rate vectors for which jointly reliable communications are possible with a given probability. This, capacity region is outer bounded by the capacity region that is determined in the

absence of MAI (achieved with probability 1 in the synchronous case).

Finally, we emphasize that (11.5) and (11.6) still depend upon the tone allocation strategy, and the power allotment to tones.

11.5 System Scenarios and Capacity Performance Comparison

Evaluation of the ccdfs (11.5) and (11.6) is carried out numerically through Monte Carlo simulations. As a result it is possible to evaluate the capacity performance of several systems that differ on the tone allocation and power allotment strategy.

11.5.1 Single Link Capacity Complementary Cumulative Distribution Function

We start considering the ccdf of the single user link (i.e., Equation (11.5)). The system under investigation is a fully loaded system scenario characterized by the following parameters: fixed number of overall carriers $M=256$, $N_U=16$ users, $K_u=16$ tones per user. A guard time is inserted such that the MAI effect due to time misalignments is null. Further, the bandwidth penalty is also ignored assuming that M is much larger than the cyclic prefix. Obviously, this assumption depends upon the cell size. However, we could always think of having some degree of centralized control that confines the time offset within the guard time length. Vice versa the frequency offset detrimental effect cannot be completely canceled out by the insertion of frequency guards. Thus, we have considered users with frequency offsets that are independent and uniformly distributed in $(-T_1\Delta f_{\max}, +T_1\Delta f_{\max})$. The maximum frequency offset is assumed to be a fraction of the sub-carrier spacing.

In Fig. 11.2 and Fig. 11.3 the users are allocated with an *interleaved tone assignment* scheme. In other words, the tones of distinct users are regularly interleaved across the overall set of M tones. All sub-carriers of all users have the same power. The signal-to-thermal-noise power ratio is set to 10 dB and 30 dB and several maximum frequency offsets are considered (the frequency offset intervals are normalized to the sub-carrier spacing). We plot a vertical line in correspondence of the capacity that is achieved by the synchronous system. This represents a capacity upper bound. For SNR=10 dB the upper bound is 3.46 bit/s/Hz, while for SNR=30 dB is 9.97 bit/s/Hz.

Now, looking for instance at Fig. 11.2, we set a percentage, say 90%, then we read the minimum capacity we can provide to a user link with that probability over all system realizations. Note that, since the system is fully loaded, the tones are regularly assigned, and the power allotment to sub-carriers is the same, all N_U links have the same ccdf. The same applies in the other schemes described in this section.

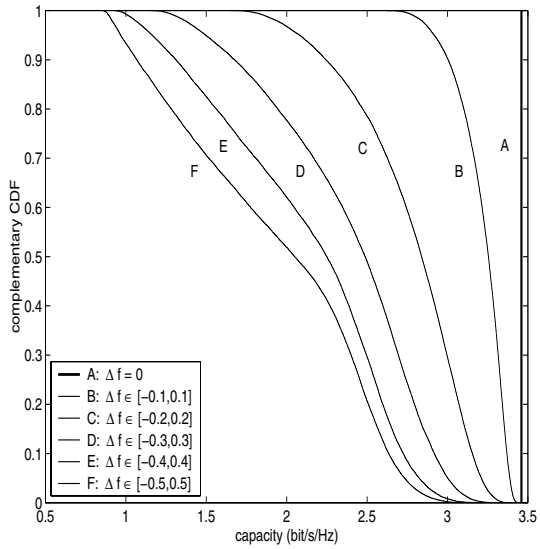

Fig. 11.2. Ccdf of the capacity of a user link for uniformly distributed frequency offsets normalized to the sub-carrier spacing. Fully loaded system with M=256, N_U=16, K_u=16. Interleaved tone assignment. Equal power tones. SNR=10 dB.

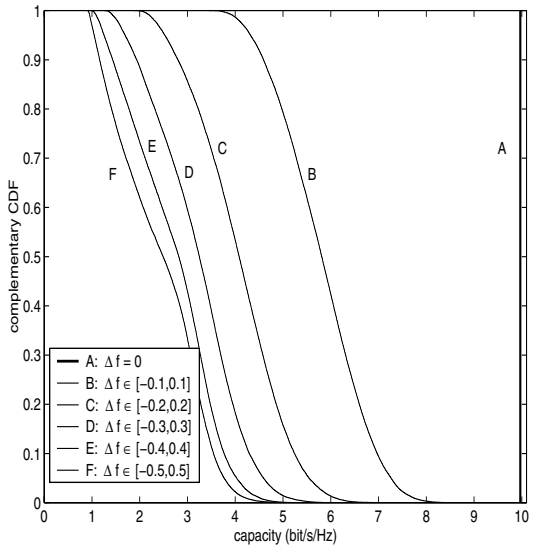

Fig. 11.3. Ccdf of the capacity of a user link for uniformly distributed frequency offsets normalized to the sub-carrier spacing. Fully loaded system with M=256, N_U=16, K_u=16. Interleaved tone assignment. Equal power tones. SNR=30 dB.

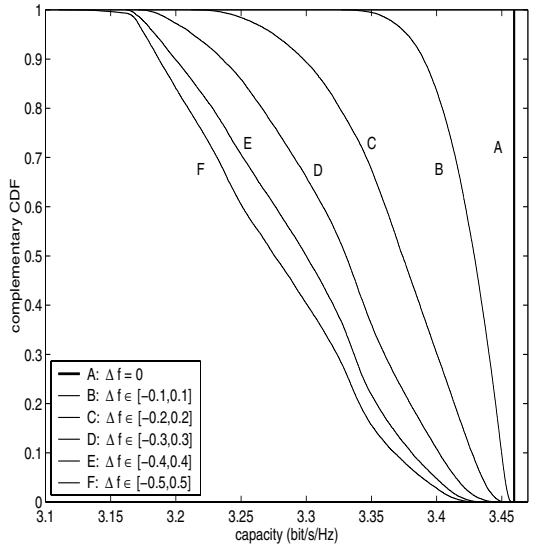

Fig. 11.4. Ccdf of the capacity of a user link for uniformly distributed frequency offsets normalized to the sub-carrier spacing. Fully loaded system with M=256, N_U=16, K_u=16. Block tone assignment. Equal power tones. SNR=10 dB.

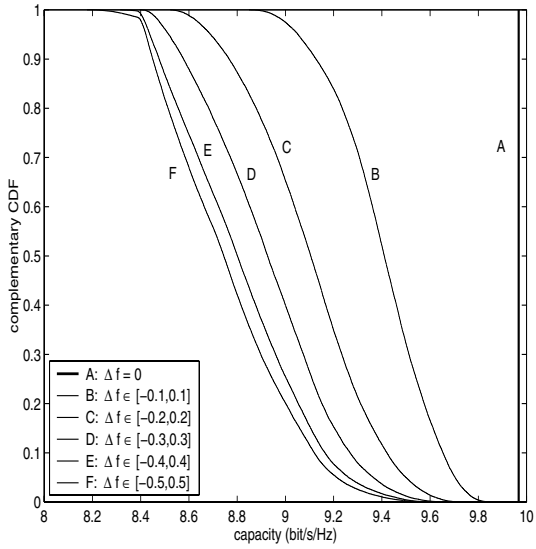

Fig. 11.5. Ccdf of the capacity of a user link for uniformly distributed frequency offsets normalized to the sub-carrier spacing. Fully loaded system with M=256, N_U=16, K_u=16. Block tone assignment. Equal power tones. SNR=30 dB.

From Fig. 11.2 it can be seen that the capacity lower bound is about 0.5 bit/s/Hz from the upper bound for 90% of the system realizations when $T_1\Delta f_{max}$=0.1 and the SNR=10 dB. The capacity loss dramatically increases to about 2.5 bit/s/Hz for $T_1\Delta f_{max}$=0.5. As the SNR increases (Fig. 11.3), the

capacity performance is dominated by the MAI, such that the difference between the lower and the upper bound is more pronounced.

In Fig. 11.4 and Fig. 11.5 we consider the same system with, however, a *block tone assignment* where disjoint blocks of K_u contiguous tones are assigned to each user. Fixed the same outage probability (i.e. 10%), the block tone allocation scheme exhibits a strong capacity improvement over the interleaved. For instance, at 30 dB SNR the block scheme provides a minimum capacity ranging from about 8.4 to about 9.1 bit/s/Hz for $T_1\Delta f_{max}$ ranging from 0.5 to 0.1. On the other hand the interleaved scheme yields capacities ranging from 1 to 4.5 bit/s/Hz.

At this point, a first approach to improve further the single link capacity can be to differentiate the power transmitted on the sub-carriers. We pursued this idea in a simplified manner. In Fig. 11.6, the tones are block allocated. Then, the power of the first and last tone of each user block is set to zero. Basically, this corresponds to inserting frequency guards. Unfortunately, this helps only for high Δf_{max} , as shown by comparison of Fig. 11.6 with Fig. 11.5. This is due to the fact that the diminished MAI level does not always compensate the capacity loss due to no transmission on two sub-carriers. In a second experiment (Fig. 11.7), the total available power is distributed in the following manner. The first and the last tone of each block have half power, while the power of two middle tones is increased by half. As Fig. 11.7 confirms, this strategy shows some improvement over Fig. 11.5.

It is clear that although we pursued an intuitive and simple method to allocate the power to sub-carriers, the results in Fig. 11.7 confirm that distributing the power uniformly among the tones is not optimal. A systematic application of the water-filling method [23] should lead to more significant improvements.

A second proposed method to improve capacity is based on *adaptively allocating* the tones to users. The main idea is that if we know for instance what the frequency offsets of the users are, we can assign block of tones in a way such that each block has adjacent blocks ordered with increasing frequency offset. This can be simply accomplished by imagining of allocating the N_U users in a circular queue of N_U cells. The user with the lowest offset is assigned to a cell. Then, pick other two users with the remaining lowest offset and allocate them one to the right and one to the left adjacent cells. Proceed until the cells are filled. This adaptive method of allocating tones in order of increasing frequency offset can be generalized to include time offsets exceeding the guard time.
The ccdf of the user link capacity with this adaptive scheme is plotted in Fig. 11.8 and Fig. 11.9. A deep improvement is found over the schemes that we have considered so far. For instance at 30 dB SNR the lower bound in capacity granted with probability 90% loses less than 1 bit/s/Hz over the

upper bound for all $T_1\Delta f_{max}$ from 0.5 to 0.1. Clearly, the practicality of such an approach needs to be investigated.

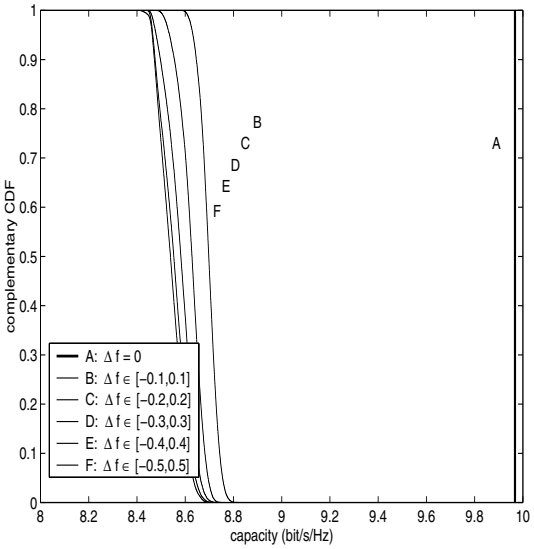

Fig. 11.6. Ccdf of the capacity of a user link for uniformly distributed frequency offsets normalized to the sub-carrier spacing. Fully loaded system with M=256, N_U=16, K_u=16. Block tone assignment. Power zero on first and last tone in each block. SNR=30 dB.

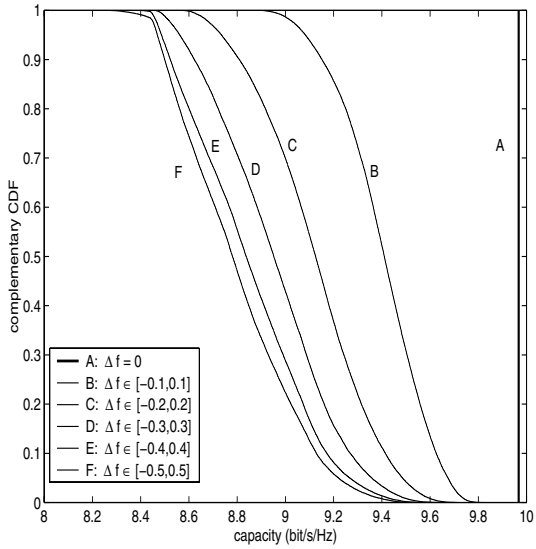

Fig. 11.7. Ccdf of the capacity of a user link for uniformly distributed frequency offsets normalized to the sub-carrier spacing. Fully loaded system with M=256, N_U=16, K_u=16. Block tone assignment. Half power on first and last tone, 3/2 power on two mid-tones. SNR=30 dB.

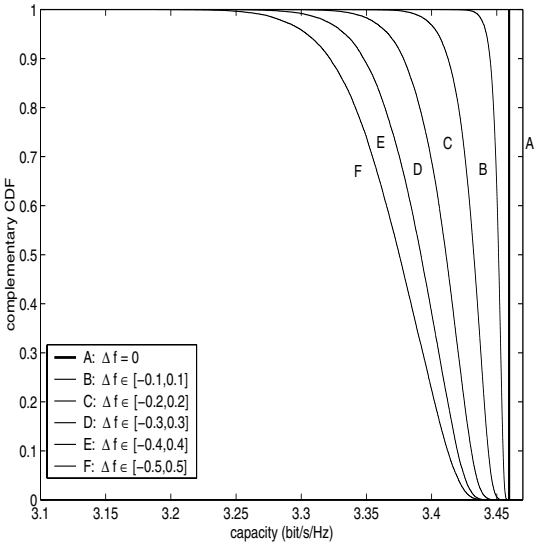

Fig. 11.8. Ccdf of the capacity of a user link for uniformly distributed frequency offsets normalized to the sub-carrier spacing. Fully loaded system with M=256, N_U=16, K_u=16. Adaptive block tone assignment. Equal power tones. SNR=10 dB.

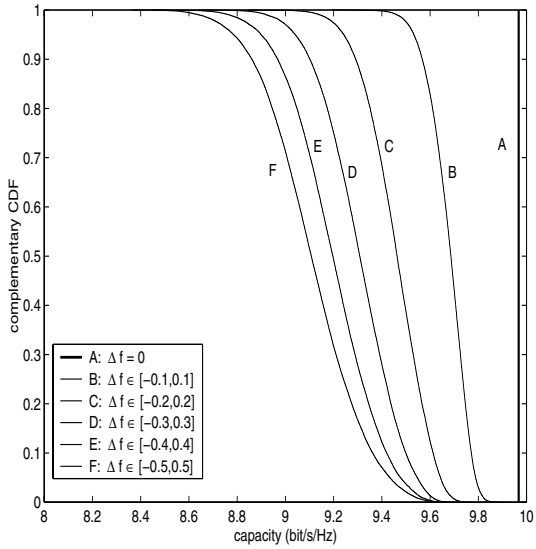

Fig. 11.9. Ccdf of the capacity of a user link for uniformly distributed frequency offsets normalized to the sub-carrier spacing. Fully loaded system with M=256, N_U=16, K_u=16. Adaptive block tone assignment. Equal power tones. SNR=30 dB.

11.5.2 Joint Link Capacity Complementary Cumulative Distribution Function

In this section we report some results obtained by numerically computing (11.6).

In Fig. 11.10 we consider a fully loaded system with $M=64$, where 2 users have $K_u=32$ tones block assigned with equal power, and experience independent frequency offsets with uniform distribution in $(-0.25/T_1 \ ,+0.25/T_1)$. The SNR is set to 30 dB. Fig. 11.11 is the contour plot of the surface in Fig. 11.10: each curve is the set of rate pairs for which joint reliable communications are possible with a given probability over all system realizations.

In Fig. 11.12 we consider a 4 users fully loaded system with $M=64$. Each user has $K_u=16$ tones block assigned with equal power, and experiences independent frequency offset with uniform distribution in $(-0.25/T_1,+0.25/T_1)$. The SNR is set to 10 B. Fig. 11.12 shows the joint ccdf of two users out of four. Fig. 11.13 is the contour plot of the surface. The closure determined by such curves can be thought to be the set of all achievable rate pairs with probability at least equal to the corresponding contour label. The capacity region that has probability one is a square, and is the one that would be determined in the case all users experienced the maximum frequency offset in all realizations.

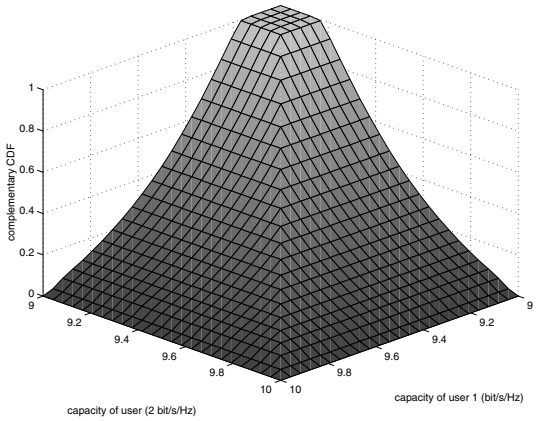

Fig. 11.10. Joint ccdf of user 1 and 2 in a fully loaded system. Block tone assignment, M=64, N_u=2, K=32. Equal power tones. SNR=30 dB. Frequency offsets uniformly distributed in [-0.25/T_1, 0.25/T_1].

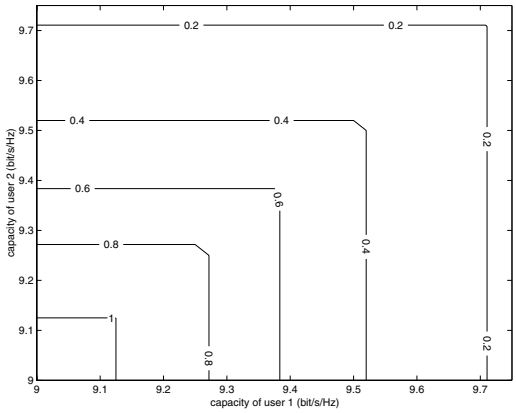

Fig. 11.11. Contour lines of joint ccdf of user 1 and 2 in a fully loaded system. Block tone assignment, M=64, N_u=2, K=32. Equal power tones. SNR=30 dB. Frequency offsets uniformly distributed in [-0.25/T_1, 0.25/T_1].

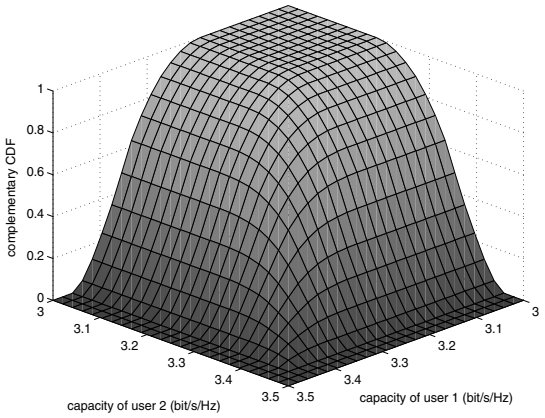

Fig. 11.12. Joint ccdf of user 1 and 2 out of 4 users in a fully loaded system. Block tone assignment, M=64, N_u=4, K=16. Equal power tones. SNR=10 dB. Frequency offsets uniformly distributed in [-0.25/T_1, 0.25/T_1].

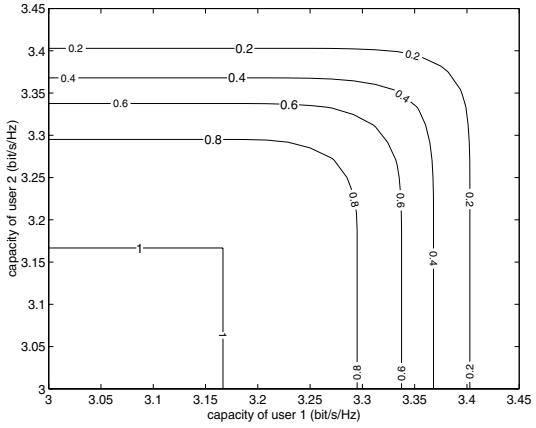

Fig. 11.13. Contour lines of joint ccdf of user 1 and 2 out of 4 users in a fully loaded system. Block tone assignment, M=64, N_u=4, K=16. Equal power tones. SNR=10 dB. Frequency offsets uniformly distributed in [-0.25/T_1, 0.25/T_1].

11.6 Concluding Remarks

In this chapter we have studied the problem of defining the achievable information rates for reliable communications of a set of time and frequency asynchronous users that share a Gaussian channel through a DMT MA access scheme. Demodulation is accomplished with a bank of single user FFT based detectors, at the output of which multiple access interference arises. We have shown that each user link can be modeled with a multiple-input multiple-output correlated Gaussian interference channel. Consequently, we have determined an inner bound to both the capacity of a given user link, and the region of achievable information rates for joint reliable communications (i.e., capacity region). These bounds are conditioned on a system realization (i.e., time and frequency offsets), and depend on the tone allocation scheme and the power allotment to sub-carriers. Thus, by treating these bounds as a random variable we have numerically computed their ccdfs for several fully loaded system scenarios characterized by different tone assignment schemes, and power allotment to sub-carriers.

Based on the results, the following conclusions and guidelines for maximizing capacity in a multiuser DMT system are derived. The insertion of an appropriate cyclic prefix completely eliminates the MAI due to time misalignments. For large cell size some degree of centralized synchronization is required to reduce the prefix length, thus save bandwidth. Multiplexing the users with a block tone allocation yields improved capacity, compared to interleaving the users tones, in

the presence of the irreducible frequency offset detrimental effect. Other capacity improvements can be obtained with a dynamic tone allocation that adaptively allocates the tones on a per user time/frequency offset base. Finally, the power of a user should be distributed in an ad hoc fashion among the user tones, following for example a water-filling approach.

12 CONCLUSIONS

In this thesis we have considered asynchronous multiuser communication systems that are based on deploying multicarrier modulation. We have proposed and deeply investigated architectures where multiple users share a communication channel through multiplexing of the available sub-carriers. The system is in general referred to as multicarrier multiple access (MC-MA) and is particularly suited for application to wireless communications, e.g., in wireless LAN and macro cellular systems. Although it is applicable to both the downlink (base to mobile) and the uplink (mobile to base), we have focused into the latter (more critical) scenario.

The key features of these architectures are determined by the choice of the sub-carrier spacing, the tone assignment strategy, and the design of the sub-channel transmit filters. As a result, the receiver sees a multitude of users that transmit their information signals through multiple narrow-band pipes (sub-channels). The sub-channels have some degree of temporal and frequency overlapping. It depends on the sub-channel transmit filters, the sub-carrier spacing, and is greatly affected by the frequency selective time-variant communication channel as well as by the presence of temporal and carrier frequency misalignment across users.

We have studied and derived efficient discrete-time system implementations that are referred to as multitone multiple access (MT-MA). Under the hypothesis of uniformly spaced sub-carriers and identical sub-channel transmit filters, a given user transmitter is efficiently implemented with a DFT module followed by a bank of low rate polyphase filters. It can be viewed as an extension of the FMT modulation concept. Therefore we refer to it as FMT multiple access (FMT-MA). If rectangular pulses are deployed the filtering operation does not take place and the system is an extension of DMT modulation and referred to as DMT multiple access (DMT-MA).

In such a scenario, we have studied the problem of defining the optimum multicarrier multiuser demodulator. The solution has been obtained by extending the multiuser detection approach to this context. The resulting receiver comprises a front-end structure followed by a maximum a posteriori detector. The front-end part is implemented with a bank of filters matched to the equivalent sub-channel impulse responses. The detector is optimum in the probabilistic sense and is capable of delivering optimum soft information on the transmitted bits/symbols of all users by running a maximum a posteriori algorithm with an appropriate metric.

We have analyzed the structure of the front-end receiver considering both static and time-variant frequency selective fading channels in the presence of temporal and carrier frequency asynchronism. Efficient digital implementations are possible and are based on using banks of adaptive polyphase digital filters followed by DFT modules.

It has been shown that intersymbol interference (ISI), intercarrier interference (ICI), and multiple access interference (MAI) arise at the front-end outputs as a function of the transmit filter shape, the tone allocation strategy, the channel time/frequency dispersion, and the time/frequency misalignment among users.

Since the complexity of the optimum detector grows exponentially with the number of users, the number of sub-channels, and the channel memory, we have considered several simplified detection approaches. These are based on iterative detection schemes where soft/hard information is exchanged between sub-trellises that are obtained by partitioning the full hyper trellis that describes the hidden multiple-input multiple-output Markov model. For instance, iterative per-symbol detection is a simple approach that performs detection by iteratively exchanging soft/hard information between the symbol detectors at the matched filter bank outputs.

Channel coding has also been considered, and iterative (turbo) multicarrier-user detection and decoding has been proposed as a practical decoding solution when interleaved codes are deployed.

Several results from simulations are reported to illustrate that multicarrier multiuser detection is capable of canceling the ISI, ICI, MAI components that arise in an asynchronous MC-MA system. In particular we wish to give emphasis to the following remarks:

A. The proposed multicarrier detector is the optimum detection scheme for both MC-MA and MT-MA systems as well as for single user FMT and DMT systems. It basically performs multiuser detection with equalization over both the temporal and the frequency dimension.
B. In DMT systems with cyclic prefix conventional DFT based demodulation with one tap equalization per sub-channel is sub-optimum. The proposed multicarrier detector is the optimal demodulator/equalizer of DMT signals. With this demodulation approach no cyclic prefix is required, which translates into higher spectral efficiency at the expense of increased complexity.
C. The optimum multicarrier detector exploits the frequency diversity provided by frequency selective fading channel as well as the temporal diversity of time-variant channels.
D. If we deploy channel coding with interleavers the concatenation of the encoders with the multitone modulator (either FMT or DMT) can be treated as a serially concatenated coded system. In particular FMT can be viewed as a form of multichannel partial response signaling. Practical decoding can follow and iterative (turbo like) approach. Performance

may exhibit turbo gains.

E. Conventional DFT based demodulation of DMT signals is not capable of exploiting the frequency diversity when no channel coding is deployed. Further, it yields dramatically poor performance in fast time-variant channels, i.e., channels that are not static over the DMT block duration. However, this simple demodulation technique can handle time dispersion and time misalignments when a sufficiently long cyclic prefix is inserted. Unfortunately, it still remains affected by the presence of carrier frequency offsets.

F. Optimal multicarrier detection may be too complex for practical applications. However, simplified implementations are possible. For instance, iterative per-symbol detection can be deployed in both uncoded and coded architectures. We have found that despite is simplicity it is capable of canceling out the interference components and it approaches the error rate bounds. It is further capable of exploiting significant fractions of the available frequency diversity.

Clearly the simplest detection scheme is based on making symbol decisions on each sub-channel matched filter output by ignoring the presence of the interference components. We refer to it as single carrier detection. It is the conventional detection scheme in a DMT system (DFT followed by one tap equalization). Its performance in general multicarrier and multitone multiuser architectures depends upon many system parameters. That is, the system design and channel characteristics determine the interference components and thus the performance of the single carrier detector. Therefore we have analytically studied the interference components for several choices of the sub-channel transmit filters and sub-carrier multiplexing. In particular we have found that:

G. With time limited filters, a frequency selective channel is responsible for ICI, ISI, and MAI. Time offsets and frequency offsets among users yield a MAI contribution. The insertion of a cyclic prefix allows counteracting the time misalignments across users as well as the echoes from a time dispersive channel.

H. With band limited filters, frequency selective channels yield no ICI at the expenses of sub-channel ISI. Time misaligned users do not introduce any interference component. However, the frequency offsets yield ICI contributions unless increased sub-carrier spacing is chosen.

I. A practical and reasonable choice for controlling the temporal and frequency overlapping of the sub-channels is to deploy Gaussian shaped filters.

J. Lower MAI is generated when the tones are allocated to users in disjoint blocks. With the block allocation of tones we can insert frequency guards in order to further separate the spectrum of distinct users.

We have focused on the DMT-MA system and analytically investigated its performance. To clarify

it and simplify the understanding we have considered first the asynchronous AWGN channel, then the asynchronous quasi-static frequency selective fading channel. Finally, the impact of fast fading has also been considered. The performance has been studied in terms of signal-to-interference power ratio, and in terms of symbol-error-rate.

With regard to the asynchronous DMT multiple access Gaussian channel, we have attacked the non-trivial problem of defining the capacity region, that is the closure of the set of data rates for which reliable communications are jointly possible. We have determined an inner bound to both the capacity of a given user link and the capacity region. Such capacity inner bounds have been treated as random variables since they depend upon the time and frequency offsets as well as upon several system parameters. Therefore, we have evaluated the associated complementary cumulative distribution functions for several system scenarios characterized by different tone assignment schemes and strategies of power allotment to sub-carriers.

Based on the above results our main conclusion is that optimal multicarrier detection should be deployed in multicarrier multiuser systems. Practical implementation with simplified schemes yields good performance. The effectiveness of simplified detection can be improved with the control of the interference components through the appropriate design of the transmit filters, the sub-carrier spacing, and the sub-carrier multiplexing across users. Improvements can be obtained with dynamic tone assignments and ad hoc power allocation across sub-carriers. Some degree of time and frequency synchronization is advisable in certain applications, e.g., macrocellular scenarios with high mobility requirements. Therefore, the appropriate design of the system can tradeoff between demodulation complexity and spectral efficiency such that the performance of the system is maximized.

13 REFERENCES

[1] Alard, M., Lassalle, R., (1987). "Principles of modulation and channel coding for digital broadcasting for mobile receivers", *EBU Riview*, no. 224, pp. 168-190, August 1987.

[2] Anderson, J. B., Mohan, S. (1984). "Sequential coding algorithms: a survey and cost analysis", *IEEE Trans. on Communications*, vol. 32, pp. 169-176, February 1984.

[3] ANSI T1E1.413 (1995). "Network and customer installation interfaces – Asymmetric digital subscriber line (ADSL) metallic interface", August 1995.

[4] Ariyavisitakul, S. L. (2000). "Turbo space-time processing to improve wireless channel capacity", *IEEE Trans. on Communications*, vol. 48, pp. 1347-1359, August 2000.

[5] Bahl, L. R., Cocke, J., Jelinek, F., Raviv, J. (1974). "Optimal decoding of linear codes for minimizing symbol error rate", *IEEE Trans. on Information Theory*, vol. 20, pp. 284-287, March 1974.

[6] Benedetto, S., Divsalar, D., Montorsi, G., Pollara, F. (1998). "Serial concatenation of interleaved codes: performance analysis, design, and iterative decoding", *IEEE Trans. on Information Theory*, vol. 44, pp. 909-926, May 1998.

[7] Benvenuto, N., Cherubini, G. (1999). "Algoritmi e circuiti per telecomunicazioni", *Libreria Progetto ed*., parte seconda, (in Italian), 1999.

[8] Benvenuto, N., Tomasin, S., Tomba, L. (2000), "Equalization methods in DMT and FMT systems for broadband wireless communications", *submitted to IEEE Trans. on Communications*, November 2000.

[9] Benvenuto, N., Tomba, L. (2001). "Multicarrier Systems", *technical report for project PRIM 2000*, Università di Padova, June 2001.

[10] Berrou, C., Glavieux, A., Thitimajshima, P. (1993). 'Near Shannon limit error correcting coding and decoding: turbo codes', *Proceedings of IEEE ICC 1993*, Geneva, Switzerland, pp. 1064-1070, May 1993.

[11] Bottomley, G. E., Chennakeshu, S. (1998). "Unification of MLSE receivers and extension to time-varying channels", *IEEE Trans. on Communications*, vol. 46, pp. 464-472, April 1998.

[12] Buehrer, R. M., Kaul, A., Woerner, B. D. (1996). "Analysis of DS-CDMA parallel interference cancellation with phase and timing errors", *IEEE Journal on Selected Areas of*

Communications, vol. 14, pp. 1522-1535, October 1996.

[13] Buherer, R. M., Arunachalam, S., Wu, K. H., Tonello, A. M. (2001). "Spatial channel model and measurements for IMT-2000 systems", *Proceedings of IEEE Vehicular Technology Conference 2001 Spring, VTC 01-Spring*, Rhodes, pp. 342-346, May 6-9, 2001.

[14] Caire, G., Taricco, G., Biglieri, E., (1998). "Bit-interleaved coded modulation*", IEEE Trans. on Information Theory*, vol. 44, no. 3, pp. 927-946, May 1998.

[15] Cariolaro G., (1996). "Modulazione", *Libreria Progetto ed*., 1996.

[16] Carleial, A. (1978). "Interference channels", *IEEE Trans. on Information Theory*, pp. 60-70, January 1978

[17] Chang, R. W. (1966). "Synthesis of band-limited orthogonal signals for multichannel data transmission", *Bell System Technical Journal*, pp. 1775-1796, December 1966.

[18] Chen, Q., Sousa, E. S., Pasupathy, S. (1995). "Performance of coded multi-carrier DS-CDMA system in multi-path fading channels", *Wireless Personal Communications*, *Kluwer Ac. Pub.*, vol. 2, pp. 167-183, 1995.

[19] Chen, Q., Sousa, E.S., Pasupathy, S. (1995). "Multi-carrier DS-CDMA with adaptive sub-carrier hopping for fading channels", *Proceedings of PIMRC 1995*, Toronto, Canada, pp. 76-80, September 1995.

[20] Cherubini, G., Eleftheriou, E., Olcer, S. (1999). "Filtered multitone modulation for VDSL", *Proceedings of IEEE Globecom 1999*, Rio de Janeiro, Brazil, pp. 1139-1144, December 1999.

[21] Cherubini, G., Eleftheriou, E., Olcer, S., Cioffi, J. M. (2000). "Filter bank modulation techniques for very high-speed digital subscriber lines", *IEEE Communications Magazine*, pp. 98-104, May 2000.

[22] Cimini Jr. L. (1985). "Analysis and simulation of a digital mobile channel using orthogonal frequency division multiplexing", *IEEE Trans. on Communications*, vol. 33, pp. 665-675, July 1985.

[23] Cover, T., Thomas, J. (1991). "Information theory", *John Wiley & Sons*, 1991.

[24] Douillard, C., Picart, A. *et al.* (1995). "Iterative correction of intersymbol interference: Turbo-equalization", *IEE European Trans. on Telecommunications*, vol. 6, pp. 507-511, September/October 1995.

[25] Edfors, O., Sandell, M., Van de Beek, J. J., et al. (1998). "OFDM channel estimation by singular value decomposition", *IEEE Trans. on Communications*, vol. 46, pp. 931-939, July 1998.

[26] ETSI, (1997). "Digital video broadcasting: Framing structure, channel coding and modulation for digital terrestrial television (DVB-T)", *standard ETSI 300 744*, Geneva, March 1997.

[27] ETSI, (1999). "Broadband radio access networks (BRAN); HIPERLAN type 2 technical specifications; Physical layer", August 1999.

[28] ETSI (1999). "GSM technical specifications 5.xx", December 1999.

[29] Eyuboglu, M. V., Qureshi, S. U. H. (1988). "Reduced-state sequence estimation with set partitioning and decision feedback", *IEEE Trans. on Communications*, vol. 36, pp. 13-20, January 1988.

[30] Fazel, K., (1993). "Performance of CDMA/OFDM for mobile communication system*", Proc. of ICUPC 1993*, Ottawa, Canada, pp. 975-979, October 1993.

[31] Fazel, K., Papke, L. (1993). "Performance of convolutionally coded CDMA/OFDM for mobile communication systems", *Proc. of PIMRC 1993*, Yokohama, Japan, pp. 468-472, September 1993.

[32] Hagenauer, J., (1996). "Iterative decoding of binary and block convolutional codes", *IEEE Trans. on Information Theory*, vol. 42, pp. 429-445, March 1996.

[33] Hirosaki, B. (1980). "An analysis of automatic equalizers for orthogonally multiplexed QAM systems", *IEEE Trans. on Communications*, vol. 1, pp. 73-83, January 1980.

[34] Hirosaki, B. (1981). "An orthogonally multiplexed QAM system using discrete Fourier transform", *IEEE Trans. on Communications*, vol. 29, no. 7, pp. July 1981.

[35] IEEE 802.11a (1999). "Wireless LAN medium access control (MAC) and physical layer specifications: high speed physical layer in the 5 Ghz band", 1999.

[36] Kaiser, S., Krzymien, W. (1999). "Performance effects of the uplink asynchronism is a spread spectrum multi-carrier multiple access system", *IEE European Trans. on Telecomm*unications, vol. 10, pp. 399-406, July-August 1999.

[37] Kammeyer, K. D., Tuisel, U., Schulze, H., Bochmann, H. (1992). "Digital muticarrier-transmission of audio signals over mobile radio channels", *IEE European Trans. on Telecommunications*, vol. 3, pp. 23-32, May-June 1992.

[38] Kondo, S., Milstein, L. B. (1996). "Performance of multicarrier DS CDMA systems*", IEEE Trans. on Communications*, vol. 44, pp. 238-246, February 1996.

[39] Le Floch, B., Halbert-Lassalle, R., Castelain, D. (1989). "Digital sound broadcast to mobile receiver", *IEEE Trans. on Consumer Electronics*, vol. 35, no. 3, pp. 493-503, August 1989.

[40] Li, X., Ritcey, J. A. (1998). "Bit-interleaved coded modulation with iterative decoding using soft feedback", *IEE Electronics Letters*, pp. 942-943, May 1998.

[41] Li, Y. G., Cimini, L. J., Sollenberger, N. R. (1998). "Robust channel estimation for OFDM systems with rapid dispersive fading channels", *IEEE Trans. on Communications*, vol. 46, pp. 902-915, July 1998.

[42] Melsa, P. J. W., Younce, R. C., Rohrs, C. E., “Impulse response shortening for discrete multitone transceivers”, *IEEE Trans. on Communications*, vol. 44., pp. 1662-1672, December 1996.

[43] Meyr, H., Moeneclaey, M., Fechtel, S. A. (1998). “Digital communications receivers”, *John Wiley & Sons*, 1998.

[44] Moher, M. (1998). “An iterative multiuser decoder for near-capacity communications”, *IEEE Trans. on Communications*, vol. 46, pp. 870-880, July 1998.

[45] Ohkawa, M., Kohno, R., Imai, H. (1995). “Orthogonal multicarrier frequency hopping-code division multiple access scheme for frequency-selective fading”, *Electronics and Communications in Japan*, part 1, vol. 78, no. 8., pp. 86-97, August 1995.

[46] Patel, P. Holtzman J. M. (1994). “Analysis of a simple successive interference cancellation scheme in a DS/CDMA system”, *IEEE Journal on Selected Areas of Communications*, vol. 12, pp.796-807, June 1994.

[47] Pollet, T., Peeters, M., Moonen, M. Vandendorpe, L. (2000). “Equalization for DMT-based broadband modems*”, IEEE Communications Magazine*, pp. 106-113, May 2000.

[48] Proakis, J. G. (1995). “Digital communications”, *McGraw-Hill*, third edition, 1995.

[49] Rainish, D. (1996), “Diversity transform for fading channels”, *IEEE Trans. on Communications*, vol. 44, no. 12, pp. 1653-1661, December 1996.

[50] Seymour, J. P., Tonello, A. M., Conner, K. (2000). "Full rate AMR over DQPSK”, *Lucent contribution to Telecommunications Industry Association TR45.3.5/00.02.22*, February 22, 2000.

[51] Sourour, E. A., Nakagawa, M. (1996). “Performance of orthogonal multi-carrier CDMA in a multipath fading channel”, *IEEE Trans. on Communications*, vol. 44, pp. 356-367, March 1996.

[52] Speth, M., Fechtel, S. A., Fock, G., Meyer, H. (1999). “Optimum receiver design for wireless broad-band systems using OFDM - part I”, *IEEE Trans. on Communications*, vol. 47, pp. 1668-1677, November 1999.

[53] Speth, M., Fechtel, S. A., Fock, G., Meyer, H. (2001). “Optimum receiver design for OFDM-based broadband transmission - part II: a case study”, *IEEE Trans. on Communications*, vol. 49, pp. 571-578, April 2001.

[54] Stuber, G. (1996). “Principles of mobile communications”, *Kluwer Acad. Publishers*, 1996.

[55] Tarokh, V., Seshadri, N., Calderbank, A. R. (1998). “Space-time codes for high data rate wireless communication: performance criterion and code construction”, *IEEE Trans. on Information Theory*, vol. 44, pp. 744-765, March 1998.

[56] ten Brink, S., Speidel, J., Yan, R. H. (1998). 'Iterative demapping for QPSK modulation', *IEE Electronics Letters*, pp. 1459-1460, July 1998.

[57] Tonello, A. M. (1996). "Spread spectrum multicarrier multiple access", *Laurea thesis* (in Italian), Università di Padova, July 1996.

[58] Tonello, A. M. (1999). "Iterative differential detector", *patent pending*, 03/01/1999, *US Patent Office S.N. 03/259949, European Patent Office S.N. 00301398.4-2206*.

[59] Tonello, A. M. (1999). "Soft output metrics generation for symbol detectors", *patent pending*, 03/24/1999, *US Patent Office S.N. 03/275147, European Patent Office S.N. 00302027.8-2216*.

[60] Tonello, A. M. (1999). "Iterative MAP detection of coded M-DPSK signals in fading channels with application to IS-136 TDMA", *Proceedings of IEEE Vehicular Technology Conference 1999 Fall, VTC 99-Fall*, Amsterdam, pp. 1615-1619, September 1999.

[61] Tonello, A. M. (2000). "Space-time bit-interleaved coded modulation with an iterative decoding strategy", *Proceedings of IEEE Vehicular Technology Conference 2000 Fall, VTC 00-Fall*, Boston, pp. 473-478, September 24-28, 2000.

[62] Tonello, A. M. (2000). "Space-time bit-interleaved coded modulation over frequency selective fading channels with iterative decoding", *Proceedings of IEEE Globecom 2000*, San Francisco, pp. 1616-1620, November 28, 2000.

[63] Tonello, A. M. (2001). "MIMO MAP equalization for turbo decoding of bit-interleaved space-time codes", *Submitted to IEEE Trans. on Communications*, January 2001.

[64] Tonello, A. M. (2001). "Performance of space-time bit-interleaved codes in fading channels with simplified iterative decoding", *Proceedings of IEEE Vehicular Technology Conference 2001 Spring, VTC 01-Spring*, Rhodes Island, pp. 1357-1361, May 6-9, 2001.

[65] Tonello, A. M. (2001). "On turbo equalization of interleaved space-time codes", *Proceedings of IEEE Vehicular Technology Conference 2001 Fall, VTC 01-Fall, Atlantic City*, pp. 887-891, October 2001.

[66] Tonello, A. M. (2001). "Array processing for simplified turbo decoding of interleaved space-time codes", *Proceedings of IEEE Vehicular Technology Conference 2001 Fall, VTC 01-Fall*, Atlantic City, pp. 1304-1308, October 2001.

[67] Tonello, A. M. (2000). "Interference cross-correlation in asynchronous DMT-MA", *Technical memorandum*, Università di Padova, February 2000.

[68] Tonello, A. M., Laurenti, N., Pupolin, S. (2000). "On the effect of time and frequency offsets in the uplink of an asynchronous multi-user DMT OFDMA system*", Proceedings of International Conference on Telecom. 2000*, Acapulco, Mexico, pp. 614-618, May 22-25, 2000.

[69] Tonello, A. M., Laurenti, N., Pupolin, S. (2000). "Capacity considerations on the uplink of a multi-user DMT OFDMA system impaired by time misalignments and frequency offsets", *Proceedings of 12th Tyrrhenian Workshop on Digital Communications – Software Radio Technologies and Services*, Springer-Verlag Del Re (ed.), Portoferraio, Isola D'Elba, pp. 93-104, September 13-16, 2000.

[70] Tonello, A. M., Laurenti, N., Pupolin, S. (2000). "Analysis of the uplink of an asynchronous DMT OFDMA system impaired by time offsets, frequency offsets, and multi-path fading", *Proceedings of IEEE Vehicular Technology Conference 2000 Fall, VTC 00-Fall*, Boston, USA, pp. 1094-1099, September 24-28, 2000.

[71] Tonello, A. M., Pupolin, S. (2001). "Discrete multi-tone and filtered multi-tone architectures for broadband asynchronous multi-user communications", *Proceedings of Wireless Personal Multimedia Communications Symposium 2001 – WPMC 01*, Aalborg, pp. 461-466, September 9-12, 2001.

[72] Tonello, A. M., S. Pupolin, (2001). "Performance of single user detectors in multitone multiple access asynchronous communications", *to appear on Proceedings of IEEE Vehicular Technology Conference 2002 Spring, VTC 02-Spring*, Birmingham (Al), May, 2002.

[73] Tonello, A. M. (2001). "Optimum multiuser detection and turbo multiuser decoding in asynchronous multitone multiple access systems", *submitted on August 2001 to IEEE International Conference on Communications 2002, ICC 2002*, New York, May 2002.

[74] Ungerboeck, G. (1974). "Adaptive maximum likelihood receiver for carrier-modulated data transmission systems", *IEEE Trans. on Communications*, vol. 22, pp. 624-636, May 1974.

[75] Ungerboeck, G. (1982). "Channel coding with multilevel/phase signals", *IEEE Trans. on Information Theory*, vol. IT-28, pp. 56-67, January 1982.

[76] Vahlin, A., Holte, N. (1994). "Optimal finite duration pulses for OFDM", *Proceedings of Globecom 94*, San Francisco, USA, pp. 258-262, November 28-December 2, 1994.

[77] Van de Beek, J., Borjesson, P.O., Boucheret M.L., et al. (1999). "A time and frequency synchronization scheme for multiuser OFDM", *IEEE Journal Selected Areas of Comm.*, vol. 17, pp. 1900-1914, November 1999.

[78] Van Etten, V. (1976). "Maximum likelihood receiver for multiple channel transmission systems", *IEEE Trans. on Communications*, vol. 24, pp. 276-283, February 1976.

[79] Vanderdorpe, L. (1995), "Multitone spread spectrum multiple access communications system in a multipath Rician fading channel", *IEEE Trans. on Vehicular Technology*, vol. 44, pp. 327-337, May 1995.

[80] Vangelista L., Laurenti, N. (2001). "Efficient implementations and alternative architectures

for OFDM-OQAM systems", *IEEE Trans. on Communications*, vol. 49, pp. 664-675, April 2001.

[81] Varanasi, M. K., Aazhang, B. (1990). "Multistage detection in asynchronous code-division multiple-access communications", *IEEE Trans. on Communications*, vol. 38, pp. 509-519, April 1990.

[82] Verdu, S., (1986). "Minimum probability of error for asynchronous Gaussian multiple-access channels", *IEEE Trans. on Information Theory*, vol. 32, pp. 85-96, January 1986.

[83] Viterbi, A. J. (1998). "An intuitive justification and a simplified implementation of the MAP decoder for convolutional codes", *IEEE Journal Selected Areas Comm*., vol. 16, pp. 260-264, February 1998.

[84] Wei, L., Schlegel C. (1995). "Synchronization requirements for multi-user OFDM on satellite mobile and two-path Rayleigh fading channels", *IEEE Trans. on Communications*, vol. 43, pp. 887-895, February/March/April 1995.

[85] Weinstein, S. B., Ebert, P. M. (1971). "Data transmission by frequency-division multiplexing using the discrete Fourier transform", *IEEE Trans. on Communications Tech.*, vol. 19, no. 5, pp. 628-634, October 1971.